POLE TIP RECESSION IN LINEAR TAPE SYSTEMS

Baogui Shi

Doctor of Philosophy

THE UNIVERSITY OF ASTON IN BIRMINGHAM

October 2005

POLE TIP RECESSION IN LINEAR TAPE SYSTEMS Baogui Shi

Aston University in Birmingham - October 2005 Doctor of Philosophy

SUMMARY

The tribology of linear tape storage system including Linear Tape Open (LTO) and Travan5 was investigated by combining X-ray Photoelectron Spectroscopy (XPS), Auger Electron Spectroscopy (AES), Optical Microscopy and Atomic Force Microscopy (AFM) technologies. The purpose of this study was to understand the tribology mechanism of linear tape systems then projected recording densities may be achieved in future systems.

Water vapour pressure or Normalized Water Content (NWC) rather than the Relative Humidity (RH) values (as are used almost universally in this field) determined the extent of PTR and stain (if produced) in linear heads. Approximately linear dependencies were found for saturated PTR increasing with normalized water content increasing over the range studied using the same tape. Fe Stain (if produced) preferentially formed on the head surfaces at the lower water contents.

The stain formation mechanism had been identified. Adhesive bond formation is a chemical process that is governed by temperature. Thus the higher the contact pressure, the higher the contact temperature in the interface of head and tape, was produced higher the probability of adhesive bond formation and the greater the amount of transferred material (stain). Water molecules at the interface saturate the surface bonds and makes adhesive junctions less likely. Tape polymeric binder formulation also has a significant role in stain formation, with the latest generation binders producing less transfer of material. This is almost certainly due to higher cohesive bonds within the body of the magnetic layer.

TiC in the two-phase ceramic tape-bearing surface (AlTiC) was found to oxidise to form TiO_2.The oxidation rate of TiC increased with water content increasing. The oxide was less dense than the underlying carbide; hence the interface between TiO_2 oxide and TiC was stressed. Removals of the oxide phase results in the formation of three-body abrasive particles that were swept across the tape head, and gave rise to three-body abrasive wear, particularly in the pole regions. Hence, PTR and subsequent which signal loss and error growth.

The lower contact pressure of the LTO system comparing with the Travan5 system ensures that fewer and smaller three-body abrasive particles were swept across the poles and insulator regions. Hence, lower contact pressure, as well as reducing stain in the same time significantly reduces PTR in the LTO system.

KEYWORDS: Magnetic tape recording, tribology, PTR, Stain, Contact pressure, Three-body particle, XPS

ACKNOWLEDGEMENTS

It is a pleasure to thank Professor Sullivan for his support throug project. His encouragement and guidance have proved invaluable in th

I am also grateful to thank Dr.Saied for her many helps and useful disc my work, and many thanks for her encouragement.

Dr.Wild and Mr.Andrew Abbot provided with many helps, maintai equipment and gave very useful discussion in this research wo McGinnity and Simon G. Kennedy (Seagate), Allan Hodkinson (HP) a (Imation) for providing heads, drives and tapes, which was jointl EPSRC.

I am also grateful all members of the Surface Science Research Gro create an excellent and warm working environment.

Thanks for my family's support during my study abroad.

Contents

Figure captions

Table captions

Glossary of Acronyms

ABS.....Air bearing Surface
AES.....Auger Electron Spectroscopy
AFM.....Atomic Force Microscope
BOT.....Beginning Of Tape
DDS.....Digital Data Storage
DLC.....Diamond-Like Carbon
EOT.....End Of Tape
GMR.....Giant Magnetoresistive (head technology)
HD.....Hard Disk
HDD.....Hard Disk Drive
LTO.....Linear Tape Open
MB/s.....Megabyte per second
ME.....Metal Evaporated (tape)
MET.....Metal Evaporation Tape
MP.....Metal Particle (Tape)
MR.....Magneto Resistive
NWC.....Normalised Water Content
PA.....Polyamid
PEN.....Polyethylene Naphthalate
PET.....polyethylene Terephthalate
PTR.....Pole Tip Recession
RH.....Relative Humidity
SAM.....Scanning Auger Microscopy
SEM.....Scanning Electron Microscopy
STM.....Scanning Tunnelling Microscope
TBS.....Tape Bearing Surface
TEM.....Transmission Electron Microscope
XPS.....X-ray Photoelectron Spectroscopy

1 Chapter 1 Theoretical Background and Literature Review

This thesis aims to accomplish a series of experimental studies on the tribology of linear data tape systems including Travan5 system and the first generation of Linear Tape Open (LTO) system. The latter is the major research area. The aim of this research is to understand Pole Tip Recession (PTR) and material transfer (stains) mechanisms occurring at the head-tape interface.

The thesis is divided into five chapters that introduces the theoretical background knowledge of the magnetic recording system and tribology literature reviews of magnetic recording systems (chapter 1); the experiments and technologies used in this project (chapter 2); experimental results (chapter 3); discussion of the experimental results (chapter 4); conclusion and future work (chapter 5).

1.1 Introduction

Information storage applications continue to grow at a rapid rate due to the successful development of business and consumer products for processing data, video, and audio signals. The demand for high data densities and capacity, good signal performance has been increased monotonically. Since the first viable commercials magnetic recording tape in the 1930's and hard disk drive in the 1950's the annual areal density growth rate remained reasonably constant at about 25 to 30% per year[1] (see Figure 1-1). However, with the introduction of thin film hard-disk media and magneto-resistive transducers in the early 1990's this growth rate increase to about 60% per year.

The areal data storage density of magnetic disk hard drives (HD) is currently increasing at a rate of 120 % per annum and it is predicted that several Tb/in^2 will be achieved before the super-paramagnetic limit is reached[2] (see Figure 1-1). The ultimate limit to storage density is the super-paramagnetic limit, where the thermal energy kT can overcome the coercive energy of the magnetic bit[3].

Computer tape provides the lowest cost storage medium for the applications, such as archival storage, backup for on-line disks, an interchange medium, sequential processing and low-cost on-line storage (library or mass storage system). Lots of works

have been done to increase the data densities and capacity. Today, the best linear tape systems have data densities of less than 200Mb/in^2, whereas, to remain competitive, densities of greater than 2 Gb/in^2 must be attained in the next few years. In spite of various measures taken by the industry[4], big problems in computer data storage are the wear between heads and tapes and the stains on the head surface that both cause the space loss between the tape and head. It is now and will increasingly in the future to be significant limiting factors in dynamic magnetic storage technology.

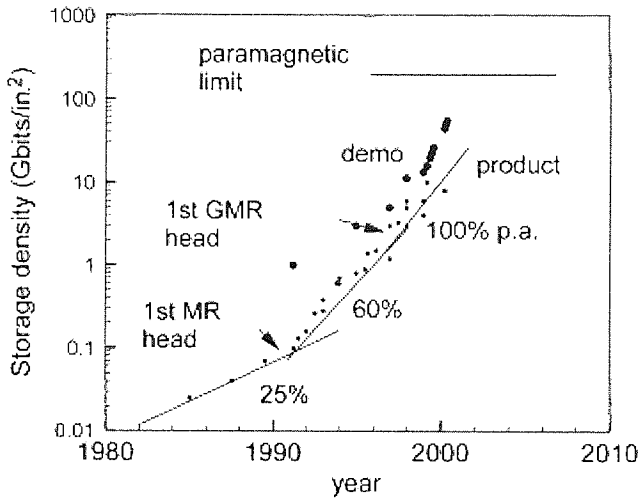

Figure 1-1 Increase in storage density of hard disk drives with date[5]

Physical spacing (d) between the head and magnetic media result in an electrical signal loss $V(d)$ which is related to the spacing (d) by the Wallace equation[6]: $V(d) = e^{-2\pi d/\lambda}$, where λ is the recording wavelength. At current wavelengths of 0.7μm every 10nm increase in d leads to 0.8dB of output loss and this will become significantly worse as wavelengths decrease. An output loss exceeding 6dB is typically considered as failure[7, 8]. Signal amplitude is only independent of the data being read if the spacing is zero. Thus, the level and more specifically the variation in head media spacing with device life must be a minimum to maximise signal output and minimise errors. Although tape is the cheapest and most efficient method of storing large amounts of data, systems will not survive if data densities can not be substantially increased. For a 2 Gb/in^2 capacity and above, the spacing must be reduced from its present value of about 50nm to a value approaching 10nm.

Pole Tip Recession is one of the most important changes because of the head tape wear; excessive recession of the poles causes an increase in the magnetic spacing. Stains or transfer film is another possible cause of spacing loss. Loose debris on the surface of the head also leads extra spacing loss in the head tape system[9,10,11]. Changes in the tape surface have also effects on the tribology between the heads and tapes.

So far Linear Tape-Open (LTO) Technology is the best available implementation of this technology in many ways. First, it enables a higher number of concurrent channels. The first generation of LTO enables up to eight channels, with future versions delivering up to 16 channels. The LTO was also developed to take advantage of the best available servo and head technologies, which are essential to provide the high degree of accuracy critical for high track densities. In addition, LTO offers a higher recording areal density (100Mbits/sq.inch) than any linear tape technology available in the industry today[12].

It is very important to understand the interaction between head and tape and its impact on signal performance. From this, methods can be developed to design and develop new generation tape-head products to meet the increasing data storage market.

1.2 Magnetic Recording

1.2.1 Magnetic Recording Principles

1.2.1.1 Physics of Magnetic Recording

A permanent magnet is composed of a material that has the property of staying magnetized in a given direction after the field that created this magnetization is removed. This property[13] is displayed by a hysteresis loop, such as that shown in Figure 1-2 (b), in which the magnetization M is plotted against the applied field H. The magnetization is not a unique function of the field but depends on the direction and magnitude of previous applied fields. There are two important parameters of the loop: first, the remanent magnetization M_r (see Figure 1-2 (b), Value of OB); second, the coercivity H_c (see Figure 1-2 (b), Value of OA), the reverse field required to reduce the magnetization to zero.

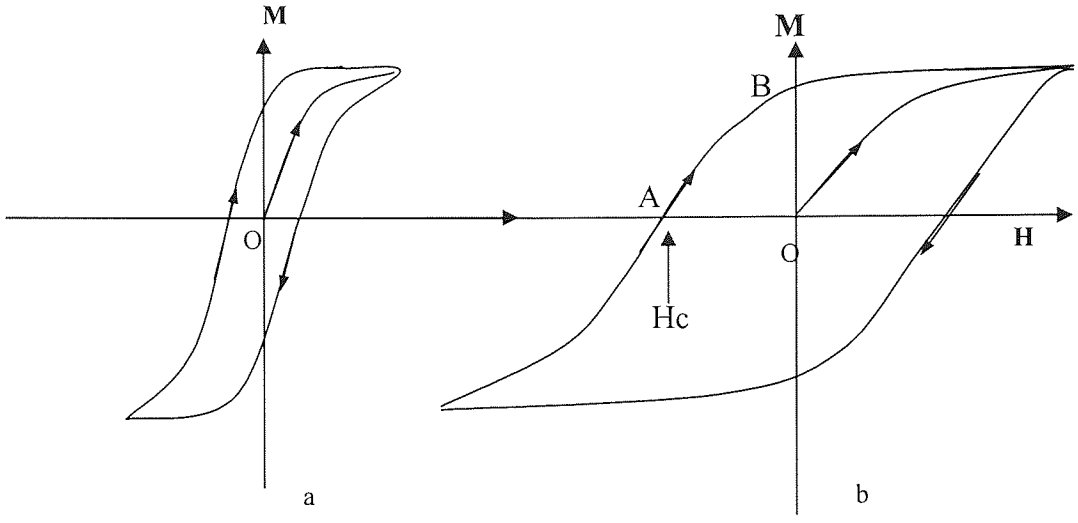

Figure 1-2 showing a typical (a) paramagnet or a soft magnet, (b) a ferromagnet or a hard magnet

The remanent magnetization indicates the extent to which the magnet stays magnetized after the applied field is removed; the coercivity expresses the degree to which the magnet resists being demagnetised. The product M_rH_c measures the strength of the magnet.

The hysteresis loops shown in Figure 1-2 (a) and Figure 1-2 (b) have two distinct shapes, which are dependent on the material. Firstly, the curve shown in Figure 1-2 (a) is long and thin with a small cross-sectional area, small remanent magnetization M_r and coercivity H_c. This is associated with a soft magnetic ($H_C \sim 10^{-2}$ Oe), which is employed to be the head writing and reading materials. Whereas, when the cross-sectional area of the loop is large the coercivity and remanent magnetization M_r high as shown in Figure 1-2 (b) the material is referred to as a hard magnetic ($H_c \sim 10^2$-10^4 Oe), this type of material that has high coercivity and magnet remanence characteristics can be used in magnetic tape to record data. In this form, most of the magnetic dipole moments of the magnetic particles are aligned in the same direction.

1.2.1.2 Magnetic Recording Process

In principle, a magnetic recording medium consists of a permanent magnet configured so that a pattern of remnant magnetisation can be formed along the length of a single track, or a number of parallel tracks, defined on its surface. Recording (or writing) takes places by causing relative motion between the medium and a recording transducer.

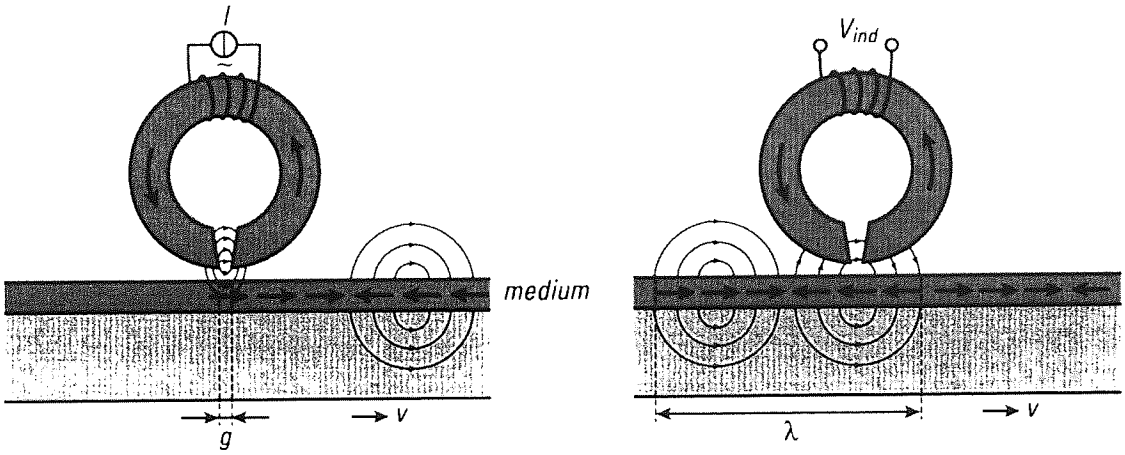

Figure 1-3 the recording (write) process (left) and reproducing (read back) process (right) with a ring head. g: gap between two pole, v is tape moving speed, λ recording wave length

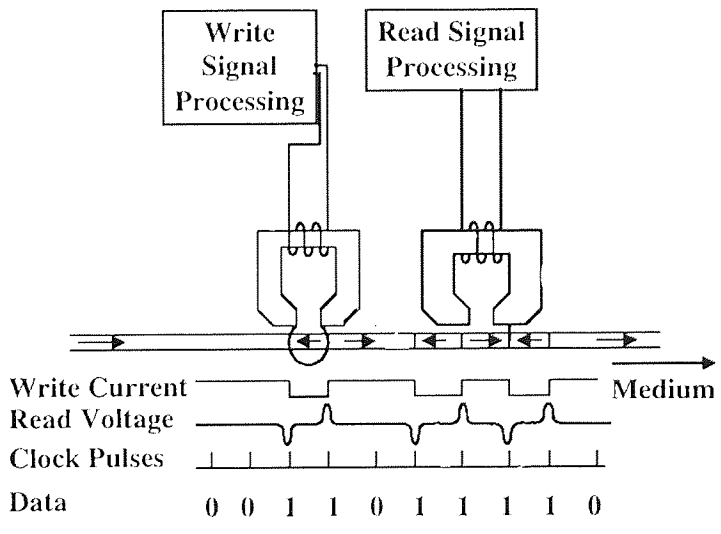

Figure 1-4 A schematic diagram of a magnetic recording system[14].

Figure 1-3 shows the simplest ring shaped electro-magnet head, with a gap facing the magnetic coating. The magnetic recording medium consists of a magnetic coating on

some form of substrate. In the case of magnetic tape, the substrate is a flexible medium. To record and play back the information one or more magnetic recording heads are used. The recording head consists of a high-permeability magnetic core with a narrow gap cut into it and a few turns of conductor wound around it. When current flows through the conductor, magnetic flux flows through the magnetic core, emanates from the core at the gap and penetrates the magnetic medium, causing it to be magnetised to the right or the left (see Figure 1-3).

A schematic of a magnetic recording system is illustrated in Figure 1-4. Highly sophisticated signal processing electronics are used to encode binary ones and zeroes into the write current waveforms in coincidence with a clock, and also to convert the waveforms sensed by the read head back into digital data. An actuator is used to servo-position the head relative to the media for accessing the desired track of data.

By changing the polarity of the write signal, the magnetic domains in the tape are aligned accordingly. Thus, data is written in bits of information, eight of these bits constitute one byte. The process is illustrated schematically in the field output from Figure 1-4, the magnetic field H produced in the writing processing is inversely proportional to the length of gap between the pole tips, g, such that

$$H = \frac{NI\varepsilon}{g} \qquad \text{Equation 1-1}$$

Where N is the number of turns in the coil, I the current in the coil and ε is a scaling factor[13, 15]. Hence, the head translates the information from electrical signals into magnetic fields and writes the information on the moving magnetic media.

If the writing signal is of a frequency f and the relative velocity is v, then the magnetisation pattern is recorded with a fundamental wavelength[13] λ,

$$\lambda = \frac{V}{f} \qquad \text{Equation 1-2}$$

The magnetic information is later read by moving the magnetised regions past the same or another head, which converts the information back into varying electrical signals. Reading does not destroy the information - it can be read again and again. Information can also be erased or overwritten by fresh data.

A similar recording head is used to sense the magnetic flux emanating from the recorded transitions in the medium during read back (see Figure 1-4 reading signal processing). In order to achieve high recording density it is imperative that the head be very close to the medium. Spacing of the order of 50 nm is used in today's head-tape system.

For the induction reading head (see Figure 1-4), the head provides an induced voltage on read back, reflecting the rate of change of magnetisation recorded on the magnetic track. This type of head would be known as inductive. In the simplest case, when the recorded medium is passed over the same head, or a reproducing head of similar construction at the same velocity, the head core intercepts the flux emanating from the medium surface, and a voltage is induced in the coil proportional to the rate of change of this flux. In the reading, or reproduction, a signal of voltage, V, is induced into the core windings according to Faraday's Law of Induction[16],

$$V = -\frac{d\phi}{dt} = -\frac{Nvd\phi}{dx} \qquad \text{Equation 1-3}$$

Where ϕ is the flux; N is the number of turns; t is time; v is the head-tape velocity and x is distance. The voltage is not an exact replica of the recording signal, but it constitutes a reproduction of it in that information describing the recording signal can be obtained from this voltage by appropriate electrical processing.

1.2.2 Recording Heads

1.2.2.1 Thin Film Magnetic Heads

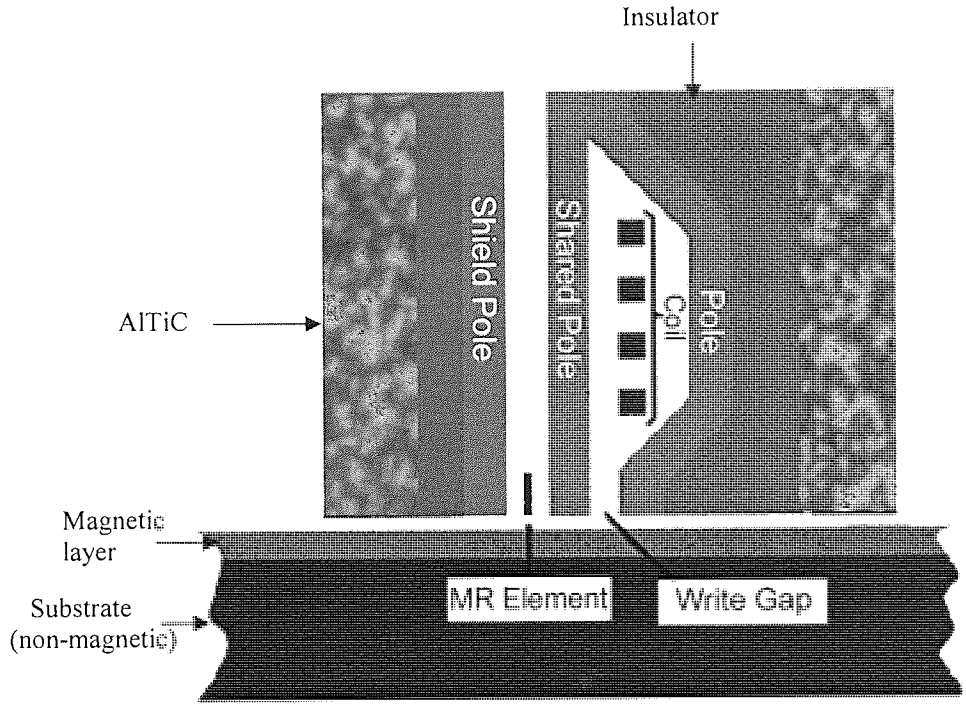

Figure 1-5 Cross-section of write-read head with magnetic media

The introduction of thin film magnetic heads[17] in the 1980's dramatically reduced the dimension of the recording gap and also the overall size of the head as compared to traditional metal tape heads, which greatly increased the recording density and data rate. Thin film magnetic heads (see Figure 1-5) are commonly used for high-density magnetic recording. For thin film heads, the read head is Magneto-Resistive (MR) type and the write head is inductive. This body of a thin film head is made of non-magnetic alumina-titanium carbide (AlTiC), and the head construction includes coating of soft magnetic alloys (Pole and shared pole and shield pole), insulating oxides (see Figure 1-5, insulator) is between the pole and shared pole and shield. Thin film magnetic heads simplified the tape head contour since the thin film magnetic elements could be easily housed within the gap area (between two parts of ceramic).

The ideal materials of pole have low coercivity, high saturation magnetic induction B_s, high permeability, low magnetostriction and high mechanical properties. High Saturation Magnetization Ms for a pole materials is beneficial for producing a high

fringing magnetic field strength across the head gap without saturating the head, and allows the head to be operated in a wide linear region (where the fringing magnetic field strength is linear to the coil current) to higher magnetic inductions without saturating the head[16]. Saturation magnetization $4\pi Ms$ values of NiFe, CoZrTa and FeAlN films are about 8-10, 12-14 and 19-20kG, respectively (see Table 1-1).

Materials	Permalloy	Amorphous Co alloys	Sendust	Hot-pressed Ferrite Mn-Zn
Composition (wt%)	19%Ni, 81%Fe	Co~ 90% Zr~5%, Ta~5%	85%Fe, 9%Si, 6%Al	$(MnO)_x(ZnO)_{1-x}(Fe_2O_3)$, (x:0.3-0.7)
Permeabilities (μ)	2000-3000	1500-3000	8000	10,000
Coercivity (Oe)	0.05	0.02	0.03	0.15
Saturation Magnetization (T)	0.8-1.0	1.0-1.4	1.0	0.5
Electrical resistivity ($\mu\Omega$·cm)	100		85	5×10^4-5×10^5
Knoop hardness (GPa)	1.2	4.9	5.4	5.9

Table 1-1 Properties of magnetic materials[18, 19, 20]

In many ways, the fabrication of magnetic recording heads resembles that of the on-chip interconnection of semiconductor integrated circuits. The processes used to fabricate a recording head comprise a combination of lithography, deposition (vacuum or plating), etching steps, precise lapping. Review papers describing the details of recording head fabrication have been published in the literature[21,22].

Amorphous Co-based alloys are regarded as materials with large M_s and soft magnetism. The addition of Ta seems to be effective not only in enhancing the fine granulation, but also in reducing the magnetostriction constant λ for improving the soft magnetism of films[18].

In Travan5 and LTO heads, Al_2O_3 insulator (see Figure 1-5) is low temperature RF-sputtered, effectively completely amorphous, Al_2O_3 insulator is used in forming the insulator deposited onto the AlTiC substrate to provide a smooth surface for head

fabrication. Inductive head pole materials are CoZrTa (R.F-sputtered, amorphous state). There are several methods[18,23] can be used to sputter Co-Zr-Ta amorphous thin film. MR element in Travan5 and LTO heads all used Permalloy (Ni-Fe). The magneto-resistive (Permalloy $Ni_{19}Fe_{81}$) is being used for read back of information in high-density recording. The MR element principle will be discussed in the next section. Leads and coils in the heads usually are copper.

1.2.2.2 Magneto Resistive Element

An alternative to inductive reading is provided by the magneto-resistive effect. Magneto-resistive (MR) read element uses the magneto-resistive effect; that is the resistance of a material changes with a change of magnetisation direction or a change of flux direction. MR sensor is only used in reading process.

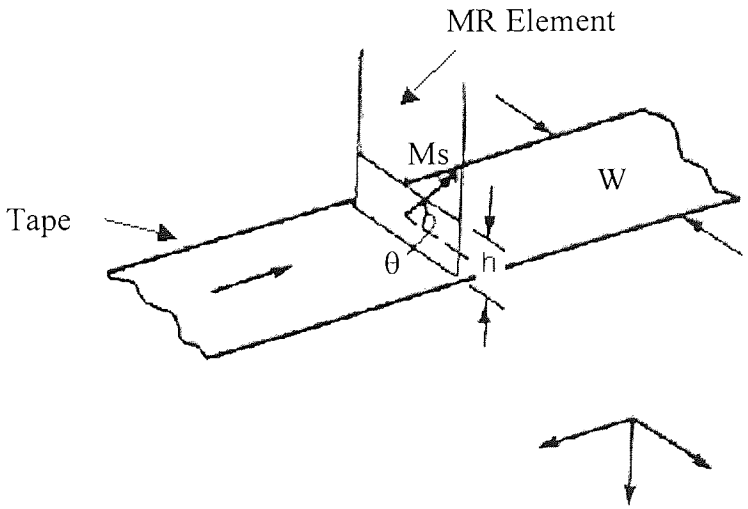

Figure 1-6 Magneto-resistive sensor stripe geometry[24]

Figure 1-6 shows the typical MR element in the heads. Basically the MR element is a stripe of magneto-resistive materials such as $Ni_{19}Fe_{81}$, Ni-Co and Co-Fe. Magneto-resistive heads are read only thin film housed between the share pole and shield pole (see Figure 1-5). Very thin Amorphous Al_2O_3 insulator is filled between the MR element and share pole and shield pole (see Figure 1-5). The measurement of resistance of MR element could be used to determine the magnetic property of the magnetic media surface; in this way the data recorded in the media could be read. The simplest form of MR element is the dependence of the resistivity of a conductor, ρ, upon the angle, θ,

between the direction of the current – density vector and the applied magnetic field, as given[24] (see Figure 1-6):

$$\rho = \rho_0 + \Delta\rho \cos^2 \theta \qquad \text{Equation 1-4}$$

For most materials of interest the increment of resistivity, $\Delta\rho$, is in the order of 2 to 6 percent of the base resistivity ρ_0, but in this function they tend to exhibit higher signal levels, especially at low velocities, comparing inductive heads.

Magneto-resistive heads are more sensitive than inductive heads and therefore produce larger signal amplitudes during read back. Another advantage of the MR head is that it senses magnetic flux ϕ, not the time rate of change of flux $d(\phi)/dt$ as an inductive head does. Consequently, whereas the inductive head output voltage is dependent on the head to medium velocity, the output voltage of an MR head is independent of velocity.

The giant magneto-resistance (GMR) effect, a phenomenon involving large changes in electrical resistance that occur in specific materials sandwiched in a number of very thin layers of metals[25, 26] has been employed in the hard disk heads. But in this research project of Aston University, MR element is used as the reader sensor in the linear recording system, so the MR sensor is the major emphasis in this study.

1.2.3 Flexible Magnetic Media

Flexible magnetic media [10,11,13] (tapes) consists of a thin magnetic coating applied to a polymeric substrate carrier film. The magnetic coating may be applied as slurry containing magnetic particles (particulate media) or as an evaporated magnetic metal film (metal evaporated media). Each of these forms of media has their own tribological problems. In addition to the magnetic side of the media there is often a backside coating applied to tape to give the desired mechanical and tribological properties, to prevent adhesion when rolled and to give anti-static protection.

1.2.3.1 Particulate Media

In particulate media, the magnetic coating consists essentially of acicular magnetic particle bound together by means of a polymeric resin[10,27]. The filled polymer in his case is complicated and consists not only of the magnetic pigment (at up to 80% by weight, 50% by volume) and the polymer binder, but also a head cleaning agent (HCA) (typically about 4 to 8% by weight of a relatively large abrasive particle such as Al or Zr oxide) and a possible combination of wetting agents (To stop the particles from accumulating in groups), cross linking agents, solvents, anti-fungal agents, carbon black (to prevent surface charging) and finally the essential lubricant (typically fatty acid/fatty acid esters)[9,10,11,13].

A lubricant is included in the binder system to increase the lifetime of the media by reducing the friction between the media and the heads since without a suitable lubricant, the condition of the media would deteriorate rapidly due to the large coefficient of friction at the head/media interface. Sullivan[10] indicated that the mean non-magnetic overlayer thickness of polymer/lubricant covering the magnetic pigment is about 4nm on the MP tapes.

Gamma Ferric Oxide (γ-Fe_2O_3) was the most common magnetic material in use during the early development of the tape industry. They are acicular (needle shaped) with an aspect ratio[10, 13] of about 5 to 10, the particle length is between 0.3-1μm, with a coercivity of around 275-375Oe (see Table 1-2), derived from their shape anisotropy,

their magnetic properties are essentially temperature-independent over the temperature range encountered in applications.

Material	Particle length,μm	Coercivity, Oe	Remanence, G	Curie temperature, °K	Density, kg/m³	SSA[a], m²/g	Mean particle volume, 10⁻¹⁸ μm³
Gamma-ferric oxide[b], γ-Fe_2O_3	0.3-1	200-300	1100-1300	870	4800	12-35	1-25
Colbalt-Substit[b] Co-γ-Fe_2O_3	0.3-0.6	600-900	1200-1700	793	4800	16-33	1-10
Chromium dioxide CrO_2	0.3-1	400-900	1400-1700	387	4800	18-36	1-10
Barium ferrite[c] $BaO\ Fe_2O_3$	0.06-0.15	400-1200	1000-1200	728	5300	20-35	<2
Metal particles[d], Fe	0.1-0.2	900-2000	3500	1043	5800	35-50	<1
Co-Ni (evaporated) 82Co18Ni		400-2000	13,000		8000		
Co-Cr (sputtered) 80Co20Cr		400-2000	10,000	1073	8000		
Gamma-ferric oxide (sputtered) γ-Fe_2O_3		400-2000	5000				

Table 1-2 Properties of hard magnetic materials for media[20]

[a]SSA, specific surface area of particle.
[b]Acicular particles with an aspect ratio of about 5 to 10.
[c]Hexagonal platelets with long dimension to thickness(easy axis)ratio of 3 to 30.
[d] Acicular particles with an aspect ratio of about 3 to 4.
[e] Co-based films are doped with elements such as Pt or Re, and γ-Fe_2O_3 films are doped with elements such as Co for high coercivity.

For the cobalt modified Gamma Ferric Oxide (γ-Fe_2O_3), the addition of cobalt to the surface of a gamma ferric oxide particle ensures that the new particle has a higher coercivity of around 1000Oe. Unfortunately this particle is thermally unstable at high temperatures (300C°) due to the diffusion of Co into the particles.

Chromium dioxide (CrO_2) tape exhibits a higher coercivity than γ-Fe_2O_3, it tends to be more abrasive than γ-Fe_2O_3, Chromium dioxide (CrO_2) is unstable as well when exposed to the atmosphere[10,11,13].

The passivated metal (Fe) acicular particles (MP media) are widely used to achieve higher recording densities. Metal particle materials were first developed for magnetic recording because of their high coercivity and magnetization intensity, both initially about twice the corresponding values of the cobalt-enhanced iron oxide and chromium dioxide particles that they have replaced. Particles of current interest are acicular in shape, with lengths on the order of 100nm, and diameters about one-fifth as large. Approximately half of the particle volume is typically taken up by the passivation shell, which contributes nothing to the magnetic properties. Commercial iron particles[28] had an oxide layer with an average thickness of 5nm, numerous other elements, such as B, Si, P, Y, Nd, Sm, La, and Pr[29,30,31] as the anti-sintering agent (less than 2%, atomic concentration) used in the manufacture of LTO MP tapes, mainly to prevent sintering between particles and to maintain the acicular[30, 32, 33]. The magnetic particles are contained within a polymer binding system; the main binders are either polyvinyl chloride (PVC) or polyester polyurethane[34].

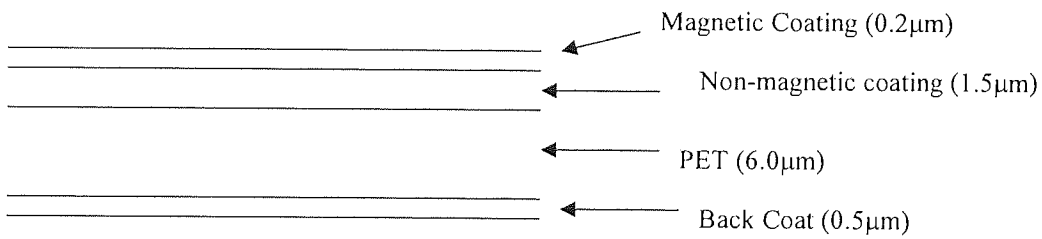

Figure 1-7 Schematic diagram structure of a double layer Particulate Magnetic Tape

Figure 1-7 shows a typical double layer metal particulate magnetic tape, from the top of the tape, the first layer was composed of metal particles with Head Cleaning Agent, lubricants, and binder materials. The under layer was composed of non-magnetic α-Fe_2O_3 fine particles with thickness around 1.5μm. This non-magnetic layer provided a much better smooth surface for the magnetic layer to deposit and in the same time reserved some lubricants for the magnetic layer. This double layer tape can achieve a smooth surface more easily than a single layer MP and have a low friction coefficient

because it has enough free lubricant in the coating layer[35]. For the single layer metal particulate magnetic tape, the magnetic coating directly deposited on the surface of PET without the non-magnetic α-Fe_2O_3 fine particles layer, the thickness of magnetic coating in single layer was normally between 1.0-1.5μm which is thicker than the double layer Mp tape magnetic layer. The other materials and structure in single layer MP tape is quite similar with double layer MP tape, but the single layer MP tape is no more used as data recording tape due the excellent performance of the double layer Mp tape.

As coercivity continues to rise, particle size continues to fall. Small particles obviously mean that a greater number of individual particles will be located within a given area. This fact, along with the higher coercivity, allows a much greater packing density rate, a greater amount of information to be stored in a given area. Detail descriptions of different tape materials are given below.

1.2.3.1.1 MP Tape Substrate

All magnetic recording tapes use ultra-thin polymeric materials as a substrate for the deposition of magnetic coating[36], currently the most commonly used substrate is polyethylene terephthalate (PET), materials with higher elastic modulus such as polyaramide (PA) and polyethylene naphtalate (PEN) are becoming increasingly popular[37]. The thickness of the film used in magnetic media applications usually falls within the range 6μm to 25μm with smaller thickness yielding greater recording capacity.

Polymers may exist in crystalline and amorphous states and in the amorphous state may be either glassy, rubbery of viscous[27]. Polymeric binders normally consist of two phases, a 'hard' glassy phase to give the system mechanical integrity and a 'soft' rubbery phase to provide the flexibility required of the media[27].

The progress proposed in the tape substrate will require improved substrate materials that are thinner, stronger mechanically and more dimensionally stable. Substrate materials should be able to withstand temperatures in excess of 100-150°C as magnetic layers are deposited or heat-treated at high temperature. PET dominates low

performance particulate tapes; PEN, which is stiffer, is used in several advanced products both for MP and ME; PA, which is even stiffer, is used in the SONY micro cassette at a thickness of only 2.5 μm. The stiffer tape usually increases the normal pressure[38], so in the same way the stiffer tape will increase the wear of the head if the other conditions are kept the same, but the thinner substrate allows a much greater packing density.

However, the cost of PET is half that of PEN and a tenth that of PA. Both PET and PEN are manufactured in very high volume for other commercial applications, which results in lower cost for the tape market. The industry faces a major challenge in the development of improved but cost-effective substrate materials.

1.2.3.1.2 Binder System of the Tape

The magnetic particles are contained within a polymer binding system. The purpose of the binder is to provide the cross linking necessary to hold all of the mix ingredients together and to ensure the coating does not shed or flake off the base film (tape substrate). The binder materials used in the tapes must have high flexibility, elasticity, wear resistance and in the same time provide low coefficient of friction and low head wear.

The term binder is a generic term covering a wide range of polymeric material such as polyurethane and vinyl chloride. The binder materials could be urethane: H_2N-NH-C(=O)-O-C_2H_5 or vinyl chlorine: (H_2C=CHCl) or the mixture of the both.

1.2.3.1.3 Tape Head Cleaning Agent (HCA)

A Head Cleaning Agent is often incorporated into the magnetic coating in order to help maintain the performance of the heads, the abrasive particles which act as the head cleaning agent are typically alumina or chromium dioxide and they help to ensure a good contact between the heads and media for the lifetime of the system by preventing a build up of debris and stains on the surface of heads.

The thickness of used head cleaning agent[39] such as α-Al_2O_3 was from 0.2 to 0.5μm, the size of HCA decreases as the tape coating decreases. The adding of HCA to MP tape can successfully prevent the formation of deposits on magnetic head but results in head wear[40]. The amount of head cleaning agent added is extremely important. If too much alumina is added certainly the abrasivity of the tape is higher and leads a rough tape surface, head life deterioration becomes an issue. If too little alumina is added the tape may not be able to keep the transport clean enough to ensure good head to tape intimacy and a poor quality recording results. HCA should be used at about 2-5wt% of the total particles in the tape surface[39]. There are many other factors that influence the abrasivity of a given tape; such as the type of particles, binder system, and other formation ingredients all play a role in determining a particular tape's abrasivity.

HCA also provides the tape hard bearing area contacted with the head during cycling. Increase in HCA increases the hard bearing area, probably also reduces hot spot temperature (during tape-head movement). Increase in HCA and reduced contact pressure combined reduce the energy dissipation at the contact areas. In Modern tape HCA has no "head cleaning" action due to the surfaces are too smooth, HCA has a purely bearings function, this is essential and is the major reason for using HCA in modern tapes.

1.2.3.1.4 Lubricants

Sliding between clean solid surfaces is generally characterised by a high coefficient of friction and severe wear due to the specific properties of the surface, such as low hardness, high surface energy, reactivity, and mutual solubility. In order to reduce the wear in the relative movement of surfaces, a lubricant is included between the moving objects.

The lubricant is included in the tape binder to increase the lifetime of the media, the lubricant does not reduce friction substantially, because the surface energy of the polymer binder is roughly the same as the surface energy of the lubricant, but the lubricants provide an easily sheared surface film and substantially reduce media wear.

The lubricants used in particulate media are generally fatty acid esters (fatty acid ester, e.g. $C_{13}H_{27}$-O-C(=O)-$C_{18}H_{37}$) since these compounds possess the stringent characteristics needed for use in particulate magnetic media. For the dual layers MP tapes, the non-magnetic layers under the magnetic layer not only provide a smooth layer for the magnetic layer to adhere, but also provide a lubricant reservoir to incorporate the lubricants and transfer the lubricants to the tape surface when the lubricants are needed.

In general, the lubricant in the surface coverage is sparse with areal coverage between 10 and 40% being typical[10]. This coverage is sufficient to protect the media surface against premature failure, tape durability increase with lubricant coverage[10,41].

1.2.3.2 Metal Evaporated Media

Figure 1-8 shows the typical structure of metal evaporation tape. The materials used for the substrate of ME media are the polyethylene terephthalate (PET) or polyethylene napthaletes (PEN) films. The magnetic layer of a metal evaporated tape is produced by the evaporation of a magnetic alloy such as $Co_{80}Ni_{20}$ onto a polymer substrate as shown in Figure 1-8. The thickness of the magnetic coating is between 100nm to 200nm. A continuous Carbon overlayer must be incorporated into the structure of thin film ME media in order to protect the tape from the effects of wear and corrosion (see Figure 1-8). Finally the inclusion of a lubricant (such as perfluoropolyether (PFPE)) on the top surface of ME media is imperative in order to give the tape good durability and low wear characteristics.

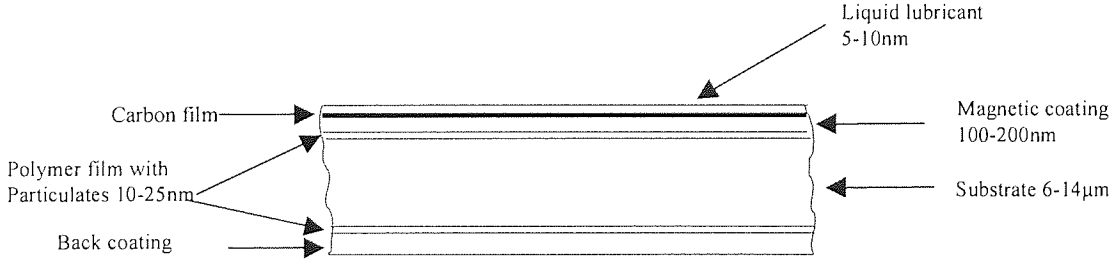

Figure 1-8 Typical metal evaporated tape structure

Metal evaporation tape (MET) was introduced late to the tape industry. The metal evaporation technique can coat extremely thin magnetic layers. The Metal evaporated media has potentially higher effective magnetisation than particulate magnetic media due to the increased magnetic grain density within the layer[10], it is unlike particulate media, surface coverage of the lubricant in metal evaporation tape must be complete, must remain for the projected lifetime of the media[10].

Generally metal evaporated tape has a higher magnetic moment and output signal than MP tape, but its durability has been a concern. Studies on the earlier version of ME tape revealed that its wear performance was worse than MP tape[42,43,44]. The wear life of ME tape has been shown to slightly improve with the addition of a Diamond like Carbon (DLC) coating[45].

1.2.4 Playback Signal Performance

The play-back or reproduce signal amplitude in magnetic recording is dependent on recording wavelength, the gap length, the head-medium separation, the magnetic properties of the medium, and its thickness. Wallace[6] gave a general expression for playback amplitude, shown in Equation 1-5:

$$e(t) = 10^{-4}\alpha NW\{\mu_r/(\mu_r+1)\}M_rU(2\pi\delta/\lambda)T(\lambda)S(\lambda)G(L)\cos(2\pi x_0/\lambda)$$

Equation 1-5

Where the major factors are:

M_r = remnant magnetisation of the media (Wb/m^2)

$= Sp\sigma_s\rho$

$T(\lambda)= \{1-\exp(-2\pi\delta/\lambda)\}/\{2\pi\delta/\lambda\}$

$S(\lambda)= \exp(-2\pi d/\lambda)$

$G(\lambda)=\{\sin(\pi g/\lambda)\}/(\pi g/\lambda)$

α = head efficiency factor

N = number of turns in the head

W = head width (mm)

μ_r = relative permeability of the core

U = relative velocity of the head to the media (m/s)

x_0 = Ut, the longitudinal position of the head along medium relative to an arbitrary reference (mm)

t = time (s)

λ = recorded wavelength (μm)

δ = thickness of medium (μm)

d = effective spacing between the head and the surface of the medium

g = gap length

$S = M_r/M_s$

p = packing fraction of particles in media (0-1.0)

σs = specific saturation magnetisation of particles (emu/g)

ρ = density of particles (g/cm^3)

The three loss functions characterised by Wallace , the tape thickness loss:

$T(\lambda) = -20\log_{10}\{2\pi\delta/\lambda\}/\{1-\exp(2\pi\delta/\lambda)\}$ Equation 1-6

The Spacing Loss

$S(\lambda) = -54.6\ d/\lambda$ Equation 1-7

The gap loss

$G(\lambda) = -20\log_{10}\{(\pi g/\lambda)/\sin(\pi g/\lambda)\}$ Equation 1-8

The contributions (in dB) of the three losses are shown graphically in Figure 1-9 as a function of δ, d and g, each expressed as multiples of the recording wavelength.

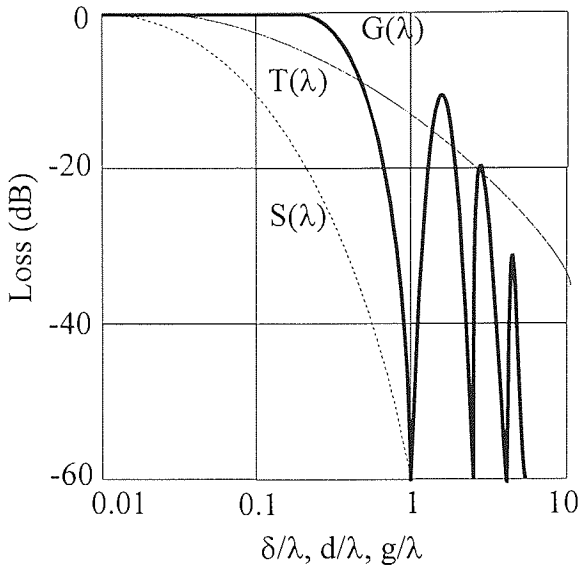

Figure 1-9 Thickness loss, T(λ); Spacing Loss, S(λ), and Gap Loss, G(λ) in magnetic recording[6]

1.2.5 Basic Introduction of tape head system

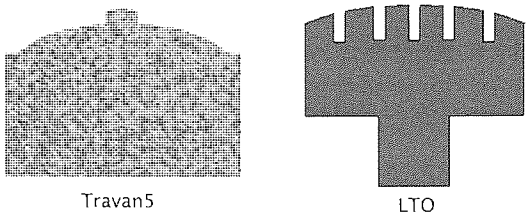

Figure 1-10 Schematic diagram of Travan5 head (left); two rails and slots of LTO head (right) (Both in the perpendicular direction to the tape moving direction)

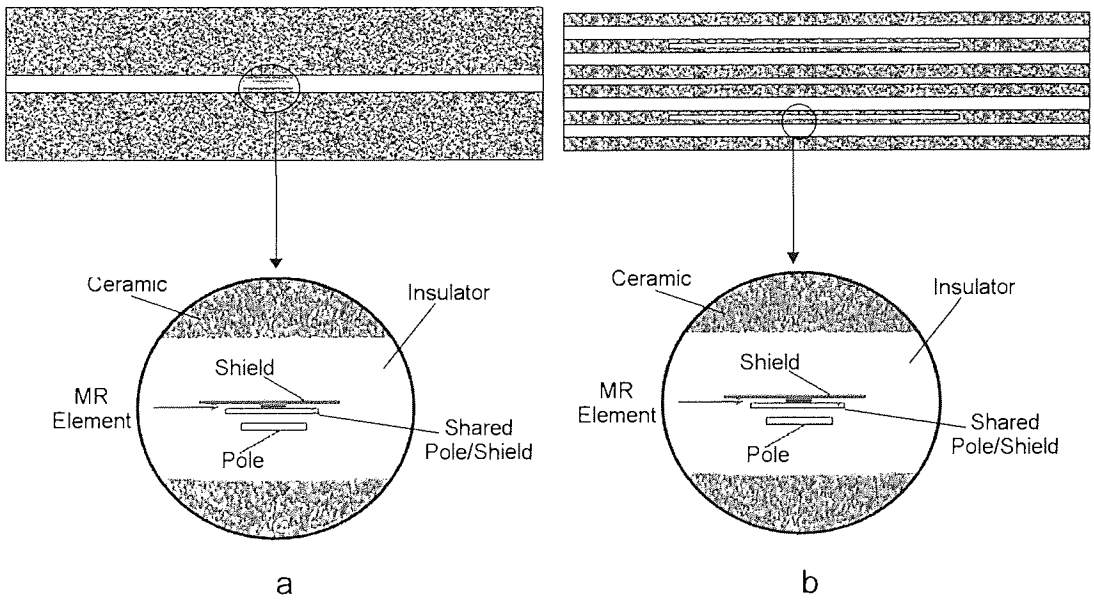

Figure 1-11 (a) Schematic diagram of Travan5 head; (b) schematic diagram of two rails and enlarged, one channel of a LTO head

Figure 1-10 and Figure 1-11 show schematic diagrams of the Travan5 head and Linear Tape Open (LTO) heads used in this research project. In both heads, the pole, shared pole/shield and shield are cobalt-zirconium-tantalum (CoZrTa) amorphous films, the insulator is sputtered Al_2O_3 and ceramic tape bearing surface is AlTiC (Al_2O_3-TiC). The magneto resistive (MR) element (reader sensor) is permalloy (Ni-Fe). The width of thin film region is around 50μm for both systems. The LTO head adopts multi-channel and slot technology[46], the LTO head has 16 channels on the two rails (see Figure 1-10 and Figure 1-11).

Modified Travan5 drives were used in this research project, Travan5 head is a thin film head, the Travan5 tape is a double layer Metal Particle tape, after connecting the drive to the power supply (5V, DC), inserting the tape, the drive automatically starts to cycling. During the tape cycling procedure, the tape is in constant contact with the Travan5 head, this causes the wear of the Travan5 head and Travan5 tape. A photo detector in the drive could sense the end of the tape (at end of tape, there is a hole inside the tape). Then the drive stops, the head move to a new position and a new cycling begins in the opposite direction until the power was turned off. The cycling time and speed and tape tension could be set before experiments start.

Linear Tape-Open (LTO) uses a linear multi-channel technology. The LTO single-reel cartridge design uses a take-up reel that is located inside the drive. The double layer LTO MP tape is engaged by means of a coupler that "grabs" a leader pin at the start of the tape and guides it around the LTO head to the take-up reel in the drive. After the leader pin is secured in the take-up reel, the reel rotates and pulls the tape through the tape path. Communication with the LTO drives and computer was established using a macro computer language named Dexter (developed by Hewlett Packard to control the tape drive operation). LTO drives use the standard computer power supply (5V, DC). The detail description of the Travan5 and LTO system could be seen in Chapter Two.

1.3 Tribology Literature Review

Tribology is the studying of the wear that occur between the moving parts of any two materials, tribology deals with the interaction of two relatively moving surfaces within a given environment.

1.3.1 Basic Mechanisms of Wear

Wear [20] is a process of removal of materials from one or both of two solid surfaces in solid-state contact. It occurs when solid surfaces are in sliding or rolling motion relative to each other. In well-designed tribological systems, the removal of material is usually a very slow process; details of different wear mechanisms are introduced below.

1.3.1.1 Adhesive Wear

Adhesive wear occurs when two nominally flat solid bodies are in rubbing contact, whether lubricated or not. Adhesion (or bonding) occurs at the asperity contacts on the interface, and fragments are pull off one surface to adhere to the other. Subsequently, these fragments may come off the surface on which they are formed and be transferred back to the original surface, or else form loose wear particles.

The interfacial adhesive junctions that form if solid materials are in contact on an atomic scale initiate adhesive wear processes. As a normal load is applied, local pressure at the asperities becomes extremely high. In some cases, the yield stress is exceeded, and the asperities deform plastically until the real area of contact has increased sufficiently to support the applied load. In the absence of surface films, the surfaces would adhere together, but very small amounts of contaminants minimize or even prevent adhesion under purely normal loading. However, relative tangential motion at the interface acts to disperse the contaminant films at the point of contact, and cold welding of the junctions can take place. Continued sliding causes the junctions to be sheared and new junctions to be formed. The chain of events that leads to the generation of wear particles includes adhesion and fracture of the mating surfaces.

For plastic contacts, it is possible to write the laws of adhesive worn volume commonly referred to as Archard's law[47] as follows:

$$V = \frac{kWx}{H} \qquad \text{Equation 1-9}$$

Where V is the volume worn away, W is the normal load, x is the sliding distance, H is the hardness of the surface being worn away, and k is a non-dimensional wear coefficient dependent on the materials in contact and their exact degree of cleanliness.

For elastic contacts which occur in materials with a low modulus of elasticity and a very low surface roughness (prevalent in magnetic media) the laws of adhesive wear[48]:

$$V = \frac{k'Wx}{E_c(\sqrt{\sigma_p / R_p})} \qquad \text{Equation 1-10}$$

Where E_c is the composite modulus of elasticity, σ_p and $1/R_p$ are the composite standard deviation and composite mean curvature of the summits of the mating surface, and k' is a non-dimensional wear coefficient.

The head stains or tape debris is typical adhesive wear in the head tape system. The stains or tape debris will contribute to the spacing loss at the head-tape interface. It must be noted that repeated stress cycling within elastic contacts may also lead to wear via fatigue, after which the wear debris may adhere to either of the mating surfaces.

1.3.1.2 Abrasive Wear

Abrasive wear occurs when a rough, hard surface slides on a softer surface and ploughs a series of grooves in it. The surface can be ploughed (plastically deformed) without removal of material. However, after the surface has been ploughed several times, material removal can occur by a low-cycle fatigue mechanism.

Abrasive wear may be described as damage to a surface by a harder material. It is also sometimes called scratching, scoring, or gouging depending on the degree of severity. There are two general situations in which this type of wear occurs. In the first case, the

hard surface is the harder of two rubbing surfaces (two-body abrasion), e.g., in mechanical operation such as grinding, cutting, and machining. In the second case, the hard surface is a third body, generally a small particle of grit or abrasive, caught between the two other surface and sufficiently harder than they are to abrade either one or both of them (three-body abrasion).

In many cases, the wear mechanism at the start is adhesive, which generates wear debris that gets trapped at the interface, resulting in a three-body abrasive wear. Rabinowicz[49] derived a simple quantitative expression for abrasive wear. It assumes conical asperities cutting through a flat soft surface (see Figure 1-12), and is given in following equation:

$$V = \frac{kWx\overline{\tan\theta}}{H} \qquad \text{Equation 1-11}$$

Where $\overline{\tan\theta}$ is a weighted average of the tanθ values of all the individual cones and k is a factor that includes the geometry of the asperities and the probability that a given asperity cuts (removes) rather than ploughs. Thus, the roughness effect on the volume of wear is very distinct.

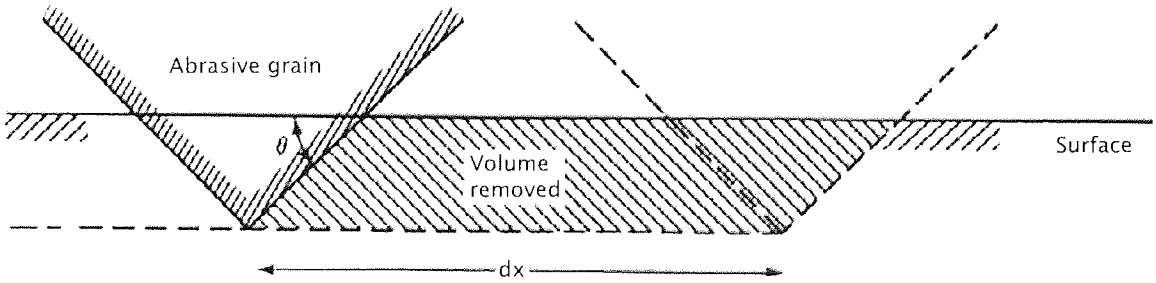

Figure 1-12 Abrasive wear model in which a cone removes material from a surface

Sullivan[27] stated that plastic deformation and hence abrasive wear can only occur in polymers if the opposing hard surface is very rough. For the very smooth tape head system, two body abrasive wear should not occur, the three-body abrasive wear is the major abrasive wear in tape head system.

1.3.1.3 Fatigue Wear

When two solids are in sliding contact[10], the maximum stress occurs not at the asperity junction, but below this surface[50, 51]. Hence for repeated contact the fatigue cracks will eventually appear, this leads to the initiation of sub-surface fatigue cracks that grow to the surface and produce delaminative removal of particles. This delaminative particles removal process is analogous to that described by Suh[52] for metal. Fatigue wear mechanism relied on the growth of surface or subsurface crack. These cracks elongate and propagate until the surface eventually breaks up, pullouts were created and large pits were left in the surfaces. The fatigue failure requires a given number of stresses cycles and often predominates after a component has been in service for a long period of time[53].

Fatigue wear not only depends on the cycling conditions on the component, but also on the previous history of the component: the presence of subsurface cracks, and the presence of voids, porosity, dislocations, grain boundaries and residual stress at the surface and subsurface. Crack propagation can also be initiated and propagated by chemical action.

1.3.1.4 Impact Wear

Impact wear is governed by the transfer of kinetic energy from the impinging particle to the mode of wear occurring within the material. The impact wear rate increases with increasing kinetic energy of the incoming particle stream, and shows an angular dependence that is different between ductile and brittle materials.

1.3.1.5 Corrosive Wear

The wear due to adhesion, abrasion, and fatigue can be explained in terms of stress interactions and deformation properties of the mating surfaces, but in corrosive wear, the dynamic interaction between environment and mating material surfaces plays a significant role[53]. This interaction gives rise to a cyclic stepwise process: In the first step, the contacting surfaces react with environment, and reaction products are formed

on the surface. In the second step, attrition of the reaction products occurs as a result of crack formation and/or abrasion in the contact interactions of the materials.

In any corrosive wear regime the exact mechanism is going to be governed by the relative rates of the tribochemical process that result in tribochemical film formation and mechanical processes leading to the wear of all components of the system. For one example of corrosive wear, the oxidation wear, these processes include the formation of the oxide film, the cyclic delamination of the oxide film, removal of the oxide then the fresh surface re-oxidation. Oxidation is not the only form of corrosive wear. Sullivan[10] reported that water vapour could produce hydrolysis and chain scission in the tape polymer and hydroxide formation on ceramic, glasses, ferrite and metals.

1.3.2 Basic Mechanisms of Friction

Friction is the resistance to motion that is experienced whenever one solid body slides over another. The resistive force F, which is parallel to the direction of motion, is called the friction force. If the solid bodies are loaded together and a tangential force (F) is applied, then the value of the tangential force that is required to initiate sliding is the static friction force (F_{static}). It may take a few milliseconds before sliding is initiated at the interface. The tangential force required maintaining sliding is the kinetic (or dynamic) friction force ($F_{kinetic}$); it is sometimes also called drag force. Kinetic friction is either lower than or equal to the static friction.

The friction force could be expressed as below. It states that the force required to initiate or sustain sliding F_t is proportional to F_N, the normal force. Thus

$$F_t = \mu F_N \qquad \text{Equation 1-12}$$

μ is the coefficient of friction.

In the magnetic recording system, static friction, the force required to initiate motions is generally higher than dynamic friction that required maintaining it[27]. The friction between sliding surfaces is due to the various combined effects of adhesion between the

flat surfaces, ploughing by wear particles and hard surface asperity, and asperity deformation. The relative contribution of these components depends on the specific material used, the surface topography, the conditions of sliding interface, and the environment.

Dynamic friction in the magnetic recording system[27] can be expressed as followed:

$$F \approx \tau A_r \qquad \text{Equation 1-13}$$

τ-Interfacial shear stress and is not constant, which is temperature and pressure dependent.
A_r is Real area of contact.

With particulate media, a fatty acid/fatty acid ester tape lubricant is normally incorporated into the bulk of the magnetic coating. The coating acts as a reservoir to preserve and replenish the surface lubricant film about 2 or 3 molecular layers thick, and coverage as low as 10%. Taking into account the presence of the lubricant, the frictional force can be written as[27]:

$$F = A_r[\tau(1-\alpha) + \tau_1\alpha] \qquad \text{Equation 1-14}$$

τ_1-Shear stress in the lubricant and α the fractional areal coverage of the lubricant.

Friction is an important parameter in the design of magnetic recording system; friction that is too high can cause speed variations or failure of drive motors and can lead to high surface temperature[10, 27]. In the same way, the higher friction can lead to the higher wear of the tapes and heads.

1.3.3 Various material properties affect the wear and friction

The microstructure of a material has an important role in physical properties, e.g., elastic modulus, hardness and toughness, chemical properties, which in turn affect the friction and wear properties

The rigidity of a solid arises because of inter-atomic bonds which hold the atoms in the solid together. There are two types of solid: crystalline and amorphous. Amorphous solids (like pole materials of the head) lack any sort of regular pattern or array of atoms in the solid. In crystalline solids (such as AlTiC), however, there is a regular order or array of the atoms in the solids. Crystalline solids include most metals and alloys as well as inorganic solids, and even some lubricating species such as solid lubricants. The spatial arrangement of atoms in a crystalline solid is strongly influenced by the nature of the inter-atomic bonds, which in turn is influenced by the electronic structure of atoms. Bonding in crystalline solids can be of four types: (a)Van der Waals, (b)Ionic, (c) metallic and (d) covalent.

The Van der Waals bond is the weakest bond holding the solids together.These forces can be represented in bonding the atoms of an inert gas, e.g., argon together when solidified. Van der Waals bonding is frequently encountered in tribological systems with the physisorption of liquid lubricants and gases to a solid surface. Ionic bonding forms between two oppositely charged ions, which are produced by the transfer of electrons from one atom to another. Ionic bonding could be very strong because there is an electron transfer. Typically the bonding of ceramic of AlTiC are ionic bonding which stand very good tribological property. The metallic bonds, sharing of the electrons between the neighbour atoms becomes delocalized. The electrons move freely between the cores of ions allowing for, and contributing to many of the metallic materials properties. The covalent bonding, sharing of electrons between neighboring atoms take place. Neutral atoms appear to be bound together by overlapping their electron distribution.

It is well known that the coefficient of friction depends on intrinsic properties of the mating materials. In the same time the coefficient of friction depends on the operations, load, sliding speed and lubricant. The microstructure of materials decides the material property. Generally speaking, the higher hardness and low surface energy materials will reduce the adhesion at the interface, which in turn affect friction and wear. The high hardness, toughness (The energy absorbed in tearing the material), and high flow strength will resist the subsurface deformation and crack nucleation and growth rate, which reduce the Fatigue wear, in the same time, the harder material is not easy cut by the abrasive cutting agent.

A simple law describing the wear of materials under a wide variety of conditions is the Archard law[27, 47].

$$w = k\frac{W}{H} \qquad \text{Equation 1-15}$$

Where w is the wear rate, the volume of materials removed per unit distance of sliding, W the applied load, H is hardness and k is a constant of proportionality sometimes known as the wear coefficient.

1.3.4 Surface topography and roughness definition and effects on wear

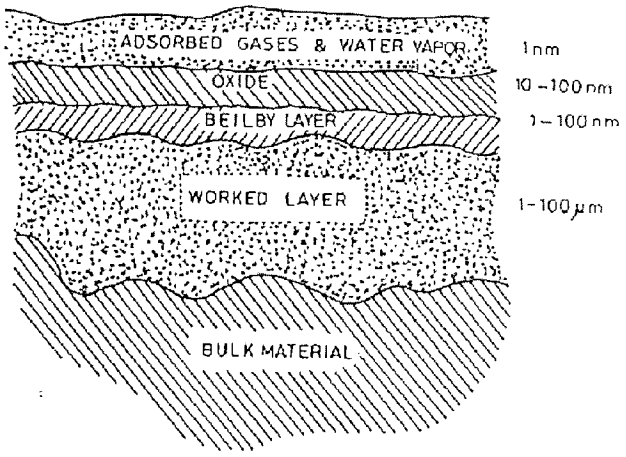

Figure 1-13 Schematic representation of a metal surface[53]

The tribological behaviour of a solid surface is directly influenced by its chemical and physical state. Understanding the surface property is very important for the studying of wear and friction. As an illumination, Figure 1-13 shows a schematic of a typical metal surface. At the base of surface layer, there is a zone of work-hardened materials on the top of which is a region of amorphous or microcrystalline structure, this is the so-called Beilby layer, which results of melting and surface flow during machining of molecular layers that are subsequently hardened by quenching. On the top of the Beilby layer is an oxide layer, the formation of which depends on the environment, on the top of the oxide layer, the whole multi-zone stack of surface contains a layer of adsorbate, which is generally water vapour or hydrocarbons from the environment that may have condensed and become physically or chemically adsorbed to the surface.

The physical adsorption process is a relatively weak process. However, a very small amount of energy is required to remove the physisorbed atoms, this process typically involves Van der Waals forces. It is observed that, if the interaction involves less than 10 kilocalories per mole material, the process is one of physisorption. If, however, the energy involves is in excess of 10 kilocalories per mole material, the adsorption may be due to chemisorption[20]. Clean surfaces are extremely active chemically. Chemisorption is a much stronger bonding than that associated with physisorption. The higher the surface energy of the solid surface, the stronger the tendency to chemisorb. All these surface and subsurface layers have to be taken into consideration in tribological interaction.

Surface topography and roughness are extremely important in the sliding of the tribology of surfaces in contact. The roughness parameter is usually used to describe the smoothness of the surface or the whole surface area. The micro-roughness[54] is most commonly measured along a single line profile and is usually characterized by one of the statistical height descriptors. If considering a profile, z(x) in which profile heights are measured from a reference line. a centre line or mean line is defined as the line such that the area between the profile and the mean line that is above the line is equal to that below the mean line (see Figure 1-14).

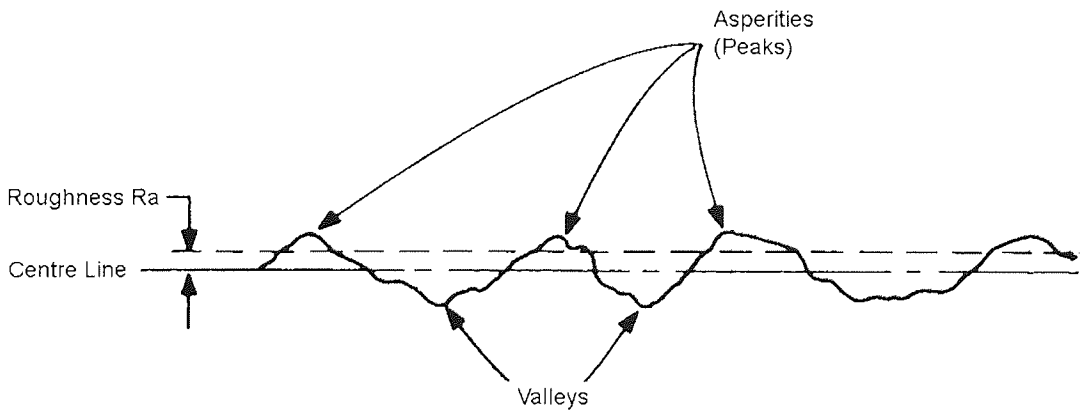

Figure 1-14 Sketch of surface roughness

$$\overline{Z} = \frac{1}{N}\sum_{i=1}^{N} Z_i \qquad \text{Mean Value} \qquad \text{Equation 1-16}$$

The definition of the mean Z value is shown above. The average roughness is given by the average deviation of the data from the average of the data. For a line containing N data points, the average roughness is determined using the standard definition (see below).

$$R_a = \frac{1}{N}\sum_{i=1}^{N} | Z_i - \bar{Z} | \qquad \text{Average Roughness} \qquad \text{Equation 1-17}$$

For a line containing N data points, the RMS roughness (root-mean-squared roughness) is given by the standard deviation of the data, determined using the standard definition:

$$R_{rms} = \sqrt{\frac{\sum_{i=1}^{N} (Z_i - \bar{Z})^2}{N-1}} \qquad \text{RMS roughness} \qquad \text{Equation 1-18}$$

Since R_{rms} contains squared term, large deviations from the average Z height are weighted more heavily than they are in the calculation of R_a. For the same reason, small deviations are given less weight in the calculation of R_{rms} than R_a.

There are some other parameters that are used in the measurement of the surface roughness as well. Three extreme value descriptor[20, 55] , R_t (or R_y, R_{max}, or P-V), R_p, and R_z are defined as follows: they are defined as the vertical distance between:

R_t (R_y, R_{max}, or P-V): the highest asperity (peak) and the lowest valley;
R_p: the highest asperity and the mean line;
R_z: the averages of five highest asperities and the five lowest valleys;

In most tribological applications, heights of highest asperities above the mean line are an important parameter because damage of an interface may be done by the few high asperities present on one of the two surfaces.

Mechanical stylus method, optical methods, Atomic Force Microscopy (AFM) and other devices can achieve the measurement of surface roughness[53]. In this research work, the topography of the sample surface was obtained by AFM.

From a wear standpoint, a surface should be relatively smooth because rougher surfaces lead to high rates of abrasive wear of the mating surfaces. The adhesive force due to meniscus effects increases for a smoother surface. Furthermore, in smooth surfaces, adhesive forces may be high due to micro capillary. Therefore, stiction increases with a decrease in surface roughness and this effect is expected to be more pronounced at higher humidity. Therefore, an optimisation in surface roughness is essential for the system. This needs a combination of good design, lower contact pressure, and harder materials.

For head tape system, the friction is largely determined by the properties of the magnetic layer, thus a high hardness, high complex modulus material should be used to reduce friction, however, due to the need for mechanical durability and to reduce spacing losses between the head and tape to a minimum, the surface needs to be as smooth as possible.

1.3.5 Contact between head and tape

When two nominally flat surfaces are placed in contact, surface roughness causes contact to occur at discrete contact spots. The sum of the areas of all the contact spots constitutes the real area of contact. Deformation occurs in the region of contact spots, establishing stresses that oppose the applied load. The mode of surface deformation is either elastic or plastic and depends on nominal stress.

A solid block of material can suffer several kinds of deformation, depending on how the force is applied. If one end of the body is held fixed and the force pulls on the other end, the deformation is a simple elongation of the body. If one side of the body is held fixed and the force pushes tangentially, along the other side, then the deformation is a shear. If the force is applied from all sides simultaneously, the deformation is a compression of the volume of the body.

Any force or distribution of forces that acts upon a body and is balanced by equal and opposite forces in the body is termed a stress, although the term is more particularly applied to the force per unit area on the body. The change in a particular dimension per unit dimension produced by the stress is called a strain. The deformation is elastic,

provided that the force and the deformation remain within some limit, which means that the body returns to its original shape once the force ceases to act. The ratio of stress to strain is a constant and is known as the modulus of elasticity of the substance.

In the case of magnetic media, Bhushan found that the assumption of peak heights having a Gaussian distribution is valid and the assumption of peak radii being constant is only approximate. At the magnetic media/head interface, the tape is in moving contact with a hard (ceramic/glass/ferrite) surface. The real contact areas depend on the physical properties of the surface. When contact occurs, the asperities may deform either plastically or elastically[10,27] depending on the materials properties, nominal load and the surface roughness. Bhushan[56] adapted the work of Greenwood and Williamson[57] and defined a plasticity index Ψ when two rougher surface contacted:

$$\psi = \frac{E_c}{Y}\left(\frac{\sigma}{R_p}\right)^{1/2} \qquad \text{Equation 1-19}$$

Where E_c is the composite modulus, given by[20]

$$\frac{1}{E_c} = \frac{(1-\nu_1^{\,2})}{E_1} + \frac{(1-\nu_2^{\,2})}{E_2} \qquad \text{Equation 1-20}$$

Where E_1, E_2, and ν_1, ν_2 are the Young's moduli of elasticity and Posson's ratio of the two contact materials, respectively. Posson's ratio is the lateral contraction per unit breadth divided by the longitudinal extension per unit length in elastic stretching or compression. Y is the tensile yield stress, σ the standard deviation or asperity heights and R_p is the equivalent rough surface mean radius of those asperity peaks. The R_{p1} and R_{p2} is the asperity radius of the two rough surfaces, respectively.

$$\frac{1}{R_p} = \frac{1}{R_{p1}} + \frac{1}{R_{p2}} \qquad \text{Equation 1-21}$$

$$\sigma = (\sigma_{p1}^2 + \sigma_{p2}^2)^{1/2} \qquad \text{Equation 1-22}$$

Here the σ_{p1} and σ_{p2} are the two rough surfaces standard deviations respectively.

If $\psi<1.8$ the contact is elastic and if $\psi>2.6$ the contact is plastic. Bhushan[58] and Bhushan, Doerner[59] found that typical head media contacts are elastic by insertion of measured value into the above equations and the dominant wear mechanism at media and head is due to fatigue[58, 60].

Typically head tape contact as described were elastic, the ratio of real area to the apparent area of the contact as follows[61, 62]:

$$A_r = 3.2\frac{W}{\psi Y} \qquad \text{Equation 1-23}$$

W-the applied load
Y-Tensile yield strength of the polymer
ψ-Plasticity index.

To minimize friction and wear in a machine, the fraction of real area of contact to apparent contact should be as low as possible; the study[20] shows that the plastic contact results in a minimum contact area. However, wear is more probable when asperities touch plastically than in pure elastic contact[20], the plastic contact would lead to undesirable permanent deformation, therefore it is desirable to design machine components in the elastic-contact regime with $\psi\sim1.8$ close to the elastic contact limit or $E_c(\sigma_p/R_p)^{1/2}$ to be as high as possible. The asperities with high E_c and low R_p produce high contact stresses and result in lower A_r for a given load, in addition, high σ_p allows contact with fewer asperities and again produces high contact stresses and results in low A_r for a given load[20].

Ideally the mean real pressure is just below the yield strength of the softer materials[20], for the mechanical durability and magnetic considerations, the low value of real area of contact should be obtained as much as possible from a higher value of E_c rather than from a rougher surface.

1.3.6 Tribology of head tape system

The areal data storage density of magnetic disk hard drives (HD) is currently increasing at a rate of 120 % per annum and it is predicted that 1 Tb/in^2 will be achieved before the super-paramagnetic limit is reached. Today, the best linear tape systems have data densities of less than 200 Mb/in^2, whereas, to remain competitive, densities of greater 2 Gb/in^2 must be attained in the next few years. In spite of various measures taken by the industry, these densities can only be attained by minimising physical spacing between media and sensors (pole tips) and reducing the wear of the head and tape. Although tape is the cheapest and most efficient method of storing large amounts of data, systems will not survive if data densities can not be substantially increased.

High-density, high-data rate magnetic recording requires a high relative speed between the tape and the head; the tape should remain in close and stable proximity to the recording head for reliable recording. The performance of the head-to-tape interface is a function of the shape or contour of the head and how the tape wraps onto the head[46]. The magnetic head has a contour that maintains a constant, low head-to-tape spacing throughout the tape tension range, especially at low tension.

It is well known that wear increases with an increase in the normal load[63, 64, 65], the wear rate is inversely proportional to the material hardness[63]. Contact pressure depends on the head load and the contact area, which is determined by head contour, and tape tension and tape stiffness. The stiffness of a magnetic tape can be directly related to the head wear[65, 66], the stiffer tapes do not conform to the head and therefore contact the head at discrete contact points which can lead to increased wear[66]. Some studies have also shown that the relative amount of headwear tends to be higher at the edges of the head when compared to the centre[65]. Hahn[67] reported that headwear might be reduced by effectively increasing the contact area by increasing the longitudinal radius. Mechanisms of head wear for the particulate tapes were dominated by adhesive and abrasion, whereas with ME tape it was adhesive[65].

The contact is almost entirely elastic for MP media[58,68, 69] and elastic/plastic for metal evaporated media as mentioned before. The adhesive wear, abrasive wear, fatigue and chemical wear are involved in the head tape system. There are two forms of abrasive wear (two-body and three body-abrasion), but due to the very smooth surface, two body abrasive wear does not occur[27].

Sullivan[10] stated forces between head and media are largely adhesive and these forces lead to transfer film and debris particle formation. For polymer/metal contacts covalent bonding occurs and for polymer/ceramic contact, ion-dipole bonds are formed[10, 70]. Introducing a boundary lubricant between the opposing surfaces and in this case by reducing the polar molecule content of the binder can reduce adhesive wear. Sullivan and Sharma[71] found lifetimes reduced by two orders of magnitude in the media without lubricant.

For head and media interactions the major corrosive elements are supplied by the atmosphere: oxygen can produce oxidative degeneration of the polymer surface and oxidation of elements of the head; and water vapour can produce hydrolysis and chain scission in the polymer and hydroxide formation on ceramic and metals. Water vapour is a major cause for concern in head/media interactions, where high humidity can result in high friction, stiction and high wear[20].

For the current thin film head, insulator and pole materials wear at a higher rate than air bearing ceramic (resulting in recession)[9]. These results suggest that wear is primarily governed by the difference in hardness between thin-film insulator, poles and the hard ceramic part of the head, insulator and pole materials wear at a higher rate primarily because they are softer.

William and Bhushan[72] adopted the Archard wear law[47], assuming that wear occurs uniformly over the head substrate. Scott and Bhushan[72] suggested a model for the Pole Tip recession of magnetic head, the wear mode for the head poles material is assumed to be three-body abrasive wear as Sullivan[10] indicated before, the wear mode for the head substrate material is assumed to be a combination of adhesive and abrasive wear[72]. Sullivan[27] and Bhushan[48] found that this is true for heads sliding against MP tape[73].

Pole tip recession and stains[48, 74] are major problems in thin film recording heads. PTR causes signal degradation as a result of spacing loss and can be minimized by matching as closely as possible the mechanical properties of the magnetic poles and insulating

layers to the harder ceramic substrate material. The detail of PTR and stains will be discussed below.

1.3.6.1 Pole Tip Recession

Pole tip recession, or PTR, is defined as the height difference between the air bearing surface, or ABS (ceramic substrate), and the pole tips. Figure 1-15 shows the definition of Pole Tip Recession. This height difference is a result of differential wear rates of the head materials[75]. PTR is influenced not only by the pole tip mechanical properties, but also by the mechanical properties of other materials in the head structure.

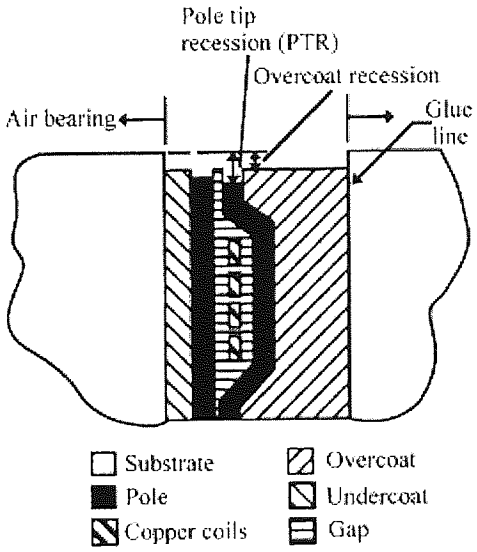

Figure 1-15 Pole Tip Recession[75]

This spacing (d) between the head and magnetic media result in an electrical signal loss $V(d)$ which is related to the spacing (d) by the Wallace equation[6]: $V(d) = e^{-2\pi d/\lambda}$, where λ is the recording wavelength. At current wavelengths 0.7μm every 10nm increase in d leads to 0.8dB of output loss and this will become significantly worse as wavelengths decrease. An output loss exceeding 6dB is typically considered as failure[7, 8].

Usually the majority of the tape-bearing surface is formed by a mechanically hard ceramic. The magnetic pole pieces are different in structure but share a common material set including similar magnetic thin films and spacers such as Al_2O_3 and SiO_2.

If dissimilar materials are at about the same level of recession, the material with poorer mechanical properties (determined primarily by both the hardness and scratch resistance) will wear and become more recessed from Air Bearing Surface[9]. However, at some point wear of this material will be reduced as a result of less severe low contact pressure interaction with tape asperities and loose debris being raking across the thin film region by the tape. The less recessed material with superior mechanical properties will now wear due to its more intimate (higher-pressure) interactions with tape asperities and loose debris being raked across the thin film region by the tape. When the materials approach a similar recession value, the cycle will begin again and the cyclic behaviour will continue until both materials approach a saturated value of recession. PTR for a given interface condition reaches a steady value after several hundred kilometres of sliding.

There are several ways to measure PTR[76], Such as stylus profilometry, optical profilometry and atomic force microscopy. Atomic Force Microscope (AFM) capable of determining accurate PTR values is limited by its speed of operation, Optical interferometers on the other hand can provide PTR measurement with high throughout. The optical PTR values are limited in resolution by the phase difference between the dissimilar substrate and pole materials[76].

Scott and Bhushan[75]used the follow methods to process the raw image of AFM. First, a zero-order flatten is applied, the flatten operation is used to eliminate bow in the slow scan direction (caused by physical bow in the instrument itself). The fast scanning direction is the tip scanning usually from left to the right. So subtracting the same value from each point on the line does not result in any difference in height between any two points on that line. Therefore, this operation cannot cause any change in the PTR measurement. Next, a first-order plane-fit is applied in the fast scan direction; the plane-fit operation is used to eliminate bow and slope in the fast scan direction. Finally the average height from the ceramic to the pole will decide the value of the PTR.

Bhushan[75] showed that no strong conclusion might be drawn about the effect of tape speed on PTR, but an increase in tape tension leads to an increase in PTR and also an increase in interface contamination also leads to an increase in PTR; the materials near the centre of the thin-film region wear faster than those near the side.

Sullivan[77] indicated that PTR is more prevalent at high humidity due to two effects. (1) Ceramic wears increased with more water content present on the interface of head and tapes. (2) Stains are not formed under higher water content condition, head stains protect the surface under low water content conditions, stains on the poles acts as a protective thin film, reducing the effect of abrasion and hence resulting in a reduction of PTR.

1.3.6.2 Head Stains

Magnetic recording head stain is defined as a build up of material on a recording head that is not easily removed by, for example, wiping with a common solvent. These deposits are not the same as common, readily removable tape debris. Stains are generally insoluble in most common solvents and require abrasive cleaning tapes for removal. Stains on the surface of head are undesirable as it introduces a spacing loss between the tape and head that causes the signal loss during the magnetic head reading and writing procedure.

The stains may contain organic or inorganic materials. Organic stains are frequently termed friction polymer. If the organic deposit results from (1) a chemical reaction (or repolymerization) of solid, liquid, or vapours and/or (2) fragmentation of polymers, these are called " friction polymers" or tribopolymers, a form of stains[78]. The inorganic stains are what usually called conventional stains; basically major compositions are the iron particles or iron oxide transferred from the tape.

The first published reference to stains was in a paper on ferrite head by Lemke[79], the stains he observed were typical brown in colour and formed on both metal and ferrite head materials.

However, stain has beneficial wear resistant and lubricating effects[10, 27]. Stain build-up corresponds to a drop in friction, suggesting that stain provides lubrication[80]. It is common to most types of head materials. The conventional stains are typically inorganic in composition. This is generally thought to be due to stain being in dynamic equilibrium. Sullivan[10, 27, 81] showed that in general there is little evidence for chemical

interaction and layer consists essentially of magnetic pigment from the media and thickness and substrate determine stain colour. However, stain can protect the poles from wearing[82], as long as stain is covering the head surface, only stain is removed instead of head materials. If the stain becomes too thick, an entire region of stain can be removed, resulting in excessive wear[83].

Prabhakaran [84] used commercial video cassette recorders (VCR) operated in the record mode, the magnetic core was made of Manganese Zine ferrite and using standard γ-Fe_2O_3 tape for wear test. They found that wear rate was significantly lower at RH 12% than at RH 60%, however deposits were found to form on both the glass and ferrite regions in all humidity ranges (25°C, 2%RH, 22%RH, 60% RH), The maximum deposit formation occurred for tests at low humidity. They found that the stains in the glass regions is not continuous but in the form of 'islands' consisting of aggregates of Fe and organic material.

Ajayi [85] discussed the dependence of deposit formation on relative humidity. They found that at low humidity the wear debris aggregate and tend strongly to the head surface resulting in stain formation. The absence of stain at high humidity could be attributed to the fact that water vapour at the head tape interface helps in separating the head surface from debris and hence reducing the Van der Waals attraction.

Bhushan[82] wrote a review about the head stains. Stains of the head surface vary from spotty to continuous with thickness ranging from 10-30nm. Stain normally only forms at low humidity – below 30-45% R.H.

Hempstock, Wild and Sullivan [86] found that higher interface temperatures might encourage the formation and growth of stains. They found more extensive deposits were observed on the left structure of the head because the MR element was active and thus greater heating consequently occurred at the head-tape interface during cycling.

Sullivan[77] states that the common features of stain production for all tapes and heads are as follows: (1) Conventional stain is not produced at high humidity. (2) The thickness of the stain is constant and is related to the magnetic pigment size and corresponds to one

particle thickness. Thickness of the films was in the range 20–30 nm, depending on tape type. (3) The stain forms a lumpy deposit in the initial stages and in general the areal coverage increased with number of passes. (4) The formation is a dynamic process. (5) Stain formation on the poles is influenced whether the pole is energised or not; it is much greater on the energised pole, an obvious temperature effect. (6) Stain does not form on the Al_2O_3 insulator and only forms preferentially on the poles and on the TiC phase in the ceramic.

A suggested theory of stain formation is that organic materials chemically bond to the head followed by a build up of oxidised material. Sullivan[10, 27] found an inverse relationship between stain formation and water vapour pressure. The initial head media contact is between the various component materials of the head and polymer surface of media. The adhesive forces at this contact may be either physical, involving Van der Waal bonds[87], or chemical involving electrostatic, ionic or covalent. Van der Waal forces will exist between the media and head and the calculations of typical bond strengths[88]show that their contributions could be significant. For polymer/metal contacts covalent bonding occurs[89] and for polymer/ceramic[90] contact, ion-dipole bonds are formed. Each of these bond types will give strong adhesive junctions.

The stain is due to the adhesive force between the head and outer polymer layer of the tape being greater than the cohesive forces within the polymeric binder under certain circumstances. This leads to dynamic formation of the transfer film that attains and maintains constant critical thickness. Strong chemical bonding[77] occur between metals and polymers and preferentially at polymer/TiC contacts. This junction is probably greater than the cohesive force between magnetic pigment and resin binder. Thus, an adhesive junction is formed at the polymer/ceramic, polymer/metal interfaces.

Staining starts as small spots and then grows into patches or continuous film. Stains only formed in the low humidity condition[82, 91]. In most normal environments, staining with chromium dioxide tapes is less common. The relatively high abrasive of chromium dioxide particles-certainly much higher than iron oxide particle tapes can explain this[82]. The main way in which stain may be controlled with particulate media is to include a

head-cleaning agent (HCA) – hard particles such as Al_2O_3 included in the binder system.

1.3.7 Head Wear

1.3.7.1 Ceramic Wear in the Magnetic Heads

Ceramics in general have high hardness, low adhesion to contacting surface and are chemically inert in a wide range of environment. Furthermore, they retain these properties over a much wider temperature range than metals. In view of these unique properties, ceramics are found to have low friction and wear under a wide range of sliding contact conditions[92].

Materials used for construction of head ceramic should be hard, wear resistant, and easy to machine, thermally conductive and electrically resistive. Non-magnetic Al_2O_3-TiC (70-30% by weight), polycrystalline and single-crystal Mn-Zn ferrite and calcium titanate materials are almost exclusively used in the construction of the Air-bearing Surface (ABS) of heads[93]. There are many studies on the wear characteristics of the constituent materials of the heads, the generally wear resistance of AlTiC is the best in the applied ceramic materials so far, the wear rate of the materials depends on the tape used[94] and the environment[20] and contact pressure.

Bhushan and Lowry[65] developed a wear measurement technique to measure the wear of various head materials sliding against different magnetic tapes in a linear mode; a nano-scratch array was produces in the centre of the head sample surface using a commercial nano indenter. Using an atomic force microscope, scratch depths were measured before and after running against magnetic tapes as a direct measure of wear on the head surface. They found that mechanisms of head wear for the particulate tapes were dominated by abrasion, whereas with ME tape it was adhesive. In all tests significant edge wear was observed. The relative wear rates of the various head materials were inversely related to their hardness.

Sullivan[10, 27] states that the contact between media and heads is complex, is largely elastic in nature and it has been shown that adhesive contacts and fatigue play major

roles in both head materials and media wear, but that other mechanisms such as abrasion and erosion must not be neglected. For the sintered ceramic, if the grain size is small, water under hydrostatic pressure can enhance crack formation and propagation in the ceramic surface. This led to increased rates of removal of the surface due to micro-fatigue that enhances polishing wear. For high wear of ceramic heads at high humidity is believed to be moisture-assisted fracture or static fatigue[20].

Evans and Marshall[95] indicate that wear of brittle materials (ceramics) at low loads (below the threshold loads needed to cause propagation of lateral cracks) involves plastic cutting. Hsu and Shen[96] have found that, in some ceramics, low loads result in wear by micro-abrasion rather than by brittle fracture.

The tribological behaviour of ceramic is significantly influenced by humidity[97, 98]. For alumina ceramics, the reduction of friction coefficient was attributed to the formation of a hydroxide on friction surface due to a tribochemical reaction[97,99]. The hydroxide is soft and has low shear strength that results in a low friction coefficient[100].

For the thin film magnetic head, that titanium element appears on the worn head pole region after cycling against tapes were found by Sullivan[77], Sourty and Sullivan[101, 102, 103]. The hard three-body abrasive particles that are swept across the pole region, preferentially wearing the softer poles. Three-body abrasive wear modes for PTR are also proposed for tape heads and disk heads by Harrison, Sullivan[104] and Xu and Bhushan[105]. Tsuchiya and Bhushan[106] gave a three-body wear mode for the thin film magnetic head; they suggested that three-body abrasion must be the wear mode for PTR because tape asperities were not able to reach the recessed thin-film surface of the head to a significant extent.

Zhang[107] found TiC of AlTiC sliders that were DLC-coated or uncoated were easily decomposed in slider/disk drag test. Zhang[108] also studied the oxidation of TiC of AlTiC, found that carbon diffusion was also accompanied by titanium oxidation at about 400°C in the air. The density of TiC is $4.9\times10^3 kg/m^3$ and the density of TiO_2 is $4.0\times10^3 kg/m^3$. The volume of TiO_2 is bigger than the TiC volume after TiC oxidation.

However the mechanism of the generation of three-body particles in head tape system was not fully understood.

1.3.7.2 Pole Material Wear in the Magnetic Head

There are several kinds of pole materials used in the magnetic recording heads (see table1-1). Sundust (FeAlSi), a magnetic alloy that exhibits low coercivity, high resistivity, and high permeability at low frequencies, has a somewhat higher saturation magnetization than ferrite. However, because of high processing temperatures, Sendust is more suited for MIG (Metal in Gap) write heads than full thin-film write heads. Permalloy (NiFe) has a high permeability, a low coercivity, and a low magnetostriction. Its saturation magnetization is comparable to that of Sendust. Permalloy's low resistivity, however, limits the usefulness of materials to low-frequency applications.

Amorphous alloys of CoZrTa are now being used in video and other tape heads systems. Its permeability is lower than that of permalloy but it is adequate for use in thin-film write heads. It is suited for high frequency application, especially those involving high-coercivity metal-particle tapes. However, amorphous materials have limited thermal stability.

For the Travan5 heads and LTO heads, the pole and share pole/shield pole are made of CoZrTa, the MR element is made of NiFe, the nano-hardness of NiFe is lower than hardness of CoZrTa, CoZrTa and Al_2O_3 are similar and about one half that of FeAlN materials. The hardness of Al_2O_3-TiC substrate is about four times that of pole CoZrTa materials[109]. Steven and Bhushan[109] found that the better mechanical properties of FeAlN pole material reduced PTR as compared with NiFe and CoZrTa pole materials.

Sullivan[77] stated two-body abrasion was not the important wear mechanism due to the two criteria. One is the calculation of the plasticity index from the Greenwood and Williamson[57] relationship for the head-tape interface by insertion of roughness and elastic parameters for the materials, shows the contact between the head-tape to be almost entirely elastic. Another is considering the ultra-smooth surfaces and the consequently vanishing small asperity included angles calculated from Halliday[110] show

that plastic deformation of the head components surface can not occur. On the basis of these two criteria two-body abrasion hardly occurs at the head-tape interface.

The head pole wear by three-body particles abrasive wear is the major reason for the pole tip recession. These three-body particles produced from the surface of the head ceramic and also possible three-body particles from the HCA in the tape, it is believed[77] that the Al_2O_3 phase of AlTiC wears by a nano-adhesive wear mechanism and as such would not result in the production of three-body abrasive particles from the Al_2O_3 phase ceramic. So the major three-body particles come from the TiC phase of AlTiC. These abrasive wear particles produced during operation and trapped at the interface between the tape and head and cause growth in PTR by three-body abrasion.

PTR is influenced not only by the pole materials mechanical properties, but also by the mechanical properties of other materials in the thin-film structure, as well as the relative recession of the various materials with respect to the Air Bearing Surface (ABS). Insulator materials should be chosen with the highest hardness and scratch resistance to further protect the pole tip and reduce PTR in heads.

1.3.7.3 Temperature and humidity effects on the head Wear

Bhushan and Khatavkar[111] studied the friction and wear behaviour of metallic (mu-metal) and ceramic (Mn-Zn ferrite) head materials sliding against CrO_2 magnetic tape, In the case of Mn-Zn ferrite, friction and wear increased steadily up to 65% RH and then increased catastrophically. The fracture stress of ceramic is known to reduce at high humidity (moisture-assisted fracture or static fatigue). In the case of mu-metal heads, water was believed to act as a lubricant in the mid-RH (relative humidity) range and to mitigate friction and wear. At high humidity, friction and wear increased dramatically and patches of debris were observed at the head gap. This increase is attributed to formation of menisci bridges at asperity contacts resulting in high adhesive friction and increased abrasive wear due to agglomeration of debris.

Sourty and Sullivan[101] found that amongst the conditions at which the heads were tested, the high humidity conditions were found to dramatically alter the pole region and increase the PTR, forming deep and wide grooves.

High wear of ceramic heads at high humidity is believed to be moisture-assisted fracture or static fatigue[20]. Static fatigue results from a stress-dependent chemical reaction between water vapour and the surface of ceramic. The higher temperature increase the materials chemical wear.

The friction or impact of the tape on to the head surface could generate the heat, the tape cycling against the head, numerous asperities contact between the two surface induce high transient temperature flashes of a few hundred degrees over surface of a few μm diameter, within a few ns to a few μs[112, 113, 114]. Bhushan[112] found that if the exposed magnetic particles or alumina particles contact the slider surface, the transient temperature rise could be more than 1000°C in the head disk system. Sullivan[27] studied the contact temperatures and found that the maximum contact temperatures for a particular linear tape system were calculated to be over 130°C. It is well knows that the higher temperature leads to the tape ages[20]. The aged tape did show a substantial increase in an extractable binder of low molecular weight, which resulted in a significant increase in friction and stick. The water vapour can produce hydrolysis and chain scission in the polymer and hydroxide formation on ceramic, glasses, ferrites and metals[27].

Environment plays a significant role in the tribology of the head-tape interface and magnetic tapes. High humidity has been shown to lead to high friction and head wear[115, 116]. Magnetic and tribological performance of the head-tape interface is the best at low temperature and low relative humidity. Increase in both temperature and humidity results in performance degradation.

1.3.8 Protective Coating on the Head Wear

Thin film read-write heads are commonly used for high-density magnetic recording in data processing tape and rigid disk drive. For inductive write heads, the head Pole Tip

Recession and stains are the major problems, potentially all problems of the PTR and stains could be solved by the application of a very thin coating to the recording head. To be viable, the coating should survive 15,000+ hours of continuous running[77].

In order to minimise separation of the head and tape surface and also reduce the wear, several kinds of wear resistant coatings over the entire air-bearing surface have been applied. The substrate temperature during coating deposition has to be kept below Curie temperature of the magnetic pole material and to maintain low residual stress in the coatings; any gap in coverage will increase mechanical weakness in the overcoat and possible failure. A lot of research works have been done in hard disk and disk-head coating comparing tape and tape-head coating, but more research work still underway in order to achieve the projected recording system.

The tribological behaviour of diamond-like carbon coating (DLC)[117, 118] has been studied. DLC film[119] is a metastable form of amorphous carbon containing a significant fraction of sp^3 bonds[119]. Basically Carbon forms a great variety of crystalline and disordered structures[119, 120] because it is able to exist in three hybridisation, sp^3, sp^2 and sp^1. In the sp^3 configuration, as in diamond, a carbon atom's four valence electrons are each assigned to a tetrahedrally directed sp^3 orbital, which makes a strong σ bond to an adjacent atom.

DLC can have a high mechanical hardness, continuous and chemically inert films, high thermal conductivity, with a surface roughness below 1nm. DLC is smooth because it is amorphous and has a low surface energy[3]. Thin DLC coatings reproduce substrate topography, not requiring any post-finishing. The friction coefficient of DLC film is extremely low in vacuum, in dry nitrogen and in atomic hydrogen, but it is high in water vapour and in oxygen environments. In general, these DLC coatings with higher fraction of sp^3 bonding result in higher hardness[121, 122].

Lee and J.W [123] used 40nm DLC films deposited on the VCR head, (deposition temperature below 100°C); found the head life is increased significantly by the wear durability of DLC films. Gupta and Bhushan[121] used several methods to deposit amorphous carbon on the surface of head, and found, the ion beam carbon coatings on

Ni-Zn ferrite and cathodic arc carbon coating on Al_2O_3-TiC exhibited the highest resistance to scratch and wear among his experiment.

Xu and Bhushan[124] found that carbon coating eliminated the PTR growth through reducing static and kinetic friction during take-off and landing in the disk-head system, and the carbon coating provided a wear-resistant protective layer and eliminating dis-similarities of air bearing surface.

Several materials other than DLC films, i.e.SiO_2, ZrO_2, have also been studied and used for overcoats for thin film disks. Bhushan and Gerard[8] used a 50-nm thick rf-sputtered chromium oxide coating on the thin film head surface, experiment shows this coating exhibits best durability. Bijker and Draaisma[125] studied the DLC and Cr/Cr_2O_3 coatings on advanced digital recording heads, and found Cr/ Cr_2O_3 coating better than DLC coating in their experiments.

The mechanism of coating wear[126] was determined by the maximum subsurface stress under the coating surface and was affected by the humidity and temperature. In the same time, the coating mechanical property and the tribology system played important role.

Although some of the coating of the heads show durability for the wear test, but the durability and thickness of the coating still do not match the demand of the industry, there are still more research work to be done in order to achieve the projected recording system.

1.3.9 Tape Wear

All magnetic recording media are lubricated to improve their mechanical reliability. Lubricants on the surface of particulate media are diminished by the operation of the media. It is believed that the lubrication performance is maintained as a result of migration of the lubricant from the Mp tape subsurface to the surface[127].

Nishida[128] studied the dynamic behaviour of lubricant migration in particulate magnetic recording media by using XPS; they confirmed that sub-surface lubricant migrates back to the surface. The lubricant of higher migration speed had better stability of friction

coefficient. The migration speed of lubricant was changed by the storage volume and kind of lubricant.

Lubricants degradation leads to severe wear of the tribology system. Zhao and Bhushan[129] studied degradation of lubricants for magnetic thin-film rigid disks, they found that the decomposition mechanism of the perfluoropolyether (PFPE) lubricants due to four degradation mechanisms: thermal and catalytic decomposition, tribo-electrical decomposition and mechanical scission. The lubricant during the wear processing decomposed due to different mechanism also could be found in REF[129, 130, 131, 132].

For the Mp tape wear, Hempstock, Wild and Sullivan[11] used XPS to analyse the surface composition changes. Synthesis of the carbon peak for the tape revealed four chemical states contributed to the total carbon peak[133,134]. The Synthesis of the carbon peak were due to O=C-O, C-O, C-N and C-C/C-H. The most intense peak (C-C/C-H) occurred at a designated binding energy of 284.6eV, the carboxyl (O=C-O) peak was known to be characteristic of both the lubricant and binder material. However, the C-N peak provided a good indication of the relative changes in the concentration of the binder materials. Results showed that in all areas of the tape, the amount of detected iron had increased, while the nitrogen (binder indicator) signal had decreased. This indicated resin binder was removed, but the lubricant coverage on the surface increased to compensate for this.

The tape wear increases as tape tension[75,135,136] increases. It is known that a rougher tape surface is more likely to generate debris during contact, especially when it is new. A rougher tape surface is also more abrasive[48, 73].

Sharma[137] and Sullivan[71] studied the durability of particulate diskettes under a variety of conditions of lubrication using optical microscopy, SEM and XPS. They found that wear proceeded in three stages: initial smoothing of a wear track leading to plastic deformation with little or no material removal, removal of lamina particles or flakes of thickness much less than the magnetic coating and finally a catastrophic phase where large areas of the wear track were destroyed. Research[10,27] on both tape and diskettes

have shown that the processes leading to wear and to ultimate catastrophic failure of all such media are similar.

ME tape has a higher magnetic moment and output signal than MP tape, but ME tape durability has been a concern. Studies on the earlier version of ME tape revealed that its performance was worse than MP tape[138]. Topoleski and Bhushan[139] found the MP tape significantly outperforms ME tape. Patton and Bhushan[140] found that the wear life of ME tape has been shown to slightly improve with the addition of a DLC coating.

The long-term exposure of magnetic tapes to a hot and humid environment has been shown to result in tape degradation[73,141]. The high temperature increases the speed of the tape aged, and aged tape has a propensity for generating extensive debris. The aged tape shows a substantial increase in an extractable binder of low molecular weight, which resulted in a significant increase in friction and stick[20].

Their absorbed water content affects the mechanical and physical properties of polymeric binder materials[20]. Usually, these materials become softer with increasing water content, and this can affect their frictional properties[20]. Sullivan[10] stated that water vapour could produce hydrolysis and chain scission in the polymer and hydroxide formation on ceramic, glasses, ferrite and metals. Water vapour is a major cause for concern in head/media interactions, where high humidity can result in high friction, stiction and high wear.

During contact of a particulate tape with the head, tape debris consisting of binder and magnetic particles can be generated by adhesive, abrasive, and impact wears. Binder debris, loose magnetic particles, worn head material, or foreign contaminants are introduced between the sliding surfaces and results in three-body abrasion of the head and tape surface. The amount of debris generated as a result of tape wear depends on the magnetic particles, binder, lubrication and cohesive and adhesive properties of the magnetic-coating formulation used to make the tape[20].

Scott and Bhushan[70, 142] studied the generation of tape debris in a linear tape drive, using thin film AlTiC and Ni-Zn ferrite heads run against commercial metal particle (MP) tape, three types of tape debris are found: magnetic particle rich, polymer rich and adherent debris (stain). Magnetic-particle-rich debris is characterised by its opaque

appearance while the polymer-rich type is characterised by its translucent appearance. Adherent debris is characterised by its inability to be removed easily with a solvent. It may only be removed using considerable mechanical action. More loose debris is generated at the head-tape interface in the case of AlTiC heads than in the case of Ni-Zn ferrite heads when run at the same conditions and over the same distance.

For the head tape contact, although contact should be elastic, high-localised contact temperatures can lead to polymer softening and plastic flow in the first stage. Repeated shearing of the asperity contacts can also result in the localized melting of binders and in a mechanically degraded polymer (coating) surface, for example, reduction in the molecular weight. The polymeric binders of lower molecular weight are sticky and could result in higher friction[20]. With repeated use, the amount and composition of the internal lubricant available at the tape surface could also be affected and could lead to changes in friction. The second stage is the result of continuous cyclic stressing of the media that leads to the initiation of sub-surface fatigue cracks that grow to the surface and produce laminar wear particles.

The environment (temperature and humidity) has a strong effect on the generation of debris. Friction is increased under high temperature and humidity conditions and usually results in increased debris formation[143].

2 Chapter 2 Experimental

2.1 Introduction

This chapter dealt with the sample generation and surface analysis techniques. Linear tapes and drives (including Travan5 and LTO system) were employed to run in a range of environmental conditions in environmental chamber. LTO heads normally cycled 100 passes, 1000passes, 5000passes against LTO tapes in a range of environmental conditions, one pass is 200 m fixed distance, Travan5 head only cycled 5000 passes against Travan5 tapes in a range of environmental conditions.

Surface analysis techniques such as Atomic Force Microscopy (AFM), X-ray Photoelectron Spectroscopy (XPS), Auger Electron Spectroscopy (AES) and Optical Microscopy with digital camera were employed to investigate the chemical and physical changes in the samples as a result of the cycling experiments. Indentations were made on the surface of the LTO heads to measure the wear rate of the heads cycling against tapes under different experimental conditions.

In order to simulate the high temperature (100°C) and extreme water content condition, AlTiC samples and unused LTO heads were boiled in the deionized water and then analysed using XPS and AFM.

2.2 Experimental Platform

The Travan5 drive and LTO Ultrium drive were used as experimental platforms. This is partly due to the interest of the collaborators try to understand the drive tribological property. In fact, using the actual real drives is the best way to study the wear occurred during real cycling situation, the drives could be available in a large quantity to simulate the real situation in the designed environment to acquire the statistic results. The tribological effects and the head media interaction could be easily isolated and wear mechanism could be understood. It is impossible to reproduce the complex contact geometries, contact pressure, and temperature and tape transport, data writing and reading in any model experimental system.

2.2.1 Travan5 drive

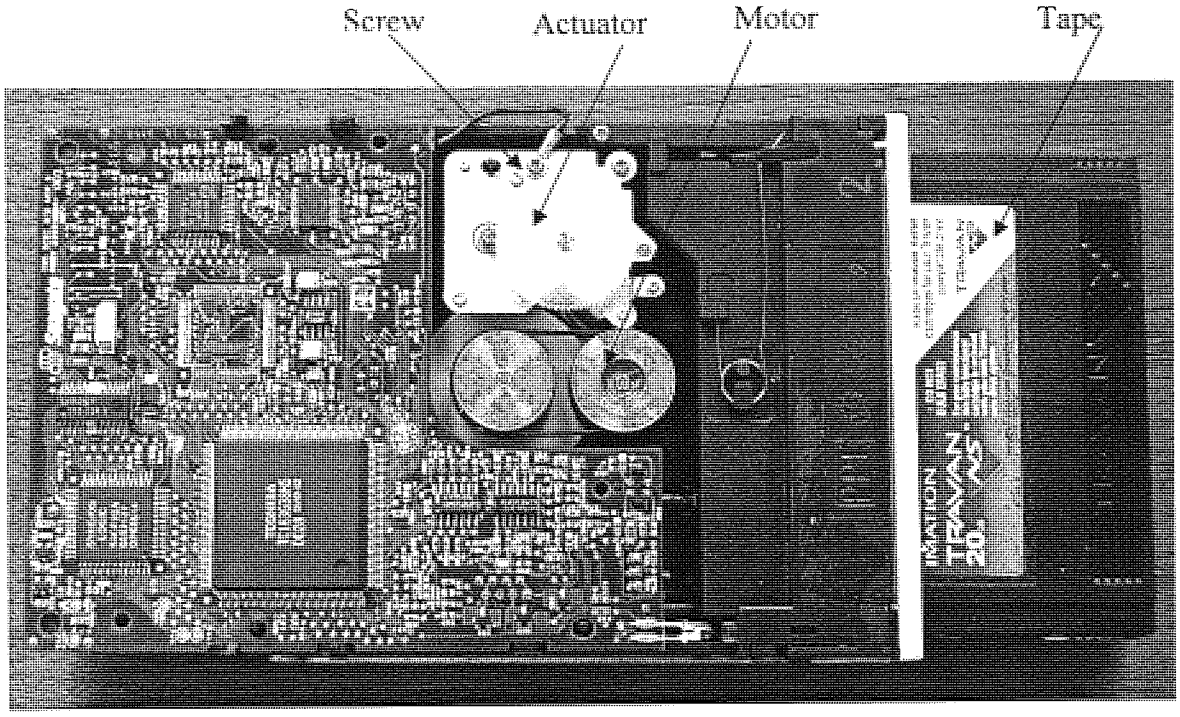

Figure 2-1 Travan5 drive and tape

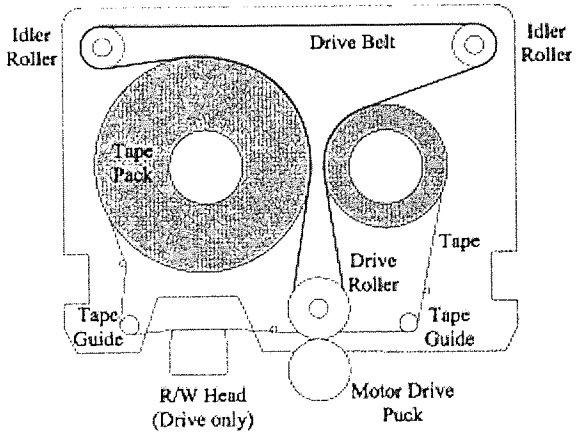

Figure 2-2 the schematic diagram of Travan5 tape cycling

The Travan5 quarter-inch cartridge (QIC), as used with the Travan5 linear tape system, it features up to 20 G bytes of capacity per cartridge and backup speeds of up to 120 Mbytes per minute. It is of a belt driven design. A polymeric belt in contact with the magnetic surface of the tape is used to control tension in the tape by driving the supply and take-up reels (see Figure 2-1 and Figure 2-2). To eliminate the problem of trapped air, the polymeric drive belt has a micro texture imparted to the surface in contact with the magnetic coating of the tape[144]. Sullivan et al[11,86] had reported the effects of the belt

on the tape surface, indicated the tape under contact with belt suffered more wear. The width of the belt is about half of the tape width. So only the central area of the tape is in contact with the belt. The belt provides for bi-direction motion of the tape[145], so that data recording and playback can be in either direction of tape travel.

Modified Travan5 drives were used in this research project, Travan5 head could be easily installed or removed from the drive (by adjusting four screws in the actuator inside the drive, see Figure 2-1), after connecting the drive to the power supply (5V, DC), inserting the tape, it automatically begins to run. A photo detector in the drive could sense the end of the tape (at end of tape, there is a hole inside the tape). Then the drive stops, the head move to a new position and a new cycling begins in the opposite direction until the power was turned off. The cycling time for a typical experiment was calculated before the experiment starts. The nominal tension and speed are 0.6 N and 2.3m/s respectively.

Physical Dimensions of the Travan5 drive are as follows: Width 4.0 in / 102 mm; Height 1.0 in / 25 mm; Length 6.36 in / 161.5 mm; Weight 1.0 lb / 0.5 kg. The working environmental conditions are min/max operating temp 5°C / 45°C, maximum operating humidity 80%.

2.2.2 LTO drive

One of the tape industry's biggest problems has been a lack of standards, with each vendor providing its own technology. Standardization means that different manufacturers' tapes and tape drives will interoperate (just as audio tape cassettes work in all tape players). Hewlett-Packard, IBM and Seagate have responded to this by collectively developing new open format specifications based on the group's Linear Tape-Open (LTO) technology. The group developed the formats to serve multiple market areas and to be supported by multiple suppliers.

Like existing tape systems, LTO uses a linear multi-channel bi-directional format. LTO adds to existing technologies timing-based servo (a device that automates a process of error correction for a mechanism), hardware data compression, enhanced track layouts, and efficient error correction code.

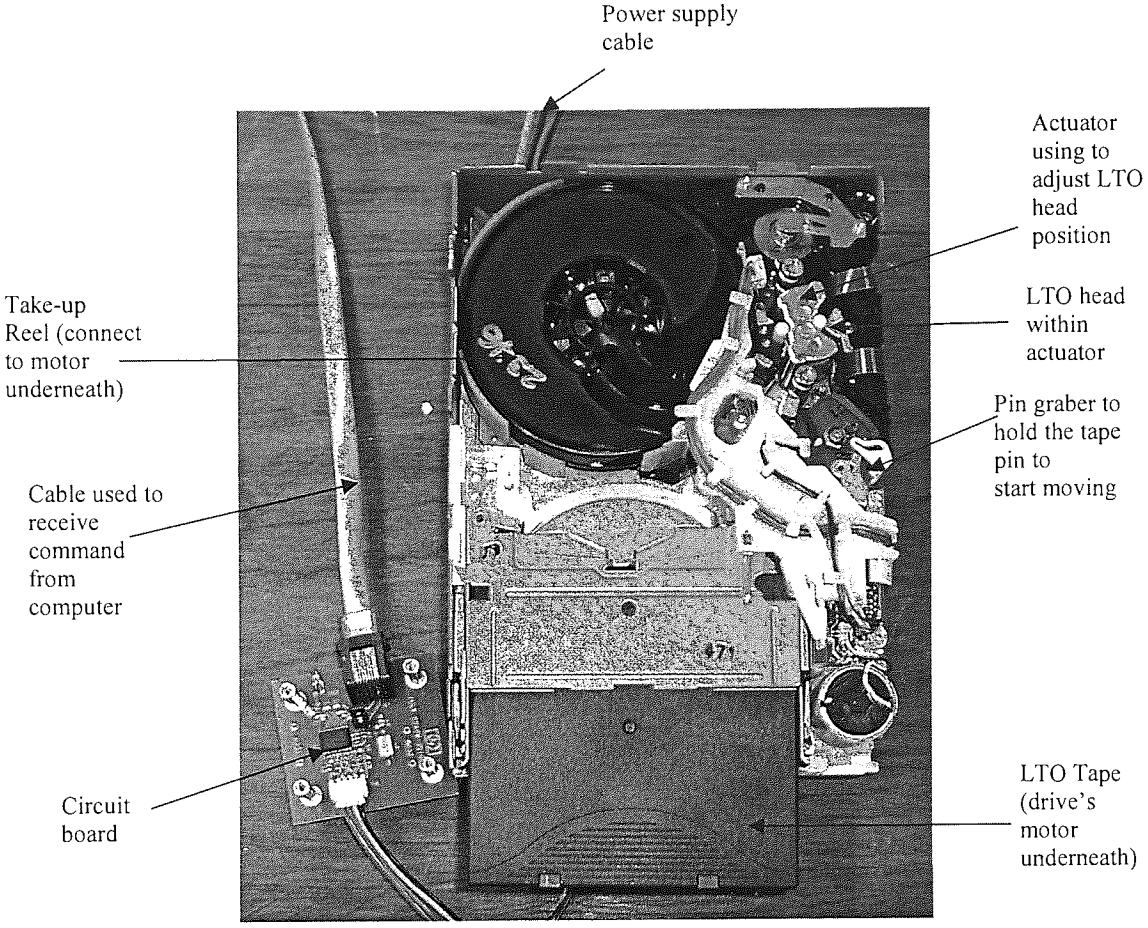

Figure 2-3 The LTO tape and LTO drive

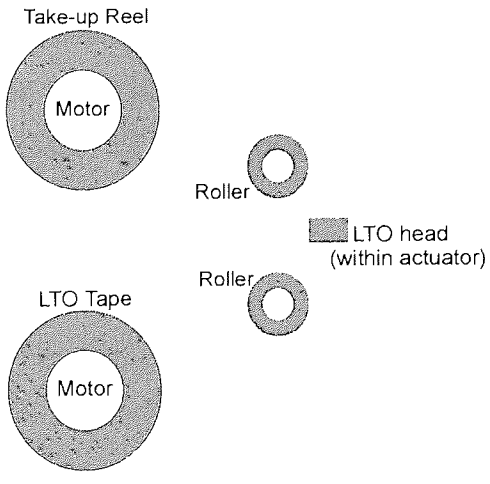

Figure 2-4 the schematic diagram of LTO drive and tape

LTO was developed in two different formats - one for fast data access (Accelis format) and another for greater storage capacity (Ultrium format). The Accelis format uses 8mm-wide tape on a two-reel cartridge that loads at the mid-point of the tape to provide

fast data access, specifically for read-intensive applications, such as online searches and retrieval functions. The Ultrium format uses a single reel of half-inch wide tape to maximize storage capacity, specifically for write-intensive applications, such as archival and backup functions.

The LTO Ultrium products were used in this research project, Ultrium based-products offer a 100-gigabyte capacity, and data transfer rates are 10 - 20 Mbps. While these figures are unheard of in other technologies, LTO specifications include plans for expected increases that will double current rates with each of the next three generations of products.

The LTO Ultrium single-reel cartridge design uses a take-up reel that is located inside the drive (see Figure 2-3 and Figure 2-4). The tape is engaged by means of a coupler that "grabs" a leader pin at the start of the tape and guides it around the tape head to the take-up reel in the drive. After the leader pin is secured in the take-up reel, the reel rotates and pulls the tape through the tape path.

The LTO head could be removed or installed by adjusting screws on the actuator (see Figure 2-3). Communication with the LTO drives and computer was established using a macro computer language named Dexter (a computer language developed by Hewlett Packard to control the tape drive operation). This allowed various tasks including tape cycling and error rate tests to be performed. LTO drives use the standard computer power supply (5V, DC). Detail of the LTO cycling methods could be seen in the experimental methods section of this Chapter.

2.2.3 Environment Chamber

Commercial Votsch VC 4034 Environmental Chamber was used in experiments. The chamber allowed independent temperature (±0.5°C) and relative humidity (±1%) control. The relative humility range of the chamber could be varied from 10% to 98%; the temperature range was from 5°C to 95°C. The water pH-value was between 6-7 in the chamber (de-ionized water was used throughout). In the environment chamber temperature and humidity were monitored by means of sensors for thermometer and hygrometer inside the chamber. A feedback electronic circuit adjusted the operation system to maintain the set-up working points.

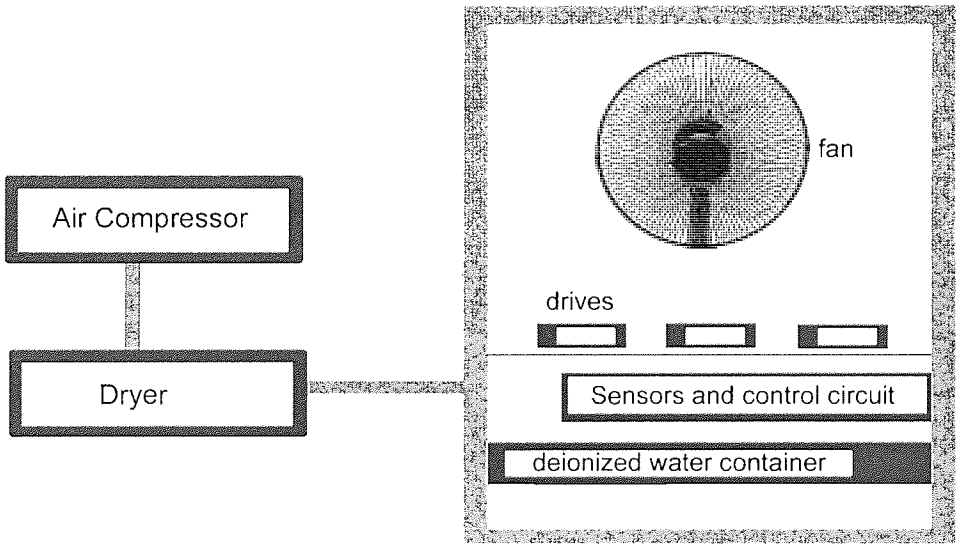

Figure 2-5 the schematic diagram of environmental chamber Votsch VC 4034

Figure 2-5 shows a schematic diagram of the chamber used in this research project; the drives and tapes were put inside the chamber. After setting the temperature and relative humidity of the chamber by a small touch screen; the experiment could begin. Normally it needs several hours to reach the setting values before the cycling experiment starts.

For Travan5 systems, the experiments were controlled by the power supply of the Travan5 drives. Normally after the chamber reached the setting experimental condition, the power supply of Travan5 drives were turned on, then the chamber door was opened and Travan5 tapes were quickly inserted into the Travan5 drives, closed the chamber door. The tape automatically started cycling until the Travan5 drive power supply was

turned off when the cycling distance was finished. The cycling time was calculated before the experiments using the cycling distance divided by 2.3m/s.

For LTO system, the LTO drives and tapes were put inside the chamber and the power supply and communication cable between the LTO drives and computer were always on, once the setting experimental conditions were obtained, the commands from the computer could be sent to control the cycling of LTO tapes by a Dexter computer language developed by HP. This will be described in experimental method in detail.

2.2.4 Relative humidity and water content

Relative Humidity (RH) is the ratio, expressed as a percentage, of the actual vapour pressure of air to the saturation vapour pressure (SVP) at the air's current temperature.

$$\mathrm{Re}\,lativeHmidity(RH) = (E / Es) \times 100 \qquad \text{Equation 2-1}$$

E_s is saturation vapour pressure and E is actual vapour pressure in millibars at the air's current temperature. The saturated vapour pressure is calculated using REF[146].

$$E_s = 6.11 \times 10^{7.5Tc/(237.7+Tc)} \qquad \text{Equation 2-2}$$

T_c is the air temperature in degree Celsius.

Water vapour pressure or normalized atmospheric water content rather than the relative humidity values (as are used almost universally in this field) are much better to compare the experimental results. At a fixed temperature, an increase of water vapour in the air corresponds to an increase in the humidity of the air, however this is not the case at differing temperatures. To ascertain the water content at the head/tape interface at different temperatures, it was necessary to use the general gas law.

$$\frac{P_1V_1}{n_1T_1} = \frac{P_2V_2}{n_2T_2} \qquad \text{Equation 2-3}$$

P = Pressure (water vapour pressure).

V = Volume of container in which the gas is enclosed.

T = Temperature (Kelvin)

n = Number of gas molecules

As the environment chamber in which the drives were enclosed is of a fixed volume, V can be cancelled from both sides of Equation, which becomes, after rearrangement,

$$\frac{P_1 T_2}{P_2 T_1} = \frac{n_1}{n_2} \qquad \text{Equation 2-4}$$

From this equation, the different water contents under the different experimental conditions can be compared.

Temperature	5°C	10°C	15°C	22°C	40°C
Saturated Water Pressure (mbar)	8.3	11.2	15.0	22.0	55.1

Table 2-1 Saturated (100%RH) water vapour pressure (mbar) in different temperature conditions

Environmental Condition	10°C/ RH10%	15°C/ RH15%	5°C/ RH80%	40°C/ RH15%	22°C/ RH40%	40°C/ RH30%	40°C/ RH45%	40°C/ RH60%	40°C/ RH75%	40°C/ RH80%
Water Pressure (mba)	1.1	2.2	6.7	8.3	8.8	16.5	24.8	33.1	41.3	44.1
Normalised Water Content (NWC)	1.0	1.9	5.9	6.7	7.5	13.4	20.1	26.8	33.5	35.5

Table 2-2 Relative Water Content Magnitude for each environmental condition
(Normalised to 10°C, RH10%)

Table 2-1 shows the saturated water pressure (RH 100%) at different temperature used in these experiments. Table 2-2 shows the water pressure at the different relative humidity/temperature conditions. At the same time the number of water molecules n inside the environment chamber were normalised to the condition of 10°C, 10% RH and will be referred to as normalised water content (NWC). The Normalised water content (the same for the absolutely water content) is the best solution to compare the water content effect happened in the different experimental conditions.

2.3 Experimental Techniques

Surface Science Group in Aston University is using VG ESCALAB 200D; it includes X-ray Photoelectron Spectroscopy (XPS), Auger Electron Spectroscopy (AES), Secondary Ion Mass Spectroscopy (SIMS) and Ion Scattering Spectroscopy (ISS). The first two techniques (XPS, AES) were intensively used in this research project. Optical Microscopy and Scanning Electron Microscopy (SEM), Atomic Force Microscopy (AFM) and Indentation techniques were used for wear rate and measuring Pole tip Recession (PTR) and topography of Head and tape surface (unused and worn).

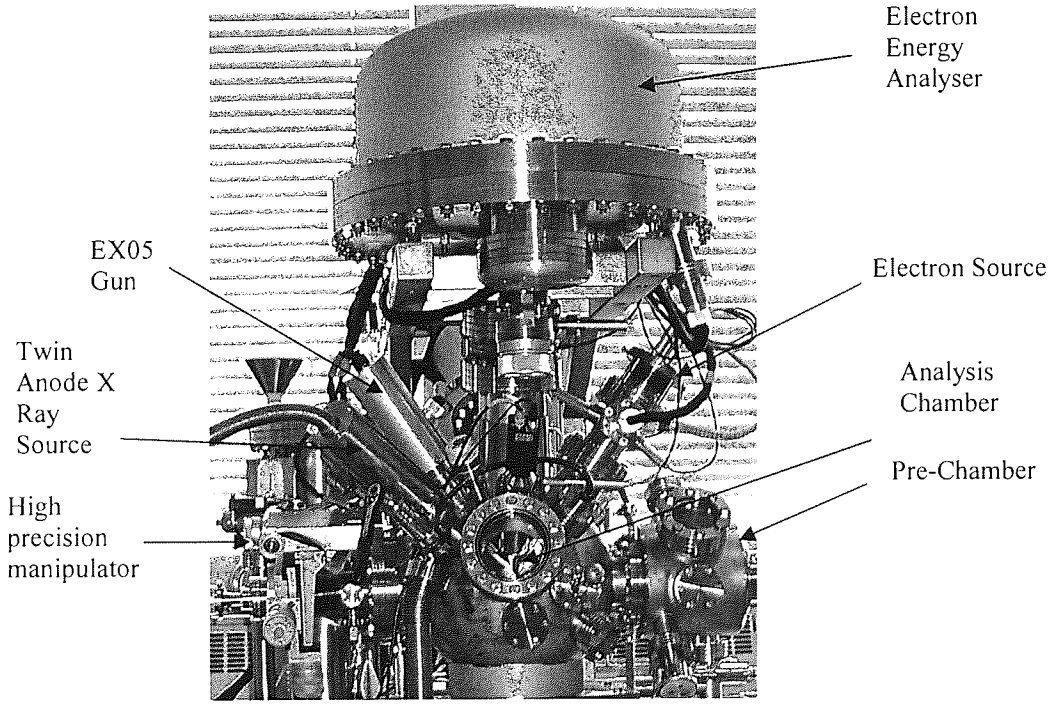

Figure 2-6 Main part of VGS ESCALAB 200D spectrometer

Surface chemical and physical analysis are essential in this project to assess the surface changes happened in the head and tape interface. XPS allowed identifying the chemical state of the surface, Auger electron spectroscopy (AES) having its spatial resolution only limited by the electron beam spot size (~0.1μm).

	Sampling Depth (monolayer)	Sensitivity (Order of)	Inform-ation	Quantif-ication	Elements Not covered	Spatial Resolution (Best)	Effective Take-off Year
XPS	3	0.3%	C, E	Easy	H, He	5μm	1967
AES	3	0.3%	C, E*	Easy	H, He	5nm	1968
SIMS (static)	2	<10ppm	C	Impossible		1μm	1970
SIMS (dynamic)	10	<1ppm	E	Possible		20nm	1975

Table 2-3 A comparisons of AES, XPS and SIMS techniques[147]

Note: C chemical, E elemental, E* means the AES has some difficult to identify the chemical state of the element.

A general comparison of the characteristics of the three analytical methods is given in Table 2-3. The principle of XPS and AES will be described in this chapter.

2.3.1 XPS

2.3.1.1 Basic Principle and consideration

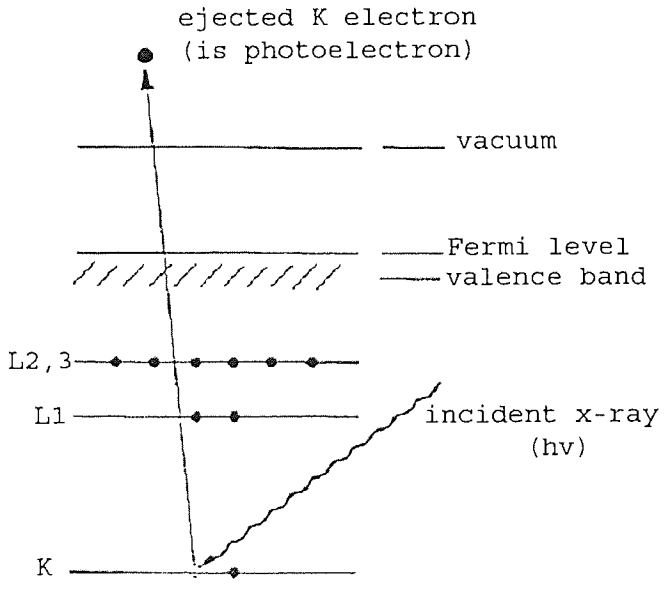

Figure 2-7 Principle of X-ray of Photoelectron Spectroscopy[148]

Surface analysis by x-ray photoelectron spectroscopy (XPS), is accomplished by irradiating a sample with monoenergetic soft x-rays and energy analysing the electrons emitted from the sample surface. These x-rays photons have penetrating power in the

solid, of the order of 1-10 micrometers. They interact with atoms in this surface region by the photoelectric effect, causing electrons to be emitted (see Figure 2-7).

An electrostatic energy analyser can measure the kinetic energy of the emitted photoelectrons, so the binding energy of electrons can be simply calculated from Einstein photoemission equation[147]:

$$E_k = h\nu - E_b - W \qquad \text{Equation 2-5}$$

E_b represents the binding energy of a core electron in the certain energy level and E_k is the kinetic energy of the electron emitted from this core level, hν is X-ray photo energy. The binding energy maybe regarded as ionization energy of the atom for the particular shell involved. Since there are a variety of possible ions from each type of atom, there are a corresponding variety of kinetic energies of the emitted electrons. The Fermi level corresponds to zero binding energy (by definition). W is called the instrument work function for a solid sample, this is the minimum energy required for an electron to escape from the sample surface and to be measure by the analyser, and it includes contributions from both sample and instrument.

Choice of materials for a soft X-ray source in XPS depends on two considerations. Firstly, the line width must not limit the energy resolution required in the technique and, secondly, the characteristic X-ray energy must be high enough that a sufficient range of core electrons can be photoejected for an unambiguous analysis. X-rays are generated in materials by bombardment with electrons of sufficient energy[147]. Mg Kα x-rays (1253.6eV, width 0.7eV) or Al Kα x-rays (1486.6eV, width 0.85eV) are ordinarily used as X-ray sources.

The electrons are not only inelastic scattered but also elastically scattered during travelling procedure, the average net distance travelled by an electron is called the attenuation length[147]. The characteristic depth from which photoelectrons can be emitted is simply in the range 2-10 atom layers, as shown in the Figure 2-8. It is this important phenomenon that makes XPS surface-sensitive techniques[147].

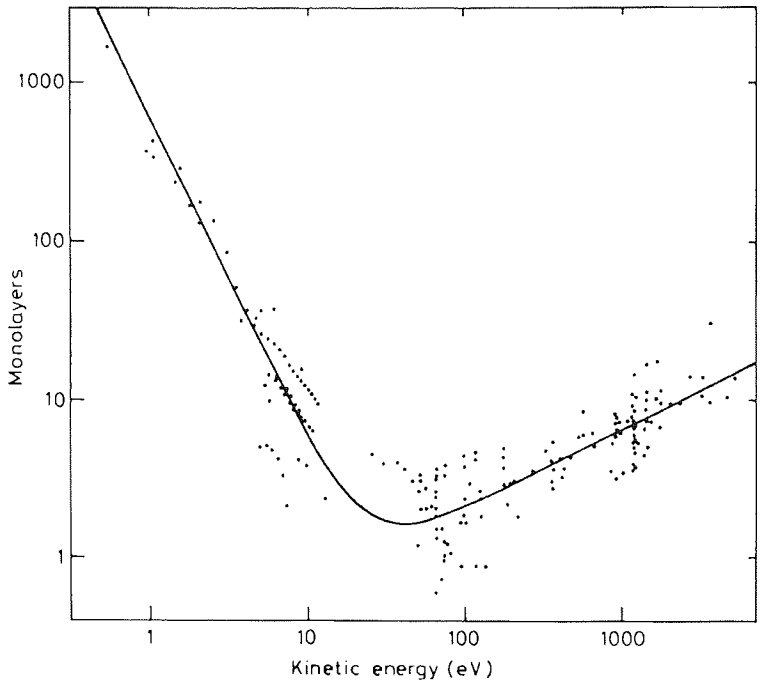

Figure 2-8 the dependence of attenuation length λ on the emitted energy for elements[147]

If λ is the attenuation length of the emerging electron then 95% of the signal intensity is derived from a distance 3λ within the solid[147]. This makes the XPS surface sensitive technology.

XPS can be used to measure most elements (except H, He) at different chemical states[147]; For VG ESCALAB 200D in Aston University, the largest analysis area for XPS is 2mm×3mm; the smallest analysis area is 150μm (diameter).

The heart of the XPS (AES) technique is the measurement of an electron energy spectrum. Such an analysis is performed by an electron energy analyser (strictly speaking, an electron velocity analyser), which is often called a spectrometer. There are two electrostatic analysers are universally employed, namely the Cylindrical Mirror Analyser (CMA) and the Concentric Hemispherical Analyser (CHA). Figure 2-9 shows hemispherical sector analyser; usually it is a multifunction energy analyser in the XPS or Auger system. By accurately measuring the electron binding energy (E_b), different atom and chemical state of the element investigation have been realised.

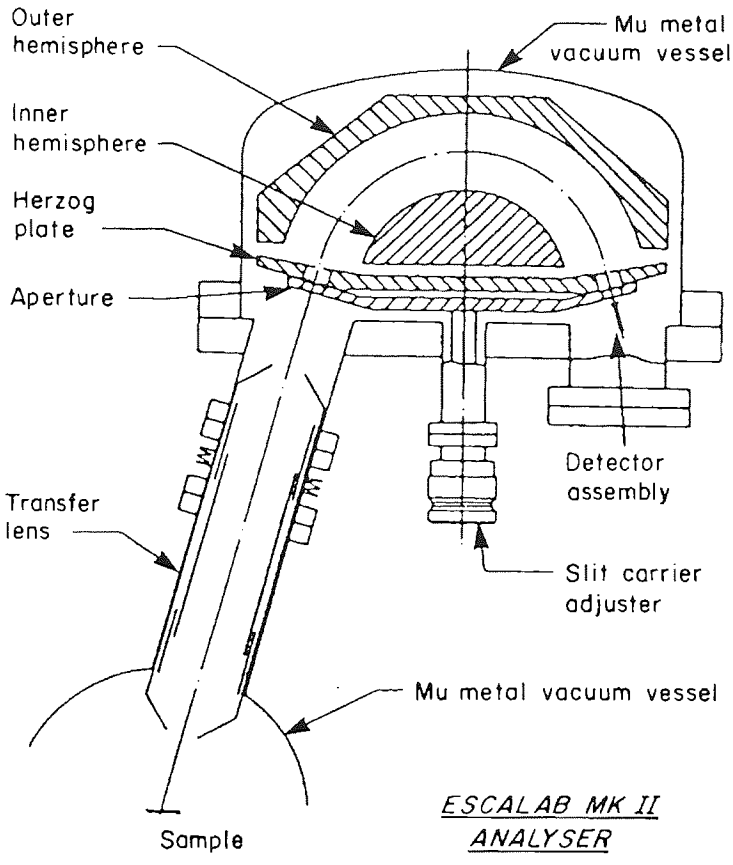

Figure 2-9 Diagram of a CHA with standard input lens systems for XPS[147]

2.3.1.2 Programming scans for an unknown sample

For a typical XPS investigation where the surface composition is unknown, a broad scan survey spectrum should be obtained first to identify the elements present. Once the elemental composition has been determined, narrower detailed scans of selected peaks can be used for a more comprehensive picture of the chemical composition. Peaks from any species thought to be radiation-sensitive or transient (for example Cl) should be run first.

2.3.1.3 Chemical Shift Theory

For the same atom in different chemical environment or chemical states, the binding energies of core level electrons vary. The binding energy shift can be briefly explained by the redistribution of electric charge that occurs in the peripheral orbital when a chemical bond is formed – so called the charge potential model[147, 149, 150], if the atomic valence electron orbital are assumed as a spherical shell of electric charge, and core

electrons reside inside this charged shell, the valence electrons may shield the core electrons. When the atom is bound to other atoms in a molecule or a crystal, the charge density of valence electrons in the atom vary due to valence electron transfer (ionic molecule) or redistribution (covalent molecule), resulting in change of binding energy of core level electrons.

2.3.1.4 XPS Spectrum Smoothing

Sometimes it is not possible to obtain data with sufficiently good signal/noise for further data analysis or for reasonable presentation. The high noise signal can arise when collecting very weak signal or when sample decomposition is occurring and fast data collection is necessary. Spectrum smoothing, which is a mathematic process to increase the correction between data points and suppress uncorrected noise, can be very useful. The smooth is a method to use either a quadratic or cubic function to fit the data to an appropriate smooth curve[147].

2.3.1.5 XPS Energy Calibration

In an original XPS spectrum, core level peaks of photoelectron may not be at the expected positions mainly due to surface charging, variation of sample work function or sometimes the inappropriate calibration of spectrometer energy scale. The best way to check the calibration is to record suitable lines from a known, conducting specimen. Typically the Au4f lines or C1s are used. C1s peak line for C-C or C-H bond (284.6eV) is the convenient for use since adventitious carbon is always present on sample surface.

2.3.1.6 Background Removal

Typical XPS spectra and AES peaks are always superimposed on a background. This background arises from photoelectrons produced within the target materials that have been subject to one or more inelastic scattering processes before emission from the surface, background removal is an important step for quantitative analysis.

A simple way is to draw a straight line between two suitably selected points, so called linear background[147]. This process can be effective when little change in background occurs. But in the case of step ground, especially there are a mixture of more than one chemical states, the end points are difficult to choose for linear background. Shirley[151] found a way to solve the background subtraction, in which the background intensity at a point is determined by an iterative analysis to be proportional to the intensity of the total peak area above the background, and to higher energy. It assumes that each unscattered electron is associated with a flat background of losses. In this research work, Shirley's method was always chosen, as it is generally the more accurate[152].

2.3.1.7 Curve Synthesis and Fitting

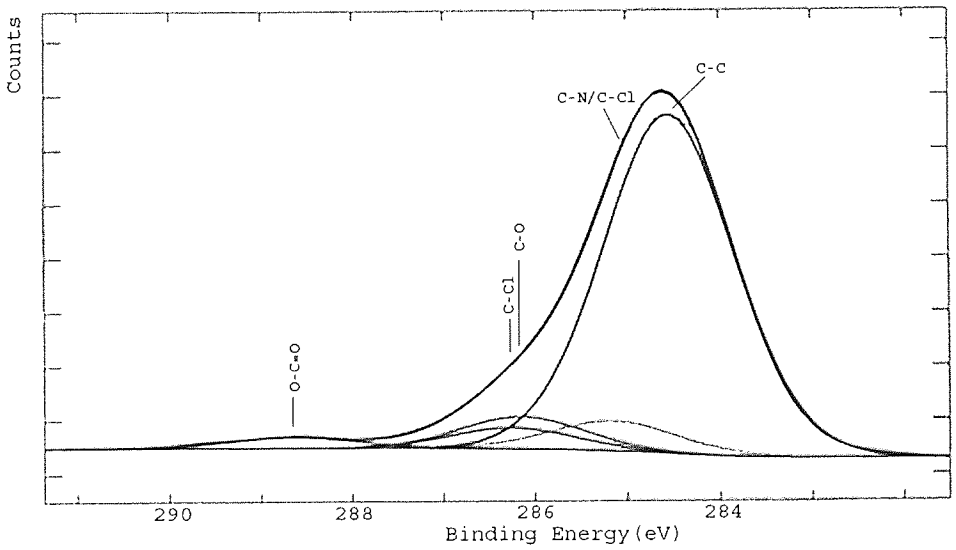

Figure 2-10 LTO Fuji tape C1S peak fitting

When the energy separation is smaller than the resolution of the system or the binding energy of the several peaks are very close together, an XPS peak may consist of several components corresponding to different chemical states of the same element, or two or more elements of similar binding energy. In such cases several curves can be fitted to the peak, simulating the individual components. The key to successful fitting methods depends upon the choice of an appropriate fitting function and a proper consideration of the background. Figure 2-10 shows a typical C1S peaking fitting in the magnetic double layer Fuji tape XPS results. There are totally six individual components in C1s peak. The fitted peaks include C-C/C-H, C-N, C-Cl, C-O; O-C=O as the binder energy

indicated in Table 2-4. The most intense peak (C-C/C-H, aliphatic and aromatic components were not resolved) occurred at a designated binding energy of 284.6eV.

Assignment	Peak (eV)
C (1S) from adventitious carbon	284.6
C (1S) from Sp^3 in DLC	285.4
C (1S) from C-N in urethane	285.2
C (1S) from C-O in urethane	286.1
C (1S) from $-\underline{C}H_2CHCl-$	285.2
C (1S) from $-CH_2\underline{C}HCl-$	286.2
C (1S) from O=C-O in urethane	288.6
Al ($2P_{3/2}$) from pure Al	72.6
Al ($2P_{3/2}$) from Al_2O_3	74.0
Al ($2P_{3/2}$) from AlOOH	74.5
Y ($3d_{5/2}$) from Y_2O_3	157.8
O (1S) from $Fe_2O_3/Fe_3O_4/FeO$	530.0
O (1S) from FeOOH/AlOOH	531.5
O (1S) from epoxy	533.1
O (1S) from Al_2O_3	531.6
Fe ($2P_{3/2}$) from pure Fe	706.7
Fe ($2P_{3/2}$) from Fe_2O_3/Fe_3O_4	710.6
Fe ($2P_{3/2}$) from γ-FeOOH	711.3
Fe ($2P_{3/2}$) from α-FeOOH	711.8
Ti ($2p_{3/2}$) from pure Ti	453.8
Ti ($2p_{3/2}$) from TiC	454.0
Ti ($2p_{3/2}$) from TiO_2	458.3

Table 2-4 XPS binding energy of the interested elements[153, 154, 155, 156, 157]

2.3.1.8 XPS Quantification

For a sample that is homogeneous in the analysis volume, the number of atoms of photoelectrons per second in a specific spectral peak is given by[154]:

$$I = nf\sigma\theta y\lambda AT \qquad \text{Equation 2-6}$$

Where n is the number of atoms of the element per cm^3 of sample; f is the x-ray flux in photons/cm^2.sec; σ is the photoelectric cross section for the atomic orbital of interest in cm^2; θ is an angular efficiency factor for the instrumental arrangement based on the angle between the photo path and detected electron; y is the efficiency in the photoelectric process for formation of photoelectrons of the normal photoelectron

energy; λ is the mean free path of the photoelectrons in the sample; A is the area of the sample from which photoelectrons are detected; and T is the detection efficiency for electrons emitted from the sample.

After rewriting the equation into following:

$$n = \frac{I}{f\sigma\theta\lambda yAT} \qquad \text{Equation 2-7}$$

The denominator of above equation can be assigned the symbol S, defined as the atomic sensitivity factor. If we consider a strong line from each of two elements, then:

$$\frac{n_1}{n_2} = \frac{I_1 / S_1}{I_2 / S_2} \qquad \text{Equation 2-8}$$

The concentration C_x of element x in a compound containing more elements measured by means of XPS may be calculated from:

$$C_x = \frac{n_x}{\sum_i n_i} = \frac{I_x / S_x}{\sum_i I_i / S_i} \qquad \text{Equation 2-9}$$

I_i is the strong line from element i, S_i is the corresponding sensitivity factor. The sum of denominator includes all the element appeared in the surface of materials. In practice, the intensity is taken using the peak area (normalised by time and step size), that is, the area under the envelop of the photoelectron peak after removing background. The sensitivity factors for the elements may be refereed to either systematically experimental measurements or based on theoretical calculation.

2.3.1.9 Angular Resolved XPS

Intensities of photoelectrons depend on their take-off angle[147]; take-off angle is the angle of electron emission to the surface normal. The surface sensitivity of XPS is based on the fact that the number of electrons is reduced exponentially by a factor of $e^{(-d/\lambda\cos\theta)}$

after travelling a distance of d in a solid. That means 95% of photoelectrons emerge from a depth of $d=3\lambda\cos\theta$, Where λ is the attenuation length, so the maximum sampling depth of XPS (when $\theta=0°$) for a specific core level on an atom is approximately 3λ.

Angular resolved XPS is a method to use and measure the intensity of photoelectrons at different take-off angles (same area) to obtain the thin overlayer information on a solid surface.

$$I = I_0 \exp(-d / \lambda \cos\theta) \qquad \text{Equation 2-10}$$

I_0 is signal intensity at saturation (without overlayer), I is signal intensity with the overlayer (d is the thickness) measured at take of angle θ. With changing the different take-off angle and measuring the intensity of photoelectron, the depth and element information of overlayer could be obtained from above equation.

2.3.1.10 Sputter Depth Profiling

An ion source for sputter removal of surface layers allows either XPS or AES to perform composition depth profiling. The most frequently used ion guns in XPS spectrometers are simple electrostatic devices where the inert gas ions are generated by collisionally excitation with electrons of typically 100eV energy from a hot filament. The positive ions are accelerated to energies between 0.5 and 5 KeV and are focused to bombard on the sample surface, creating a sputtering spot diameter of typically 1-5mm in diameter[150].

Sputtering is a destructive method. A small fraction of the energy is transferred to surface atoms and causes them to leave the sample; they are sputtered away. Thus, the sample is successively decomposed in an abraded part which can be analysed, e.g. by SIMS, AES or XPS. The sputtering method could also be used to clean a sample by sputtering away the contaminant layer.

2.3.2 AES

AES is a surface analytical method in which the sample is bombarded by a beam of low energy electrons. This process could be illustrated in Figure 2-11. When the electron beam hits a sample, core electrons may be ejected, the core holes are then filled by an internal process in the atoms where electrons from higher energy levels fall into the core hole and release the extra energy to the third core electrons. These third electrons are called Auger electrons; these Auger electrons obtained kinetic energies unique to each type of atoms and were ejected from sample surface. Auger electrons are collected and analysed by an electron energy analyser like XPS does then AES spectrum can be obtained, which provides information on surface composition and chemistry. AES is commonly used in elemental analysis and is particularly useful in micro area studies since it is easy to reduce the spot size of an electron beam into a few hundreds Å by an electrostatic or magnetic focusing lens. AES can be used to measure most elements (except H, He).

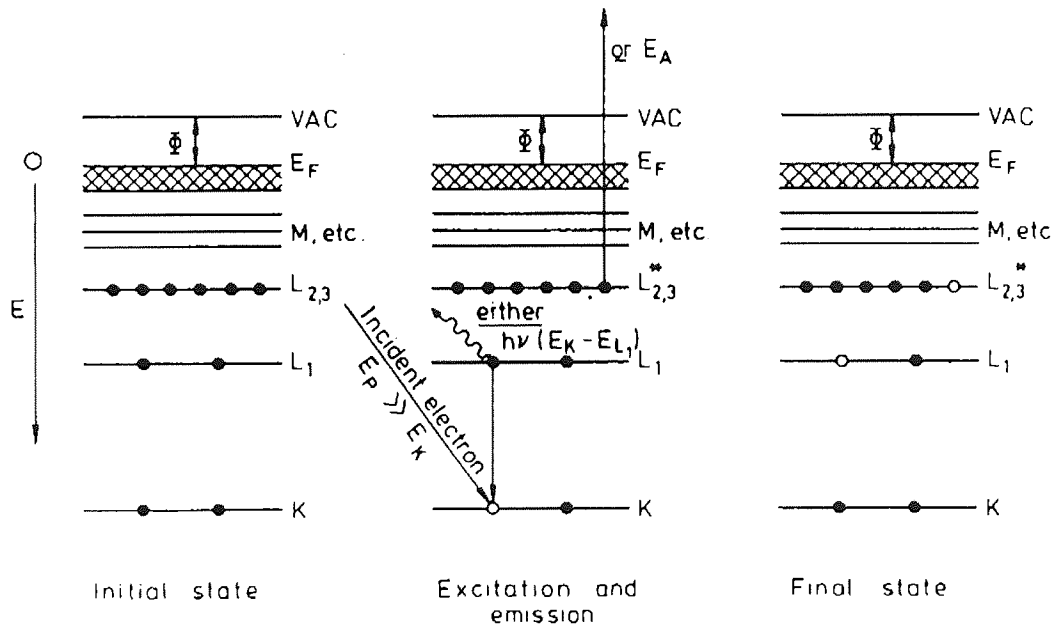

Figure 2-11 Schematic diagram of the process of Auger emission in a solid [147]

In Figure 2-11, the initial state of the system is shown at the left. In the centre an incident electron of energy E_p has created a hole in the core level K by ionisation; for this to occur efficiently E_p should be more than $5E_k$. The hole in the K shell is filled by an electron from L_1, releasing an amount of energy (E_k-E_{L1}), which can appear as a

photo of energy hν=(E_k-E_{L1}) or can be given up to another electron. In this example the other electron is in the $L_{2,3}$ shell, and it is then ejected with energy (E_k-E_{L1}-$E^*_{L2,3}$); $E^*_{L2,3}$ is starred because it is the binding energy not of $L_{2,3}$ in its ground state but in the presence of a hole in L_1. The energy of the ejected Auger electron in the example of Figure 2-11 is

$$E_{k/1/2,3} = E_k - E_{/1} - E^*_{/2,3} \qquad \text{Equation 2-11}$$

Two types of electron source are used in AES, the thermionic (LaB_6) and the field emission, with the former being much more common. After leaving the emitter the electron current has to be collected into a beam and then focused down an electron optical column. If E_0 is the incident electron beam energy, these energetic electrons can ionise atoms in the solid in core level X, which level subsequently de-excites by an electron falling from a higher level Y, the energy balance being removed by the ejection of an electron from level Z. This last electron, the so-called XYZ Auger electron, The emitted Auger electron is then detected by an electron spectrometer with transmission efficiency, $T(E_{AXYZ})$, and an electron detector of efficiency, $D(E_{AXYZ})$. Thus, the Auger electron current, I_{AXYZ}, may be written with some simplification[147]:

$$I_A = I_0 \gamma \sigma_A(E_0) \sec\alpha[1 + r_m(E_{A,}\alpha)]T(E_A)D(E_A)\int_0^\infty N_A(z) \times \exp[-\frac{Z(E_A)}{\lambda_m}\cos\theta]dZ$$

Equation 2-12

Where I_0 is the primary electron beam current and $N_A(Z)$ is the A atom distribution with depth Z into the sample surface. E_0 the energy of incident electron beam, Where θ is the angle of emission from the surface to normal, $r_m(E_{A,}\alpha)$ the back-scattering term, is dependent on the Matrix M in which the A atoms are embedded and the angle α to the surface normal of the incident electron beam; The emitted Auger electron is then detected by an electron spectrometer with transmission efficiency $T(E_A)$; $D(E_A)$ is an electron detector of efficiency; λ_m is the attenuation length in the matrix; $\sigma_A(E_0)$ is the total ionisation cross-section for the A atoms; The ionised core level X decays with a γ probability of Auger electron emission through the XYZ transition.

Practically the method to acquire the element composition in Auger is using the similar method as XPS – peak area combining relative sensitivity factor.

Scanning Auger Microscopy enables images of the elements in the near surface layer of conducting samples to be acquired. SAM (Scanning Auger Microscopy) is a combination of the techniques of SEM and AES. An electron beam is scanned over the surface and the electrons excited from the surface are energy analysed to detect Auger peaks. The intensity of the Auger peaks as a function of the position of the electron beam provides an image of the element to which the Auger peak corresponds. Usually a well-defined peak was chosen for the element of interest. Then the electron beam was raster-scanned over an array of points partitioning the selected area, the resultant image signal was determined by the following equation:

$$R = \frac{(P - B)}{B} \qquad \text{Equation 2-13}$$

R is the signal density of the resultant image, P is the peak energy of the selected element peak, B is the energy of adjacent background. The results of R were computed by the computer to present the mapping of the detected element. As for AES, the near surface layer typically means the first 2 or 3 atomic layers of the surface. Scanning AES allowed mapping on a selected surface area the occurrence of a given element.

It is normal to operate AES at a constant relative resolution. A typical resolution used would be 2.5×10^{-3}, under which condition the absolute resolution in the middle of the energy range at, say, 500eV kinetic energy would be 1.25eV,which is quite adequate.

In AES the only function of the incident electron beam is the ionisation of core levels to initiate the Auger process. For this purpose the precise energy in the beam is unimportant, provided it is high enough to ionise all core levels of interest with efficiency both high and uniform.

The charging and carbon contamination are the two undesirable effects in AES. Charging is caused by the accumulation of electrons brought by the incident electron beam in the insulating parts of the samples. Charging could lead energy shift, peak

broading and distortion on the collected spectra or element map. This charging caused instability and noise of the spectra. Charging could be reduced by reducing the acceleration voltage and current of the electron beam, it had been found essential to mount the sample at a grazing angle with respect to the electron beam, which increases the secondary electron emission from the sample[147]. Another technique has been used to reduce sample charging by providing better electronic contact to the sample[147]. Carbon contamination is sample exposition to the electron beam, ion etching is the normal way to remove the carbon contamination, but great care needed to not remove the stains on the heads or other element you are interested to analyse.

2.3.3 AFM

Atomic Force Microscope (AFM) was developed by Gerd Binnig et al. in 1985. It is capable of investigating surfaces of scientific and engineering interest on an atomic scale[158,159]. The AFM relies on a scanning technique to produce very high resolution, three-dimensional images of sample surfaces. AFM measures ultra small forces (less than 1nN) present between the AFM tip surface mounted on a flexible cantilever beam, and a sample surface.

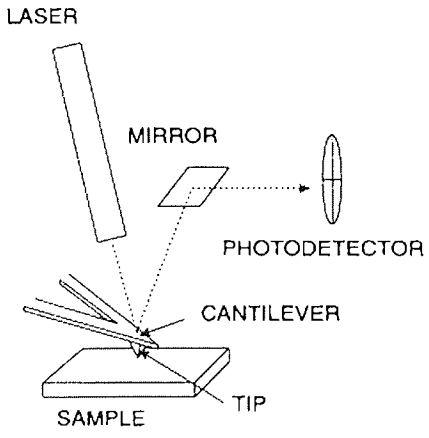

Figure 2-12 Principle of AFM[160]

The Thermo microscopes Auto-probe M5 is the AFM used in this research work. The major scanning system is sitting on the air table. The detail of scanning head and tip could be seen in Figure 2-12. The scanning tip is directly under the scanning head. A cantilever beam with a spring constant of about 1 N/m or lower is desirable. Tips have to be as sharp as possible. Tips with a radius ranging from 10 to 100 nm are commonly

available[161]. All the systems are sealed in an isolated chamber to prevent the interfering from outside.

Typical Atomic Force Microscopy (AFM) is comprised of a sensing probe, piezoelectric ceramic, a feedback electronic circuit, and a computer for generating and presenting images[160]. A tip is mounted on the cantilever such that, when the cantilever moves, the light beam from a small laser moves across the face of a four-section photo detector (see Figure 2-12). The amount of motion of the cantilever can then be calculated from the difference in light intensity on the photo sectors.

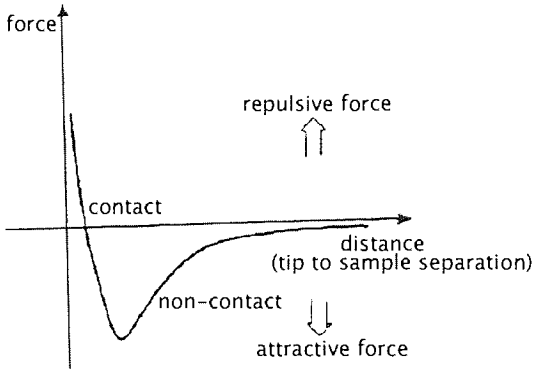

Figure 2-13 Interatomic force vs. distance curve[160]

Figure 2-13 shows an interatomic force vs distance curve, which illustrates the force between atoms on a cantilever tip and atoms on a sample surface vs. the separation distance between the tip and the sample. AFM is working on precisely measuring the force between the tip and sample.

Hooke's law gives the relationship between the cantilever's motion, x, and the force required to generate the motion, F.

$$F = -kx \qquad \text{Equation 2-14}^{160}$$

It is possible to fabricate a cantilever with a force constant, k, of 1 Newton/meter. Since motion of less than 1 angstrom can be measured, force less than 0.1 nano-Newton are detectable.

The control of the AFM sensor over extremely small distances is made possible by the use of piezoelectric ceramic. These materials are constructed such that a change in their

physical dimensions occurs when an electric field is applied. Ceramics are fabricated into a variety of shapes and configurations. Each type of ceramic has a unique expansion coefficient that allows the calculation of physical distortion upon the application of a potential. The coefficients range from 1 angstrom/volt up to 3000 angstroms/volt. As a result, this ceramic permits the accurate positioning of the probe tip. For example, a ceramic with a 1 angstrom/volt expansion coefficient will move 0.1 angstrom when excited with a 100 millvolt potential source. Three discrete pieces of piezoelectric ceramic are mounted orthogonally. These create positive or negative scan motion in the X, Y, or Z directions as voltage is applied to the appropriate piezo (see Figure 2-14).

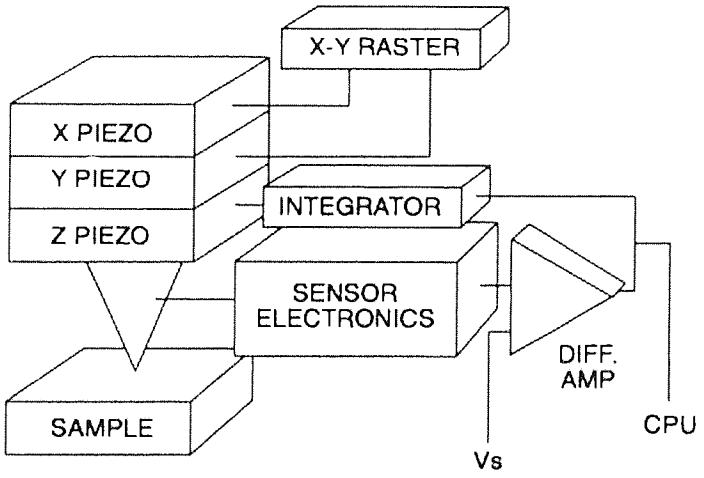

Figure 2-14 An AFM image of a surface is generated by rastering the sensor over the surface and storing the piezo driver signal on the computer

An electronic feedback circuit uses the output of the probe/sensor to drive the Z piezoelectric ceramic to create the Z-positioning mechanism. The error signal is the difference between the sensor signal and a user-defined set point. The feedback response is based on an equation which combines terms proportional to the error signal, the integral of the error signal, and the derivative error signal to set the Z position of the probe so as to maintain a constant sensor signal.

Imaging modes can be classified as "contact"(repulsive forces) or "non-contact (attractive forces)" depending on the net forces between the probe and sample (see Figure 2-13). In the contact AFM method, the probe tip scans across the sample surface, coming into direct physical contact with the sample. Non-contact AFM is preferred to measure soft or fragile samples.

The Specifications and performance of Thermomicroscopes Auto-probe M5 are as follows: Scan range: Maximum lateral scan range is 100μm; Maximum vertical scan range is 7.5μm. Scanner resolution: Maximum lateral resolution: 0.25Å, Maximum vertical resolution: 0.025Å.

2.3.4 Optical Microscopy

Olympus optical microscopy was used to examine the head surface before and after wear. There is an Olympus digital camera fitted on the optical microscopy. So the images of the head could be taken and stored in the computer.

The maximum magnification of the Olympus optical microscopy is 400 times, the optical images clearly show the 1μm objects, such as the grains of the ceramic and the pole and shared pole of the heads. The brown Fe stain on the pole and some tape debris on the heads could be clearly identified.

2.3.5 Indentation and wear measurement

Indention is mostly used to determine the hardness of materials; this method involves the formation of permanent (plastic) indentations on the surface of the material to be tested. The hardness number being determined by the normal load divided by either the curved surface area (Brinell hardness number and Vickers hardness number) or the projected area (meyer hardness number, Knoop hardness number and Berkovich hardness number) of the contact between the indenter and the material being tested under load[162].

Indentation tests differ with regard not only to the shape of the indenter (ball, cone, or pyramid) but also to the load range employed. The Knoop indenter is a rhombic-based pyramidal diamond with longitudinal edge angles of 172.5° and 130°. If L is the long diagonal in millimetres, W is the imposed load in kilograms, Knoop hardness number (K or HK) is given by the load divided by the projected area of the indentation, that is,

$$HK = 14.229W / L^2 \qquad \text{Equation 2-15}^{162}$$

The long diagonal and depth of the indention has the following relation:

$$L = 30.5d \qquad \text{Equation 2-16}^{162,163}$$

The forces used in indentation were carefully chosen. Higher force would crack the head AlTiC surface while smaller force would not make an indent big enough to measure preciously and last for several thousands kilometres tape cycling.

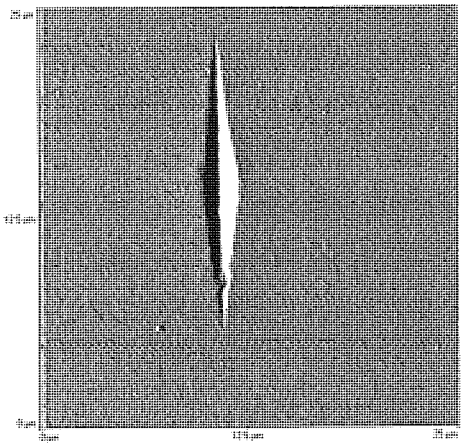

Figure 2-15 AFM image of a typical indentation made on the ceramic (AlTiC) surface of LTO head (25μm×25μm)

Figure 2-15 is a typical indentation on the LTO head ceramic part (AlTiC) of the head surface. As the material wears, the depth (d) of the indentation decreases, but the ratio L/d remains constant effectively giving a wear magnification of the order of 30 times. By measuring the diagonal-length periodically during the wear test using AFM, the depth of materials removed from the surface can be calculated. Great care is required in using the AFM because of the relatively small changes in the diagonal-length during the wear test. For each indent, multi measurements were employed to obtain good statistical results.

2.4 Experimental Materials

2.4.1 Travan5 Head

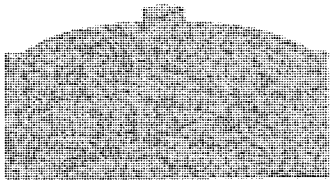

Figure 2-16 Schematic diagram of Travan5 head in the perpendicular direction to the tape moving direction

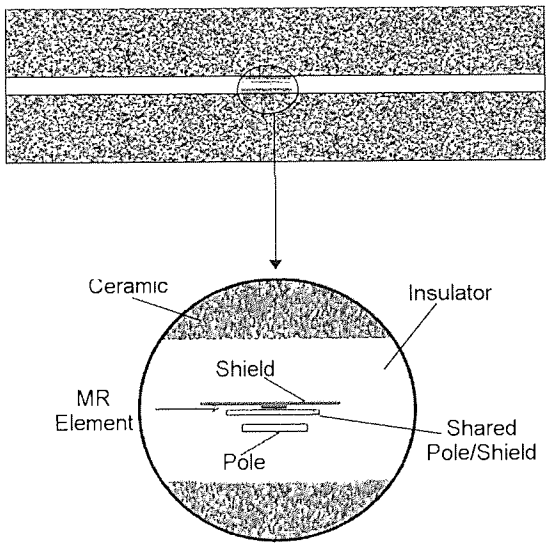

Figure 2-17 Schematic diagram of Travan5 head

Figure 2-16 and Figure 2-17 show schematic diagrams of a Travan5 thin film head and the main constituent parts. The pole, shared pole/shield and shield are each constructed from cobalt-zirconium-tantalum (CoZrTa) amorphous film, around the CoZrTa thin film is the rf- sputtered Al_2O_3 insulator. The insulator consists of low temperature sputtered Al_2O_3. The thin-film structure is sandwiched between a two-phase, much harder ceramic (Al_2O_3-TiC). The coils and leads in the thin film heads are copper. The ceramic substrate is manufactured from non-magnetic alumina-titanium carbide (Al_2O_3-TiC) which is a two phase material consisting of approximately 70 wt% alumina (Al_2O_3) and 30 wt% titanium carbide (TiC). It is a hot isostatically pressed, high-density ceramic materials. Grain size of TiC is limited to 1-1.5μm. TiC particles are added to Al_2O_3

limits the Al_2O_3 grain growth in the matrix during sintering. This results in a higher strength and hardness, but also can retard crack propagation[164]. The magneto resistive (MR) element is Permalloy (Ni-Fe). Table 2-5 shows the ceramic materials properties involved in the head materials and also some related other materials.

Materials	Crystalline Structure	Density Kgm^{-3}	Knoop micro hardness Gpa ($kgmm^{-2}$)	Fracture Toughness (K_{1c}) $MPa{\cdot}m^{1/2}$	Thermal Conductivity $Wm^{-1}K^{-1}$	Electrical Resistivity $\mu\Omega$ cm	Melting or Decomposition Temperature/ Operating Temperature C°/ C°
TiC Metallic ceramics	Cubic f.c.c	4,920	27.5 (2800)	4.0	27	60	3065/700
Al_2O_3 (ionic) oxides	Hexagonal	3,980	20.4(2100)	4.9	35	10^{20}	2050/1800
Covalent: diamond	Cubic	3,515	78.4-102.0 (8000-10,400)	_	900-2100	10^{13}-10^{26}	3800/1000
SiO_2(fused Silica)	Amorphous	2,200	5.4-7.4 (550-750)		1.2	10^{15}-10^{18}	1650/575
Cr_2O_3	Hexagonal	5,210	12.7(1300)		7.5		2300/1000
TiO_2	rutile or cassiterite structure	4,000	7.0-10.0		6.7		1800/1000

Table 2-5 Selected properties of ceramic[162, 165]

2.4.2 Travan5 tape

Travan5 tape used in this study was double layer Metal Particles tape. Every tape cartridge had 200 m length of tape. The compressed capacity of Travan5 tape was up to 20 GB, Native Capacity Up to 10 GB. Native Sustained Transfer Rate up to 60 MB/min Compressed Sustained Transfer Rate up to 120 MB/min.

The magnetic particles are contained within a polymer binding system; this has commonly been a polyester polyurethane copolymer. The filled polymer in his case is complicated and consists not only of the magnetic pigment (at up to 80% by weight, 50% by volume) and the polymer binder, but also a head cleaning agent (HCA) (typically about 4 to 8% by weight of Al and Zr oxide) and a possible combination of wetting agents, cross linking agents, solvents, anti-fungal agents, carbon black (to prevent surface charging) and finally the essential lubricant (typically fatty acid/fatty acid esters). The coercivity of the metal particle is around 1650 Oe. The mean particle length is on the order of 100nm[27]. Acicular particles with an aspect ratio are about 3 to

4. The passivated metal (Fe) acicular particles (MP media) are widely used to achieve higher recording densities. MP materials were developed for magnetic recording because of their high coercivity and magnetization intensity. The magnetic coating is on the surface of PET material. The detail property of PET material could be found in Chapter one.

Fe Particles of current interest are acicular in shape; approximately half of the particle volume is typically taken up by the passivation shell, which appears to contribute little or nothing to the magnetic properties. Commercial iron particles[28] had an oxide layer with an average thickness of 5nm.

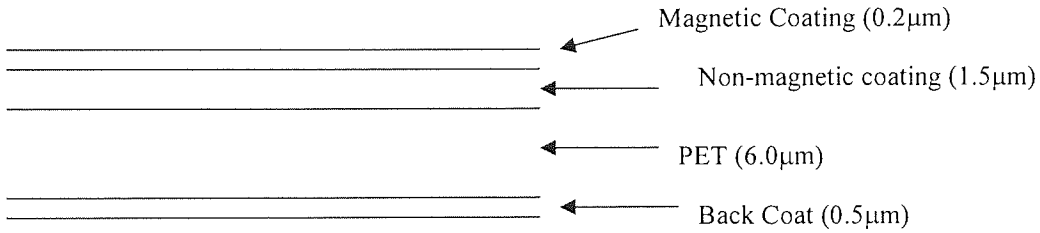

Figure 2-18 Schematic diagram structure of Travan5 double layer MP tape

Figure 2-18 shows Travan5 double layer metal particulate magnetic tape, from the top of the tape, the first layer was composed of metal particles with Head Cleaning Agent, lubricants, and binder materials. The under layer was composed of non-magnetic α-Fe_2O_3 fine particles with thickness around 1.5μm. This non-magnetic layer provided a much better smooth surface for the magnetic layer to deposit and in the same time reserved some lubricants for the magnetic layer. This double layer tape can achieve a smooth surface more easily than a single layer MP and have a low friction coefficient because it has enough free lubricant in the coating layer[166].

2.4.3 LTO Head

Linear Tape-Open Technology (LTO) combines the advantages of linear multi-channel bi-directional tape formats in common usage today with enhancements in the areas of timing based servo, hardware data compression, optimised track layouts and high efficiency error correction code to maximize capacity and performance.

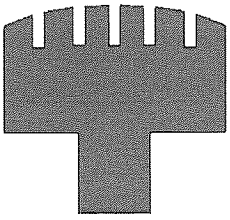

Figure 2-19 Schematic diagram of two rails and slots in the perpendicular direction to the tape moving direction

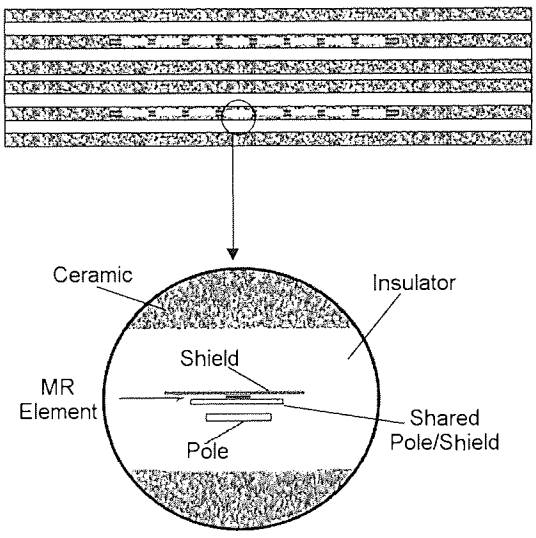

Figure 2-20 Schematic diagram of two rails and enlarged, one channel of a LTO head

Figure 2-19 and Figure 2-20 show schematic diagrams of a LTO thin film head and the main constituent parts. Each LTO head has two rails; each rail has eight channels for reading and writing the data. The head materials used in LTO heads are exactly the same materials as those used in the Travan5 head, but the head structure is different. In order to increase the recording density and reduce the contact pressure, the LTO system adopted the multi-channel and slots technology[46]. This reduces the head-tape spacing due to the negative pressure between the head and tape.

LTO heads are thin film heads, the read head is magneto resistive (MR) type and the write head is inductive. The write coil (inside) generates the magnetic flux in the write pole and shared pole, and the field generated between the write pole and shared pole writes information on a tape. The layers between write pole and shared pole define the write gap (typically 1μm); it determines the linear density of writing. The read element

is between the shield and shared pole, the shield and shared pole protect the MR element (Permalloy), MR element can read only when information is between the shared pole and shield. The distance between the shared pole and shield is referred to as read gap; it determines the linear density of reading.

2.4.4 LTO tapes

	LTO Fuji Tape	LTO Imation Tape	LTO Maxell Tape	LTO Mp1 Tape	LTO Mp3 Tape
Tape type	Commercial Ultrium 1 tape	Commercial Ultrium 1 tape	Commercial Ultrium 1 tape	Specially produced tape	Specially produced tape
Dual layer tape	yes	yes	yes	yes	yes
Metal particle length	100nm	100nm	100nm	100nm	50nm
Binder materials	Urethane and vinyl chlorine	Urethane and vinyl chlorine	Urethane and vinyl chlorine	Urethane	Urethane and vinyl chlorine
Cartridge Capacity	100 GB	100 GB	100 GB	100 GB	100 GB
Tape length	609 m	610 m	609 m	600 m	609 m
Tape width	12.65mm	12.65mm	12.65mm	12.65mm	12.65mm
HCA	Al oxide	Al oxide	Al oxide	Al and Zr oxide	Al oxide
Coercivity Hc	2200Oe	2200Oe	2200Oe	1650Oe	2540Oe
Substrate Thickness	6μm.	6μm	6μm	6μm	6μm
Magnetic Coating Thickness	0.15μm.	0.15μm.	0.15μm.	0.20μm.	0.15μm.
Lubricant	Unknown	Unknown	Unknown	Unknown	Unknown

Table 2-6 LTO tapes used in the experiment

The Ultrium format drives were employed to test the wear of the heads and different LTO tapes in this research project. Five different dual layers LTO Ultrium format MP tapes were used through out these experiments are shown in Table 2-6. The LTO tape has a magnetic layer of about 0.2μm thickness, under which is a nonmagnetic layer of about 1.5-2.0 μm thickness of acicular alpha iron oxide particles, then the substrate usually the PET or PEN, although substrate is normal 6μm thickness, usually PET or PEN, The one difference between PET and PEN is that the substrate of PET film might be a little less stiff than PEN[167]. The structure of these LTO tapes used in these experiments is quite similar with Travan5 tape, but the materials involved in LTO tapes are different such as binder materials, size of MP particles etc except LTO Mp1 tape which is quite similar with Travan5 tape.

Due to the commercial confidentiality, the manufacturers did not provide the full details of materials used in the different tapes. The normal tape materials have already been introduced in Table 2-6. The Mp1 tape materials were the similar tape materials as Travan5 tape as manufacturer informed. Between the LTO Fuji Tape, LTO Imation tape and LTO Maxell tape, the lubricant level and materials varied. But the materials involved in these LTO tapes were unknown. For LTO Mp3 tapes are quite similar with LTO Imation tape except the Fe metal particles inside Mp3 tape are smaller than Imation LTO tape. Typical LTO tape thickness is around thickness 8.5 μm. Lubricant normally used inside the tape, but what kind of lubricant used were not known due to confidentiality.

2.5 Experimental Methods

2.5.1 Travan5 Experiment Procedures

Commercially available Travan5 cartridges were used throughout the experiments. Tapes were cycled for 5000 passes in custom built Travan5 drives located in the Votsch environment chamber, for each of the conditions detailed in Table 2-7. One pass consisted of the tape moving forward from the beginning to the end of the tape, the next pass was the tape rewinding from the end to the beginning. Each pass represented the passage of 200 m of tape. The tape speed during operation was 2.3ms^{-1}, the normal operating speed for standard drives. An unused head and tape was utilised for each experiment. Three drives were run at each series of environmental conditions to improve reproducibility of results.

Environmental Conditions	Tape Type	Number of Tapes Heads	Tape Speed	Tape Tension	Running Time (Hours)	Analysis Methods
15°C/RH15%	Travan5 Dual layer MP Tapes	Each condition used three virgin tapes and three unused Travan5 heads	Fixed 2.3m/s	Fixed 0.6N	Each experiment needs 127 hours	AFM and XPS for tapes AFM and AES for Heads
5°C/RH80%						
40°C/RH15%						
22°C/RH40%						
40°C/RH30%						
40°C/RH45%						
40°C/RH60%						
40°C/RH75%						
40°C/RH80%						

Table 2-7 The Travan5 experimental condition

Modified Travan5 drives were used in this research project, every time unused Travan5 heads were installed prior to commencing any of the cycling experiments. Travan5 head could be easily installed or removed from the drive (by adjusting four screws in the actuator inside the drive, see Figure 2-1), after connect the drive to the power supply (5V, DC), inserting the tape, it automatically begins to run. A photo detector in the drive could sense the end of the tape (at end of tape, there is a hole inside the tape). Then the drive stops, the head move to a new position and a new cycling begins in the opposite direction until the power was turned off. The cycling time (see Table 2-7) for a typical

experiment was obtained from calculation and tape cycling time measurement. The nominal tape tension was 0.6 N. More information about Travan5 drives could be seen in experimental platform section of this chapter.

The unused head was initially lapped with a diamond film and then tested with normal tape for quality assurance.

Examination of the tape samples was performed by means of X-ray Photoelectron Spectroscopy (XPS) in a VG ESCALAB 200D electron spectrometer equipped with a HSA energy analyser. Mg K_α X-radiation was employed for the XPS examination, at a source excitation energy of 14KeV and emission current of 20mA. The area of analysis was chosen to be 2mm x 3mm for each tape analysis. The centre and edge of tape were analysed separately.

Survey scans were first recorded for all samples at analyser take-off angles of 0^0 and then narrow region energy scans were collected for all the elements identified on the surface at 0^0 take-off angle. Analyser pass energy of 20eV with step size of 0.1eV and dwell time of 100ms was used throughout. Relative atomic concentrations were calculated for each sample from the intensities of the major photoelectron spectral lines by means of codes incorporated in the VG Eclipse V 2.0 instrument data system.

Auger electron spectroscopy (AES) was used to analyse the heads due to the small size of the areas being studied. AES enabled elemental compositions to be determined at different points on the surface of the heads with micron resolution. For the ceramic or insulator region, AES was performed using an area of 30 μm^2 otherwise point analysis was used. The Auger elemental images were collected for some head samples.

The base pressure within the spectrometer during examinations was always better than 8 x 10^{-10} mbar and this ensured that all signals recorded were from the sample surface and not due to system contamination.

Topographical information regarding the physical structure of the Travan5 heads and tapes was obtained using a ThermoMicroscope AFM operated in contact mode. Image enhancement was restricted to the use of shading and levelling algorithms. The contact

force was 10.8 nN, the scanning rate was 1.0 Hz. The AFM instrument was calibrated using standard samples. The scanning direction of AFM was from left to right.

Various methods for measuring Pole Tip Recession (PTR can be seen in Chapter one) via AFM have been employed, usually dictated by the software available with the AFM. The method[168] used for this research project required that a 0^{th} order Flatten be applied to the raw image. Secondly a 2^{nd} order XY plane fit auto on the AlTiC surface in the AFM image fast scan direction was applied. The profile of the head generated by the AFM has two curvature components: 1) the form of the head; for the Travan5 head the head radius is 2.28mm. 2) The bow created by the AFM scanner. If the tape was assumed to follow the form of the head, then the AlTiC on both sides of the alumina could be used to generate a profile or surface that could be subtracted from the entire image. This subtraction not only subtracted the head form, but also subtracted the scanner bow (which is generally uniform here). A second order plane fit provided the ability to subtract an sphere/parabola from the image. Actually the pole and shared pole recession were not generally equal, in this case, the PTR was taken for the more deeply recessed pole or shared pole[169].

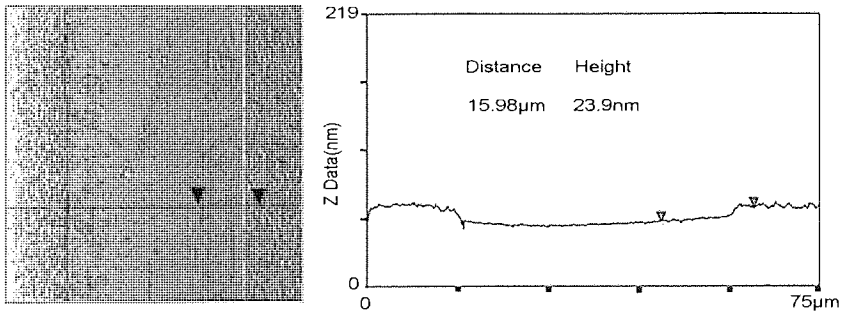

Figure 2-21 the AFM image show Pole Tip Recession measurement for unused head

Figure 2-21 shows Pole Tip Recession measurement for unused head after software processing the raw AFM image. A scan rate of 0.4-1 Hz was used and 512 data points were collected along each of the 512 scan lines. Great care must be taken in obtaining raw data from AFM. It is common to have electrostatic forces to deal with in AFM. Charge build-up on heads, e.g. in regions of highly insulating materials, can cause large forces on AFM tips, giving false topographic output. Use of a static eliminator device,

which ionizes the air surrounding the sample, could reduce and usually eliminates this problem.

2.5.2 LTO experiment Procedures

Tapes were cycled for certain passes in custom built LTO drives located in the Votsch environment chamber, Table 2-8 includes the LTO experiments carried in this research project and the experimental condition involved in the experiments. Detail information of LTO drive could be obtained in the experimental platform section in this chapter.

LTO Tape Type	Environmental Conditions	Number of Tapes Heads	Tape Speed (fixed)	Tape Tension (fixed)	Analysis Methods
LTO dual layer Fuji Tapes	10°C/RH10%	Each condition three virgin tapes and three unused heads	2.3m/s	0.8N	XPS, AFM for tapes AFM, AES for heads
	40°C/RH15%				
	22°C/RH40%				
	40°C/RH80%				
LTO dual layer Imation Tapes	10°C/RH10%	Each condition three virgin tapes and three unused heads	2.3m/s	0.8N	XPS, AFM for tapes AFM, AES,XPS for heads
	40°C/RH15%				
	22°C/RH40%				
	40°C/RH80%				
LTO dual layer Maxell Tapes	10°C/RH10%	Each condition three virgin tapes and three unused heads	2.3m/s	0.8N	XPS, AFM for tapes, heads AFM, XPS, AES for heads
	40°C/RH15%				
	22°C/RH40%				
	40°C/RH80%				
LTO dual layer Mp1 Tapes	10°C/RH10%	Each condition three virgin tapes and three unused heads	2.3m/s	0.8N	XPS, AFM for tapes AFM, AES for heads
	40°C/RH15%				
	22°C/RH40%				
	40°C/RH80%				
LTO dual layer Mp3 Tapes	10°C/RH10%	Each condition three virgin tapes and three unused heads	2.3m/s	0.8N	XPS, AFM for tapes AFM, XPS, AES for heads
	40°C/RH15%				
	22°C/RH40%				
	40°C/RH80%				

Table 2-8 The LTO experiment table

Environmental Condition	10°C/ 10% RH	40°C/ 15% RH	22°C/ 40% RH	40°C/ 80% RH
Normalised Water Content (NWC)	1.0	6.7	7.5	35.5

Table 2-9 Environmental conditions used in the LTO experiments with Normalised Water Content (Normalised to 10°C, 10%RH)

The effect of water vapour on the tribology of these systems is very important. The actual water content (termed normalised water content (NWC)) on the head/tape interface of the LTO system was present in Table 2-9.

Communication with the LTO drives and computer was established using a macro computer language named Dexter (a computer language developed by Hewlett Packard to control the tape drive operation). This allowed various tasks including tape cycling and error rate tests to be performed; also, the head position could be set at any point across the width of the tape[170, 171]. The format specification divides the full tape width into four data bands. The tape head spans one band, and fills each data band sequentially[170, 171]. At the top and bottom of each data band is a servo band. The servo bands provide location information to the head as it writes and verifies data tracks within that band. The process of positioning the head on the tape is an interaction between the head, the media, and the servo elements of the system. To simulate the serpentine motion of a head across a tape the head was placed at four positions (four bands evenly) across the width of the tape during cycling[171].

For the first generation of LTO system, there are eight channels either side of the LTO head (see Figure 2-20), as the tape moves beneath the head, the one side eight elements write the data to the tape. When the data passes the other eight elements, it is immediately checked for errors. If any errors are found, the block of data is rewritten farther down the tape.

An unused head and cartridge was used for each experiment. Three drives were run at each series of environmental conditions to improve the reproducibility of results. The tape speed during operation was $2.3ms^{-1}$. The tape tension was 0.8 N during the operation and the LTO head radius is 6.55 mm.

Tape Position /m	Number of Passes	Total Number of Passes Endured by Head	Total distance Endured by Head
600-400	100	100	20 km
200-400	900	1000	200 km
0-200	4000	5000	1000 km

Table 2-10. Breakdown of cycling experiments

The tape length in each cartridge was around 600m long. The availability of cartridges was limited so to generate tape samples for analysis, the 5000 passes of tape was divided as in Table 2-10.

Examination of the tape samples was performed as for Travan5 tape samples. XPS was also employed to analyse the head surface before and after wear test. Auger electron spectroscopy (AES) was used to analyse the heads as Travan5 heads did.

For time constraints, analysis of the heads was restricted to channels No4 and No7 of the left rail for every LTO head. For LTO experiments, the LTO Heads were removed after 100 passes, 1000 passes then at the end of the experiment, 5000 passes to do the head AFM scanning. The PTR of LTO head was obtained by the same method as in Travan5 experiments procedure.

In this research work, a Buehler Micromet4 microhardness indenter was employed to make indent on the surface of the heads to measure the wear rate, an indenter force of 50g, 25g, 10g and dwell time of 15s were applied to the ceramic area, insulator area and pole area individually. Detail indentation technology could be found in REF[162,163]. By carefully measuring the long diagonal of the indentation on the surface of the head before and after wear using AFM, the depth changes of the indentation could be obtained and in this way, the wear rate of the interested materials on the head surface could be found in the specific experimental condition.

2.5.3 AlTiC samples and LTO head boiling experiment

The unused head and unused AlTiC samples were ultrasonically-cleaned in Methanol for five minutes, then washed by de-ionized water before boiling.

Unused AlTiC samples and unused LTO Head were boiled in de-ionized water for 30 hours. The unused AlTiC samples and LTO heads were scanned by AFM and analysed by XPS before and after boiling.

3 Chapter 3 Experimental Results

This chapter presents the results obtained from Travan5 heads after Travan5 tapes cycling and Linear Tape Open (LTO) heads using different LTO tapes such as Fuji, Imation, Maxell, Imation Mp1 and Mp3. During each section, XPS and AES were extensively employed to analyse the chemical and physical changes in the head and tape surface. AFM was used to observe the head and tape topography including Pole Tip Recession, tape roughness, ceramic pullout, and stains on the surface of the heads. Optical microscopy was used to observe the stains and tape debris.

3.1 Experiment results of Travan5 heads with Travan5 tapes

In this section, the experimental results of Travan5 system are presented.

3.1.1 Travan5 head wear

3.1.1.1 Travan5 unused head

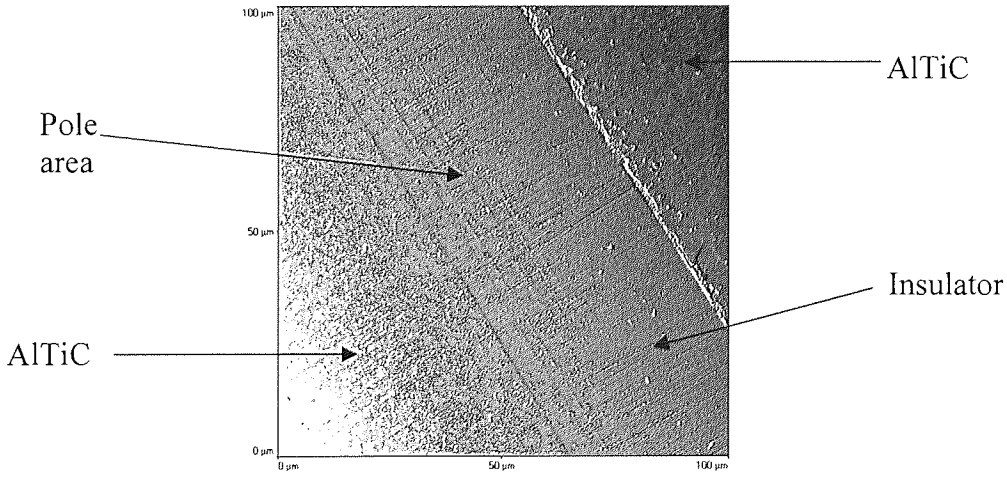

Figure 3-1 Travan5 unused head AFM image (100µm×100µm)

Figure 3-1 to Figure 3-5 show the typical topography of the unused Travan5 head. The typical pole area had about 2nm recession compared with surrounding insulator. The pole tip recession value was between 25nm to 28nm for the unused Travan5 heads. This initial PTR was results of differential wear that occurred in contour lapping during head manufacturing. Some of the unused heads were from the different batch products. Even in the same batch, the value of the PTR of the unused heads was not exactly the same.

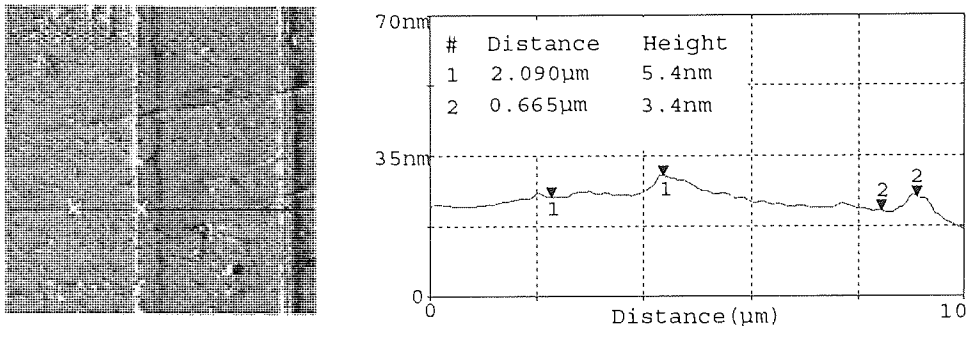

Figure 3-2 Travan5 AFM image showing unused head pole area (10µm×10µm)

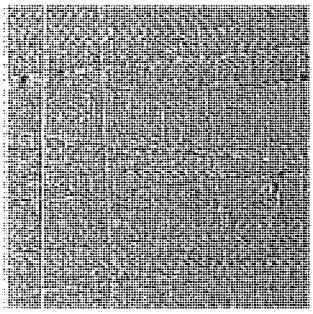

Area Ra	3.0 nm
Area RMS	3.5 nm
Avg. Height	13.3 nm
Max.Range	21.1 nm

Figure 3-3 Travan5 AFM image showing unused head insulator area (10µm×10µm)

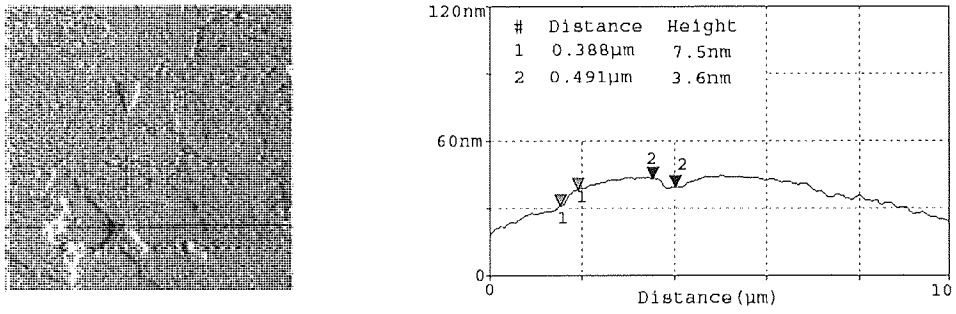

Figure 3-4 Travan5 AFM image showing unused head ceramic pole side (10µm×10µm)

The ceramic surface topography was measured by AFM. The recessed area corresponds to the AlTiC ceramic pullout or delamination; see Figure 3-4 and Figure 3-5. The distance of the deepest recessed area of the head AlTiC ceramic to the head tape-bearing surface (non recessed ceramic area) determined the greatest depth of the pullout.

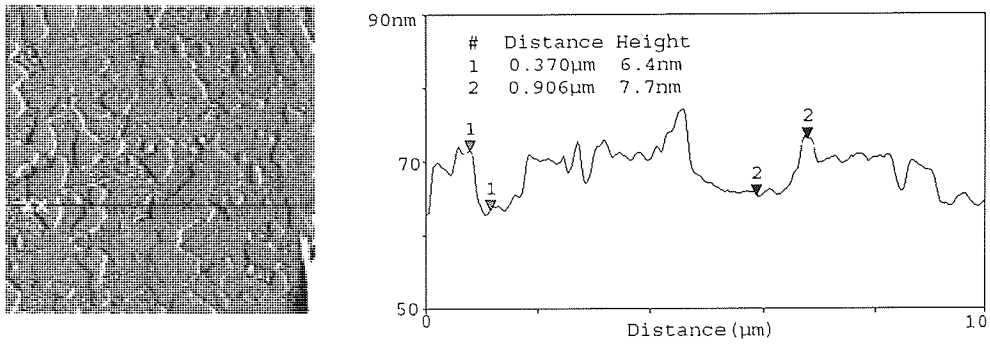

Figure 3-5 Travan5 unused head AFM image showing ceramic shield side (10μm×10μm)

The greatest depth of pullout in the virgin AlTiC ceramic area was around 5-7nm. The TiC grain size on the ceramic pole side was larger than the area in the ceramic shield side due to the materials used in manufacturer. The RMS roughness of the Al_2O_3 amorphous insulator area was around 3nm (RMS).

3.1.1.2 Travan5 Head Wear after 5k Passes at RH 80%, 5°C

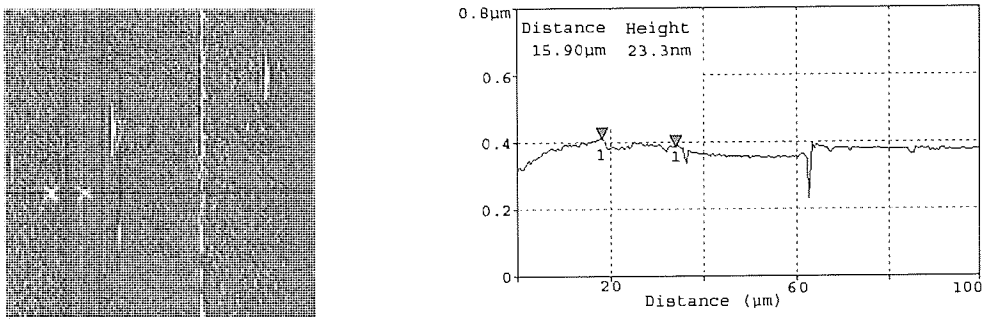

Figure 3-6 AFM Image of Travan5 head after RH 80%, 5°C, 5k Passes (100μm×100μm)

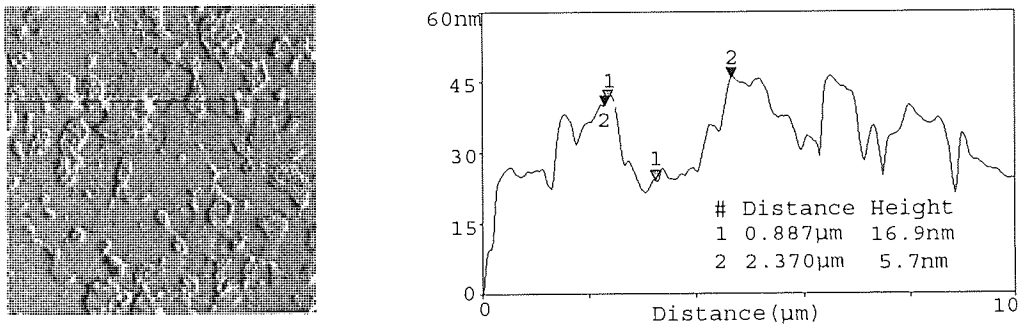

Figure 3-7 AFM image of Travan5 head ceramic shield side (RH 80%, 5°C, 5k passes) (10μm×10μm)

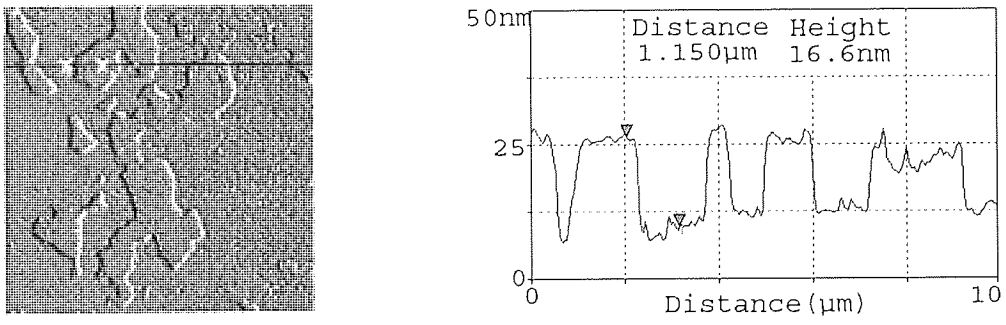

Figure 3-8 AFM image of Travan5 head ceramic pole side (5°C, 80%RH, 5kpasses) (10μm×10μm)

Figure 3-6 shows a typical example of Pole Tip Recession (PTR) measurement of a head after cycling 5k passes Travan5 tape cycling at RH 80%, 5°C experiment

condition. The average PTR was about 50nm (including 30nm thickness of stain, the thickness of the stain measurement will be shown in Figure 3-55).

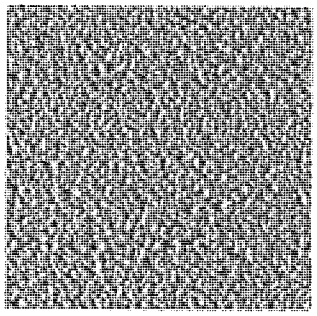

Area Ra	4.0 nm
Area RMS	5.0 nm
Avg. Height	23.1 nm
Max.Range	40.2 nm

Figure 3-9 AFM image of Travan5 head insulator (5°C, 80%RH, 5kpasses) (10μm×10μm)

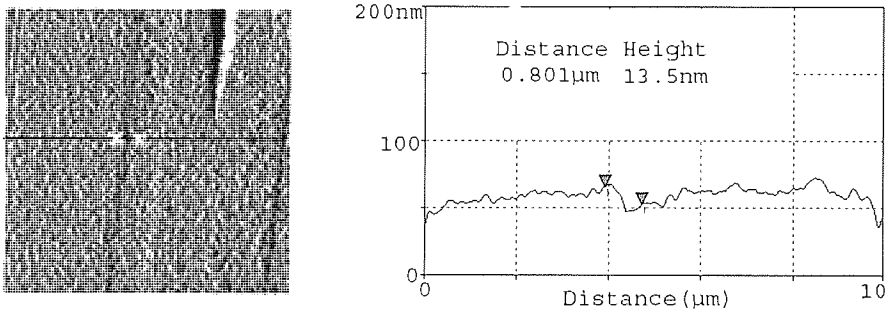

Figure 3-10 AFM image of Travan5 head pole (5°C, 80%RH, 5kpasses) (10μm×10μm)

Extensive stains covered the insulator area; the pole and shared pole were fully covered with stains. The greatest depth of pullout in the ceramic area was around 18nm. The pullout size on the ceramic pole side was larger than the area in the ceramic shield side due to larger TiC grain size on the ceramic pole side. The RMS roughness of insulator area was around 5nm (10μm×10μm scan), the amorphous insulator was always very smooth.

3.1.1.3 Travan5 Head Wear after 5k Passes at RH 15%, 15°C

Figure 3-11 shows a typical example of the PTR of the head at RH 15%, 15°C experimental condition. This was quite similar to the 5°C, RH 80% condition, the average PTR was about 50nm (including 30nm stain thickness), and some tape debris was found on the surface of the head. Pole and shared pole protruded slightly above with insulator. The depth of pullout in the ceramic area was around 21nm (see Figure 3-12 and Figure 3-13).

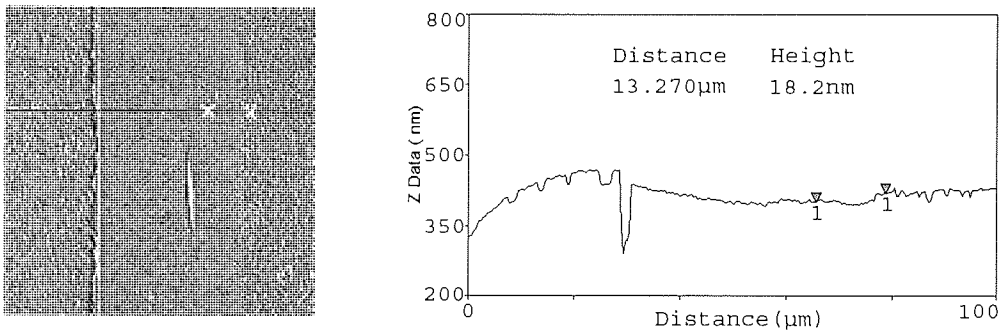

Figure 3-11 Travan5 head AFM image (15%RH, 15°C, 5k passes) (100µm×100µm)

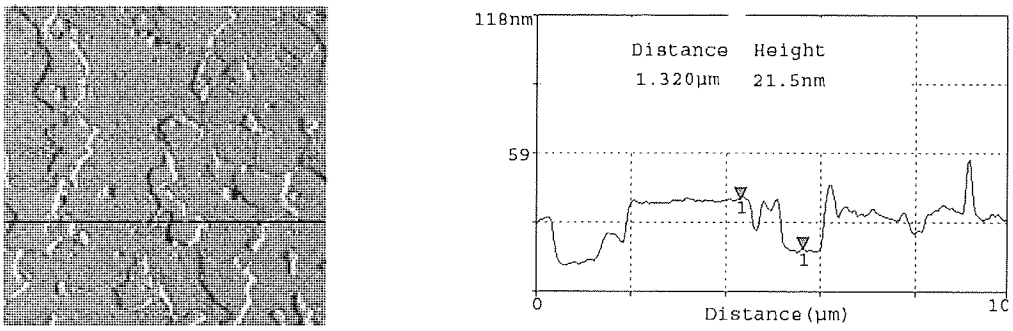

Figure 3-12 AFM image of Travan5 head ceramic pole side (15%RH, 15°C, 5k passes) (10µm×10µm)

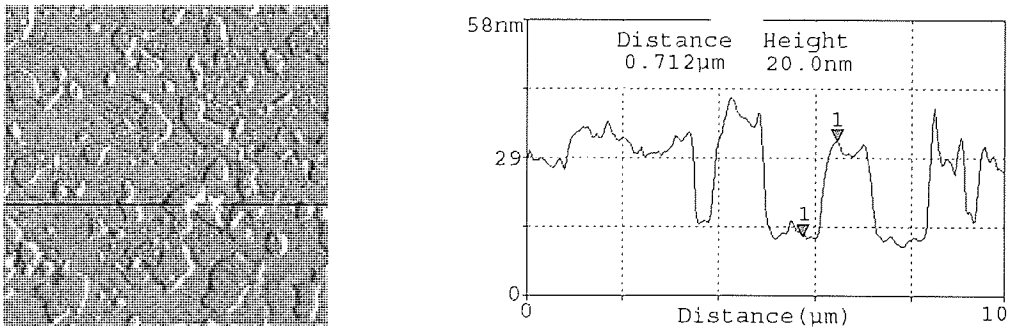

Figure 3-13 Travan5 head AFM image ceramic shield side (15%RH, 15°C, 5k passes) (10µm×10µm)

The RMS roughness of insulator area (Figure 3-14) was around 4nm (10μm×10μm scan). Figure 3-15 shows the pole and shared pole of the head. The poles in this case were not visible due to extensive stains.

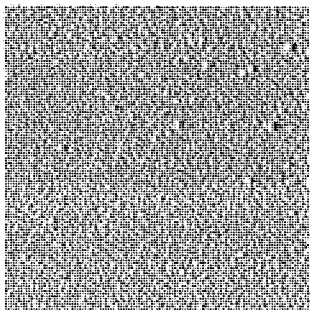

Area Ra	3.0 nm
Area RMS	3.9 nm
Avg. Height	14.9 nm
Max.Range	65.8 nm

Figure 3-14 Travan5 head AFM image insulator (15%RH, 15°C, 5k passes) (10μm×10μm)

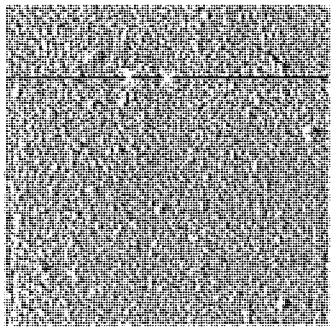

Figure 3-15 Travan5 head AFM image pole (15%RH, 15°C, 5k passes) (10μm×10μm)

3.1.1.4 Travan5 Head Wear after 5k Passes at RH 40%, 22°C

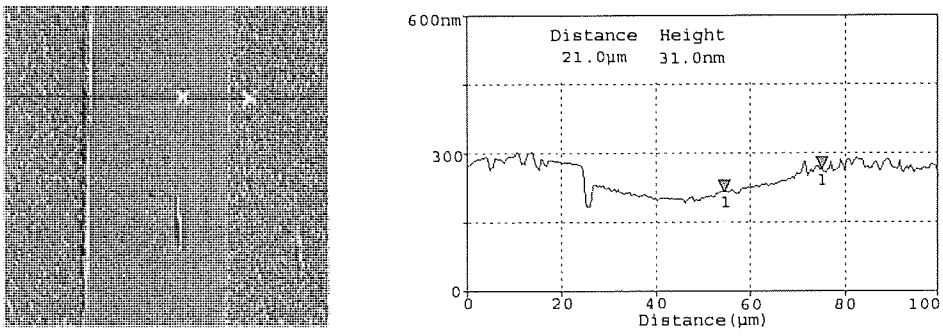

Figure 3-16 Travan5 head AFM image (40%RH, 22°C, 5k passes) (100μm×100μm)

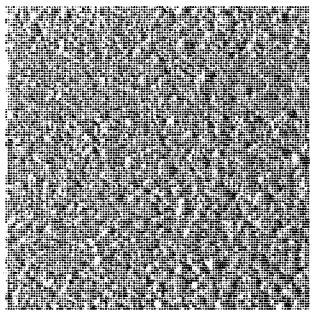

Area Ra	3.7 nm
Area RMS	4.4 nm
Avg. Height	17.5 nm
Max.Range	30.5 nm

Figure 3-17 Travan5 head AFM image insulator (40%RH, 22°C, 5k passes) (10μm×10μm)

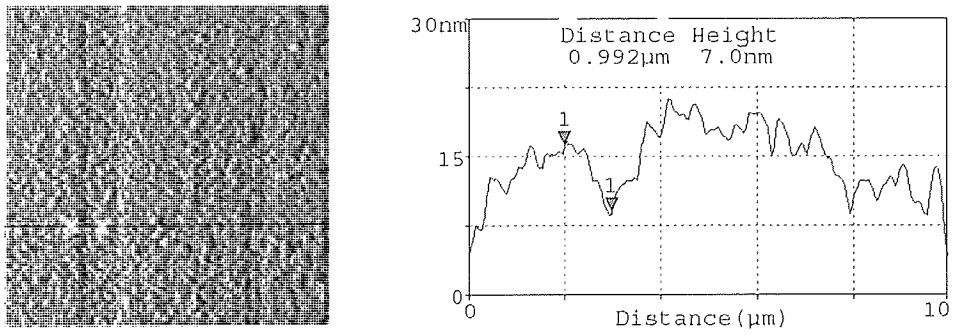

Figure 3-18 Travan5 head AFM image pole area (40%RH, 22°C, 5k passes) (10μm×10μm)

The PTR measurement at RH 40%, 22°C experimental condition was shown in Figure 3-16, the average PTR was 63nm (including 30nm stain thickness), pole and shared pole slightly protruded compared with insulator. The depth of pullout in the ceramic area was around 22-25nm (see Figure 3-19 and Figure 3-20). The RMS roughness of insulator

area was around 5nm (10μm×10μm scan). Extensive stain still was observed on the poles and insulator area.

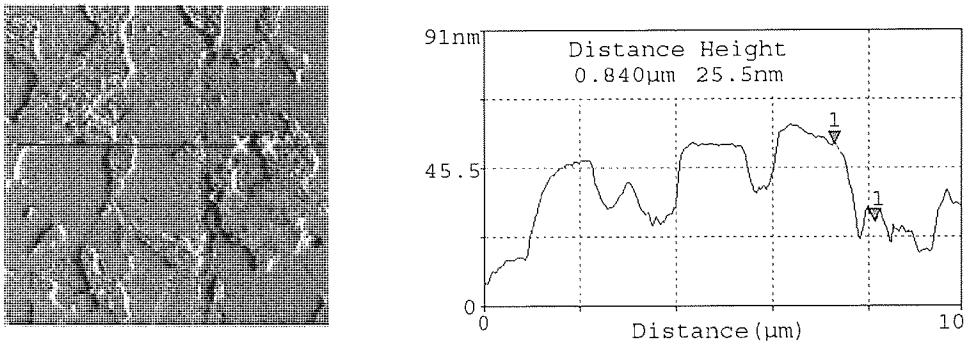

Figure 3-19 Travan5 head AFM image ceramic pole side (40%RH, 22°C, 5k passes) (10μm×10μm)

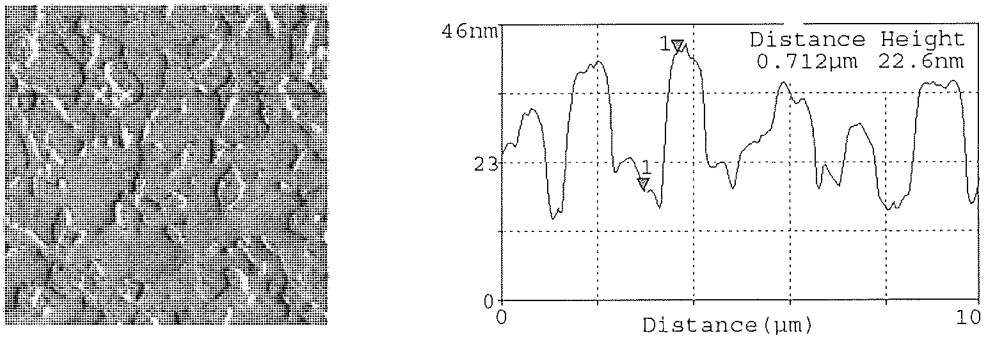

Figure 3-20 Travan5 head AFM image ceramic shield side (40%RH, 22°C, 5k passes) (10μm×10μm)

3.1.1.5 Travan5 Head Wear after 5k Passes at RH 15%, 40°C

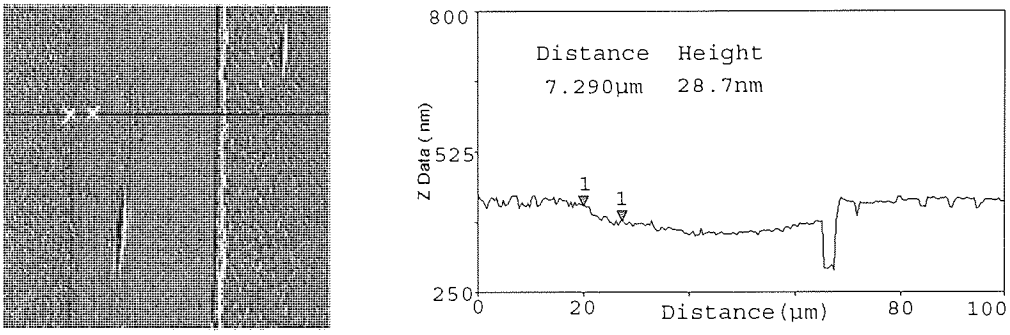

Figure 3-21 Travan5 head AFM image (15%RH, 40°C, 5kpasses) (100μm×100μm)

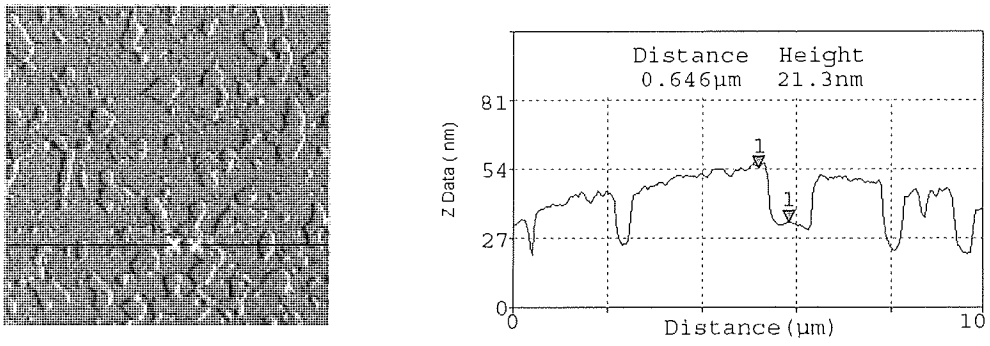

Figure 3-22 Travan5 head AFM image ceramic shield side (15%RH, 40°C, 5kpasses) (10μm×10μm)

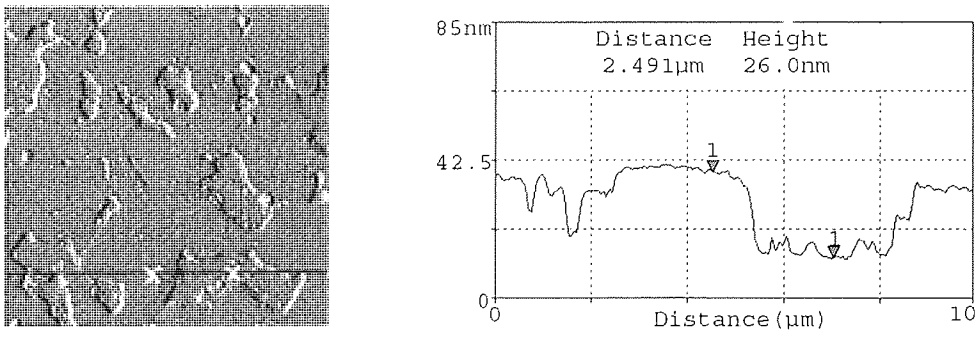

Figure 3-23 Travan5 head AFM image ceramic pole side (15%RH, 40°C, 5kpasses) (10μm×10μm)

At RH 15%, 40°C experiment condition, the average PTR was about 57nm (including 30nm stain thickness), some tape debris was found on the surface of the head, pole and shared pole slightly protruded above the insulator. The depth of pullout in the ceramic

area was around 23-25nm (see Figure 3-22 and Figure 3-23). The RMS roughness of insulator was around 7nm (10μm×10μm scan). It was difficult to observe the pole due to the stain covering.

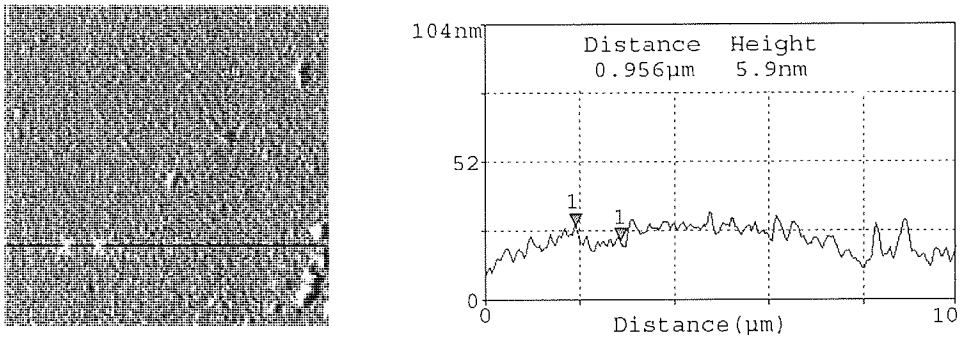

Figure 3-24 Travan5 head AFM image pole area (15%RH, 40°C, 5kpasses) (10μm×10μm)

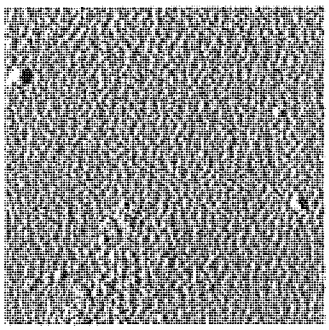

Area Ra	4.9 nm
Area RMS	7.0 nm
Avg. Height	32.9 nm
Max.Range	151.3 nm

Figure 3-25 Travan5 head AFM image insulator (15%RH, 40°C, 5k passes) (10μm×10μm)

3.1.1.6 Travan5 Head Wear after 5k Passes at RH 30%, 40°C

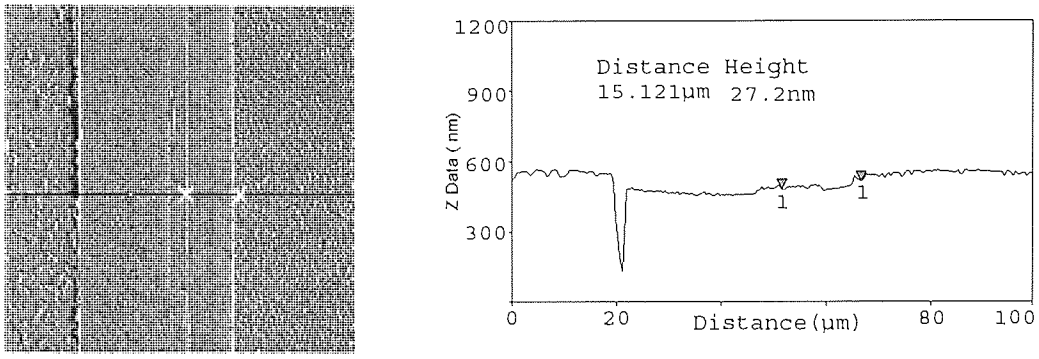

Figure 3-26 Travan5 head AFM image (30%RH, 40°C, 5k passes) (100µm×100µm)

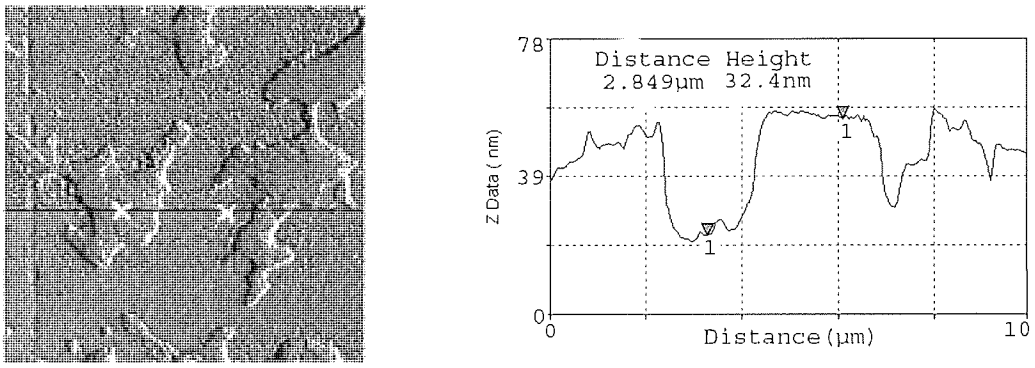

Figure 3-27 Travan5 head AFM image ceramic pole side (30%RH, 40°C, 5k passes) (10µm×10µm)

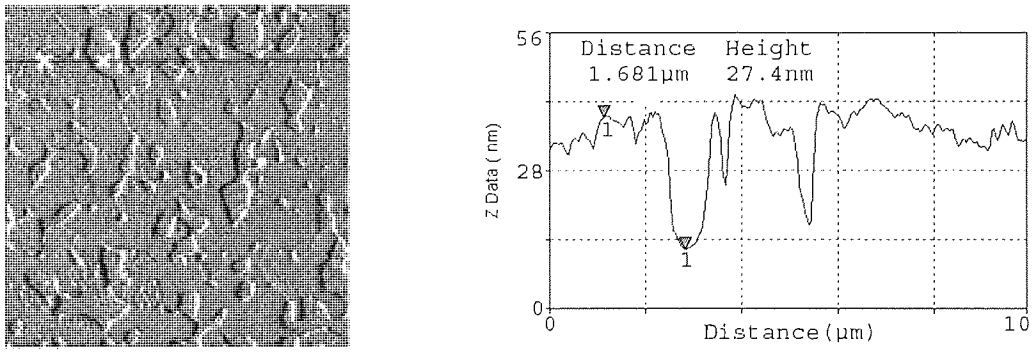

Figure 3-28 Travan5 head AFM image ceramic shield side (RH 30%, 40°C, 5k passes) (10µm×10µm)

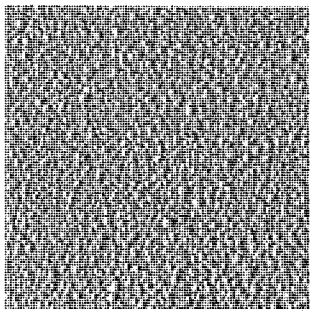

Area Ra	4.1 nm
Area RMS	5.1 nm
Avg. Height	17.6 nm
Max.Range	44.9 nm

Figure 3-29 Travan5 head AFM image of insulator area (RH 30%, 40°C, 5k passes) (10μm×10μm)

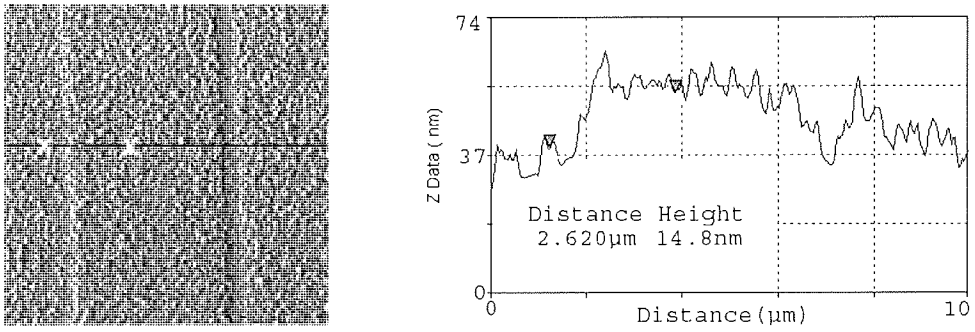

Figure 3-30 Travan5 head AFM image of pole area (RH 30%, 40°C, 5k passes) (10μm×10μm)

At 30%RH, 40°C experiment condition, the average PTR was about 57nm (including 30nm Fe stain thickness). Extensive stain was observed on the pole and shared pole area. Some tape debris was found on the surface of the head. The pole and shared pole slightly protruded above the insulator. The depth of pullout in the ceramic area was 27-32nm (Figure 3-27 and Figure 3-28). The RMS roughness of the insulator area was around 5nm (10μm×10μm scan).

3.1.1.7 Travan5 Head Wear after 5k Passes at RH 45%, 40°C

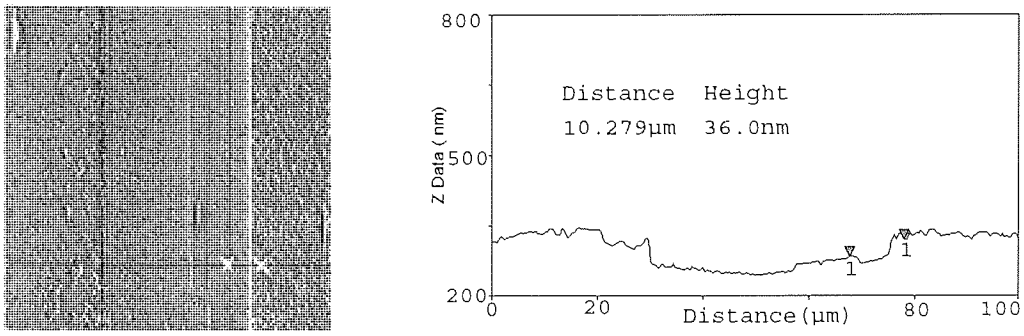

Figure 3-31 Travan5 head AFM image (RH 45%, 40°C, 5k passes) (100μm×100μm)

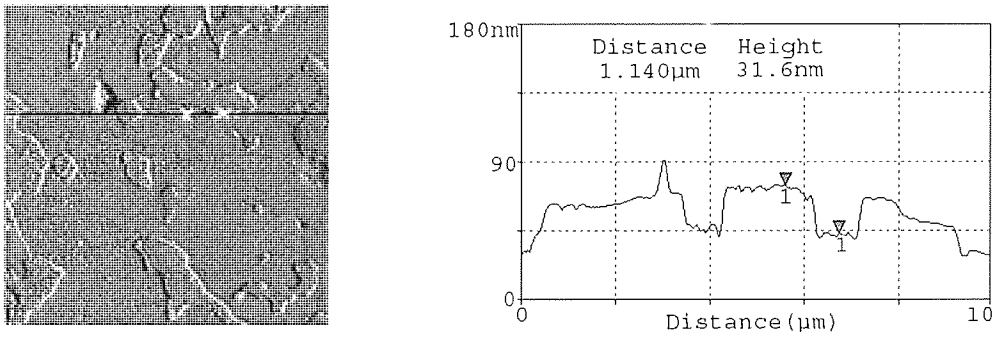

Figure 3-32 Travan5 head AFM image of ceramic pole side (RH 45%, 40°C, 5k passes) (10μm×10μm)

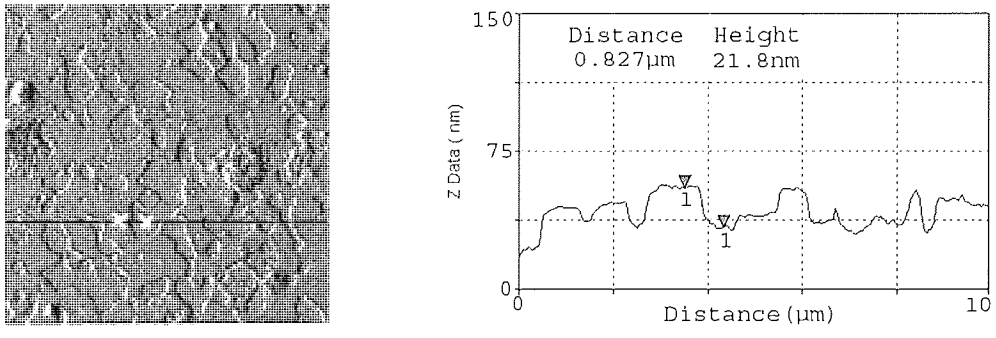

Figure 3-33 Travan5 head AFM image of ceramic shield side (RH 45%, 40°C, 5k passes) (10μm×10μm)

A typical PTR measurement of the head after tape 5k cycling at RH 45%, 40°C experimental condition was presented in Figure 3-31, the average PTR was about 61nm (including 30nm stain thickness). Some tape debris was found on the surface of the head. Pole and shared pole slightly protruded compared with insulator the depth of pullout in the ceramic area was around 30nm. The RMS roughness of the insulator

surface was around 3nm (10μm×10μm scan area) that indicated very smooth surface. Insulator area before and after wear showed some stains deposited on the some part of the insulator, but the stain was not fully covered the insulator.

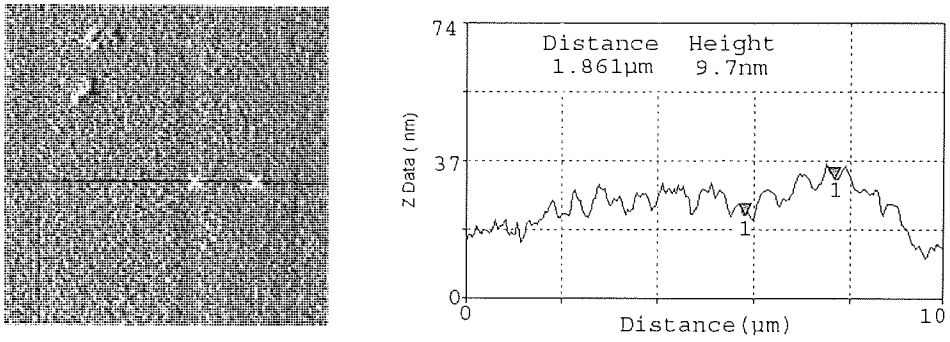

Figure 3-34 Travan5 head AFM image of pole area (RH 45%, 40°C, 5k passes) (10μm×10μm)

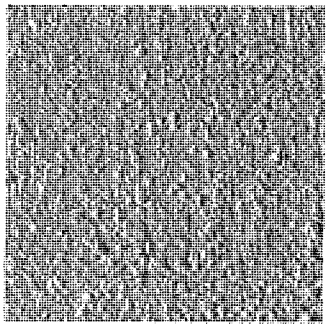

Area Ra	2.3 nm
Area RMS	2.9 nm
Avg. Height	14.6 nm
Max.Range	26.8 nm

Figure 3-35 Travan5 head AFM image of insulator area (RH 45%, 40°C, 5k passes) (10μm×10μm)

3.1.1.8 Travan5 Head Wear after 5k Passes at RH 60%, 40°C

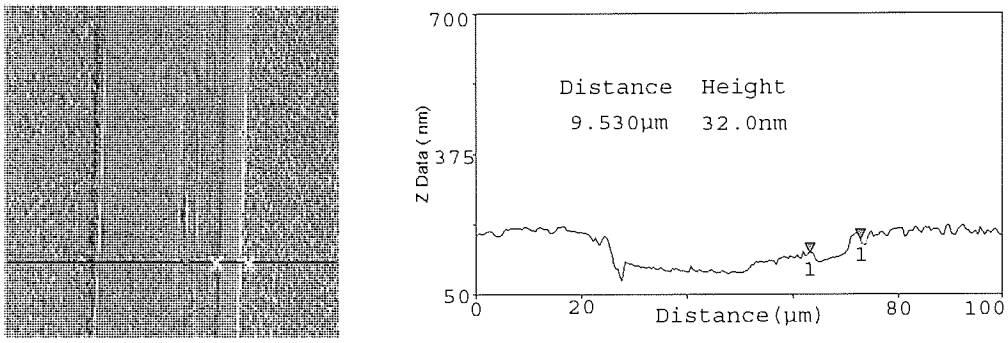

Figure 3-36 Travan5 head AFM image (RH 60%, 40°C, 5k passes) (100μm×100μm)

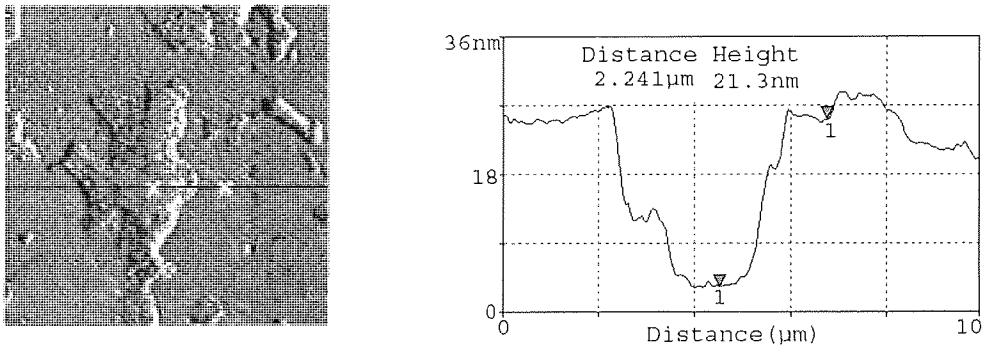

Figure 3-37 Travan5 head AFM image of ceramic pole side (RH 60%, 40°C, 5k passes) (10μm×10μm)

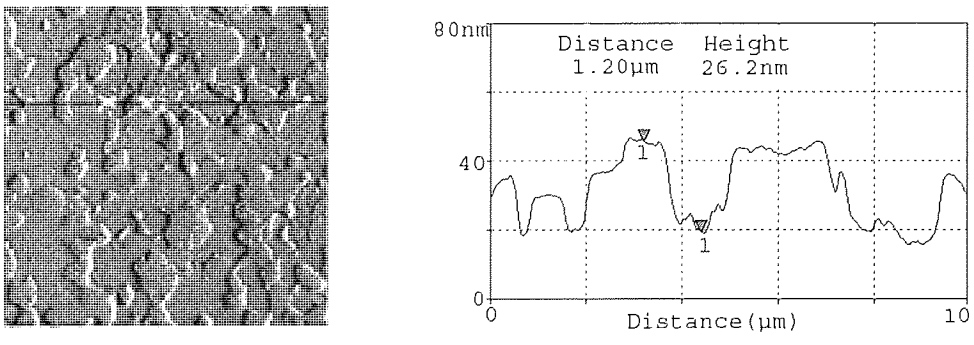

Figure 3-38 Travan5 head AFM image of ceramic shield side (RH 60%, 40°C, 5k passes) (10μm×10μm)

At RH 60%, 40°C experiment condition, the average PTR was about 60nm (including 30nm Fe stain thickness), pole and shared pole slightly protruded above the insulator. The depth of pullout in the ceramic area was around 26nm. The RMS roughness of

insulator was around 3nm (10μm×10μm scan). Island-like stains were found on the surface of insulator. Pole and shared pole area were fully covered by the stain.

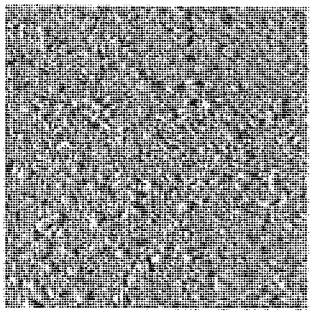

Area Ra	2.6 nm
Area RMS	3.3 nm
Avg. Height	18.6 nm
Max.Range	34.2 nm

Figure 3-39 Travan5 head AFM image of ceramic shield side (RH 60%, 40°C, 5k passes) (10μm×10μm)

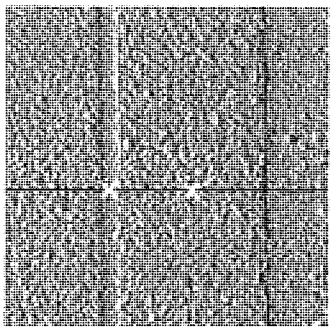

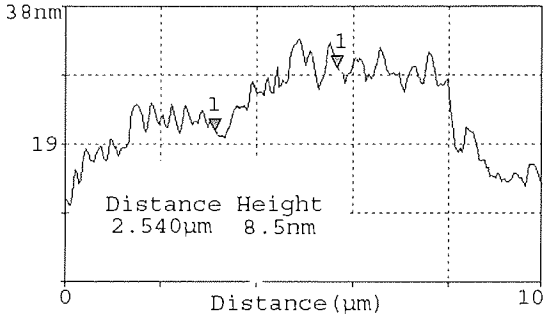

Figure 3-40 Travan5 head AFM image of pole area (RH 60%, 40°C, 5k passes) (10μm×10μm)

3.1.1.9 Travan5 Head Wear after 5k Passes at RH 75%, 40°C

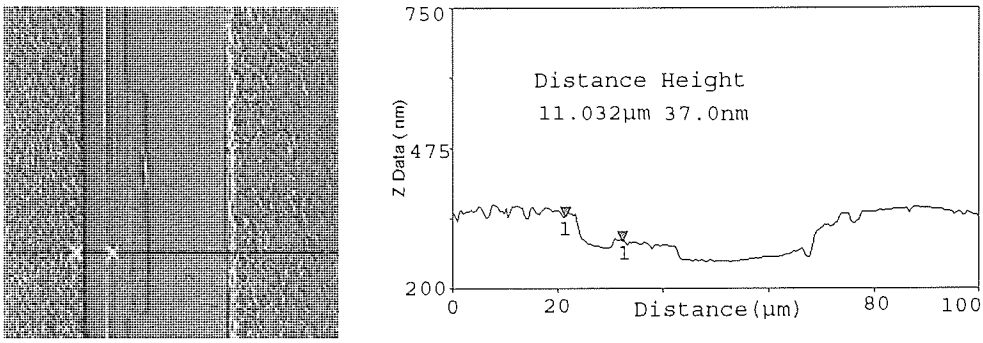

Figure 3-41 Travan5 head AFM image (RH 75%, 40°C, 5k passes) (100μm×100μm)

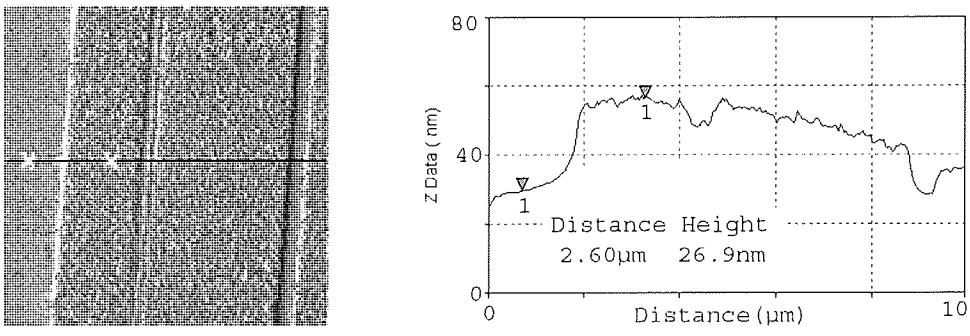

Figure 3-42 Travan5 head AFM image of pole area (RH 75%, 40°C, 5k passes) (10μm×10μm)

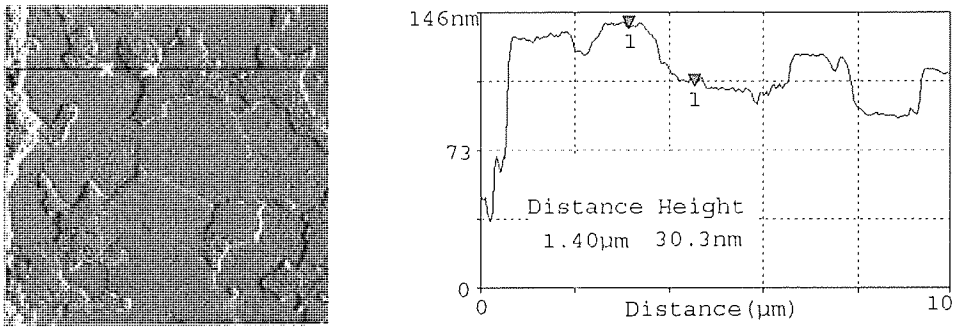

Figure 3-43 Travan5 head AFM image of ceramic pole side (RH 75%, 40°C, 5k passes) (10μm×10μm)

A typical PTR measurement of the head after 5k passes tape cycling at RH 75%, 40°C experimental condition was shown in Figure 3-41, PTR was about 65nm (including 30nm Fe stain thickness). The pole and shared pole protruded compared with insulator. The depth of pullout in the ceramic area was around 27-30nm. There was very little

stain on the surface of insulator area of the head, but stain was still observed on the pole and shared pole area.

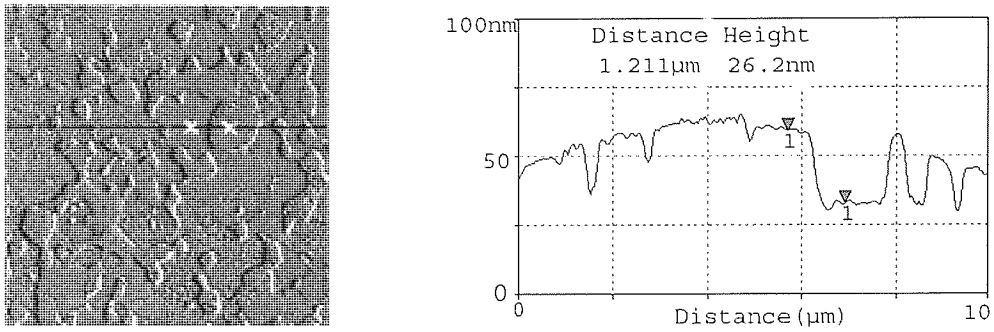

Figure 3-44 Travan5 head AFM image of ceramic shield side (RH 75%, 40°C, 5k passes) (10μm×10μm)

3.1.1.10 Travan5 Head Wear after 5k Passes at RH 80%, 40°C

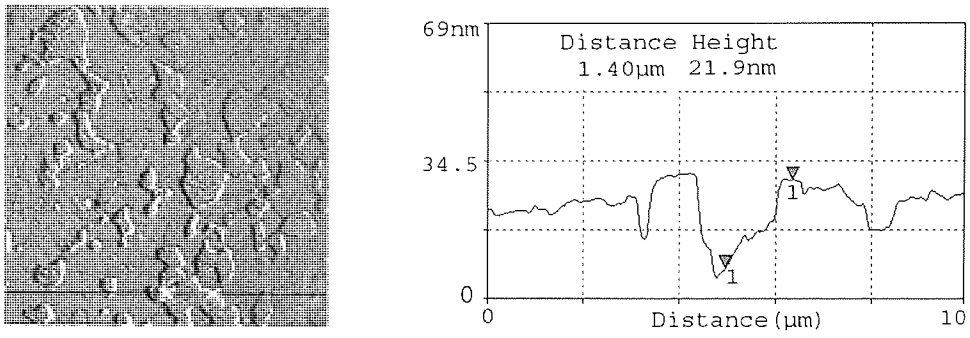

Figure 3-45 Travan5 head ceramic shield side (RH 80%, 40°C, 5k passes) (10μm×10μm)

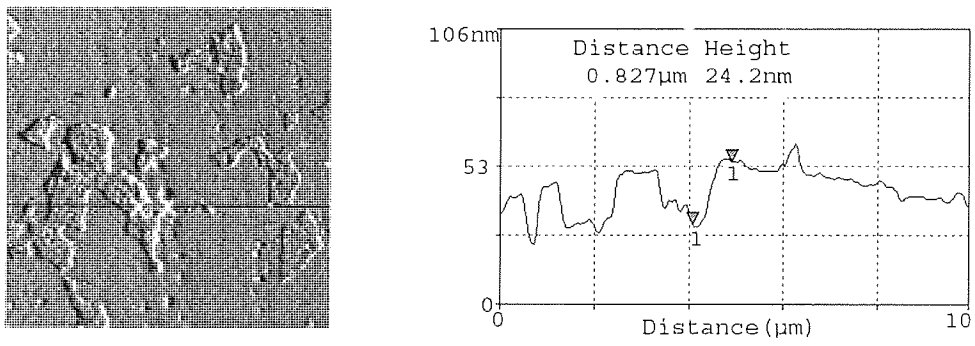

Figure 3-46 Travan5 head ceramic pole side after RH 80%, 40°C, and 5k passes (10μm×10μm)

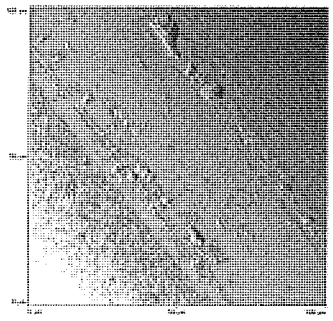

Figure 3-47 Travan5 head AFM image (RH 80%, 40°C, 5k passes) (100μm×100μm)

At RH 80%, 40°C experiment condition, the average PTR was more than 70nm due to the more materials deposited on the surface of the pole and shared pole (the average height of the deposit in three heads was 70nm higher than the surrounding area, see Figure 3-49), pole area and glue line were covered with material. These worn heads showed there were substantial deposits on the surface, especially along the boundary

between the glued AlTiC and insulator; these deposits could not be easily removed by brushing. Substantial amount of material transferred from tape at this high temperature and high humidity condition. The depth of pullout in the ceramic area was around 25nm. Unusually in this condition, material was observed to cover the insulator. The roughness of insulator was around 3nm.

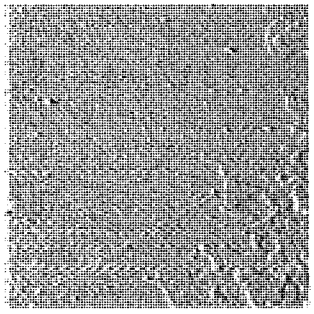

Area Ra	2.4 nm
Area RMS	2.9 nm
Avg. Height	11.1 nm
Max.Range	35.7 nm

Figure 3-48 Travan5 head AFM image of insulator area (RH 80%, 40°C, 5k passes) (10μm×10μm)

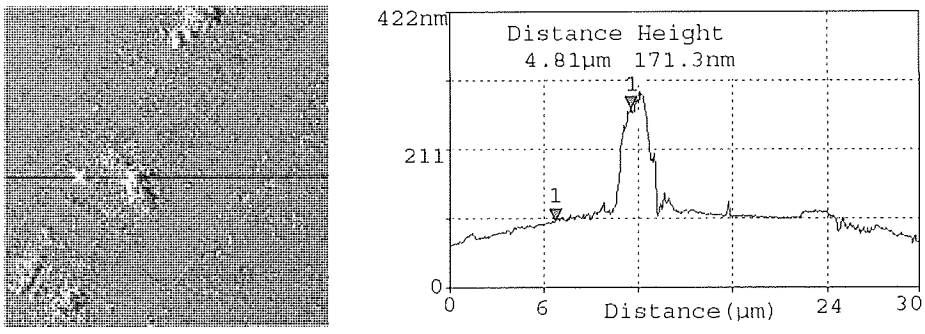

Figure 3-49 Travan5 head AFM image shows deposits on the pole and shared pole surface (RH 80%, 40°C, 5k passes) (30μm×30μm)

3.1.1.11 Summary Results of Travan5 head Wear

Experimental Conditions	Relative Water content	Stain	PTR (±2nm)	Pullout in the ceramic (±2nm)
Unused head		Basically clean surface	25nm	5-7nm
5k passes 15°C/RH 15%	1.9	Fe stain everywhere, more on pole/shared pole	50nm	20nm
5k passes 5°C/RH 80%	5.9	Fe stain everywhere, more on pole/shared pole	50nm	21nm
5k passes 40°C/RH 15%	6.7	Fe stain everywhere, more on pole/shared pole	57nm	24nm
5k passes 22°C/RH 40%	7.5	Fe stain everywhere, more on pole/shared pole	63[c]nm	23nm
5k passes 40°C/RH 30%	13.4	Fe stain everywhere, more on pole/shared pole	57nm	29nm
5k passes 40°C/RH 45%	20.1	Fe stain everywhere, more on pole/shared pole	61nm	28nm
5k passes 40°C/RH 60%	26.8	Spotty Fe stain on pole/shared pole, less stains on insulator, less on ceramic	60nm	26nm
5k passes 40°C/RH 75%	33.5	Spotty Fe stain on pole/shared pole, no stains on insulator, less on ceramic	65nm	27nm
5k passes 40°C/RH 80%	35.5	Substantial stain covers all head surface	~70nm	25nm

Table 3-1 Summary Results of Travan5 heads (Water content Normalised to 10°C, 10%RH)

[a]PTR value already includes the 30nm thickness of the Fe stains covered the surface of poles/share poles.
[b]Pullout of ceramic is the average highest value.
[c]Only one value from one Travan5 head available

Ceramic on the pole side of the head structure had larger TiC grain than that on the ceramic at the shield side of the structure. Fe signal was consistently higher on the ceramic with larger TiC grain structure.

3.1.2 Travan5 Head stain

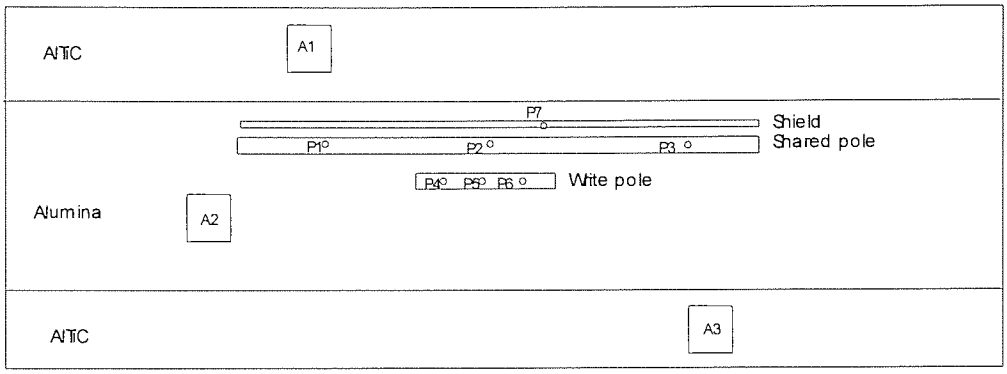

Figure 3-50 Sketch of AES analysis area

AES analysis was conducted on the surface of the heads (see Figure 3-50). For the pole and shared pole, the point AES analysis was conducted, for the insulator and ceramic, the area analysis was conducted ($30\mu m^2$).

Constituent part	C	Ti	O	Fe	Co	Al
Pole	81.6	0.0	8.3	0.0	10.2	0.0
Pole/shield	82.1	0.0	7.8	0.0	10.1	0.0
Shield	78.3	0.0	9.0	0.0	12.7	0.0
Insulator	63.1	0.0	20.8	0.0	0.0	16.0
Ceramic (pole side)	51.3	17.7	17.3	0.0	0.0	13.7
Ceramic (shield side)	65.3	8.0	15.8	0.0	0.0	10.9

Table 3-2 Typical atomic percentage concentration of AES analysis of unused Travan5 heads

Constituent part	C	Ti	O	Fe	Co	Al
Pole	74.4	1.4	12.6	11.2	0.4	0.0
Pole/shield	78.2	0.0	10.8	8.6	1.3	1.0
Shield	82.7	0.0	9.3	7.0	1.1	0.0
Insulator	77.4	0.0	13.8	6.8	0.0	2.0
Ceramic (pole side)	64.1	2.0	17.2	6.3	0.0	10.4
Ceramic (shield side)	75.5	3.0	11.2	2.2	0.0	8.1

Table 3-3 Typical atomic percentage concentration of AES results of Travan5 heads after 5k passes at RH80%, 5°C

Constituent part	C	Ti	O	Fe	Co	Al
Pole	63.4	0.0	17.4	17.2	0.9	0.9
Pole/shield	61.2	0.9	18.5	18.7	0.7	0.0
Shield	61.1	0.0	20.3	18.3	0.3	0.0
Insulator	64.7	0.0	16.2	13.6	0.0	5.2
Ceramic (pole side)	52.3	5.6	22.1	9.7	0.0	10.9
Ceramic (shield side)	53.8	5.7	22.3	4.3	0.0	13.9

Table 3-4 Typical atomic percentage concentration of AES results of Travan5 heads after 5k passes at RH15%, 15°C

Constituent part	C	Ti	O	Fe	Co	Al
Pole	68.5	0.0	15.1	13.7	1.14	1.4
Pole/shield	71.1	0.0	14.2	12.0	1.6	1.1
Shield	72.6	0.7	13.3	11.6	1.8	0.0
Insulator	72.3	0.0	14.3	11.2	0.0	2.2
Ceramic (pole side)	58.0	3.4	18.7	6.0	0.0	13.8
Ceramic (shield side)	61.7	4.5	19.5	2.5	0.0	11.9

Table 3-5 Typical atomic percentage concentration of AES results of Travan5 heads after 5k passes at RH40%, 22°C

Constituent part	C	Ti	O	Fe	Co	Al
Pole	48.9	0.0	24.1	22.9	2.9	1.1
Pole/shield	52.9	1.0	21.0	20.6	2.5	1.7
Shield	61.1	0.0	19.1	17.4	2.4	0.0
Insulator	68.3	0.9	13.7	11.4	0.0	5.3
Ceramic (pole side)	41.2	7.1	25.6	10.8	0.0	15.4
Ceramic (shield side)	53.1	9.0	22.3	4.3	0.0	11.4

Table 3-6 Typical atomic percentage concentration of AES results of Travan5 heads after 5k passes at RH15%, 40°C

Constituent part	C	Ti	O	Fe	Co	Al
Pole	54.2	0.0	21.1	21.4	2.1	1.2
Pole/shield	64.4	0.0	17.5	15.8	2.4	0.0
Shield	63.0	0.0	17.9	15.3	2.5	1.3
Insulator	63.9	0.0	17.4	13.2	0.0	5.6
Ceramic (pole side)	62.0	2.6	17.1	10.3	0.0	80
Ceramic (shield side)	60.1	3.47	21.1	6.54	0.0	8.8

Table 3-7 Typical percentage concentration of AES results of Travan5 head after 5k passes at RH30%, 40°C

Constituent part	C	Ti	O	Fe	Co	Al
Pole	58.5	2.1	18.8	17.2	1.6	1.7
Pole/shield	60.7	1.7	17.6	16.1	1.9	2.0
Shield	68.3	0.0	15.4	14.5	1.7	0.0
Insulator	61.6	0.9	18.2	13.6	0.0	5.6
Ceramic (pole side)	61.5	3.7	18.9	3.9	0.0	11.9
Ceramic(shield side)	56.5	4.5	24.1	2.0	0.0	12.9

Table 3-8 Typical atomic percentage concentration of AES results of Travan5 head after 5k passes at RH45%, 40°C

Constituent part	C	Ti	O	Fe	Co	Al
Pole	42.4	0.0	28.7	23.3	3.5	2.1
Pole/shield	50.9	2.4	22.9	19.1	3.3	1.3
Shield	54.7	0.0	24.1	17.7	2.5	0.9
Insulator	42.2	0.0	34.4	8.8	0.0	14.6
Ceramic (pole side)	36.8	7.0	35.3	5.4	0.0	15.5
Ceramic(shield side)	50.3	5.9	27.9	1.9	0.0	14.1

Table 3-9 Typical atomic percentage concentration of AES results of Travan5 head after 5kpasses at RH60%, 40°C

Constituent part	C	Ti	O	Fe	Co	Al
Pole	32.2	0.0	34.4	25.8	5.9	1.6
Pole/shield	40.5	1.7	28.6	23.0	5.3	0.9
Shield	46.8	0.0	27.1	20.6	4.7	0.8
Insulator	21.3	0.7	46.2	0.0	0.0	31.9
Ceramic (pole side)	47.3	5.8	31.2	5.0	0.0	10.7
Ceramic (shield side)	36.3	10.2	32.1	3.0	0.0	18.4

Table 3-10 Typical atomic percentage concentration of AES results of Travan5 heads after5k passes at RH75%, 40°C

Constituent part	C	Ti	O	Fe	Co	Al
Pole	66.9	0.0	22.3	0.0	8.9	1.9
Pole/shield	80.1	0.0	13.4	0.0	5.8	0.7
Shield	75.5	0.0	18.1	0.0	6.3	0.0
Insulator	64.2	0.0	18.5	0.0	0.0	17.2
Ceramic (pole side)	63.3	3.8	16.9	0.0	0.0	15.9
Ceramic (shield side)	59.7	7.9	17.5	0.0	0.0	14.9

Table 3-11 Typical atomic percentage concentration of AES results of Travan5 heads after 5k passes at RH 80%, 40°C

Test condition	Fe/Co (average)
Virgin Head	0
5k passes RH15 % 15°C (water 1.9)	28.6
5k passes RH80 % 5°C (water 5.9)	9.6
5k passes RH15 % 40°C (water 6.7)	7.8
5k passes RH40 % 22°C (water 7.5)	8.3
5k passes RH30 % 40°C(water 13.4)	7.6
5k passes RH45 % 40°C(water 20.1)	9.0
5k passes RH60 % 40°C(water 26.8)	6.4
5k passes RH75 % 40°C(water 33.5)	4.3
5k passes RH80 % 40°C (water 35.5)	0

Table 3-12 Fe/Co atomic ratio in the pole and share pole area after different conditions cycling (Water Content Normalised to 10°C, 10%RH)

AES results showed Fe stain was observed in most experimental conditions (except for RH80%, 40°C), more Fe stain was seen on poles and shared pole area. Some loose debris was also found on the surface of the head. Table 3-12 and Figure 3-51 show the Fe/Co (average Mean value) decreased with water content increased at different experimental conditions. The reason for measuring Fe/Co ratio is to compare the stain change at different experimental condition since the only source of Fe on the head was coming from the tape. The smaller water content, the higher was the Fe/Co value. The more water content, the smaller was the Fe/Co value. After water content reached more than 35.5 (RH 80 %, 40°C condition), the Fe stain stopped forming, polymer materials covered the whole head surface. From here it showed that Fe stain connected with water content. The more Fe stain covered the pole and shared pole during lower water content condition.

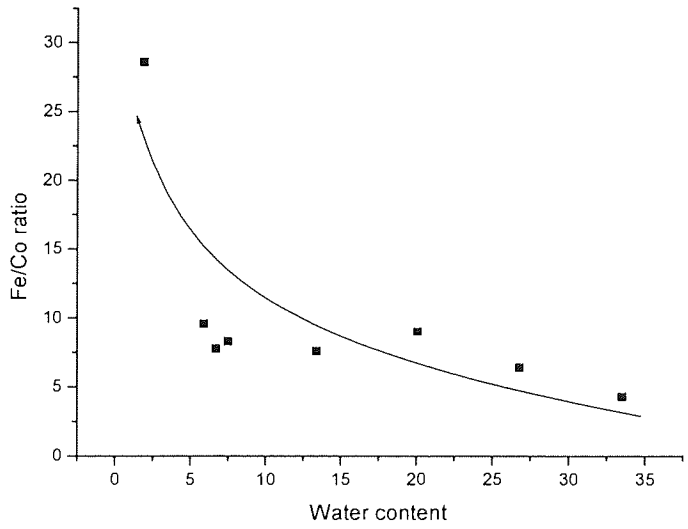

Figure 3-51 Changes in Fe/Co ratio as a function of water content

(Water Content Normalised to 10°C, 10%RH)

As the water content increased, the Fe stain on the surface of the heads changed to a discontinuous film, until water saturation of active sites on the head material surfaces prevented the formation of Fe stains (RH 80%, 40°C). At RH 80%, 40°C (NWC 35.5), AFM showed a substantial amount material transferred to the head surface, AES confirmed the material was tape binder and lubricant material and AES did not detect Fe on the surface of heads at the RH 80%, 40°C condition.

Figure 3-52 is the optical microscopy of the pole area for Travan5 at different environmental conditions respectively. For the unused head pole area, the gap between the pole and shared pole was 1 μm. Both the pole and the TiC grains, metal-like materials were expected to appear clear, the white dots in the ceramic region represented the TiC grains. For the worn head, the brown stain was clearly seen on the pole area. For Travan5 at condition of 40°C, RH 80%, polymer deposits were seen in the pole area.

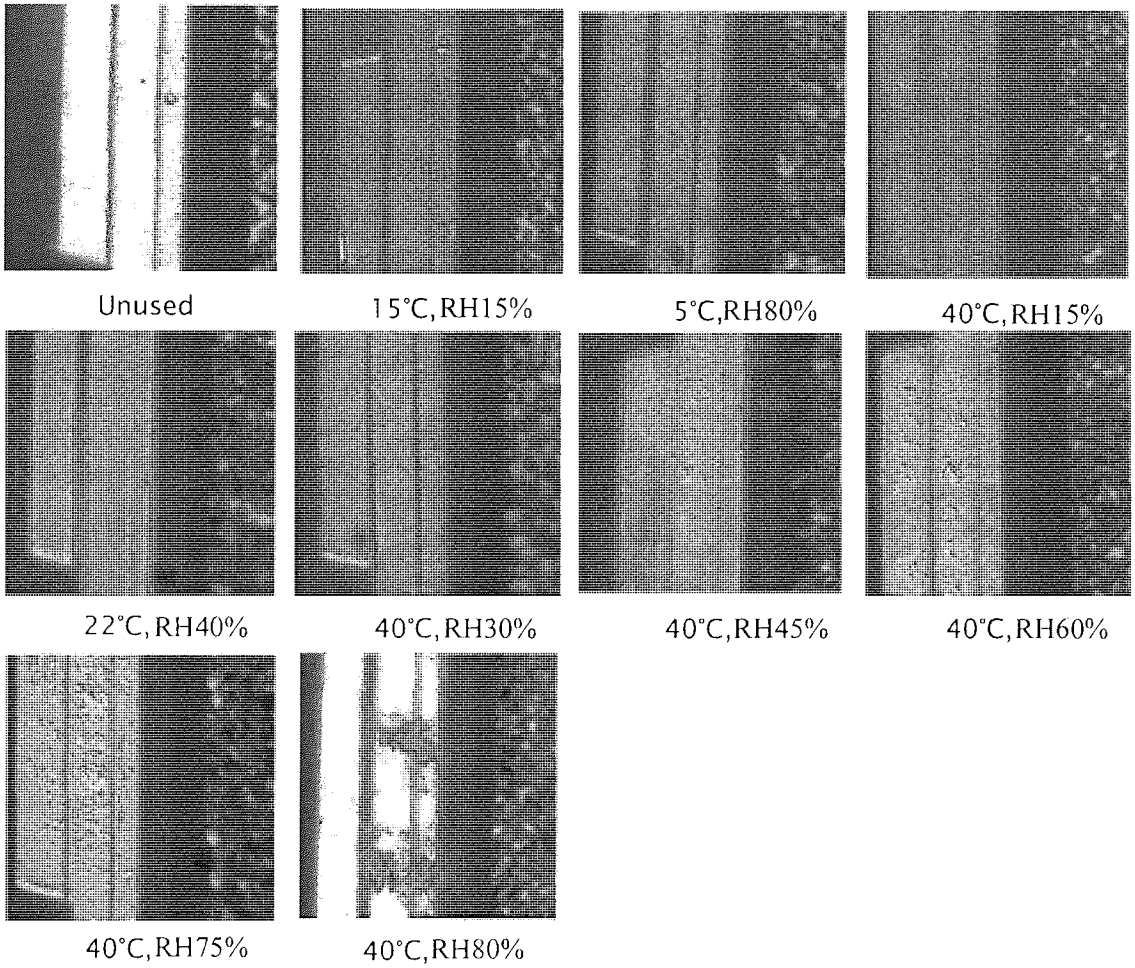

Figure 3-52 Optical micrographs of Travan5 head pole area, unused and worn heads after 5k passes cycling against tapes in different environmental conditions (400×)

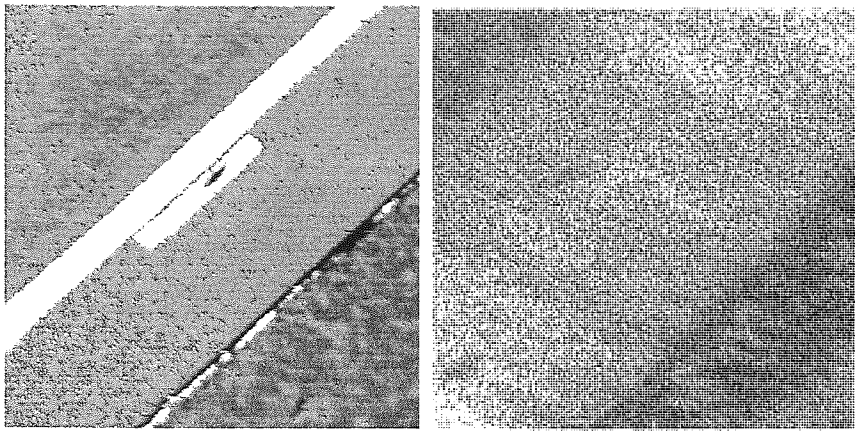

Figure 3-53 At 22°C, RH 40% condition 5kpasses Travan5 tape cycling, SEM image (left), AES Fe element mapping image (right)

Figure 3-53 (left) is SEM image of a Travan5 head surface; Figure 3-53 (right) is AES elemental mapping result for the Travan5 head after 5k passes of Travan5 tape cycling; the white colour areas represent Fe composition. The Fe stain was found formed on the surface of the pole and shared pole area, extensive Fe stain covered insulator area as well.

3.1.3 Travan5 head PTR

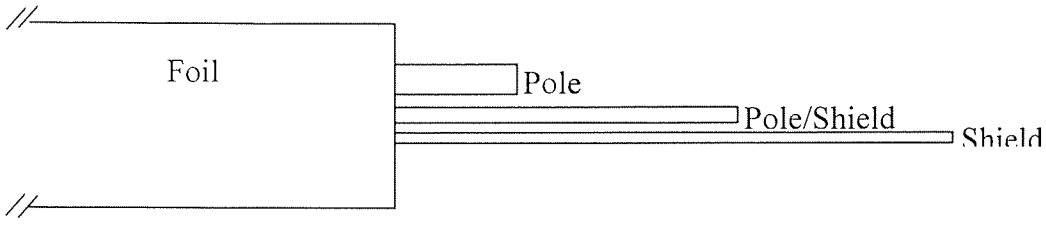

Figure 3-54 Schematic of the set-up for the stain thickness experiment

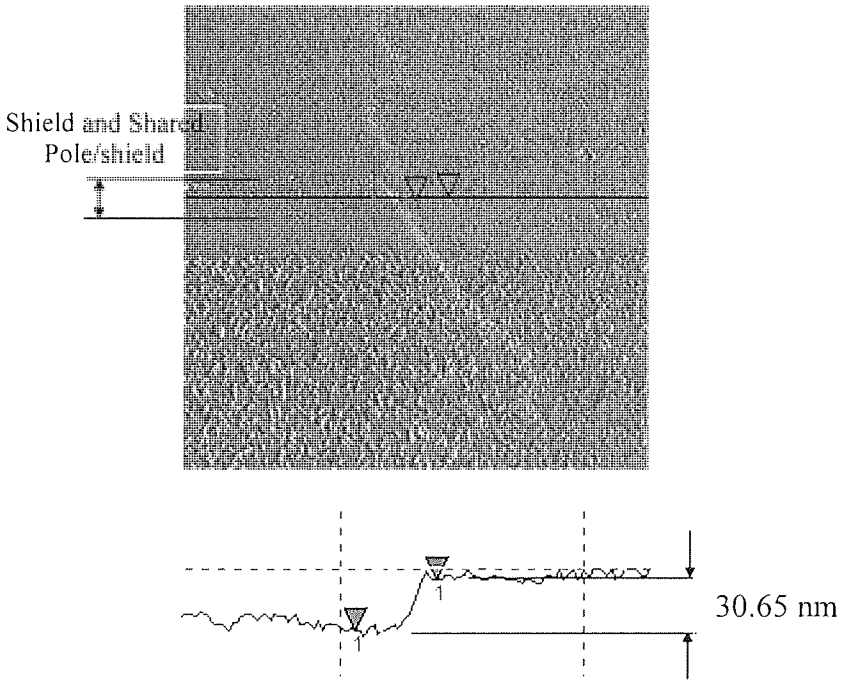

Figure 3-55 Measurement of stain thickness via AFM line scan

Supplementary experiments designed to determine stain thickness were performed on a Travan5 head subject to 5000 passes of Travan5 tape at 40°C, 15% RH. The pole areas were masked off half way along their lengths using aluminium foil that was held in place with fine wire (Figure 3-54). This protected stain covered by the aluminium foil from being affected by the experiment. AES was first performed on the pole/shield without covered by the aluminium foil, allowed three points to be analysed and averaged. The head was then etched using ion current of 2μA with 3KeV energy Ar^+ ions as the etchant.

AES was recorded at certain intervals (1 minute) of this sputtering to produce a depth profile of the detected elements. The sample was etched until the detected Fe content was below 5% indicating that stain was almost completely removed. After removing the aluminium foil, AFM images of the pole areas were then collected and the depth from the etched stain/pole to unetched stain was measured (see Figure 3-55).

Test condition	PTR (nm)
Virgin Head	25
RH 15 %, 15°C (water 1.9)	20+stain
RH 80 %, 5°C (water 5.9)	20+stain
RH 15 %, 40°C (water 6.7)	27+stain
RH 40 %, 22°C (water 7.5)	33+stain
RH 30 %, 40°C (water 13.4)	27+stain
RH 45 %, 40°C (water 20.1)	31+stain
RH 60 %, 40°C (water 26.8)	30+stain
RH 75 %, 40°C (water 33.5)	35+stain
RH 80 %, 40°C (water 35.5)	~70

Table 3-13 PTR of Travan5 heads after 5k passes at different environmental conditions (Water Content Normalised to 10°C, 10%RH)

The measurement of PTR was taken from the ceramic region on the pole side of the head to the surface of the stain material covering the pole. The detail PTR measurement had already been described in Chapter Two. An assumption was made in that, at each condition the thickness of the stain covering the pole was the same (approximately one particle thick plus binder~30nm), as such, the PTR measurements were an indication of pole wears. The degree to which PTR had occurred after 5000 passes of tape was shown in as a function of increasing NWC (see Table 3-13). As the NWC increased PTR was seen to increase.

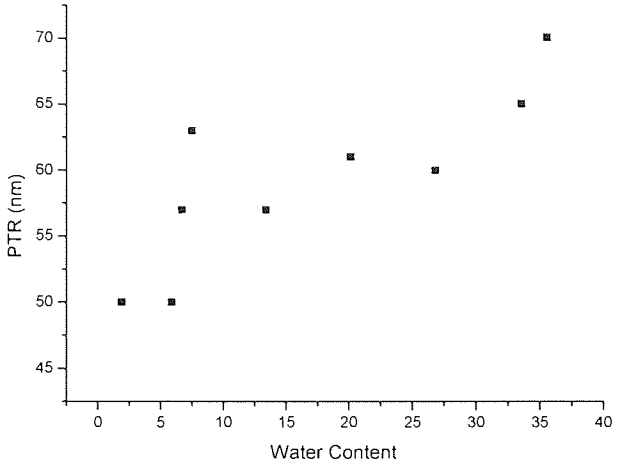

Figure 3-56 Travan5 head PTR after 5000passes in different cycling condition (Water content Normalised to 10°C, 10%RH)

Figure 3-56 shows that PTR in these experimental conditions increased as the atmosphere water vapour content increased.

3.1.4 Travan5 Tape Wear

3.1.4.1 Travan5 Virgin Tape

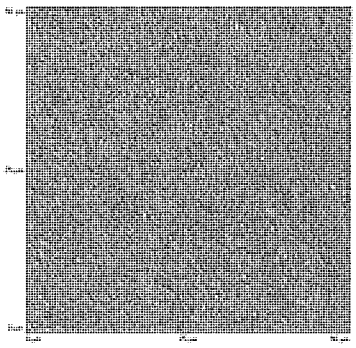

Area Ra	12.4 nm
Area RMS	15.7 nm
Avg. Height	88.5 nm
Max.Range	153.7 nm

Figure 3-57 Virgin Travan5 tape AFM image

XPS analysis was performed at the edge and centre of each Travan5 tape due to the different contact pressure at the centre and at the edge of tapes (centre area of the tape contacts with the belt, the edge of the tape is away from the belt, see section 2.2.1). XPS wide scan (Figure 3-58) showed that elements in the surface of the tape were as follows: Iron (Fe), Carbon (C), Oxygen (O), Nitrogen (N), Aluminium (Al) and Zirconium (Zr).

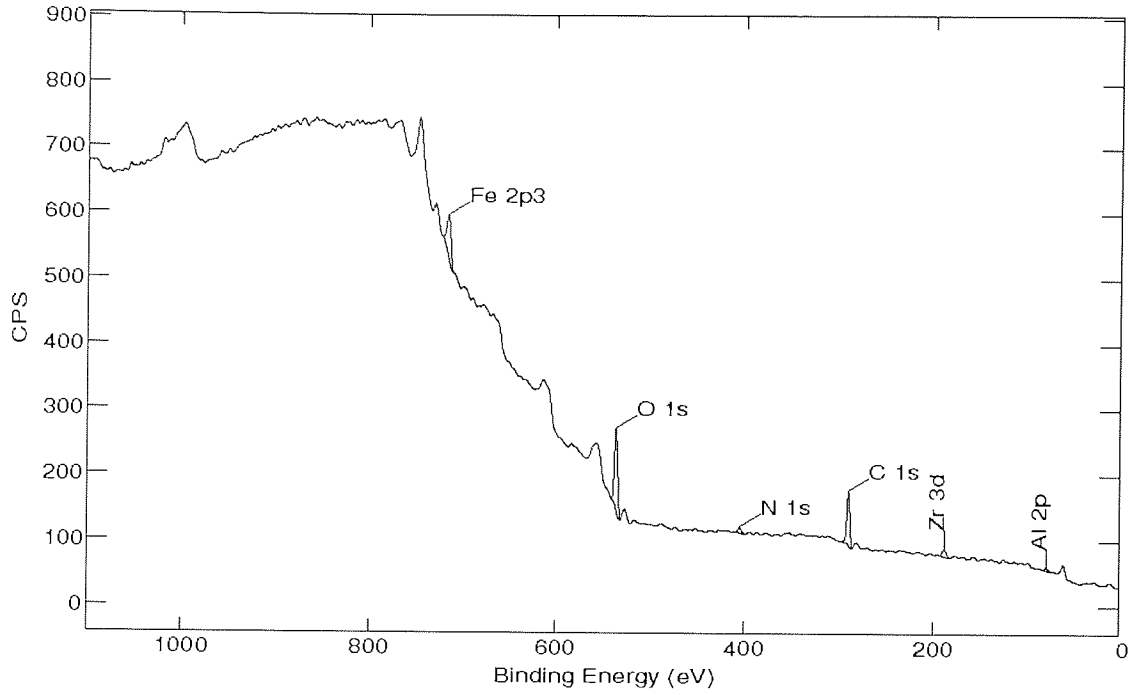

Figure 3-58 Wide scan spectrum for virgin Travan5 tape

C was mainly from the binder (urethane: H_2N-NH-C(=O)-O-C_2H_5); and lubricant (fatty acid ester, e.g. $C_{13}H_{27}$-O-C(=O)-$C_{18}H_{37}$) but also from a hydrocarbon contamination layer on the outer surface of the tape; the Fe originated from the magnetic pigment; O from the binder, lubricant, Fe oxide and Al and Zr oxides; the presence of N was due entirely to the constituents of the binder, Al was present in the tape as a head-cleaning agent, as was Zr.

3.1.4.2 Travan5 tape XPS results after different condition cycling

Table 3-14 summarized the experimental conditions and water content involved in the Travan5 experiments.

Environmental Condition	10°C/ RH10%	15°C/ RH15%	5°C/ RH80%	40°C/ RH15%	22°C/ RH40%	40°C/ RH30%	40°C/ RH45%	40°C/ RH60%	40°C/ RH75%	40°C/ RH80%
Water vapour Pressure (mba)	1.1	2.2	6.7	8.3	8.8	16.5	24.8	33.1	41.3	44.1
Normalised Water Content (NWC)	1.0	1.9	5.9	6.7	7.5	13.4	20.1	26.8	33.5	35.5

Table 3-14 Relative water content magnitude for each environmental condition (Normalised to 10°C, 10%RH)

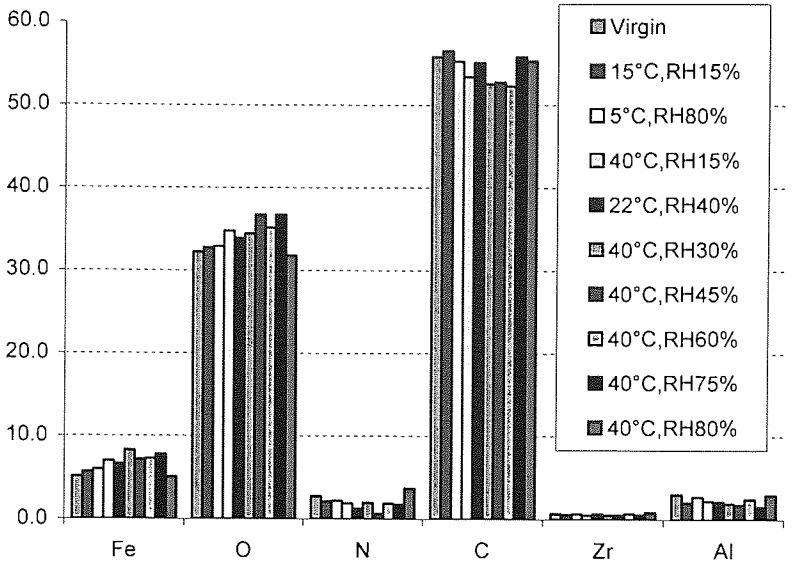

Figure 3-59 Change in relative atomic percentage as a function of temperature and NWC (centre area of the tape)

It is well known that the typical error of XPS quantitative analysis for a well-defined peak is less than one percent of the value itself. Figure 3-59 is the result of the different element composition changes obtained by XPS narrow scans. The changes were limited to reduction in the N concentration compared with virgin tape as previously found indicating binder depletion had occurred (N reduced more than 20% of original value). At the same time, the Fe signal increased compared with virgin tape. Comparing the Figure 3-59 and Figure 3-60, the centre area of the tape, the binder (N) change was more than that at the edge of the tape which indicates the higher contact pressure increases the wear of the tape. Only at 40°C, 80%RH, the worn tape showed similar with virgin tape, actually in this case tape degradation happened and possible top magnetic layer was removed. The detail tape wear mechanism will be discussed in Chapter 4.

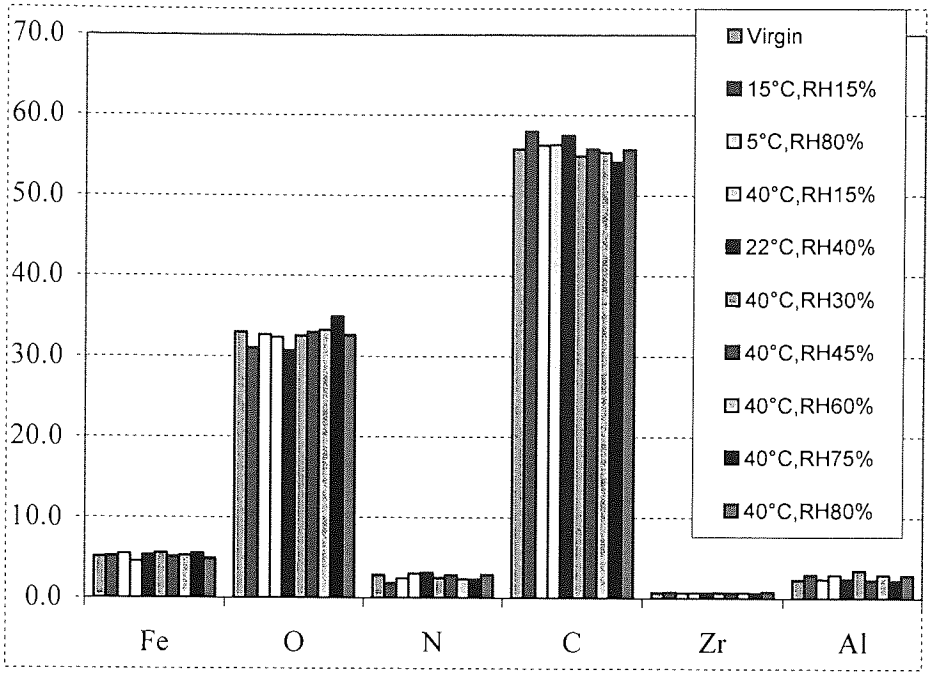

Figure 3-60 Change in relative atomic percentage as a function of temperature and NWC (edge area of the tape)

3.1.4.3 Synthesis of Carbon Peak for the Travan5 Tape

Synthesis of the carbon peak [11, 172] for each tape revealed four chemical states contributed to the total carbon peak for Travan5 tape. The peaks common to tapes were due to O=C-O, C-O, C-N and C-C/C-H (aliphatic and aromatic components were not resolved). The most intense peak (C-C/C-H) occurred at a designated binding energy of 284.6eV and was used as a reference for the other peak identification. From knowledge of the formulations used to manufacture each tape, the carboxyl (O=C-O) peak was known to be characteristic of both the lubricant and binder material. As such, it was not a particularly useful indicator of the relative concentration of constituents in the near surface region of the tapes. However, C-N peaks provided a good indication of the relative changes in the concentration of the binder materials, since these components must originate from polymeric fragments in the binder resin.

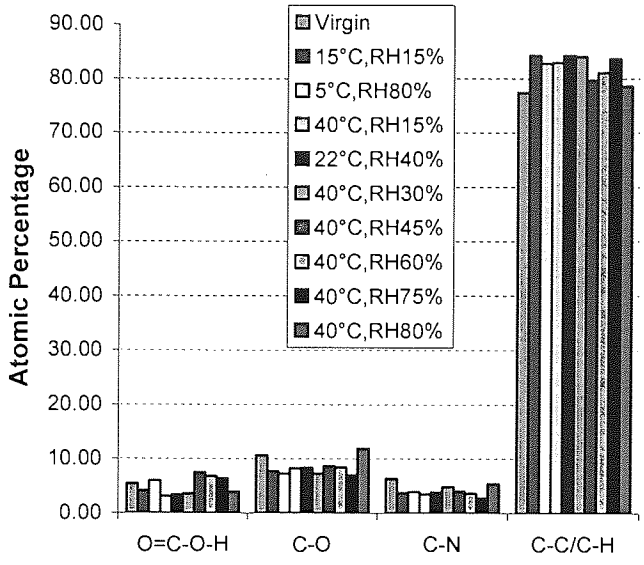

Figure 3-61 Change in synthesised carbon components as a function of temperature and NWC (centre area of the tape)

Figure 3-61 shows the XPS C1s synthesised result of the tape centre area surface after 5k passes at different temperature and relative humidity, Figure 3-62 shows the XPS C1s synthesised result of the tape edge area surface after 5k passes at different temperature and relative humidity. These results showed there was C-N changes in the centre area and the edge area of the tape which indicated tape wear happened. The detail discussions will be seen in the chapter4.

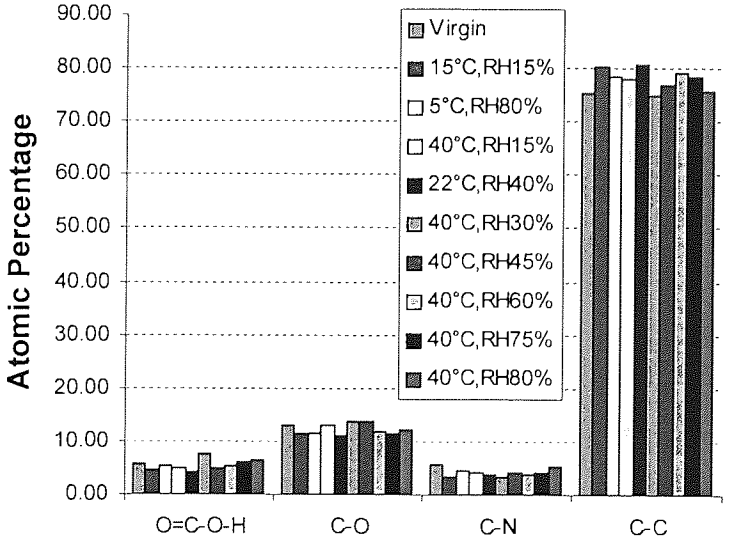

Figure 3-62 Change in synthesised carbon components as a function of temperature and NWC (edge area of the tape)

3.1.4.4 Travan5 tape debris

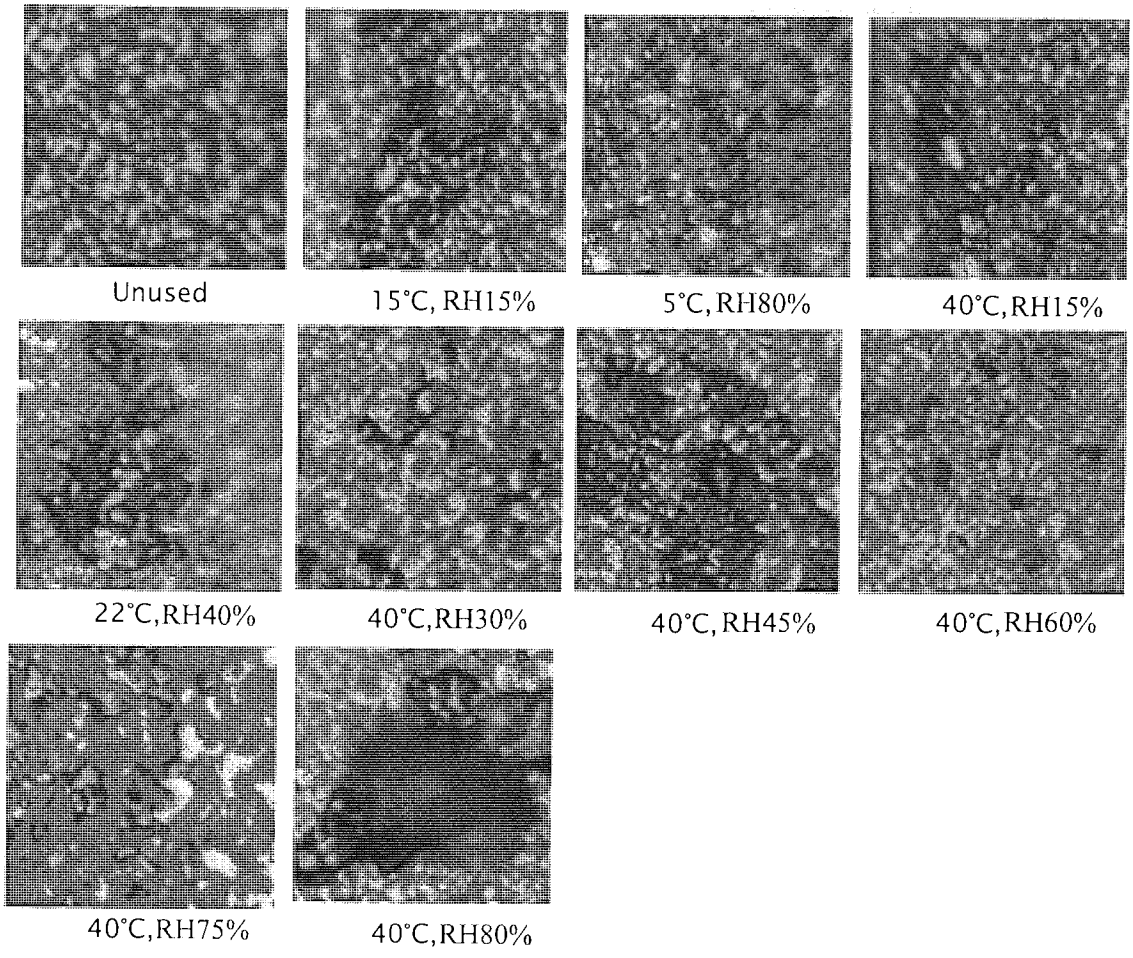

Figure 3-63 Optical micrographs of typical LTO head ceramic debris for unused, worn head after 5k passes cycling against tapes at different environmental conditions (400×)

Figure 3-63 shows typical debris distribution at the Travan5 ceramic surface. Generally speaking there was more tape debris per unit area for Travan5 heads at the higher temperature and higher water content conditions, indicating tape degradation at the higher temperature and high water content conditions.

3.1.4.5 Travan5 tape roughness

Table 3-15 is the Travan5 tape roughness result obtained from 100μm×100μm AFM scan from different conditions. Generally speaking, the worn tapes became smoother than the virgin tapes except the condition 5k passes RH 80% 40°C this case, large amount of tape materials were transferred from tape to the head and also other places. In

the same time, worn tape roughness became rougher at this RH 80% 40°C condition, indicating the degradation of the surface of the tape under these conditions.

Experimental conditions	Tape Roughness RMS (nm)
Virgin	15.7
RH 15%, 15°C (water 1.9)	13.1
RH 80%, 5°C (water 5.9)	13.1
RH 15%, 40°C (water 6.7)	8.4
RH 40%, 22°C (water 7.5)	9.4
RH 30%, 40°C (Water 13.4)	11.4
RH 45%, 40°C (Water 20.1)	9.1
RH 60%, 40°C(Water 26.8)	11.4
RH 75%, 40°C (Water 33.5)	7.6
RH 80%, 40°C (water 35.5)	39.7

Table 3-15 Surface roughness of Travan5 tape after cycling 5k passes at different environment conditions (Water content Normalised to 10°C, 10%RH)

3.2 Experiment Results of LTO heads with Mp1 tapes

3.2.1 LTO Head Wear with Mp1 Tapes

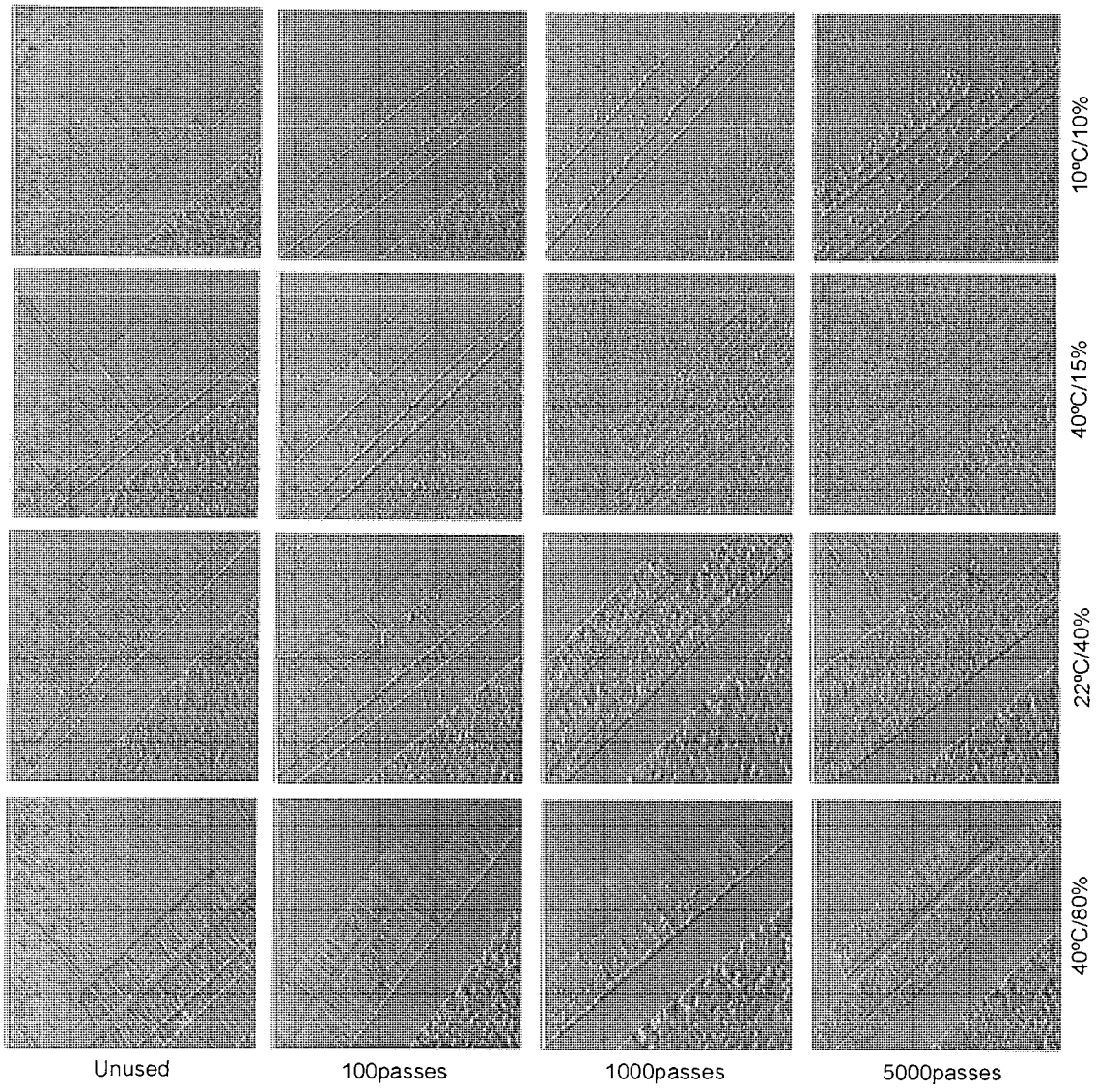

Figure 3-64 AFM images of LTO head pole area after Mp1 tapes cycling in different environmental conditions (30μm×30μm)

Figure 3-64 shows virgin head poles were slightly recessed about 2nm compared with insulator, after 100passes (20km) Mp1 tapes cycling, the height of pole was very similar with the height of insulator area, stain did not cover the pole area. Some scratches can be observed on the surface of heads. After 1k passes (200km) cycling against Mp1 tapes, stain started to build up in the condition of 40°C, RH 15% and 22°C, RH 40%, other condition also had some stains but less than these two conditions. Some island like stain was found on the surface of pole and shield pole.

After 5k passes of tape, the pole and shared pole was completely covered with stain except at the 10°C, RH10% condition. The lack of stain at low temperature and low relative condition (10°C, RH10%) was totally different to our former work and that of other workers who reported more stain at low temperature and low humidity conditions. This will be explained in the Chapter 4.

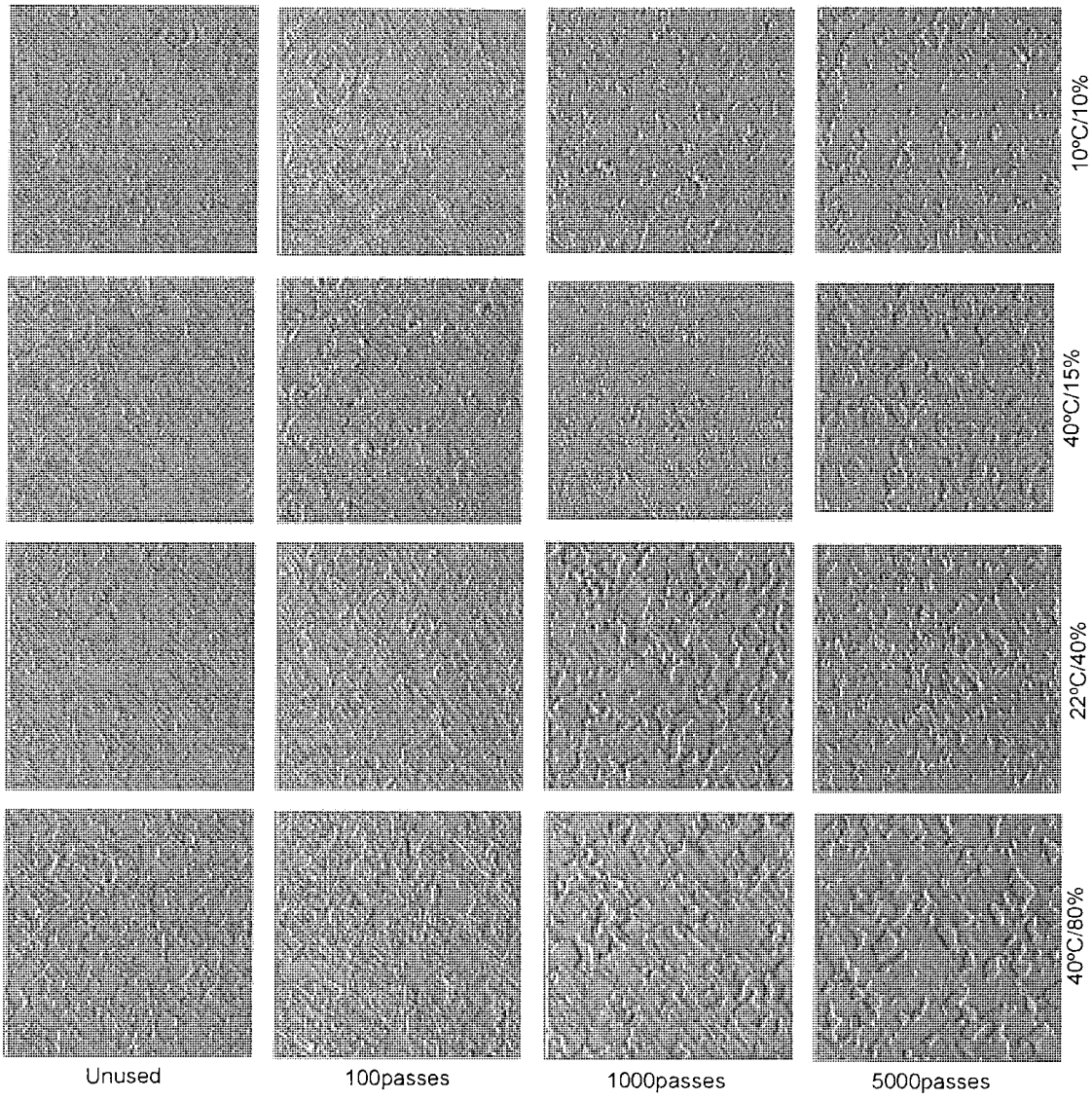

Figure 3-65 AFM images of LTO head ceramic area after Mp1 tapes cycling in different experimental conditions (15μm×15μm)

In all the LTO experiments involved in Mp1 tapes, the typical pullouts in the ceramic region was around 4-6nm for the virgin heads, this kind of pullouts were produced during the manufacturing processing, after 5k passes (1000Km) of the Mp1 tapes

cycling, the experiments showed the typical depth pullout was around 15-18nm except the 40°C, RH80% condition the typical depth of pullout reached around 22nm. The insulator and pole materials had very close hardness. The ceramic pullout happened here compared with Travan5 heads was smaller.

The abrasions visible on the insulator in the direction of tape motion (diagonally across the image from left to right) were common to all conditions. Micro-abrasion and adhesion of the insulator regions occurred as a result of contact with the tape or three-body particles abrasive wear.

3.2.2 LTO head PTR with Mp1 tapes

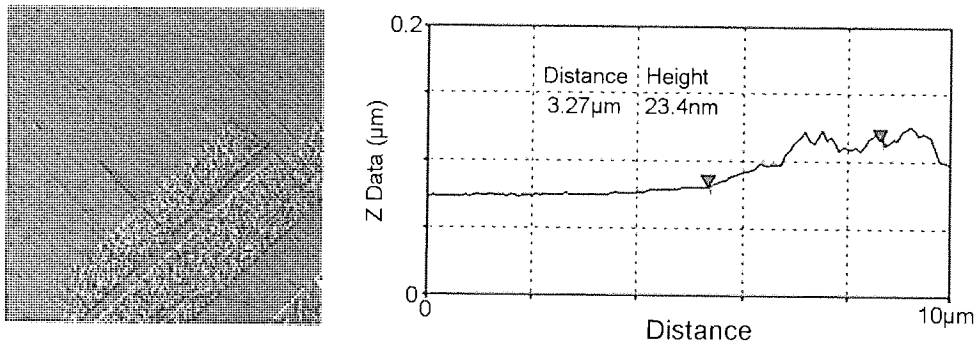

Figure 3-66 The typical thickness of stain, this AFM image is LTO head after 5k passes in the condition of 40°C, RH 80%

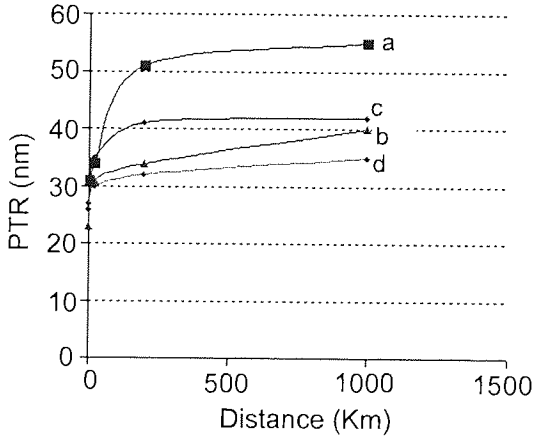

Figure 3-67 PTR of LTO heads after tape cycling at (a) 40°C, RH 80%(NWC 35.5) (b) 22°C, RH40% (NWC 7.5) (c) 40°C, RH15% (NWC 6.7) (d) 10°C, RH 10%(NWC 1.0)

The PTR value measurement had already considered the stains on the surface of pole, first of all the average distance from the pole covered with Fe stains to the air-bearing

surface (ceramic) was measured. After the thickness of stains was added, the true PTR was obtained. Some parts of pole and share pole were still not completely covered with stain (Figure 3-66). So the distance from the uncovered pole to the pole covered with stain determined the thickness of stains. The average thickness of stain measured here was around 25nm.

The PTR after 5000 passes were shown in Figure 3-67. For similar water content condition, the PTR values were quite similar (Figure 3-67 (b) and Figure 3-67(c)). Figure 3-67(a) indicates the PTR value reached the highest in the highest temperature and highest water content condition, which means the worst wear occurred in the highest water content and highest temperature condition. At the lowest water content and lowest temperature, the PTR was lowest (Figure 3-67 (d)). The average PTR for the unused LTO head was around 25nm. The PTR measurement clearly showed the higher water content and higher temperatures lead to the higher wear.

3.2.3 LTO Head stain with Mp1 tapes

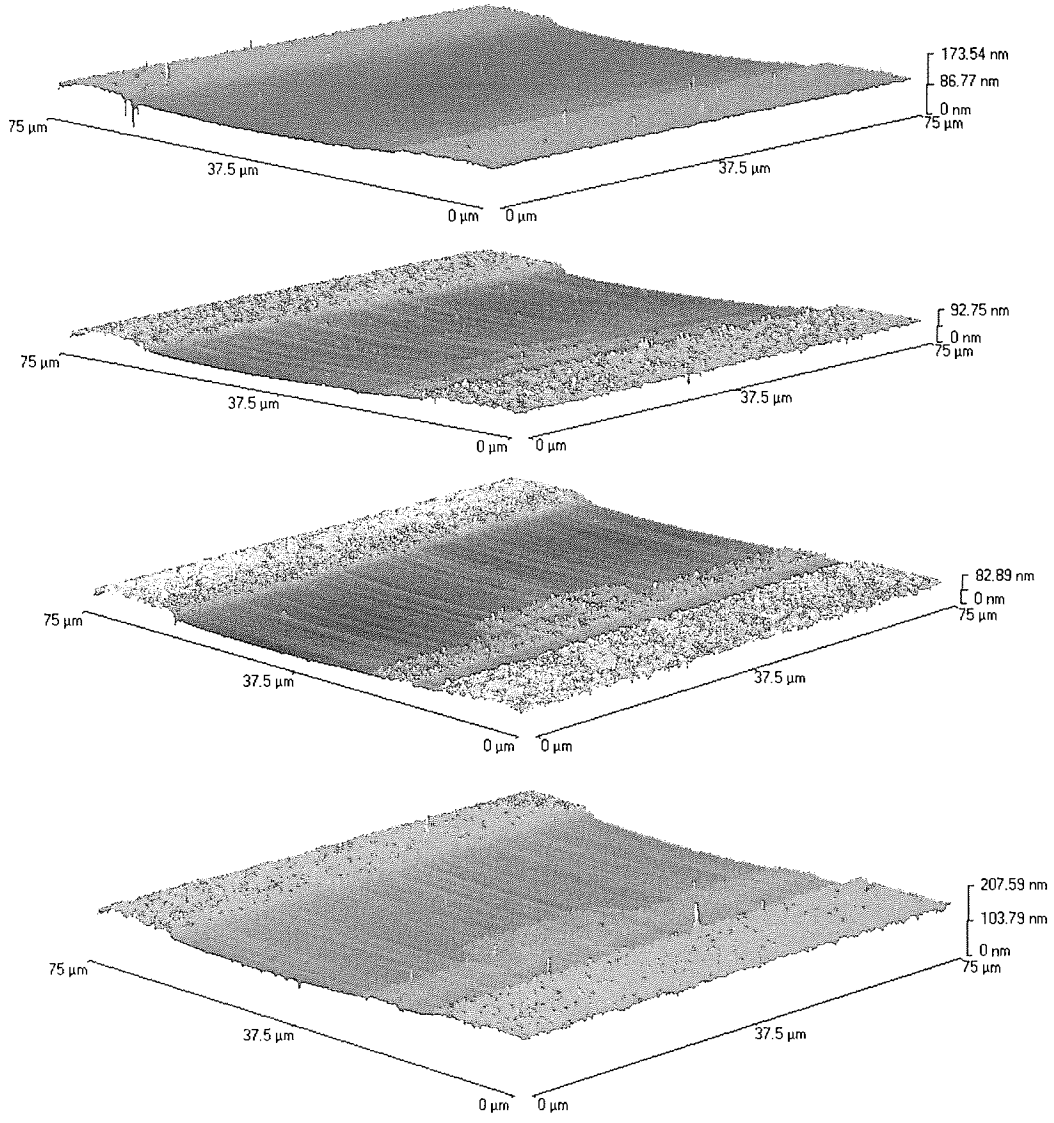

Figure 3-68 AFM 3D images of LTO heads, virgin, 100passes, 1k passes, 5k passes (from top to bottom) at 22°C, RH40% condition

Figure 3-68 shows the progression of stain and wear in the LTO head with Mp1 tapes; the virgin head showed a clean surface, after 100passes (20km) Mp1 tape cycling, some fine particles appeared on the surface of heads; after 1k passes the image clearly showed the stain build up on the pole area, the stain at this stage was island-like, not completely covering the pole area; but after 5k passes Mp1 tape cycling, the image showed the pole area to be completely covered with stain. No stain was seen on the insulator. AES results showed some Fe stain in the ceramic region, but major Fe stain was on the pole and shared pole areas.

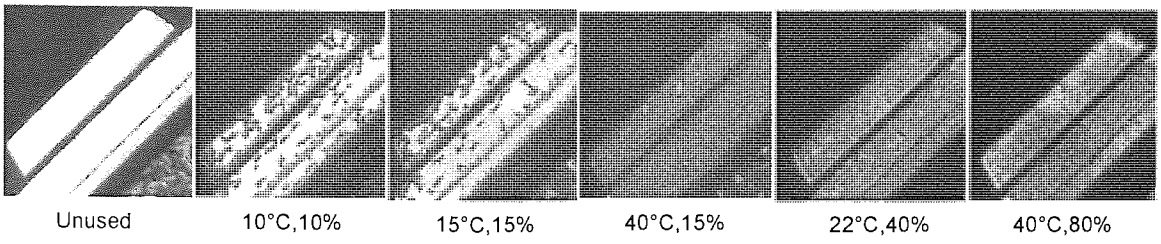

Figure 3-69 Optical Microscopy images of LTO head pole area after cycling 5k passes against Mp1 tapes in different environmental conditions

Optical microscopy of the pole area for LTO head after Mp1 tape cycling at different environmental conditions is showing in Figure 3-69, for the unused head pole area, the white dots in the ceramic region represent the TiC grains. For the unused head, the pole area showed the very clear white colour. For the worn head, the brown Fe stains were clearly spotted on the pole area. The more stain was observed at 40°C, RH15% and 22°C RH 40% conditions. In this LTO Mp1 experiment, 15°C RH15% (NWC 1.9) condition was added to study the low temperature effect on stain formation. Stain on the heads was very similar between 10°C, RH10% and 15°C, RH15% conditions.

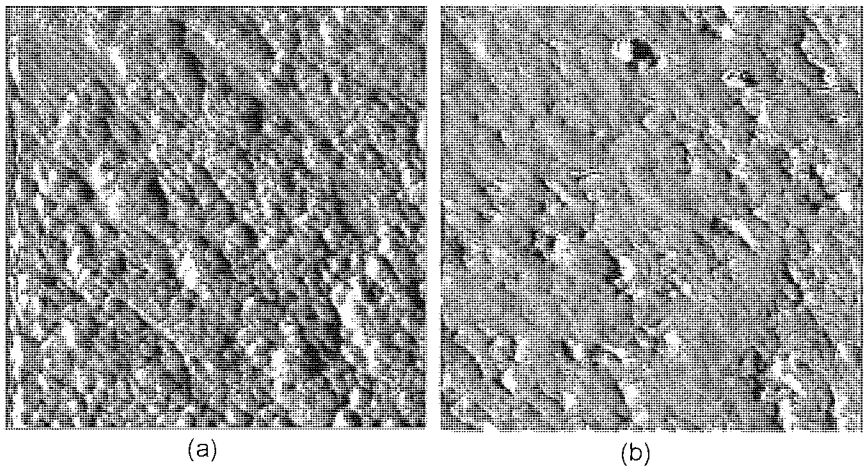

Figure 3-70 High resolution (2μm ×2μm) stains AFM image at the pole surface after Mp1 tape 5k passes (a) 40°C RH80% (b) 40°C, RH15%

Figure 3-70 (a) and (b) show stain formed using Mp1 tape. Figure 3-70 (a) clearly shows incomplete stain coverage at 40°C, RH 80%, the agglomerates of Fe particles is clearly visible on the surface of the pole. In contrast Figure 3-70 (b) shows almost complete coverage of stain on the poles at 40°C RH15%.

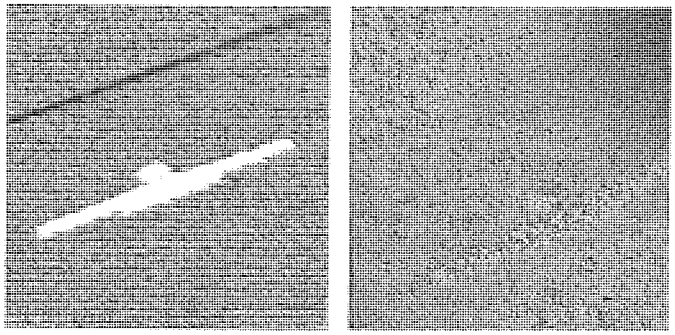

Figure 3-71 At 22°C, RH 40% condition 5kpasses Mp1 tape cycling, SEM image (left), AES Fe element mapping image (right)

Figure 3-71 is a typical AES elemental mapping result for the LTO heads after 5k passes Mp1 tape cycling, for all experimental conditions, the AES analysis showed the similar results (white colour areas stand for Fe signal). The Fe stain was found formed on the surface of the pole and shared pole area, little Fe particles were found on the ceramic regions.

In order to study the structure of Fe based stain, XPS analysis was conducted on both tape and stain (before and after etching). Samples chosen for XPS analysis were the head at 40°C RH 15% where stain coverage was greatest.

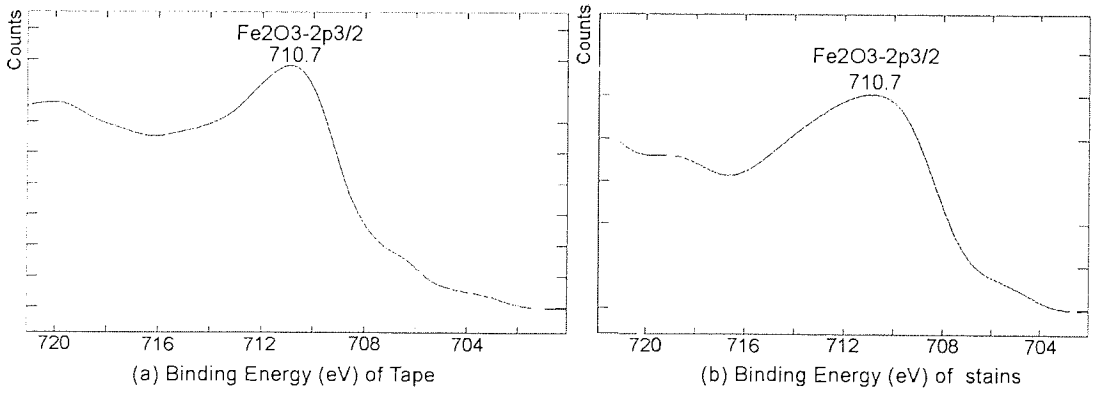

Figure 3-72 XPS spectrum of Fe 2p3 for (a) LTO tape (b) Stain on the head surface

C, O, Fe and traces of N were observed in the stain on the poles. For both head stain and tape samples the Fe2p3/2 peaks of iron appeared at a binding energy 710.7eV (see Figure 3-72(a) and (b)). This value agrees with the Fe_2O_3 2p3/2 value[153]. The magnetic particles in this formulation tape consists of Fe core passivated with α-Fe_2O_3. The

passivated shell was around 5nm thick[28]. Due to its surface sensitivity XPS does not detect the pure Fe core inside tape.

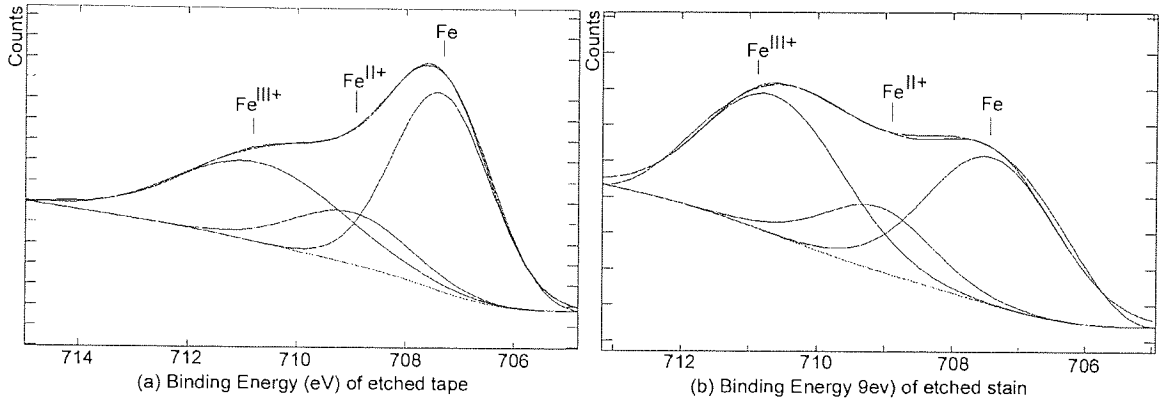

Figure 3-73 (a) XPS spectrum of Fe 2p3 for the LTO tape etched sample (Ar^+ 3keV energy, current 2.0μA/cm^2, etching 10minutes) (b) XPS spectrum of Fe 2p3 for the LTO head stains etched sample (Ar^+ 3keV energy, current 2.0μA/cm^2, etching 10minutes)

Figure 3-73 (a) and (b) shows the XPS spectrum of Fe 2p3 peaks for etched tape and etched head stain respectively. Ar^+ ion etching was employed at beam energy of 3keV energy, current 2.0μA/cm^2 for 10minutes. The 10 minutes etching time was chosen to be great enough to remove sufficient material from the passivated MP particles to reveal the metallic Fe core, but not to cause too much bombardment induced reduction of the Fe oxide[173]. These two spectra clearly show metallic Fe peaks at 707.2 eV, which can only be due to metallic Fe. The other peaks present on the etched stain and tape are due to the Fe^{III+} peaks from the Fe_2O_3 passivation layer and a further peak at due to ion induced reduction of the Fe^{III+} to Fe^{II+} during the Ar ion etching process[173].

3.2.4 LTO Mp1 Tape Wear

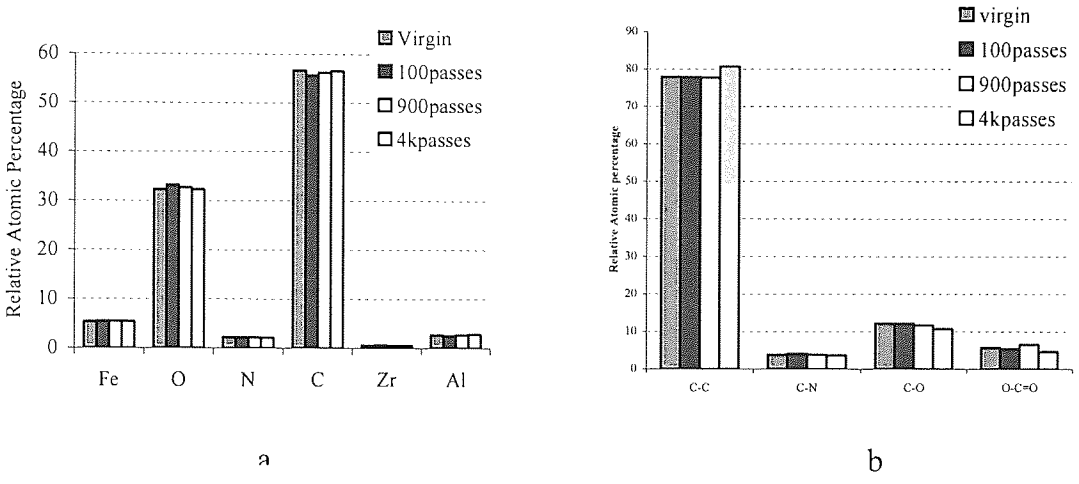

a b

Figure 3-74. At 10°C, RH 10% (a) Elemental trends in the tape surface as a function of number of passes (b) Synthesis of carbon as a function of increasing number of passes

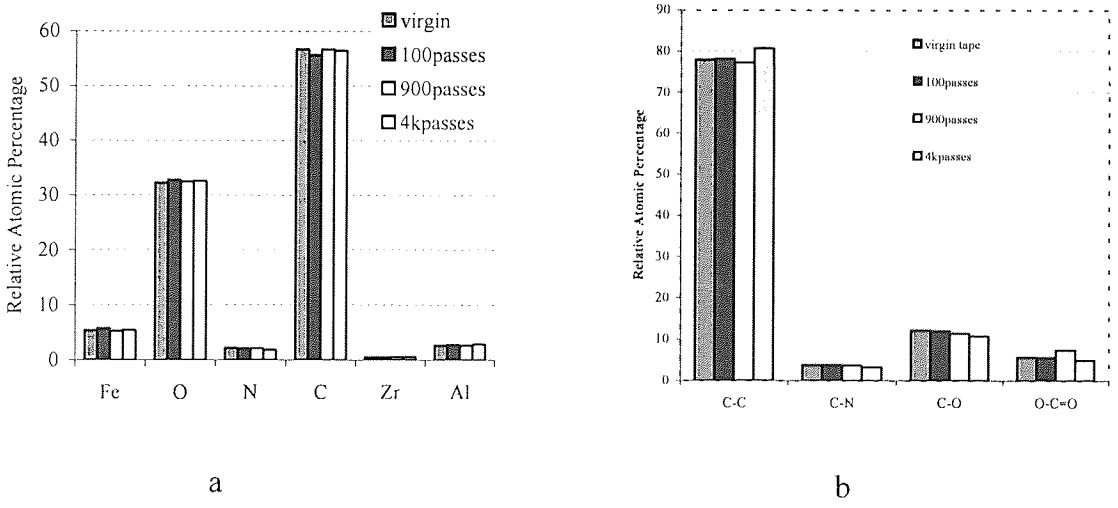

a b

Figure 3-75. At 40°C, RH 15% (a) Elemental trends in the tape surface as a function of number of passes (b) Synthesis of carbon as a function of increasing number of passes

XPS analysis of the Mp1 tape surfaces showed that N (binder indicator) had no significant changes after 1k passes cycling; N could be seen slightly change after 4k passes cycling. Synthesis of the C 1s peak showed that the C-C/C-H component of the C peak increased after 4k passes, indicating that lubricant was immigrating to the surface of the tape with cycling. Mp1 tape has the exactly similar tape formation as Travan5 tape; the wear of Mp1 tape is quite small comparing with Travan5 tape.

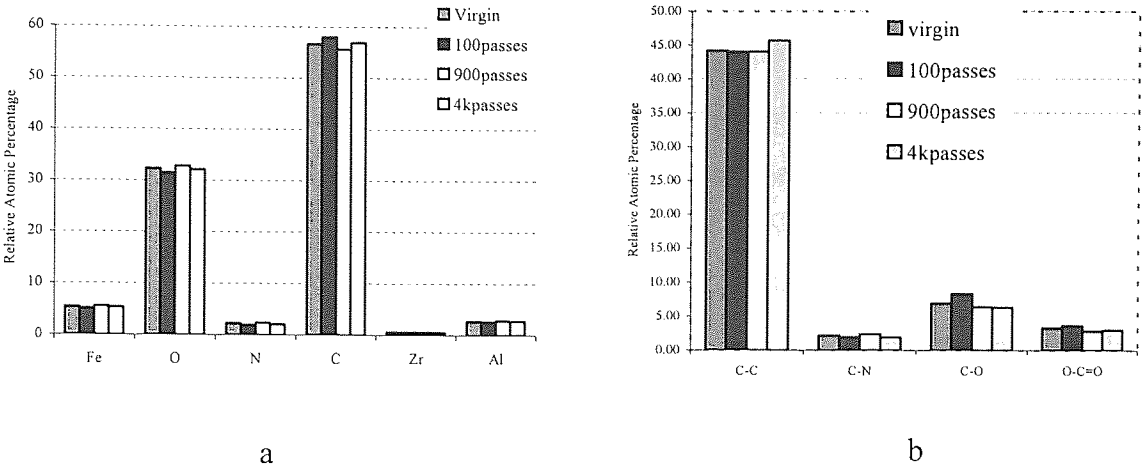

Figure 3-76. At 22°C, RH40% (a) Elemental trends in the tape surface as a function of number of passes (b) Synthesis of carbon as a function of increasing number of passes

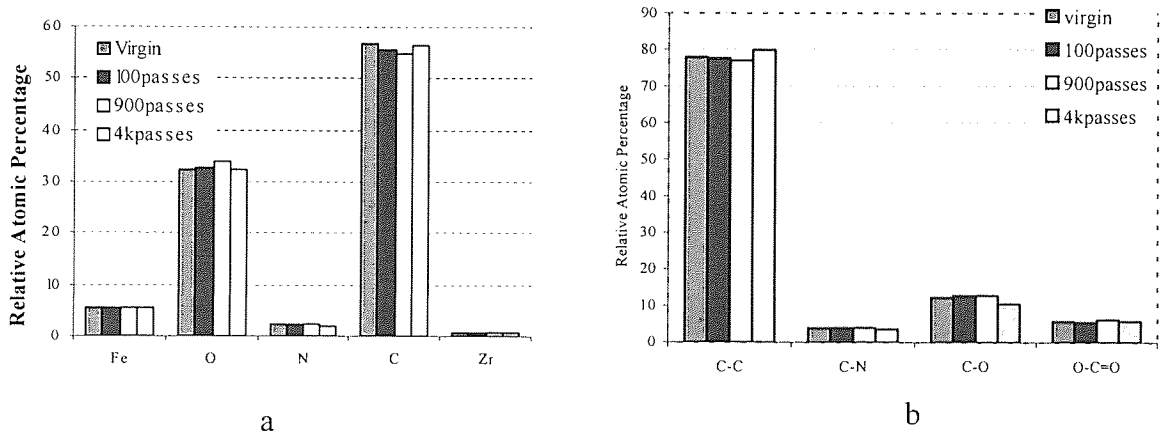

Figure 3-77. At 40°C, RH80% (a) Elemental trends in the tape surface as a function of number of passes (b) Synthesis of carbon as a function of increasing number of passes

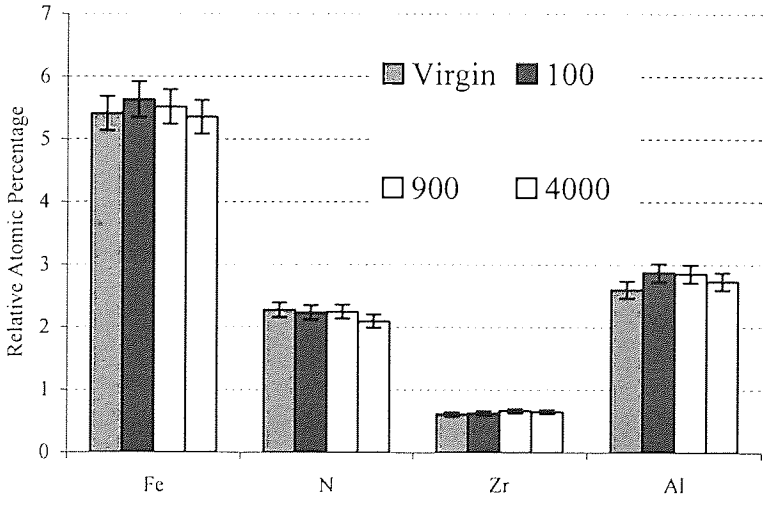

Figure 3-78 At 40°C, RH 80%, elemental trends in the tape surface as a function of number of passes, error bars correspond to standard error of mean

As a typical example of error analysis, MP1 tape results at 40°C, RH 80% is shown. It is well known that for a well defined XPS peak, the error of the atomic ratio in XPS composition analysis is less than one percent, for a weak peak signal, the error of the atomic ratio in XPS is less than ten percent. The typical error analyse of XPS here was chosen at 40°C, RH 80% for Mp1 tape. Figure 3-78 clearly shows the trend of decreasing of N in the surface of the tape. The N composition changed only after 4k passes cycling.

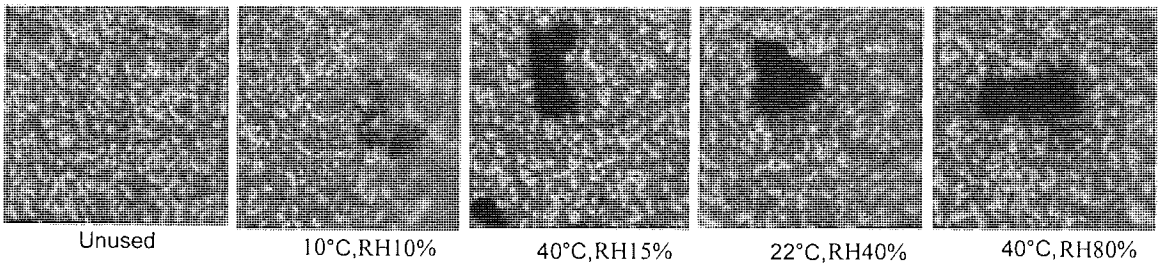

Figure 3-79 Optical micrographs of typical LTO head ceramic debris for Unused, worn head after 1000km cycling against Mp1 tapes in different environmental conditions (400×)

Figure 3-79 shows typical debris distribution at the ceramic surface of the LTO head cycling against Mp1 tapes, there are less tape debris per unit area for LTO head cycling with Mp1 tape comparing with Travan5 system in the same experimental conditions. Increasing temperature and water content; there was more tape debris produced indicating tape degradation in the higher temperature and high water content.

3.3 Experiment results of LTO heads with Fuji tapes

3.3.1 LTO Head Wear with Fuji Tape

3.3.1.1 Unused LTO head

Figure 3-80 shows AFM generated images of a typical unused LTO head. For an unused head, the pole was slightly recessed from the insulator by about 2-3nm, whilst the pullout depth for the ceramic region, was around 5-7nm. These pullouts were formed during manufacturing processing, insulator was very smooth, roughness (RMS) was around 5nm. The LTO heads are very similar with Travan5 heads, but LTO heads adopt multi-channel and slot technique as mentioned early in Chapter Two.

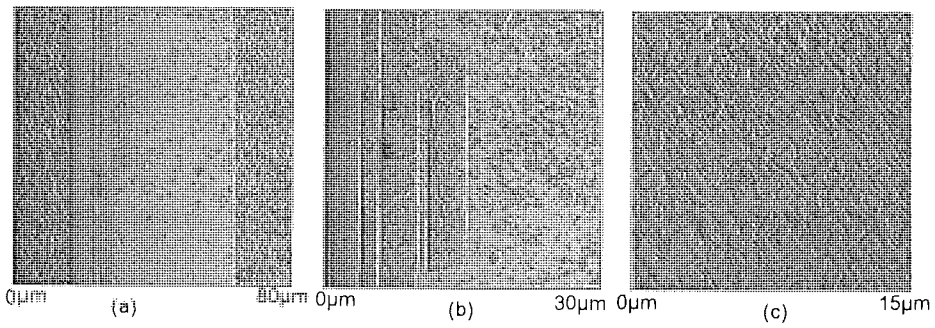

Figure 3-80 (a) Virgin LTO head (one channel), (b) pole area, (c) ceramic area.

3.3.1.2 LTO head Wear cycling against Fuji tape

Figure 3-81 shows after 100passes, the poles were still slightly recessed from the insulator and some fine, small particles could be seen on the surface of the head. After 1k passes, it was very clearly seen that some wear occurred in the surface of the poles. After 5k passes of tape cycling, the poles were seen to be similar height to the insulator. Fine particles had been deposited on the surface of the heads (pole area). The less extensive and patchy deposits (at 10°C, RH 10%, 5k passes) were polymer deposits (identified by AES). The insulator and pole wear also can be seen from images. Amongst the conditions at which the heads were tested, the high humidity and high temperature conditions were observed to produce deep and wide grooves in the pole region. Three-body particle scratches can be clearly seen (see Figure 3-81 pole area

40°C, RH 80% after 5K passes). The particles on the pole had been identified Ti bearing particles by AES, which had also reported by our group's former work as well[77,86, 101].

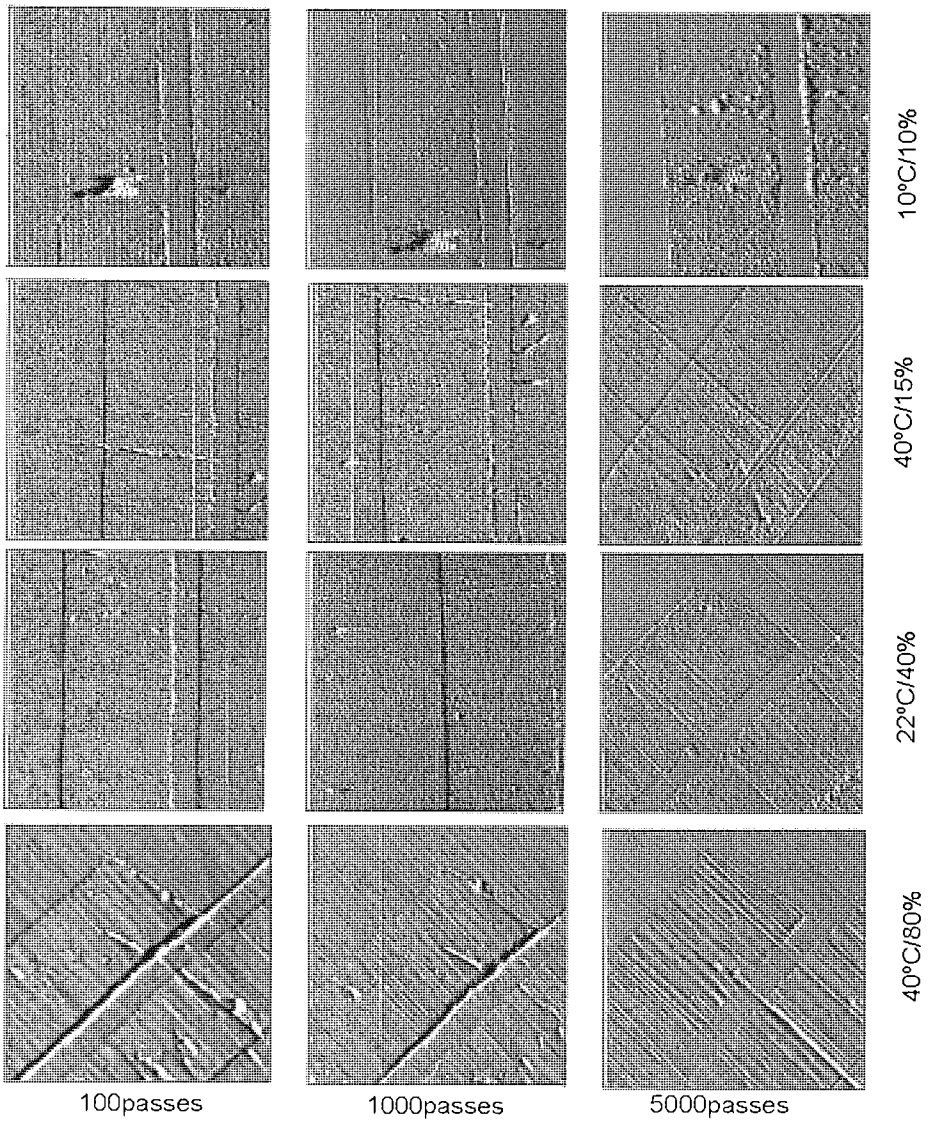

Figure 3-81 AFM images of head pole area cycling different passes at different conditions with Fuji tapes (10μm×10μm)

For the condition of 10°C RH 10%, 22°C RH 40%, 40°C, RH 15%, Figure 3-82 shows the wear of the ceramic region, the unused head ceramic pullout was around 5-7nm. The depth of the pullout in the ceramic region was quite similar to the unused head after 100passes of the tapes cycling. After 1k passes, the pullout depth was around 9-10nm. After 5k passes, the pullout depth reached around 15-18nm.

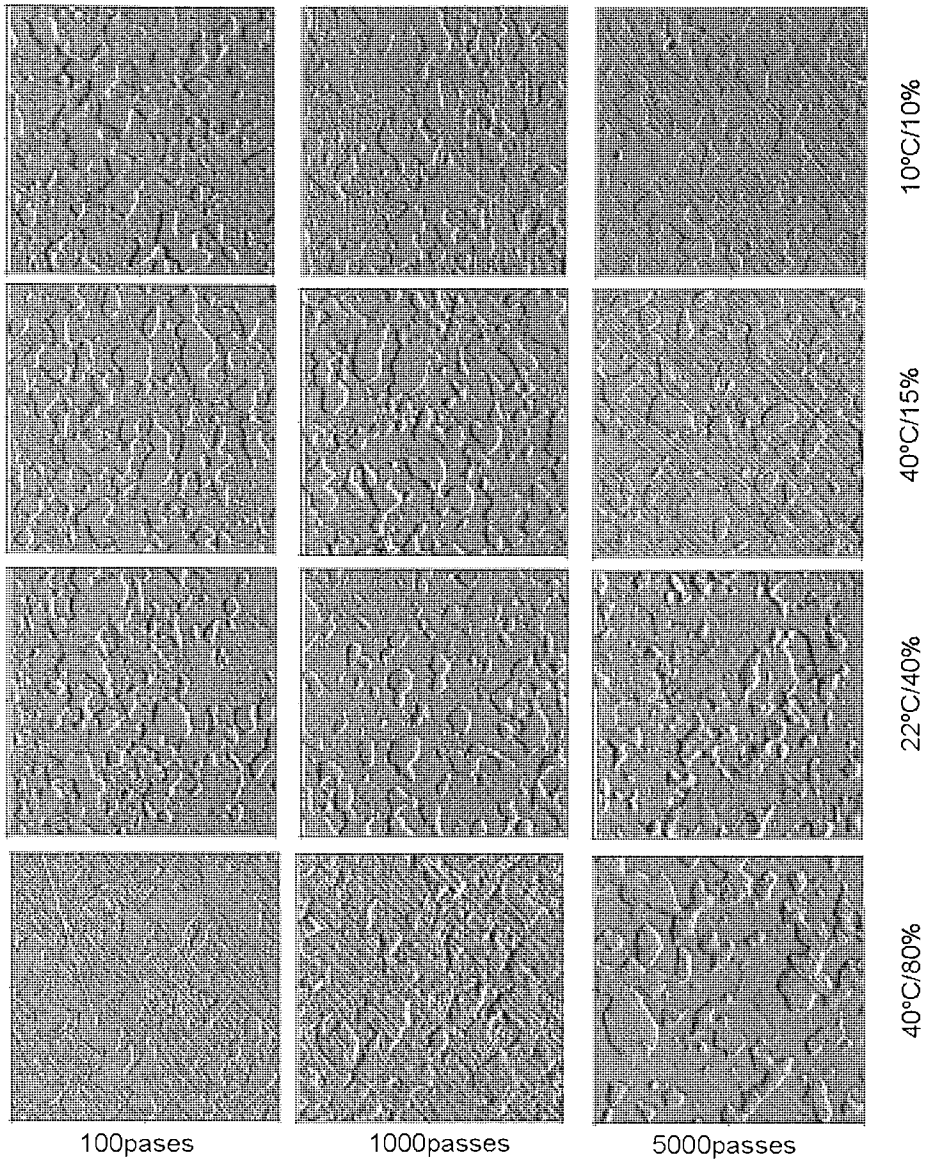

Figure 3-82 AFM images of head ceramic wear after different passes in different conditions with Fuji tapes (10μm×10μm)

For the condition of 40°C, RH 80%, after 5000passes, the pullout depth of the ceramic had increased to around 22nm with large pullouts and scratches in the ceramic region.

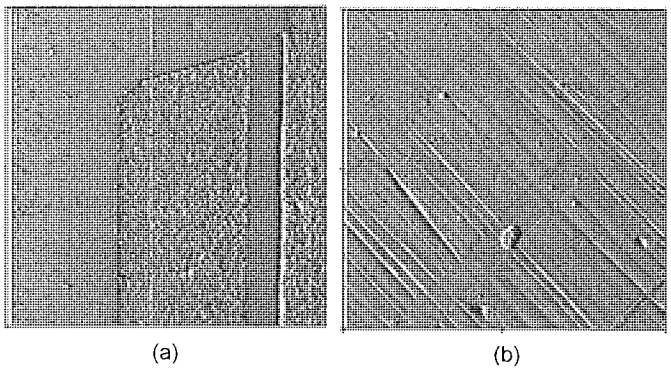

Figure 3-83 LTO Ceramic and pole wear after cycling with Fuji tape at 40°C, RH 15% (a) unused Pole area (10 μm×10 μm) (b) Worn pole area after 5k passes of tape (10 μm×10 μm)

A worn head pole surface was shown in Figure 3-83, it clearly shows grooves and scratches on head pole surfaces after the wear test. Particles were clearly spotted on the worn pole area. The particles appeared on the surface of the head were found to be Ti bearing particles by AES.

3.3.2 LTO Head stain with Fuji tape

The Table 3-16 to Table 3-19 showed the AES results of the head surface after cycling against LTO Fuji tape, Fe stain was not found. Ti element was observed on the surface of pole and insulator which only source was coming from AlTiC pullout.

Constituent part	C	Ti	O	Fe	Co	Al
Pole	43.5	1.2	20.3	0.0	34.9	0.0
Pole/shield	62.4	0.0	14.4	0.0	23.1	0.0
Insulator	48.5	0.0	36.1	0.0	0.0	15.5
Ceramic (pole side)	68.6	3.1	16.8	0.0	0.0	11.6
Ceramic (shield side)	68.1	4.5	16.2	0.0	0.0	11.2

Table 3-16 the atomic percentage concentration of AES results of LTO head with Fuji tape (RH10%, 10°C, 5k passes)

Constituent part	C	Ti	O	Fe	Co	Al
Pole	78.8	0.0	16.6	0.0	4.6	0.0
Pole/shield	80.5	0.9	13.6	0.0	4.9	0.0
Insulator	66.6	0.0	17.7	0.0	0.0	15.5
Ceramic (pole side)	66.0	6.4	17.4	2.2	0.0	7.9
Ceramic (shield side)	65.8	4.8	18.1	2.1	0.0	9.3

Table 3-17 the atomic percentage concentration of AES results of LTO head with Fuji tape (RH40%, 22°C, 5k passes)

Constituent part	C	Ti	O	Fe	Co	Al
Pole	64.5	0.0	19.3	0.0	16.3	0.0
Pole/shield	71.8	0.0	12.9	0.0	15.3	0.0
Insulator	66.3	0.0	17.9	0.0	0.0	15.4
Ceramic (pole side)	58.4	11.3	21.0	0.0	0.0	9.3
Ceramic (shield side)	45.9	9.8	26.3	0.0	0.0	17.9

Table 3-18 the atomic percentage concentration of AES results of LTO head with Fuji tape (RH80%, 40°C, 5k passes)

Constituent part	C	Ti	O	Fe	Co	Al
Pole	77.5	2.2	8.5	0.0	11.8	0.0
Pole/shield	84.3	0.0	5.6	0.0	10.1	0.0
Insulator	70.4	0.0	16.4	0.0	0.0	13.2
Ceramic (pole side)	65.5	5.6	18.7	0.0	0.0	10.2
Ceramic (shield side)	64.8	7.8	17.7	0.0	0.0	9.7

Table 3-19 the atomic percentage concentration of AES results of LTO head with Fuji tape (RH15%, 40°C, 5k passes)

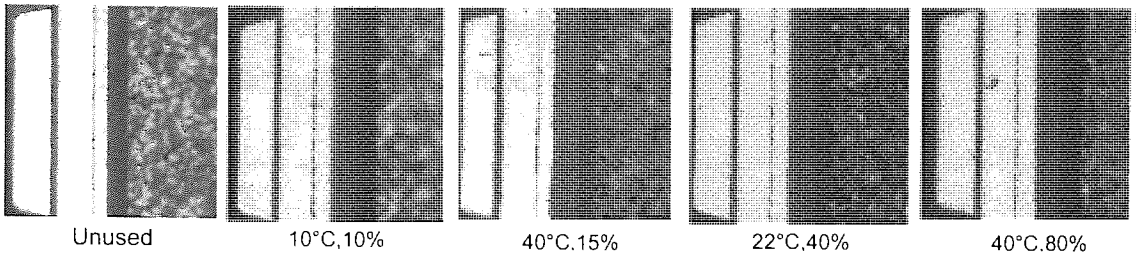

Figure 3-84 Optical micrographs of LTO head pole area, unused and worn heads after 5k passes cycling against Fuji tapes at different environmental conditions (400×)

Figure 3-84 shows the worn head pole area is basically clear, confirms the AFM and Auger results, indicating there was no Fe stain on the surface of the pole area; No Fe stain was detected on the pole/shared pole, AES analyse only showed trace of Fe particles on the ceramic surface of head.

3.3.3 LTO head PTR with Fuji tape

The effects of increasing water content on PTR were shown in Table 3-20. For the similar water content conditions the PTR was similar, for the highest humidity and highest temperature the wear of the head was highest, and also the PTR reached the highest. The PTR for the unused LTO head was around 25nm.

Environmental condition	10°C/ RH10%	22°C/ RH 40%	40°C/ RH 15%	40°C/ RH 80%
Normalised Water Content (NWC)	1.0	7.5	6.7	35.5
Pole Tip Recession (After 5000passes)	(36±2) nm	(38±2) nm	(40±2) nm	(53±2) nm

Table 3-20 Pole Tip Recession of the LTO heads after different passes and different environmental working conditions.

PTR of LTO heads was less than the Travan5 system. Both systems showed the more wear at the higher temperature and higher water content conditions. The reason for less wear in LTO systems will be discussed in the chapter 4.

3.3.4 LTO Fuji Tape Wear

Typical Fuji virgin tape XPS analysis was shown in Figure 3-85, C, O, Fe, N, Cl, Y and Al were found on the top layer of the tape.

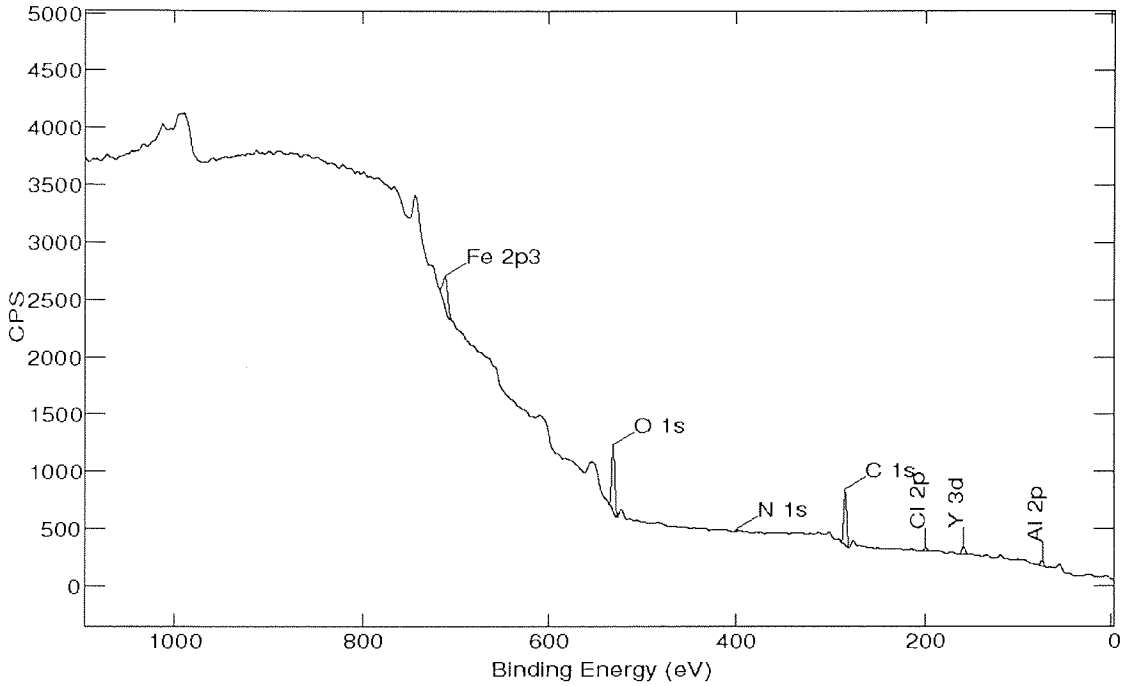

Figure 3-85 Wide scan spectrum for virgin LTO Fuji tape

XPS analysis of Fuji tape showed as following, C was mainly from the binder (urethane: H_2N-NH-C(=O)-O-C_2H_5 or vinyl chlorine :H_2C=CHCl) and lubricant (fatty acid ester, e.g. $C_{13}H_{27}$-O-C(=O)-$C_{18}H_{37}$) but also from a hydrocarbon contamination layer on the outer surface of the tape; the Fe originated from the magnetic pigment; O from the binder, lubricant, Fe oxide and Al and Zr oxides; the presence of N and Cl were due entirely to the constituents of the binder, Al was present in the tape as a head-cleaning agent, as was Zr. Y possibly as an anti-sintering agent for the Fe particles.

However, as mentioned before the C-N and C-Cl provided a good indication of the relative changes in the concentration of binder material since each of these peaks arises from bonds within the binder.

Figure 3-86 shows at 10°C, RH 10%, elemental trends in the tape surface as a function of number of passes, as mentioned early, the typical error of XPS quantitative analysis is less than one percent of the value itself for a well defined peak. Figure 3-87 clearly

revealed the binder N and Cl decreased with the tape cycling, C1s peak fitting results (Figure 3-88) showed the similar trends of the tape wear.

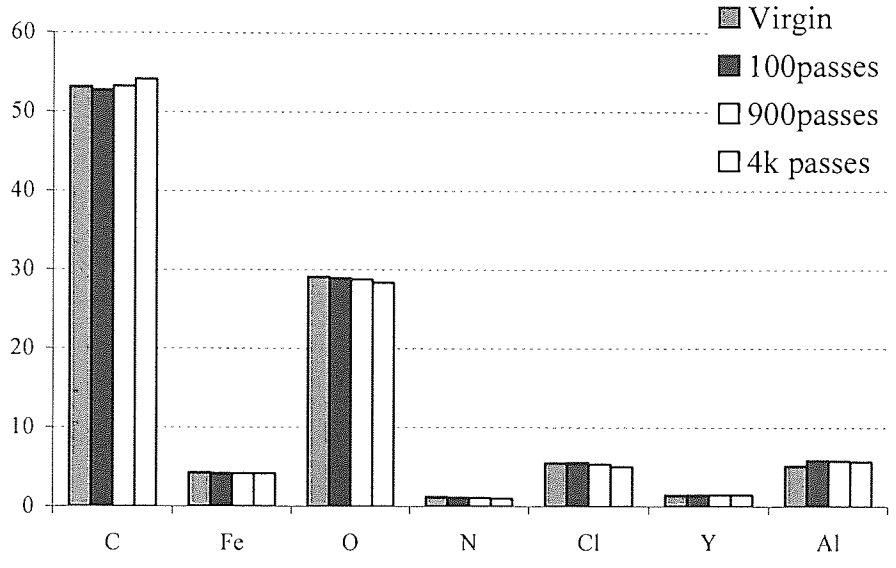

Figure 3-86 At 10°C, RH 10%, elemental trends in the tape surface as a function of number of passes

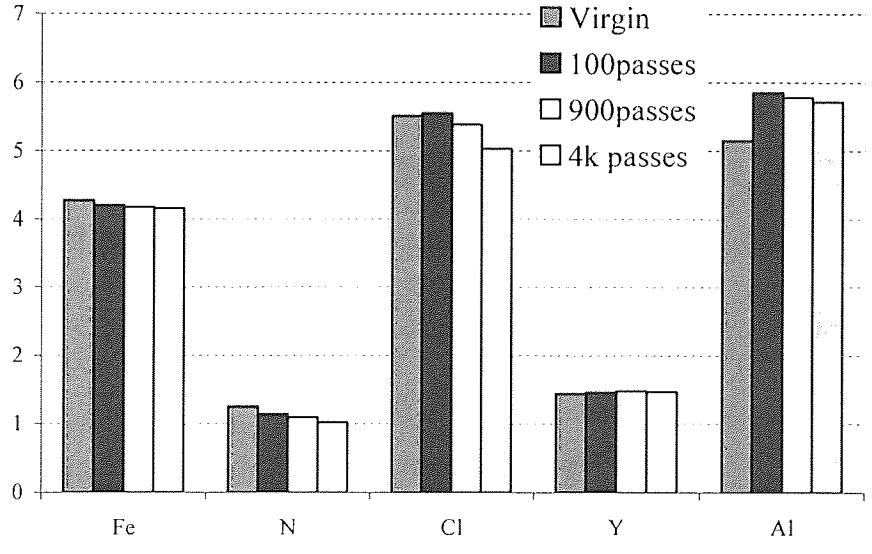

Figure 3-87 At 10°C, RH 10%, enlarged elemental trends including Fe, N, Cl Al and Y in the tape surface as a function of number of passes

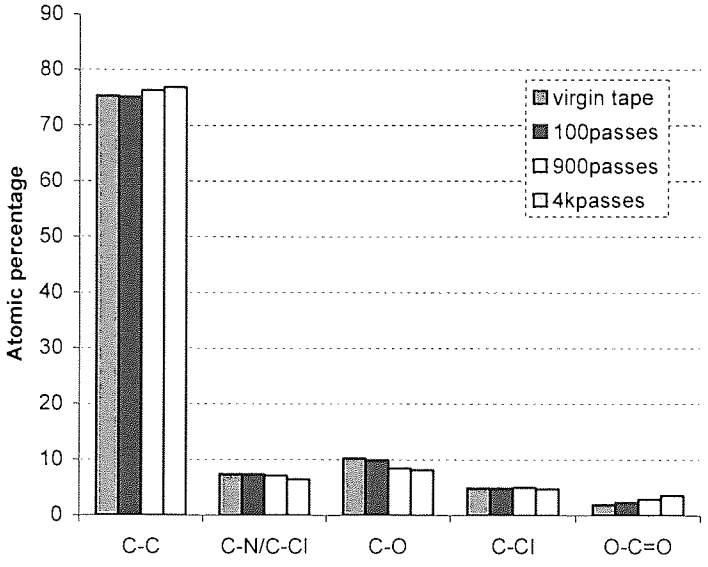

Figure 3-88 At 10°C, RH10%, synthesis of carbon as a function of increasing number of passes

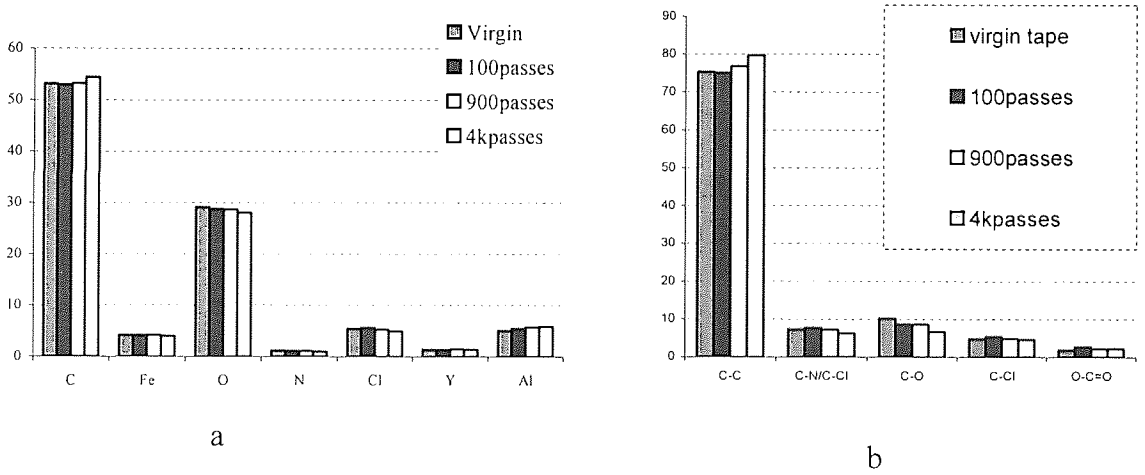

Figure 3-89 At 40°C, RH 15% (a) Elemental trends in the tape surface as a function of number of passes (b) Synthesis of carbon as a function of increasing number of passes

From Figure 3-86 to Figure 3-91, it is clear that the tape wear was very small, common wear trends can be obtained. For each set of environmental conditions XPS analysis of the tape surfaces showed that N and Cl and hence binder had slightly decreased with cycling. The Fe was quite similar to virgin tape. However, the C signal was seen to increase with cycling for each condition (the highest concentration was at the 40°C, RH 80%). Synthesis of the C 1s peak showed that the increase was wholly due to the aliphatic C-C/C-H component of the C peak, indicating that lubricant was immigrating to the surface of the tape with cycling, some binder had been lost. Migration of lubricant to the surface kept the surface layer in the tape at an approximately constant thickness

covering the magnetic particles. This small loss in binder was probably transferred to the head surface as a very thin polymeric film.

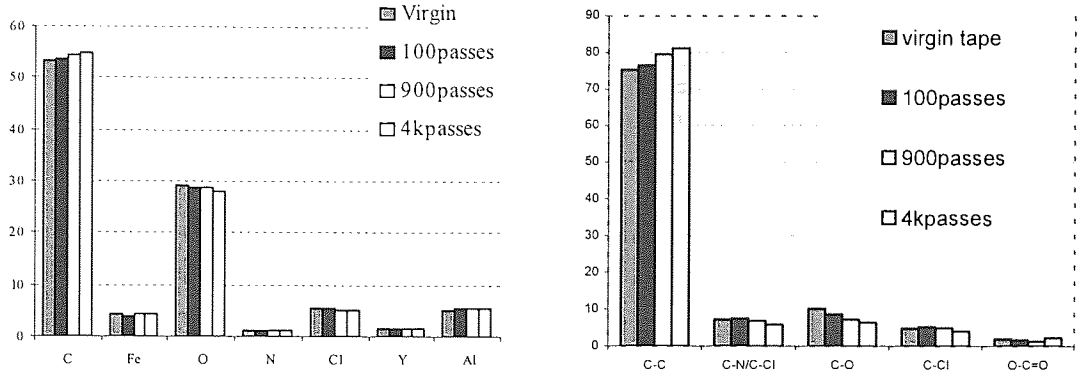

a b

Figure 3-90 at 22°C, RH 40% (a) Elemental trends in the tape surface as a function of number of passes (b) Synthesis of carbon as a function of increasing number of passes

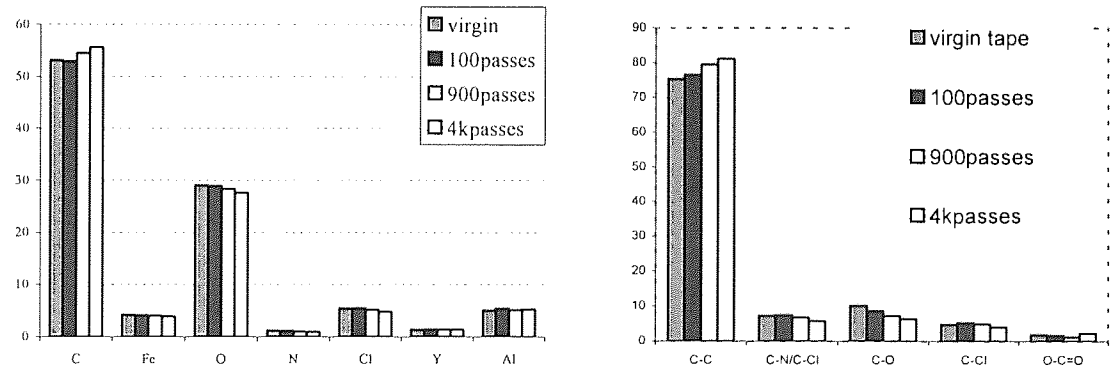

a b

Figure 3-91 at 40°C, RH 80% (a) Elemental trends in the tape surface as a function of number of passes (b) Synthesis of carbon as a function of increasing number of passes

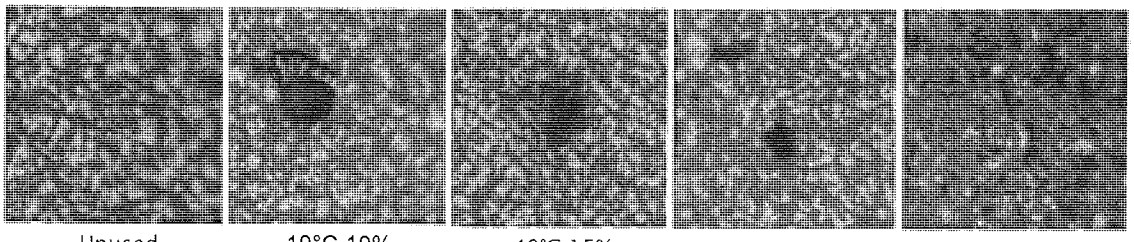

Figure 3-92 Optical micrographs of typical LTO head ceramic debris for unused, worn head after 1000km cycling against Fuji tapes in different environmental conditions (400×)

Optical pictures in Figure 3-92 show the tape debris distribution on the ceramic of the head, which indicated that more tape debris was generated at the high temperature and high water content condition.

3.4 Experiment results of LTO heads with Maxwell tapes

3.4.1 LTO head wear with Maxell tapes

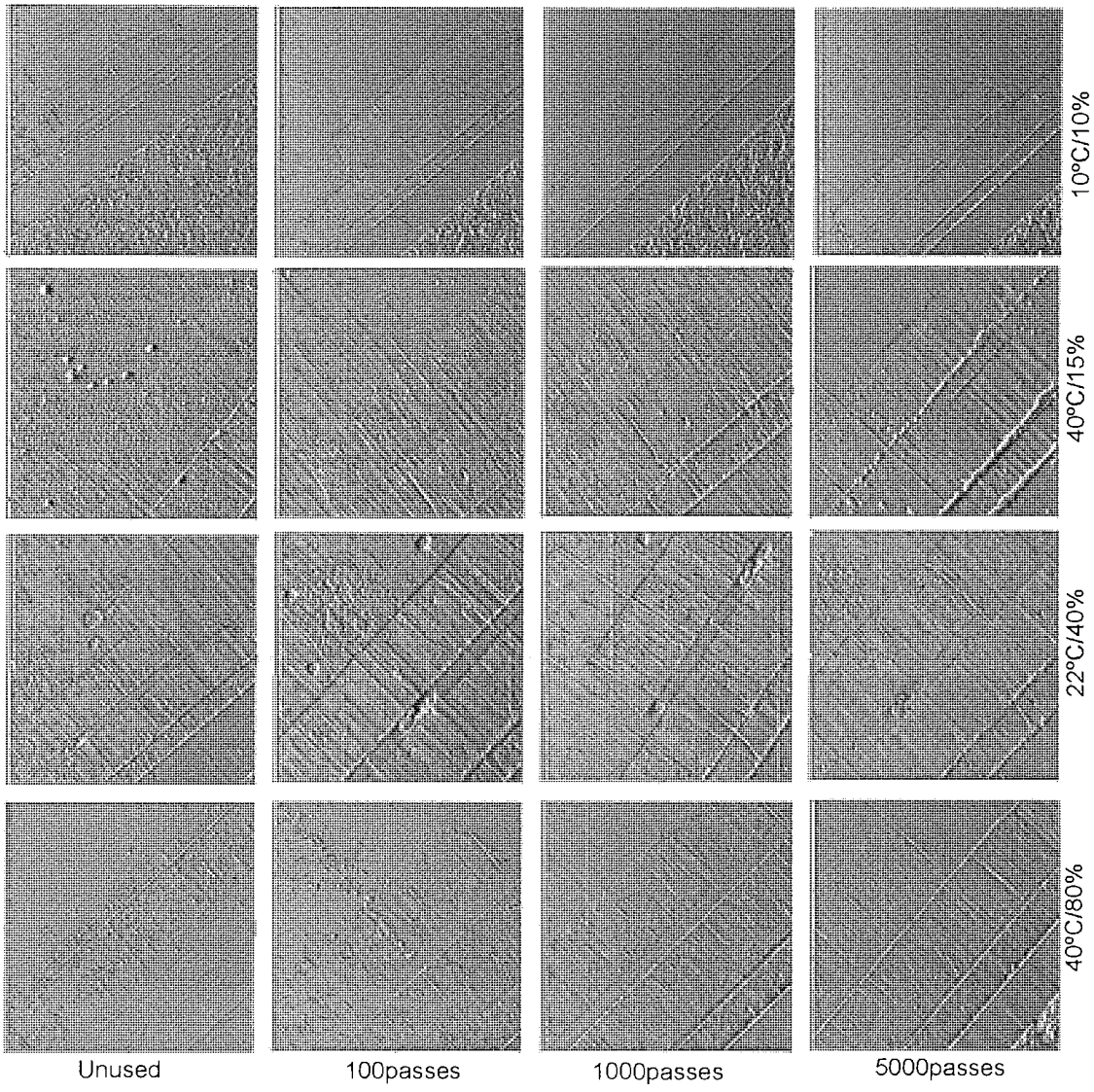

Figure 3-93 AFM images of Head pole area at condition of 10°C, RH 10% (30μm×30μm), Other conditions images are 15μm×15μm scale

Figure 3-93 shows the AFM images of surfaces of the poles generated after experiments performed over a variety of environmental conditions. Environmental conditions were the same used for the experiment conducted with other LTO tapes. No deposits (stain) were seen on the surface of heads after cycling LTO Maxell tapes; Auger electron spectroscopy results also confirm this result. Some scratches can be seen on the pole surface of the head that indicating three-body abrasive wear of the heads. A little tape

material was transferred to the heads gap between the pole and insulator at the 40°C, RH 15% condition.

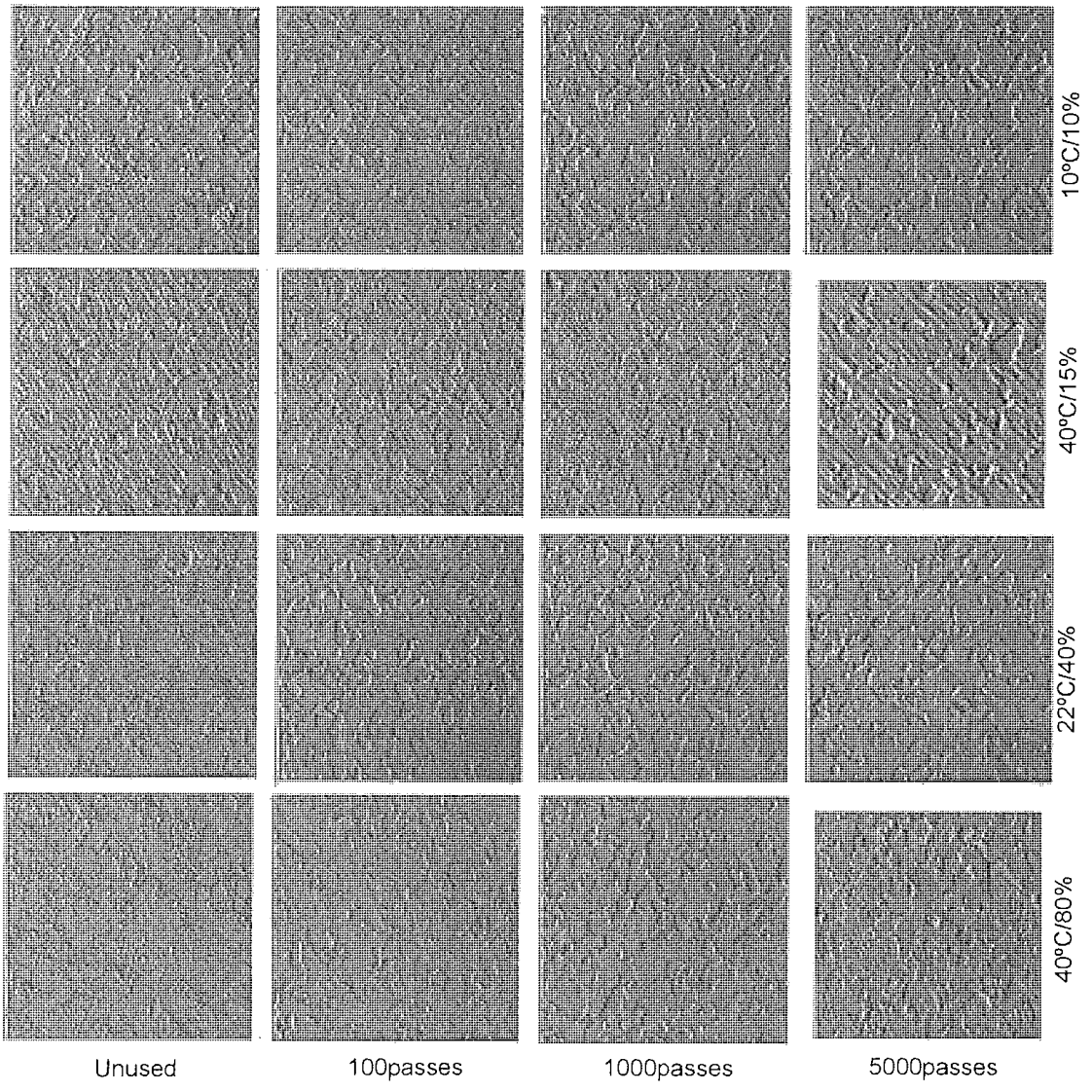

Figure 3-94 AFM images of head ceramic wear after different passes at different conditions (15μm×15μm)

Figure 3-94 shows AFM surface images of ceramic after cycling LTO Maxell tapes. Only at the 40°C conditions, was some transfer material observed on the ceramic surface and this was very little. This was an indication of the tape degradation that is known to occur at higher temperatures[174]. Some scratches can be seen on the head surface. Ceramic surface pullout from the TiC grains of the unused heads averaged 4nm. This increased to around 15-17nm after 5k passes of tape sliding.

3.4.2 LTO Head stain with Maxell tapes

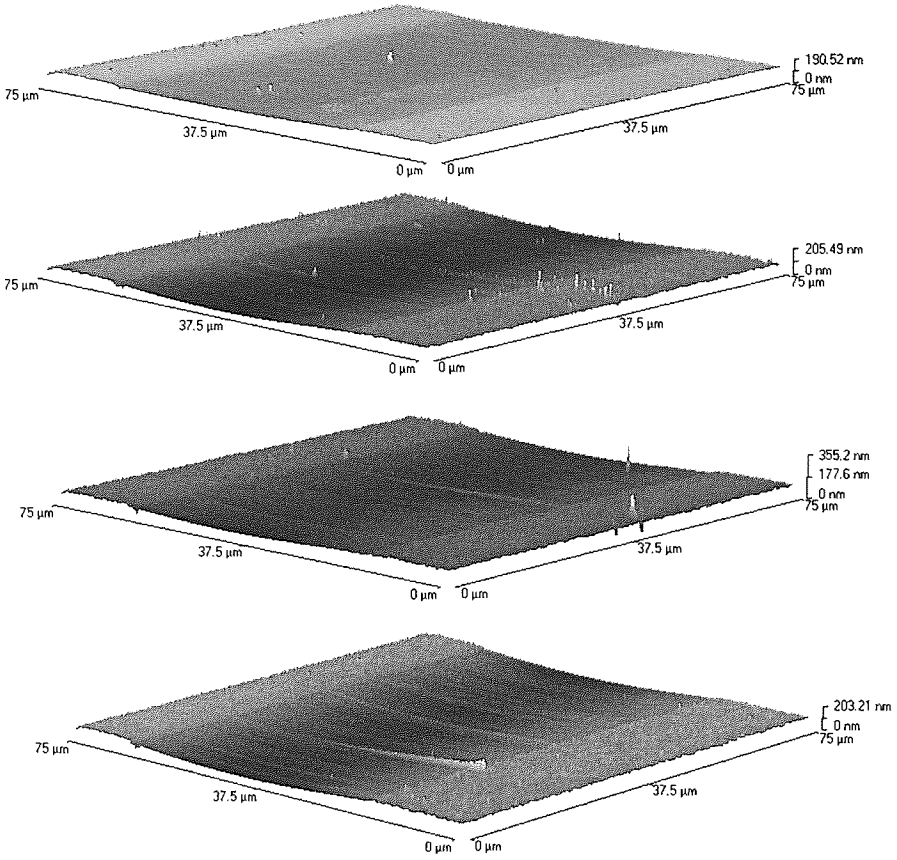

Figure 3-95 AFM 3D images of LTO heads, unused, 100 passes, 1k passes, 5k passes (from top to bottom) at 40°C, RH 80% condition with Maxell tapes

Figure 3-95 shows the progression of wear in the LTO head system; the unused head surface was clean, with PTR around 25nm; after 100passes cycling with tape, some fine particles appeared on the surface of heads; after 1k passes the image clearly showed the pole area and insulator area were recessed compared with unused head. After 5k passes cycling against tape, the image showed a further increase in recession of pole areas, AES and AFM results confirmed that there were no Fe stains or polymer stains developed on the surface of heads.

Figure 3-96 optical images show the worn head pole area was very clear, confirmed the AFM and Auger results and indicating that there was no Fe stain on the surface of the pole area.

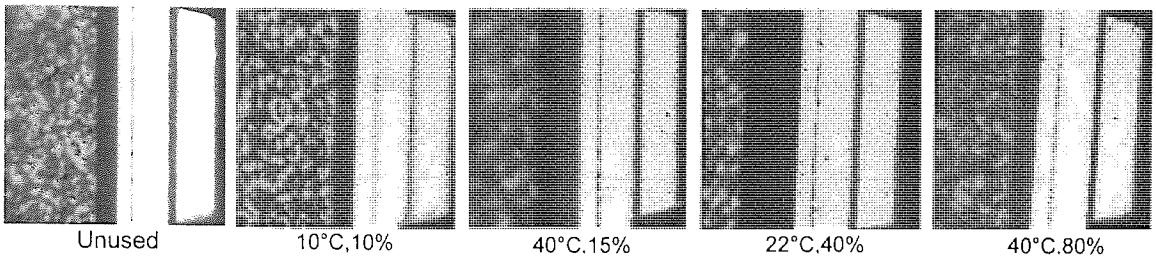

Figure 3-96 Optical micrographs of LTO head pole area, unused and worn heads after 1000km cycling against Maxell tapes in different environmental conditions (400×)

3.4.3 Effects of water on the AlTiC ceramic of LTO heads—XPS

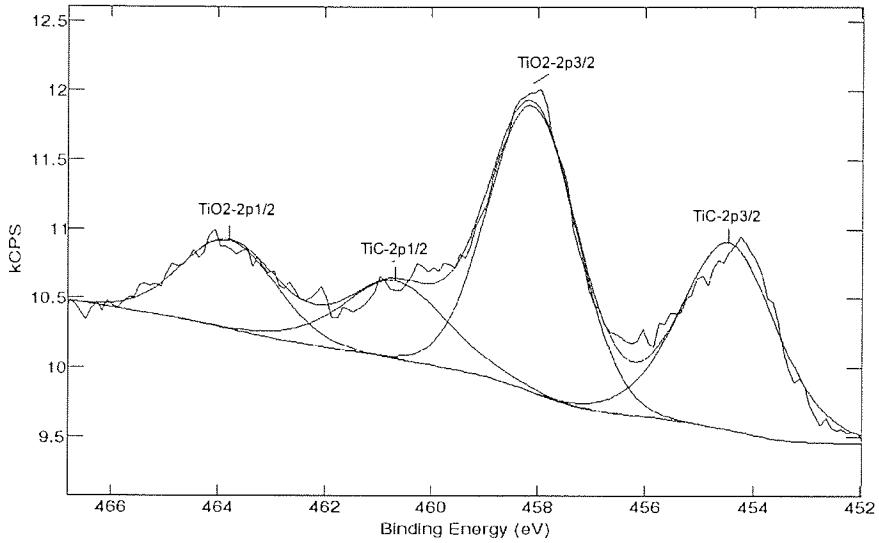

Figure 3-97 the typical Ti2p core-level XPS peaks of TiO_2 and TiC existing in the same AlTiC sample

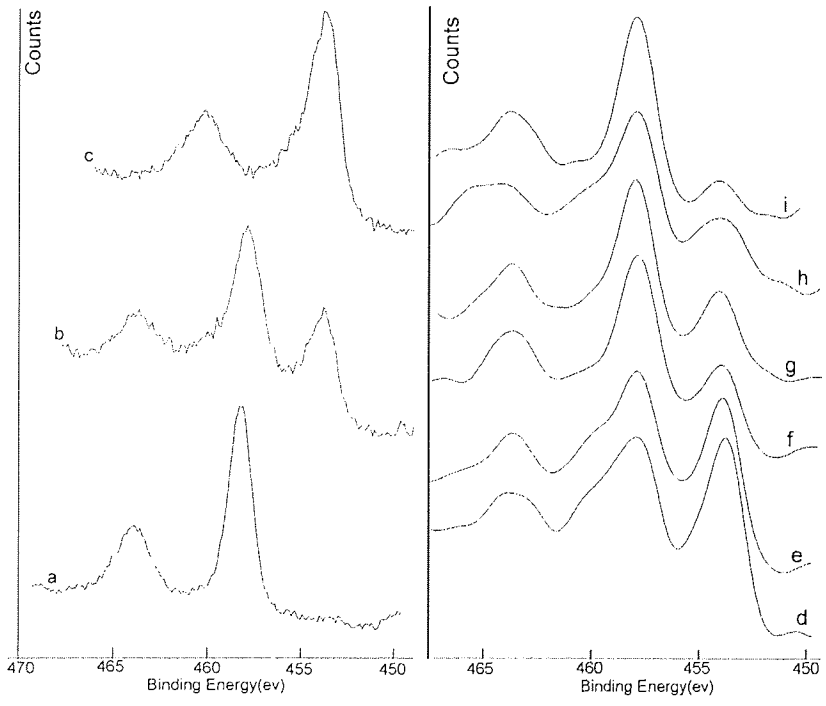

Figure 3-98 Ti2p photoelectron peaks (a) Boiled AlTiC sample for 30hrs in de-ion water; (b) Virgin AlTiC; (c) Pure AlTiC without TiO_2; (d)Unused LTO head Ceramic; (e) Head after RH10%, 10°C,5k passes cycling; (f) Head after RH15%, 40°C,5k passes cycling; (g) Head after RH40%, 22°C,5k passes cycling; (h) Head after RH80%, 40°C,5k passes cycling; (i)Boiled real LTO head for 30hrs

Figure 3-97 is a typical spectra showing Ti2p core-level XPS peaks of TiO_2 and TiC from AlTiC sample. The individual components had been synthesised using codes inherent in the VG ECLIPSE data system after applying a Shirley background subtraction. All peaks were referenced to the adventitious C1s at binding energy of 284.6eV, the C1s component from C in TiC, also visible in the C 1s spectra which has a binding energy of 281.5eV. In the spectra shown in Figure 3-97, the Ti $2p_{3/2}$ peaks at 454.0eV and 458.3eV were due to TiC and TiO_2 respectively. Peaks at 460eV and 463.9eV were the corresponding $Ti2p_{1/2}$ peaks for these compounds[153].

Figure 3-98 show XPS Ti2p photoelectron spectra from (a) a sample of AlTiC boiled for a period of 30hrs in deionized water (b) an unused "as received" sample of AlTiC and (c) a sample of AlTiC which had been etched in a solution of 0.7 gram ammonium bifluoride per litre deionized water to remove all the TiO_2. All samples were flat, 2mm×3mm slabs of AlTiC, roughly 1mm thick. The results for boiling the pure AlTiC sample, Figure 3-98 (a) shows the surface of the TiC to be totally converted to TiO_2 after boiling. From knowledge of the surface sensitivity of the XPS technique, the TiO_2 layer must be at least 10nm thick. In Figure 3-98 (c) for pure AlTiC with the TiO_2 removed, only the $Ti2p_{3/2}$ due to TiC were present, In Figure 3-98 (b) the "as received" AlTiC sample, both TiC and TiO_2 were present. These binding energy values from this series of analyses were used to unequivocally identify the compounds found in the tribological samples.

Figure 3-98 (d)-(h) show the effect of atmospheric water content and temperature on the relative concentrations of the TiC and TiO_2 after cycling real heads against tape ((d) is unused head). The spectra from (d) to (I) show that the peaks due to the TiO_2 ($Ti2p_{3/2}$ 458.3eV, $Ti2p_{1/2}$ 463.9eV) progressively increasing in intensity as the TiC peaks ($Ti2p_{3/2}$ 454.0eV, $Ti2p_{1/2}$ 460.0eV) decrease in intensity. This indicated an increasing thickness (and possible areal coverage) of TiO_2 on the surface of the TiC grains with increased atmospheric water content. In all the experiments performed the Al_2O_3 signals were unchanged, indicating no changes in the Al_2O_3 phase of the ceramic. C contamination levels were also similar for all samples.

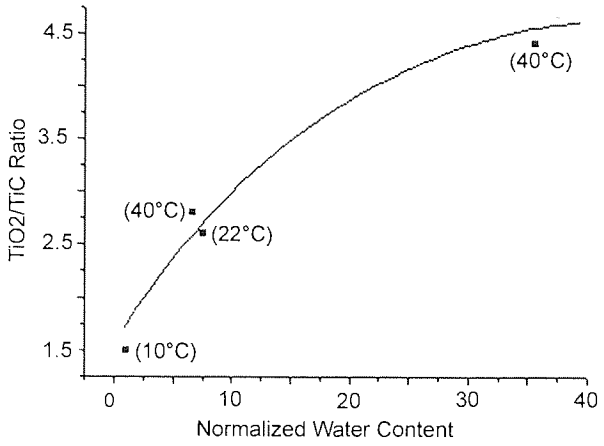

Figure 3-99 the ratio of TiO_2 to TiC on the surface of heads with water content increases

Head condition	Unused Head	10°C, RH10% 5k passes NWC 1.0	40°C, RH15%, 5k passes NWC 6.7	22°C, RH 40%, 5k passes NWC 7.5	40°C, RH 80% 5k passes NWC 35.5	Boiled Head
(TiO_2/TiC) Ratio	1.0	1.50	2.8	2.7	4.4	7.2

Table 3-21 the ratio of TiO_2 to TiC on the surface of heads changes with water content increases corresponding to Figure 3-98 (d)-(I)

Figure 3-99 and Table 3-21 show the variation of TiO_2 : TiC ratio with increase in atmospheric water content. This clearly shows that oxidation rate at the TiC grain surface increased as water content increase. It also indicates that the oxidation rate was relatively insensitive to changes of ambient temperature in the range employed in these experiments.

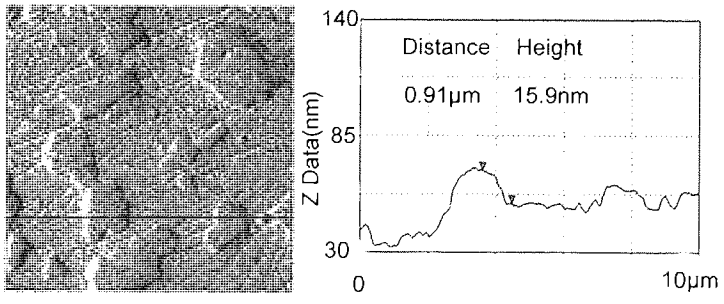

Figure3-100 AFM image of Virgin AlTiC sample

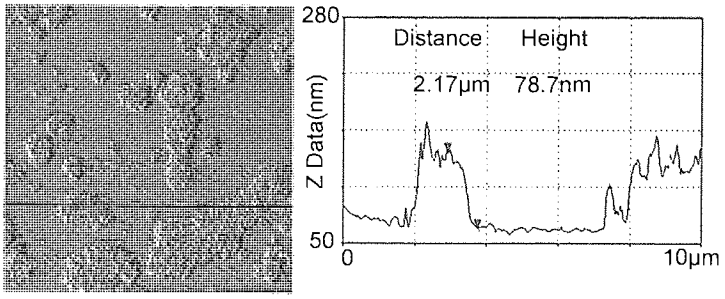

Figure3-101 AFM image of AlTiC sample boiled in de-ion water for 30hrs

Figure3-100 shows an AFM image of an "as received" ALTiC sample and Figure3-101 shows AlTiC sample after boiling in de-ionised water for 30hrs to simulate operation in an extreme saturated environment. Both samples clearly showed eruptions on the TiC grains of the ceramic surface. AFM line scan measurements indicated that the height of these eruptions was about 15nm above the general ceramic surface for the unused sample and about 70nm for the boiled sample. Similar, but less pronounced results were found for the ceramic of a real head subject to boiling, the boiled sample was fully covered with TiO_2 shown by XPS, this was different from "as received" sample.

3.4.4 LTO heads PTR with Maxell tapes

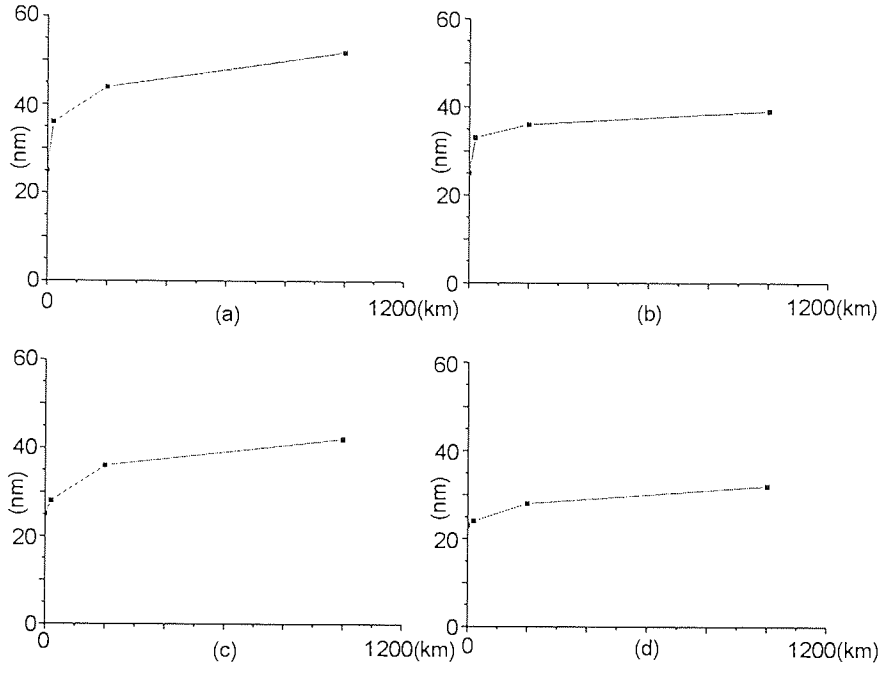

Figure 3-102 PTR of LTO heads cycling with Tape (a) 40°C, RH 80%(NWC 35.5) (b) 22°C, RH40% (NWC 7.5) (c) 40°C, RH15% (NWC6.7) (d) 10°C, RH 10%(NWC 1.0)

The PTR of LTO heads cycling with LTO tapes was smaller than that previously reported for the Travan5 system, this is the case for LTO head with Maxell tape as well. Figure 3-102 (d) shows the lowest PTR value, which showed that the lowest temperature and lowest water content produced the smallest PTR. In Figure 3-102 (b) and Figure 3-102 (c) the water contents were similar; the PTR values of these two conditions were also close. From Figure 3-102 (a), it was clear that higher water content and higher temperature produced higher PTR; it is known that the PTR value reached saturated value in less than 5k passes of tape cycling.

3.4.5 LTO Maxell Tape Wear

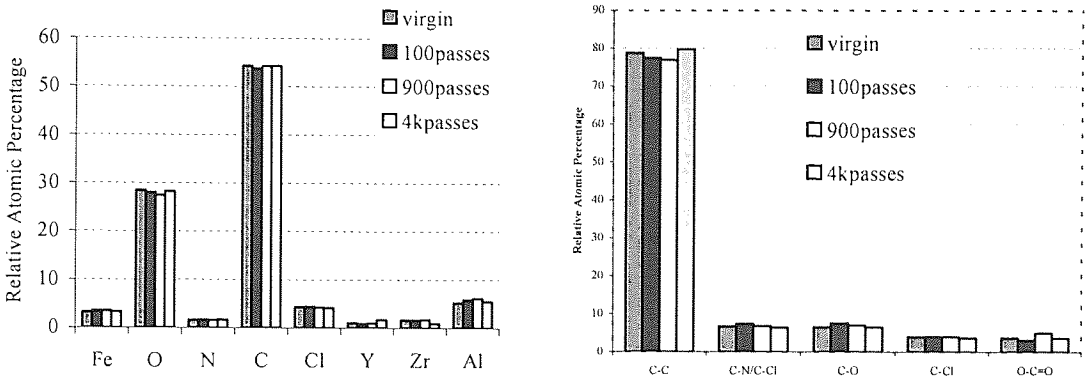

a b

Figure 3-103. At 10°C, RH 10% (a) Elemental trends in the tape surface as a function of number of passes (b) Synthesis of carbon as a function of increasing number of passes

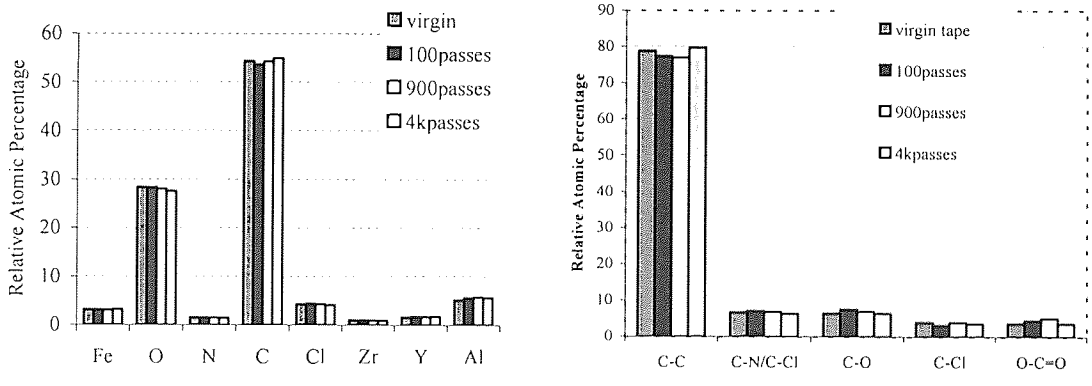

a b

Figure 3-104. At 40°C, RH15% (a) Elemental trends in the tape surface as a function of number of passes (b) Synthesis of carbon as a function of increasing number of passes

The wear of LTO Maxwell tape was very small. XPS analysis of the tape surfaces showed that N and Cl (binder indicator) had no significant changes with cycling at each condition. However, the C signal was seen to increase with cycling for each condition. Synthesis of the C 1s peak revealed that the increase was due to the C-C/C-H component of the C peak, showing that lubricant was migrating to the surface of the tape with cycling.

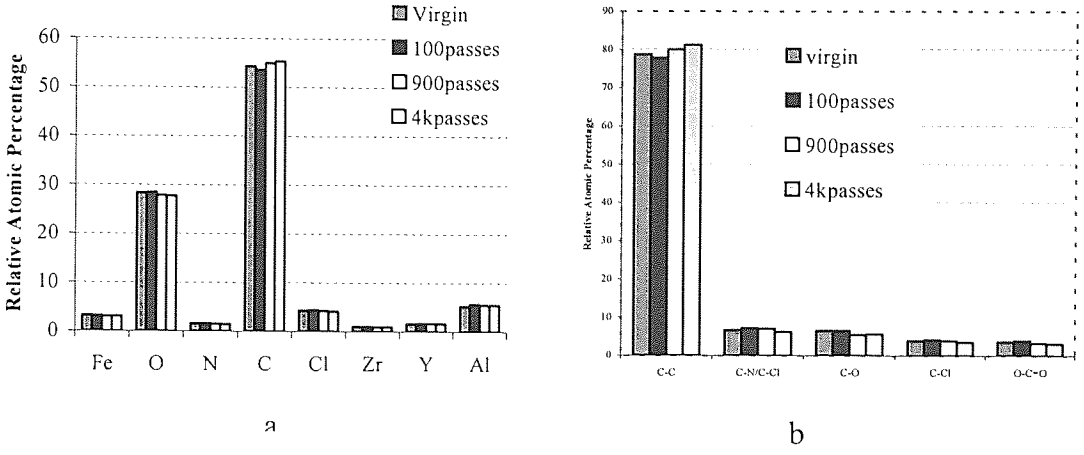

Figure 3-105. At 22°C, RH40% (a) Elemental trends in the tape surface as a function of number of passes (b) Synthesis of carbon as a function of increasing number of passes

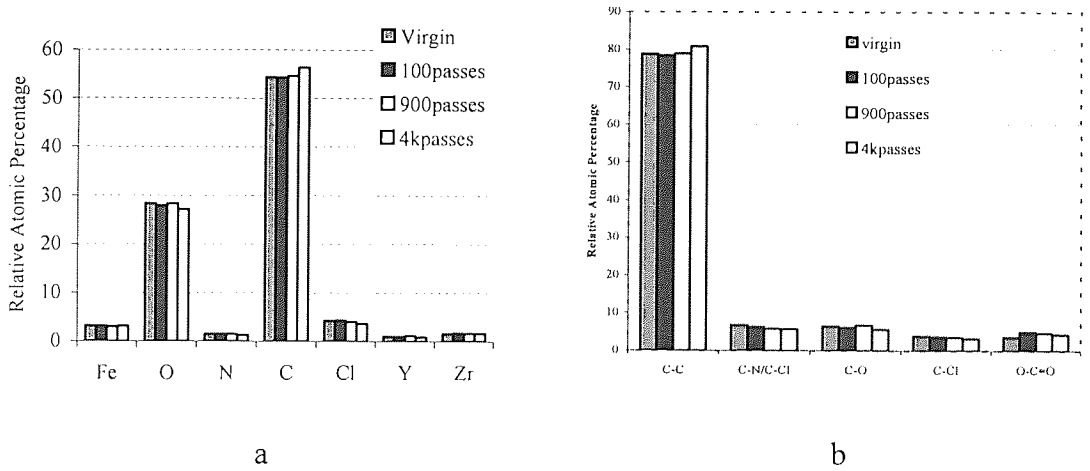

Figure 3-106. At 40°C, RH 80% (a) Elemental trends in the tape surface as a function of number of passes (b) Synthesis of carbon as a function of increasing number of passes

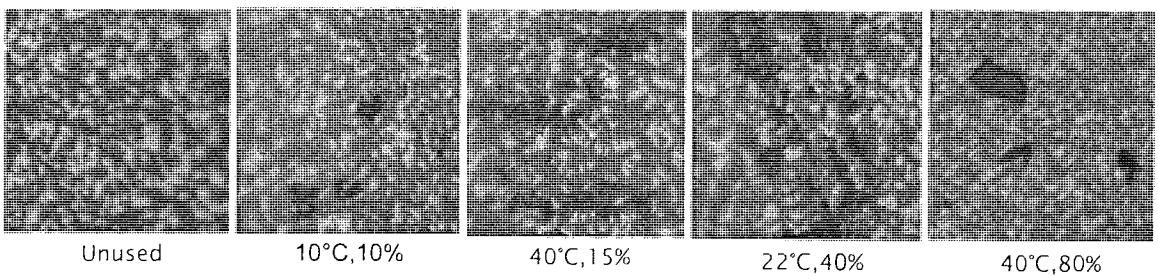

Figure 3-107 Optical micrographs of typical LTO head ceramic debris for unused, worn head after 5k passes cycling with Maxell tapes at different environmental conditions (400×)

Figure 3-107 shows the tape debris on the ceramic of the head, tape debris distribution was quite similar with Fuji tape results, there was more tape debris in the high temperature and high water content condition, but comparing with Travan5 tape debris, the size and number of debris in LTO was less.

3.5 Experiment Results of LTO heads with Imation tapes

3.5.1 LTO Head Wear with Imation Tapes

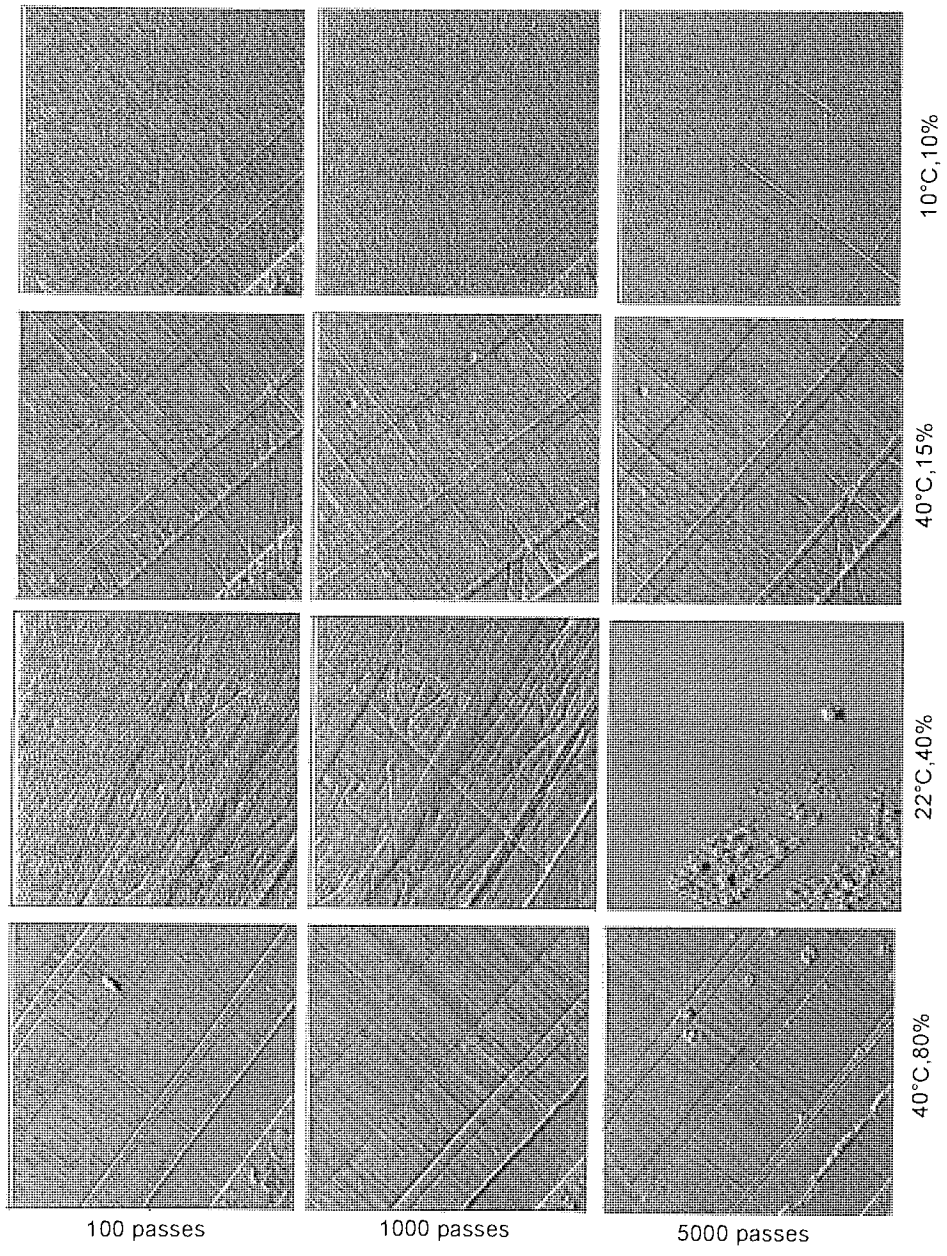

Figure 3-108 AFM images of head pole area cycling different passes at different conditions using Imation tapes (15μm×15μm)

Figure 3-108 shows pole area changes after 100passes, 1k passes, 5k passes cycling against the Imation tapes at four conditions. Generally speaking, the pole areas stayed clean except some deposit at 22°C, RH 40%. At 22°C, RH 40% some deposits on the surface of pole after 5k passes were observed. The deposit was not continuous, but was in the form of lumpy island. The AES results show the deposit on the pole area was

polymeric material (no Fe was detected), which indicated polymer deposit formed in this situation. For 10°C, RH 10%, 40°C, RH 15%, 40°C, RH 80%, the head surface were largely clean surface, even after 5k passes. The scratches on the pole area still can be seen. These scratches were caused by the pullout particles (three-body particles) from the head ceramic regions or by HCA particles from the tape.

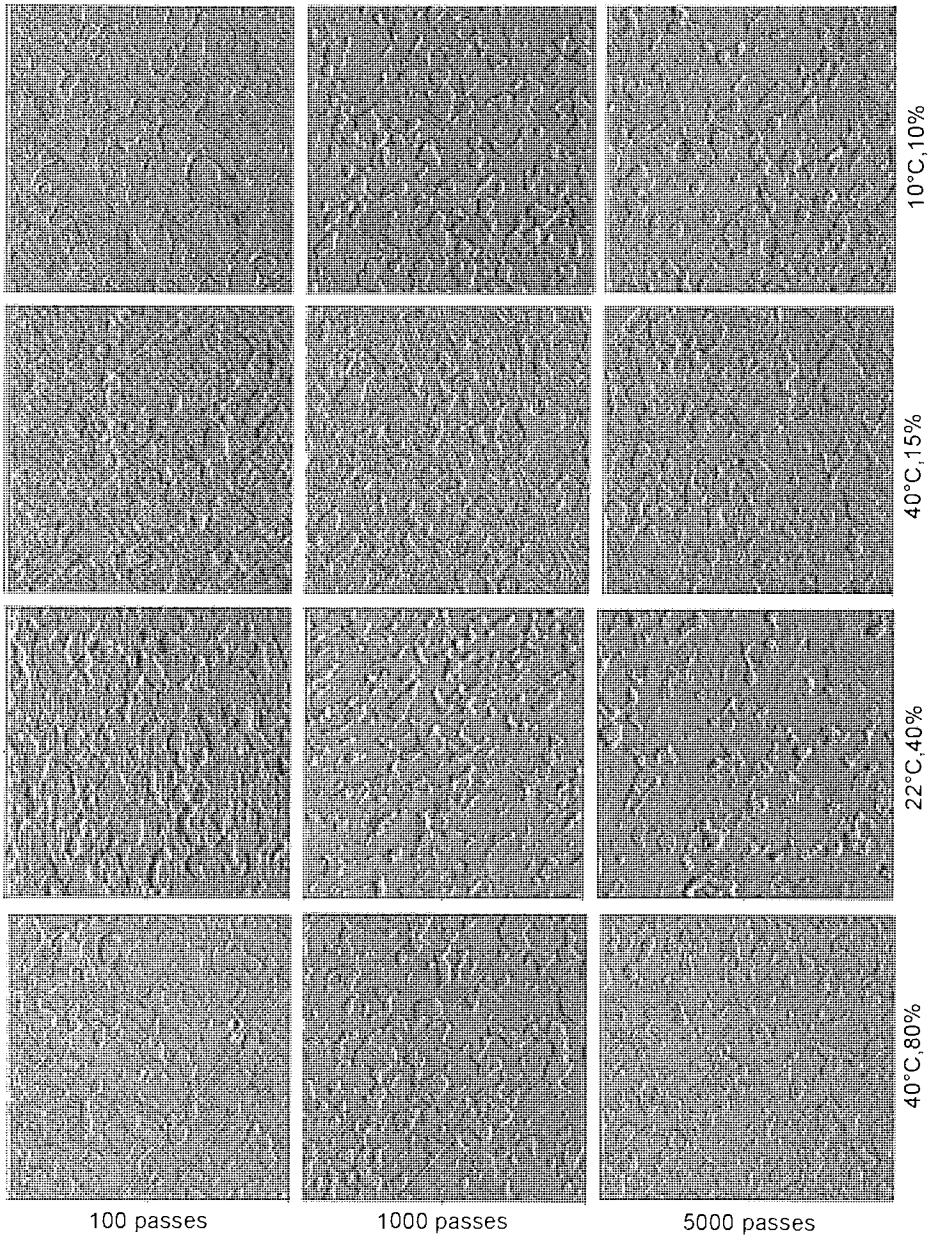

Figure 3-109 AFM images of head ceramic wear after different passes in different conditions using Imation tapes (15μm×15μm)

Figure 3-109 shows the ceramic wear occurred after tape cycling. The wear of the head including the pole area and ceramic area were clearly observed after 5k passes tape

cycling. The depth of the pullout increased from 5-7nm of the unused head to the 15-18nm after 5k passes cycling against the LTO Imation tapes.

3.5.2 LTO Head stain with Imation tape

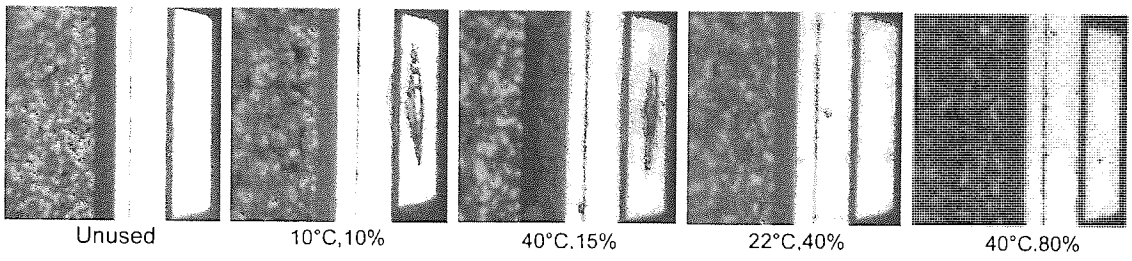

Figure 3-110 Optical micrographs of LTO head pole area, unused and worn heads after 1000km cycling against Imation tapes in different environmental conditions (400×)

Optical pictures of worn head pole area were very clear shown in Figure 3-110, AFM and Auger results also indicated there was no Fe stain on the surface of the pole area, some of material, probably polymeric debris filled the indents.

3.5.3 Effects of water on the AlTiC ceramic of LTO heads—XPS

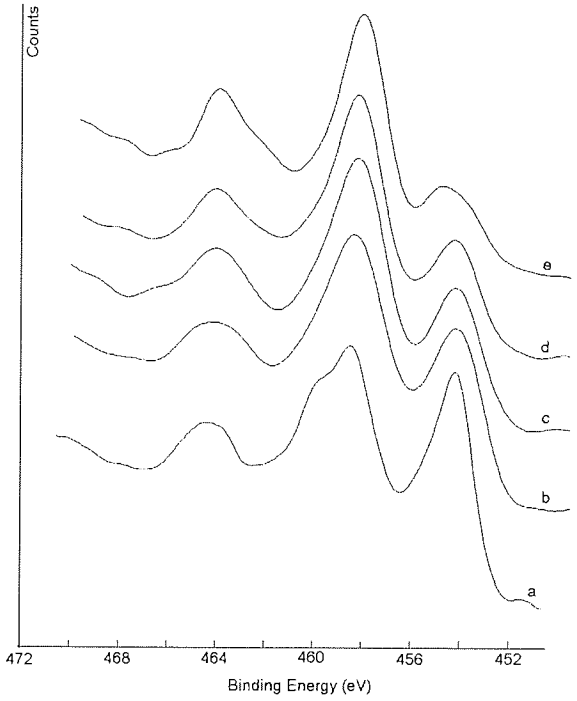

Figure 3-111 Ti2p photoelectron peaks (a)Unused LTO head Ceramic; (b) Head after RH10%, 10°C,1000km cycling; (c) Head after RH15%, 40°C,1000km cycling; (d) Head after RH40%, 22°C,1000km cycling; (e) Head after RH80%, 40°C,1000km cycling against Imation tapes

All peaks analysis was referenced to the same analysis method as section 3.4.3 did. The Ti $2p_{3/2}$ peaks at 454.0eV and 458.3eV were due to TiC and TiO_2 respectively. Peaks at 460eV and 464.0eV were the corresponding $Ti2p_{1/2}$ peaks for these compounds. Figure 3-111 spectra from (a) to (e) show that the peaks due to the TiO_2 ($Ti2p_{3/2}$ 458.3eV, $Ti2p_{1/2}$ 464.0eV) progressively increasing in intensity as the TiC peaks ($Ti2p_{3/2}$ 454.0eV, $Ti2p_{1/2}$ 460.0eV) decrease in intensity. The TiO_2 progressive increase indicates an increasing thickness (or possible areal coverage) of TiO_2 on the surface of the TiC grains with increased atmospheric water content after the cycling against the tapes.

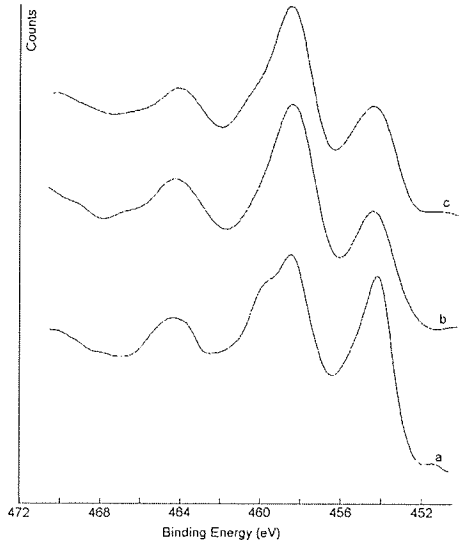

Figure 3-112 Ti2p photoelectron peaks (a)unused LTO head ceramic (b) head after RH15%, 40°C,5k passes of Imation tape cycling; (c) Head after RH15%, 40°C,10k passes Imation tape cycling

Head condition	Unused head	10°C,RH 10% 1000km NWC 1.0	40°C, RH15%, 1000km NWC 6.7	40°C, RH15%, 2000km NWC 6.7	22°C, RH 40%, 1000km NWC 7.5	40°C, RH 80% 1000km, NWC 35.5
(TiO_2/TiC) Ratio	1.0	1.6	1.9	2.0	2.2	4.9

Table 3-22 TiO_2 and TiC ratio changes after cycling against Imation tapes in different conditions

Comparing Figure 3-112 (b) and Figure 3-112(c) it maybe see that the concentrations of TiO_2 are quite similar after 1000km and 2000km cycling. Table 3-22 shows the TiO_2 : TiC ratio increases with the water content (data from Figure 3-111 and Figure 3-112). The results show that the presence of water vapour during tape cycling can have a significant effect on TiC oxidation and that tribo-chemical wear increased with the atmospheric water content.

3.5.4 LTO head PTR with Imation tapes

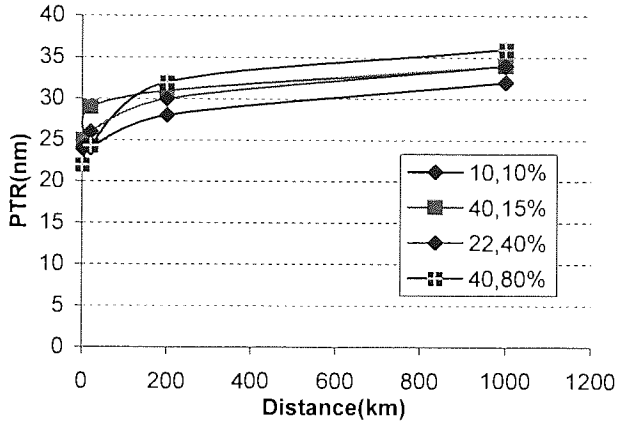

Figure 3-113 PTR of LTO heads cycling with Imation tapes at 10°C, RH 10%, 40°C, RH15% , 22°C, RH 40% and 40°C, RH80% conditions

Figure 3-113 shows that PTR of LTO heads cycling after Imation tapes at different environmental conditions. Although it did not show much different in PTR for different conditions, possibly due to the higher lubricants in the Imation tapes which leads to the less wear of the heads. The higher temperature and higher water content resulted in the PTR reaching its highest value.

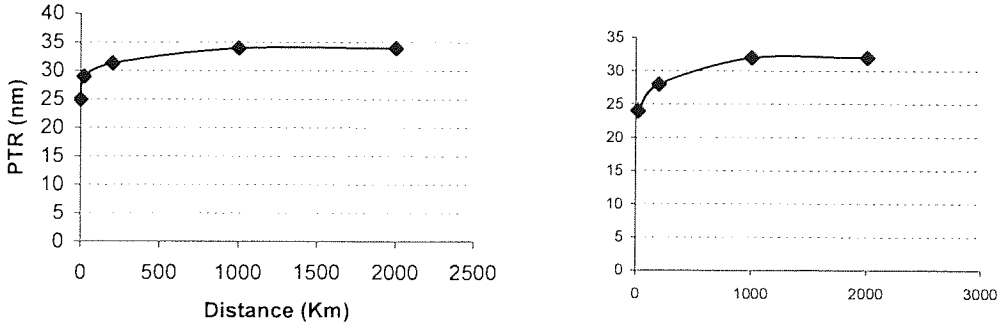

Figure 3-114 PTR of LTO heads cycling with Imation tapes at 40°C, RH15% (left) 10°C, RH 10% (right), Up to 10k passes

Results from Figure 3-114 shows PTR of LTO heads reached saturated value after 5k passes cycling with Imation tapes at 10°C, RH 10%, 40°C, RH15% conditions.

3.5.5 LTO head wear rate with Imation tapes

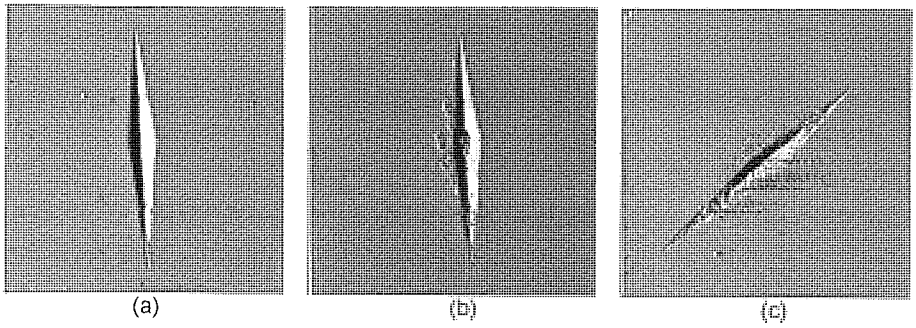

Figure 3-115 Indentation changes on the insulator surface (a) unused, after (b) 5k, (c) 10k passes at 10°C, RH10% (each AFM image is 25μm×25μm)

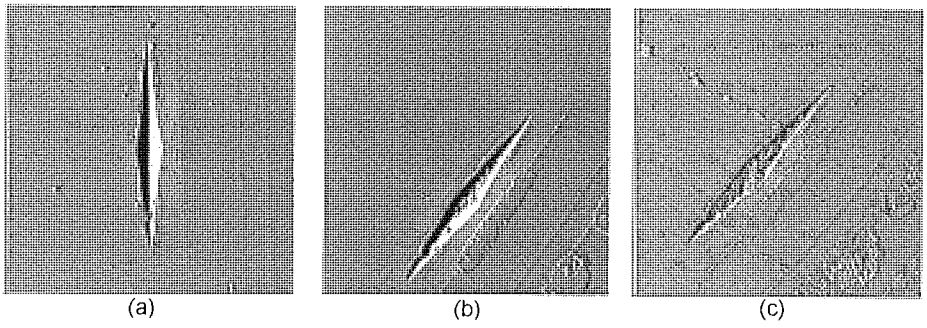

Figure 3-116 Indentation changes on the pole surface (a) unused, after (b) 5k, (c) 10k passes at 40°C, RH15% (each AFM image is 25μm×25μm)

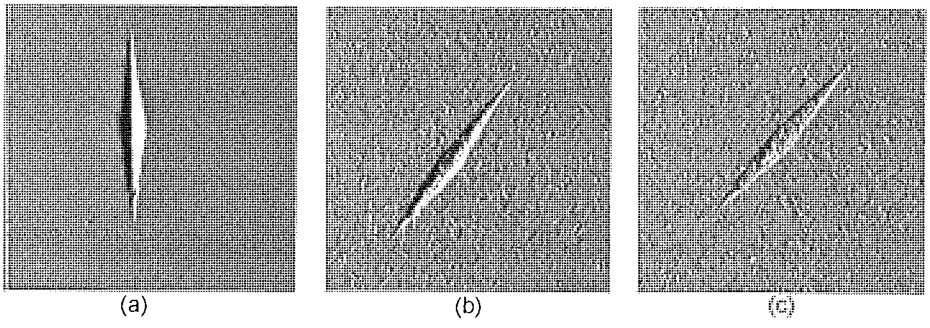

Figure 3-117 Indentation changes on AlTiC surface (a) unused, after (b) 5k, (c) 10k passes at 40°C, RH15% (each AFM image is 25μm×25μm)

Detail experimental method had already been described in Chapter two. Since TiC particles are not perfectly imbedded homogenously into the Al_2O_3 substrate, the length of indentations measured by AFM showed some statistical spread (see Table 3-23 and Table 3-24), since good shape of indents were observed for most of the indents, this led to the reliable wear measurement although hardness of AlTiC varied. For a typical indent on AlTiC, before wear test, ten times measurements of this indent were taken, the

mean value plus the standard error of mean of this indent could be written as $L_1 \pm \Delta L_1$ μm. Using the same method, the same indent after 1000km tape cycling, the length of this indent changed to $L_2 \pm \Delta L_2$ μm (mean value plus standard error of mean), the error of wear measurement in this 10 times measurement for this indent will be $(\Delta L_1 + \Delta L_2)/(L_1 - L_2)$. The typical value for $(\Delta L_1 + \Delta L2)$ is 0.1 μm corresponding $(L_1 - L_2)$ is 0.3 μm for AlTiC, from estimation of the error; the maximum error of wear rate measurement involved could be about 30%. Figure 3-115, Figure 3-116 and Figure 3-117 show the typical indentation changes in the pole, insulator and ceramic area after cycling after Imation tapes at different conditions. The L/d ratio is 30.5 for the measurement, after measuring the length of indentation; the depth (d) changes of the indentation could be obtained.

Condition 40°C, RH15%	Indentation Force (mN) Time (Second)	Virgin Average length (μm)	Length after 5k passes (μm)	Length after 10k passes (μm)	Wear (±30%) in first 5k passes	Wear (±30%) in second 5k passes
AlTiC	490mN, 15S	17.7	17.4	17.1	10nm	10nm
Insulator	245mN, 15S	19.8	19.1	18.8	22nm	9nm
Pole area	98mN, 15S	17.4	16.9	16.6	18nm	9nm

Table 3-23 Average length of indentations and wear rate after different passes at 40°C, RH 15%

Condition 10°C, RH10%	Indentation Force (mN) Time (Second)	Virgin Average length (μm)	Length after 5k passes (μm)	Length after 10k passes (μm)	Wear (±30%) in first 5k passes	Wear (±30%) in second 5k passes
AlTiC	490mN, 15S	17.0	16.7	16.4	10nm	9nm
Insulator	245mN, 15S	21.7	21.2	20.9	17nm	9nm
Pole area	98mN, 15S	16.5	15.9	15.6	19nm	10nm

Table 3-24 Average length of indentations and wear rate after different passes at 10°C, RH 10%

Table 3-23 and Table 3-24 shows that insulator and pole wear rates were higher at the first 5k passes cycling than that in the second 5k passes cycling. The AlTiC ceramic wear according to what we measured the wear rate, basically the constant with the cycling distance and around 9nm per 5k passes tape cycling. The wear rate of pole and insulator is similar but significant higher than AlTiC. The different wear rate of different materials led to the PTR of worn heads. Wear was however very limited in LTO system due to the low contact pressure and very smooth surface.

During second 5k passes tape cycling, the wear rate of different part of the heads was quite similar, this was quite fitting with the PTR measurement, indicating the PTR value maintained constant after it reached equilibrium value. From what it was measured here, it was difficult to tell the temperature and water content effect from these two environmental conditions.

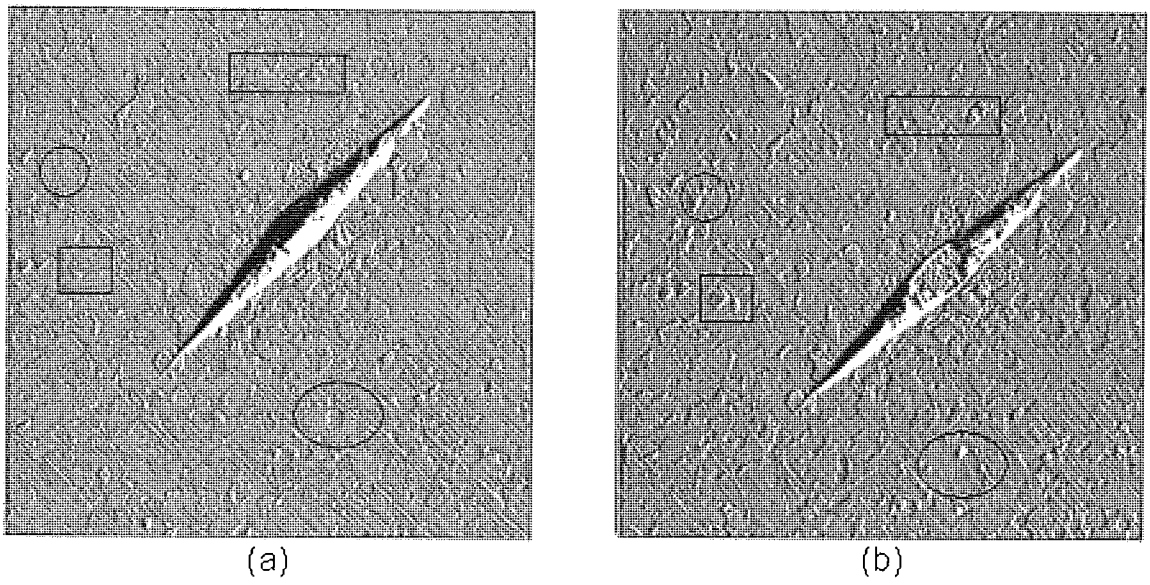

Figure 3-118 AFM Images of the ceramic region after (a) 5k passes and (b) 10k passes at 40°C, RH 15% (24μm×24μm)

Figure 3-118 shows 40°C, RH 15% condition the AlTiC ceramic part after 5k, 10k passes of tape cycling, the surface changes, from the AFM images it is clearly seen some of the AlTiC ceramic pullouts happened on the surface of the heads. The matching pattern in each image corresponds to the areas where a pullout has occurred. The pullouts happened on the AlTiC surface and removal in the later tape cycling procedure.

3.5.6 LTO Imation Tape Wear

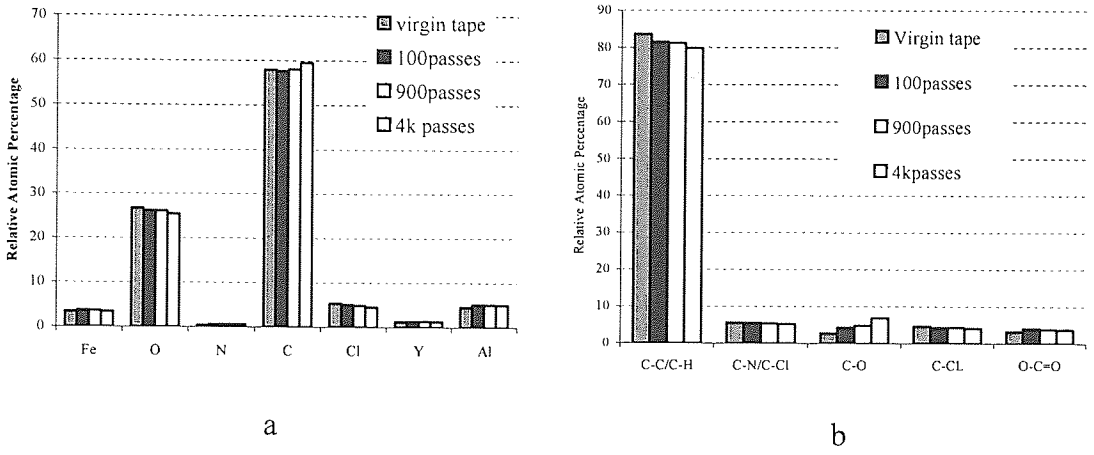

Figure 3-119. At 10°C, RH10% (a) Elemental trends in the tape surface as a function of number of passes (b) Synthesis of carbon as a function of increasing number of passes

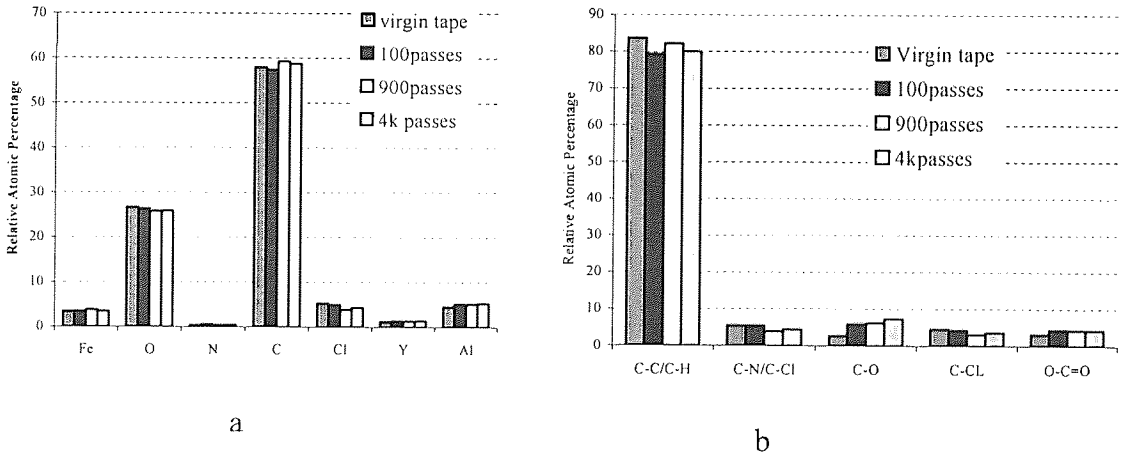

Figure 3-120. At 40°C, RH 15% (a) Elemental trends in the tape surface as a function of number of passes (b) Synthesis of carbon as a function of increasing number of passes

XPS analysis of the tape surfaces showed that the tape composition changed during the cycling. These were shown in Figure 3-119 to Figure 3-122. For each set of environmental conditions XPS analysis of the tape surfaces showed that N and Cl did not change significantly. The N composition in Imation tape was considerable lower than Travan5 tape and LTO Fuji tape. However, the C signal was seen to increase with cycling for each condition. Synthesis of the C 1s peak showed that the decrease of the C-C/C-H component of the C peak, indicating that lubricant was depleted in the surface

of the tape with cycling, for LTO Imation tape, the C composition was higher than the LTO Fiji tape which indicates there were more lubricate on the surface of Imation tape than Fuji tape.

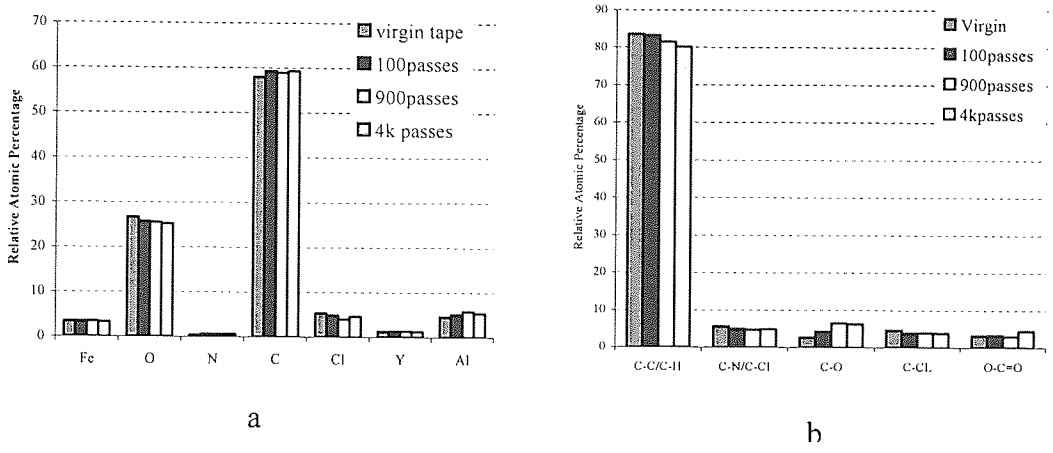

a b

Figure 3-121. At 22°C, RH40% (a) Elemental trends in the tape surface as a function of number of passes (b) Synthesis of carbon as a function of increasing number of passes

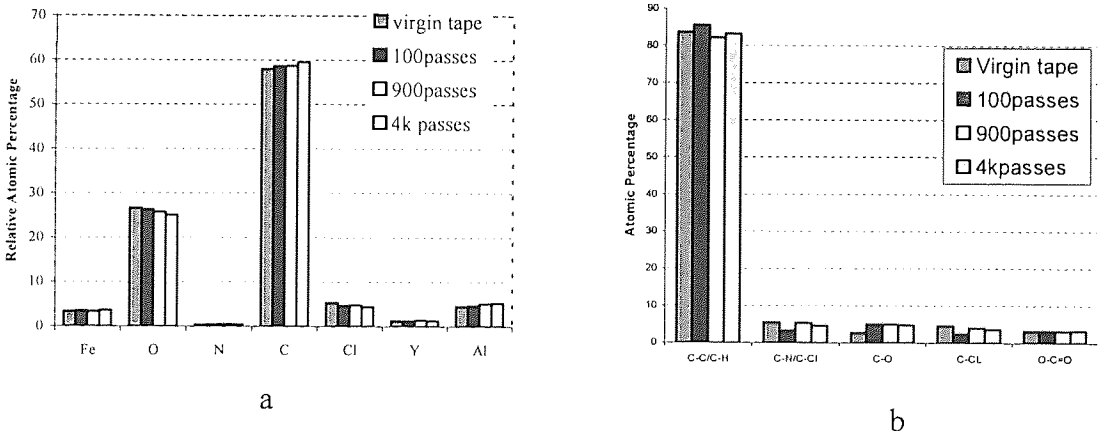

a b

Figure 3-122. At 40°C, RH80% (a) Elemental trends in the tape surface as a function of number of passes (b) Synthesis of carbon as a function of increasing number of passes

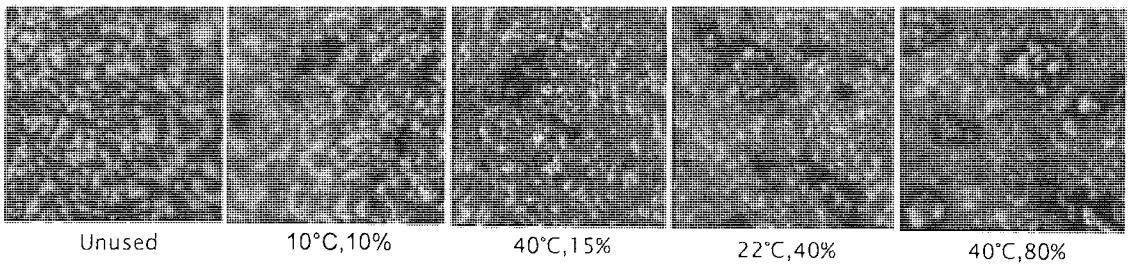

Figure 3-123 Optical micrographs of typical LTO head ceramic debris for unused, worn head after 1000km cycling against Imation tapes at different environmental conditions (400×)

Figure 3-123 shows the debris distribution on the ceramic of the head, which indicated that more tape debris were generated at the high temperature and high water content condition.

3.6 Experiment Results of LTO heads with Mp3 tapes

3.6.1 LTO Head Wear with Mp3 Tapes

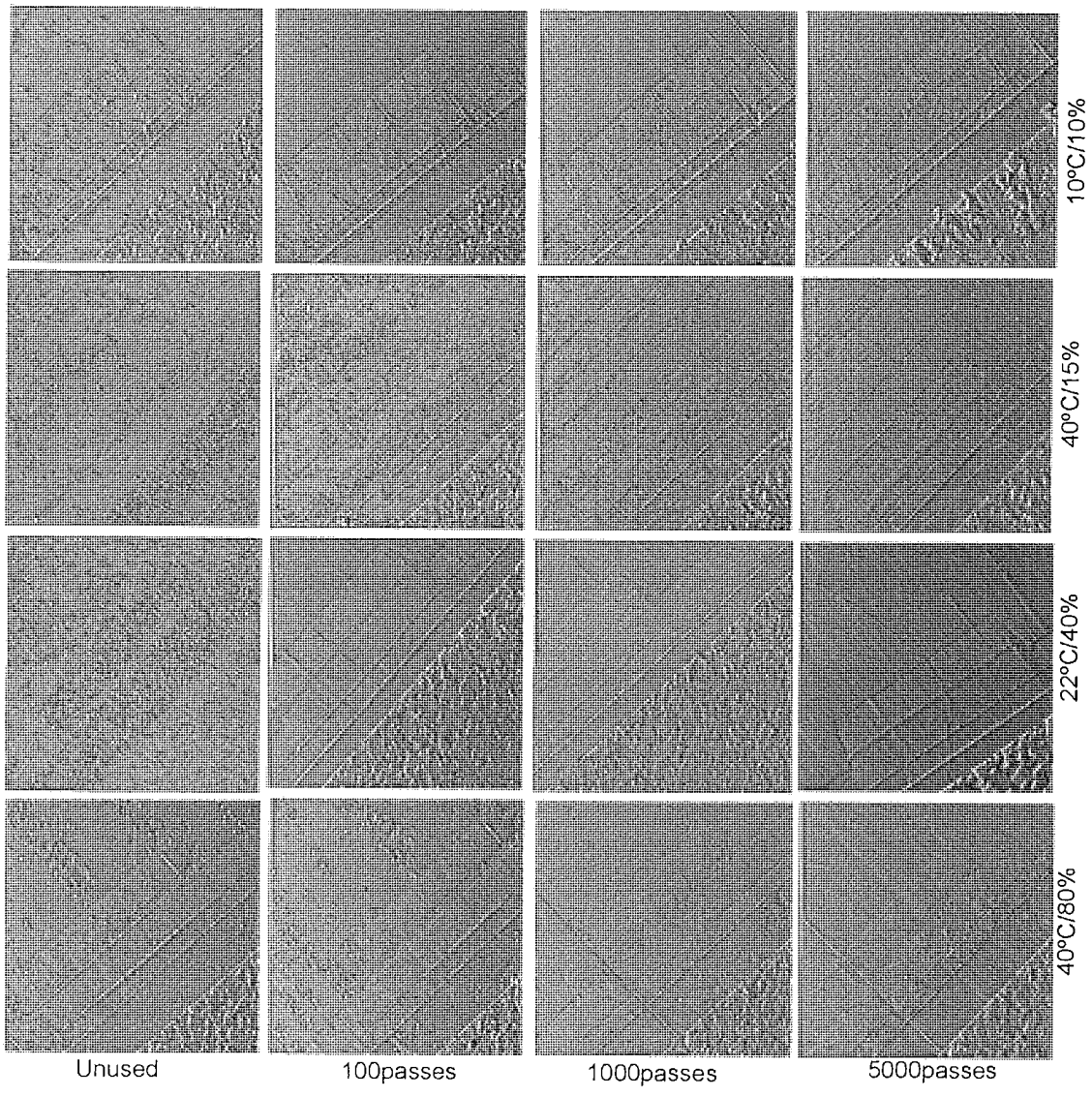

Figure 3-124 AFM images of head pole area wear after different passes at different conditions (30μm×30μm)

Figure 3-124 shows AFM images of the surfaces of the poles generated after experiments performed over a variety of environmental conditions. The unused head, with PTR around 25nm, normally shows clean surface. Auger electron spectroscopy results confirmed there were no Fe stain on the surface of the worn head pole area, conventional Fe stain was not found on the head surface after 5k passes of LTO Mp3

tape cycling. For the worn heads, new scratches on the head pole area after 5k passes tape cycling was clearly seen, indicating the pole wear due to the three-body particles.

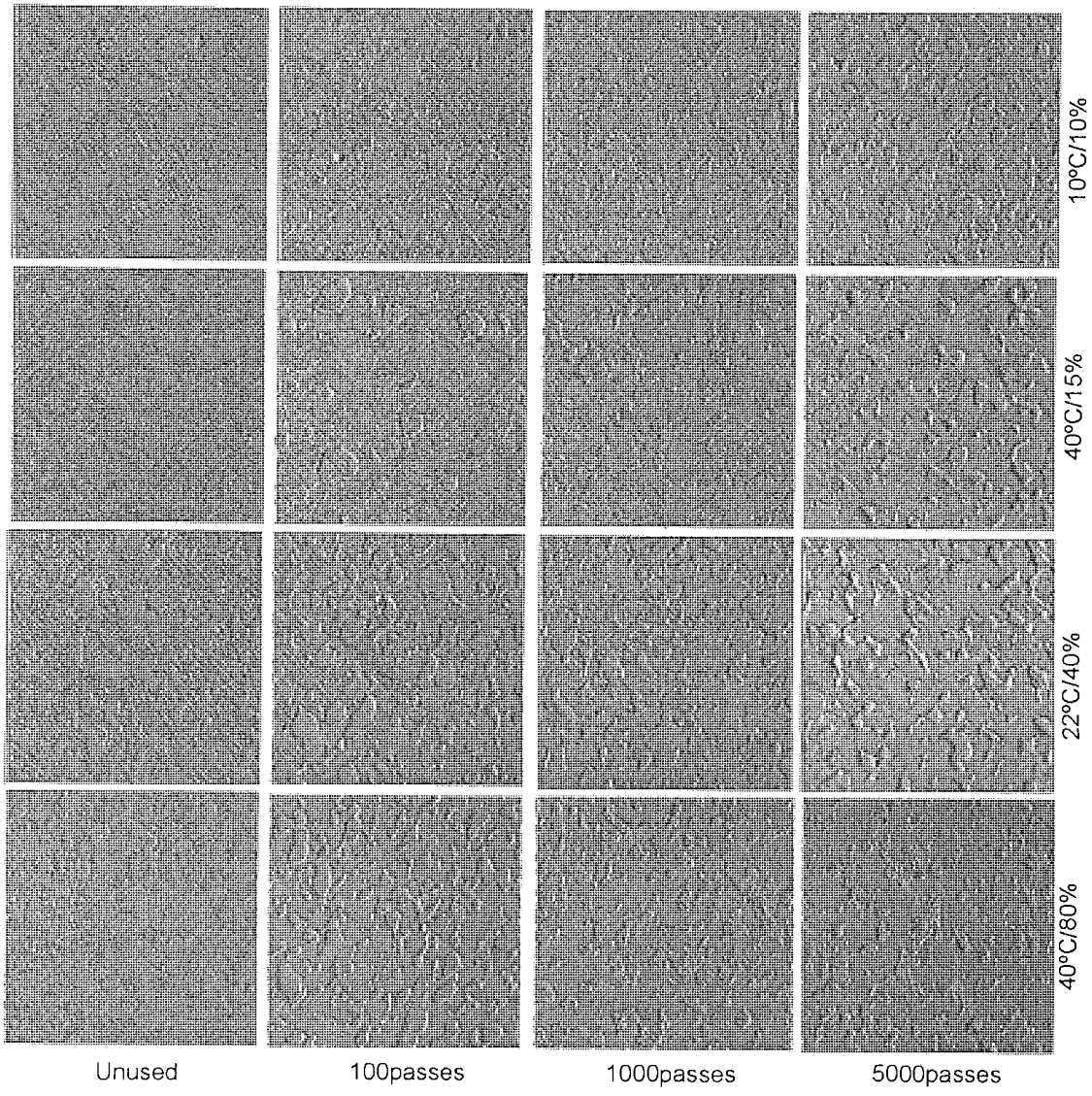

Figure 3-125 AFM images of head ceramic wear after different passes in different conditions (15μm×15μm)

Figure 3-125 shows how the ceramic wear occurred on the surface of the LTO ceramic area. However, few and shallow ceramic pullout (<6nm) could be seen on the unused ceramic part of the head. From the AFM images of the four conditions, the pullout of the ceramic on the worn head reached 14-17nm after 5k passes Mp3 tape cycling. The higher water content (40°C, RH 80%), and the greater (17nm) the pullout produced on the AlTiC ceramic surface.

3.6.2 LTO head Stain with Mp3 Tapes

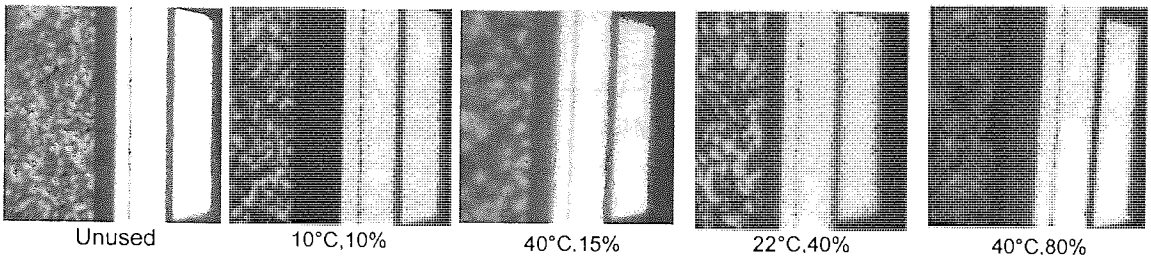

Figure 3-126 Optical micrographs of LTO head pole area, unused and worn heads after 5k passes Mp3 tapes cycling in different environmental conditions (400×)

Figure 3-126 shows the clear pole surface of the LTO head after cycling of Mp3 tape, AES results shows there were no Fe stains on the surface of the pole. The tape wear of Mp3 is quite similar with Fuji, Maxell tape, showing loss of binder material and lubricant renewal.

3.6.3 LTO head PTR with Mp3 tapes and the stand errors of PTR

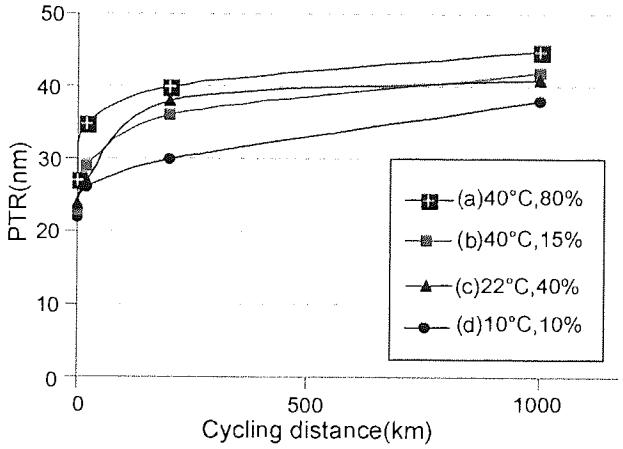

Figure 3-127 PTR of LTO heads after cycling of Mp3 tape (a) 40°C, RH 80%(NWC 35.5) (b) 40°C, RH15% (NWC6.7) (c) 22°C, RH40% (NWC 7.5) (d) 10°C, RH 10%(NWC 1.0)

Figure 3-127 shows the PTR value for the four different environmental conditions for LTO head using Mp3 tapes. This shows that the lowest temperature and lowest water content (10°C, RH 10%) produced the smallest PTR (38nm). For the 40°C, RH 15% and 22°C, RH 40%, which the water contents were similar, and PTR for these two conditions were also similar. The PTR value increased with the water content increasing and reached maximum at the 40°C, RH 80%. The PTR results show a similar trend in

that the more wear occurred at the higher temperature and higher water content condition.

PTR (nm)	Head1	Head2	Head3
Virgin	29.3, 24.5, 31.0, 26.7,29.1,29.6	23.7, 22.9,24.1, 25.4,25.3, 22.0	31.1, 30.3, 32.2, 32.4, 32.4,29.6
Virgin (Mean ± Standard error of mean)	27.7nm±0.8nm		
100passes	37.1,39.6,33.1, 37.5,38.3, 34.4	34.7,31.6,38.4, 35.2,34.8, 37.1	35.5,32.3,38.6, 38.2,34.7,35.0
100 passes (Mean ± Standard error of mean)	35.6±0.6nm		
1k passes	37.8,36.4,35.7, 37.2,42.3,39.9	43.2,43.5,39.7, 41.7,42.0,40.0	43.5,43.2,44.6, 41.7,40.3,41.8
1k passes (Mean ± Standard error of mean)	40.3±0.8nm		
5k passes	48.2,48.3,45.6, 44.5,45.8,48.5	43.7,49.4,44.6, 46.4,45.6,42.8	44.8,43.7,42.0, 42.1,43.7,43.8
5k passes (Mean ± Standard error of mean)	44.6±0.9nm		

Table 3-25 Typical PTR values and the standard deviation of PTR for LTO heads using Mp3 tapes at RH 80%, 40°C

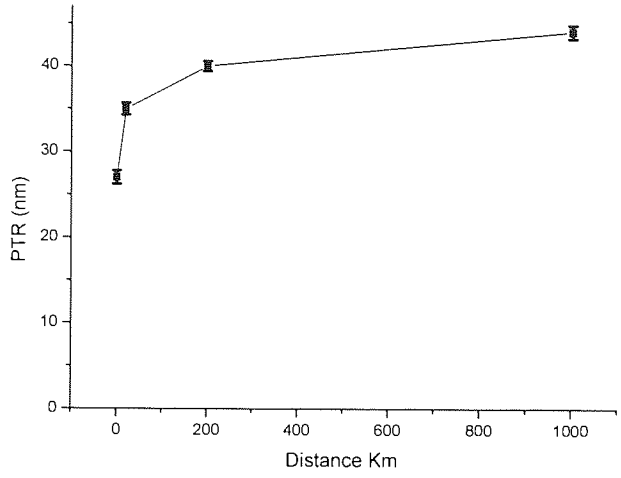

Figure 3-128 PTR values and the standard error of mean of PTR of LTO heads using Mp3 tapes at RH80%, 40°C

Table 3-25 and Figure 3-128 show the stand errors of mean for the PTR values in LTO heads after LTO Mp3 tapes cycling. From the calculation of PTR value, it clearly showed the standard error of mean of the PTR value was very small. This result was a typical analysis of the error assessment in the PTR measurement. For PTR values involved in other conditions with different tapes, the similar standard errors of mean were observed.

3.7 Summary results of LTO head and tape wear

3.7.1 Summary of LTO head wear

	Used Tape	Ceramic pullout	Head stain	PTR	Note
Unused head		4-6nm	Clean surface	around 25nm	AlTiC ceramic was studied by XPS, AES, AFM
Head with Mp1 tape	Mp1 tape	After 5k passes, pullout reached 15-22nm, higher T and higher water content, greater pullout.	stain covered pole area and some ceramic, no stain on insulator	After 5k passes, reached 36-55nm, PTR higher at higher Temperature and water content condition	Contact pressure effect for Travan5 and LTO using the exactly similar tape was compared (PTR, stain structure, ceramic pullout et al)
Head with Fuji tape	Fuji tape	After 5k passes, pullout reached 15-22nm, higher T and higher water content, greater pullout.	No stain, clean surface	After 5k passes, reached 36-53nm PTR higher at higher Temperature and water content condition	Ti bearing 3 body particles was observed on the pole area. Temperature and water content effect was studied.
Head With Imation tape	Imation tape	After 5k passes, pullout reached 15-18nm, higher T and higher water content, greater pullout.	No stain, clean surface	After 5k passes, reached 33-37nm PTR higher at higher Temperature and water content condition	Head material wear rates were measured. Head AlTiC ceramic oxidation was studied
Head with Maxell tape	Maxell tape	After 5k passes, pullout reached 15-17nm, higher T and higher water content, greater pullout.	No stain, clean surface	After 5k passes, reached 34-52nm. PTR higher at higher Temperature and water content condition	Head AlTiC ceramic oxidation was studied, and oxidation rate increased with water content
Head with Mp3 tape	Mp3 tape	After 5k passes, pullout reached 14-18nm, higher T and higher water content, greater pullout.	No stain, clean surface	After 5k passes, reached 38-46nm, PTR higher at higher Temperature and water content condition	PTR standard error of mean was assessed

Table 3-26 Summary of LTO head wear

Table 3-26 summarized major experimental results involved LTO head system.

3.7.2 Summary of LTO tape wear

	Tape property	Binder	Stain	Wear
Mp1	Exactly like Travan5	Urethane	Yes	Loss binder after 4k passes, less wear comparing with Travan5 due to low pressure in LTO
Fuji	Possible better binder material than Mp1	Urethane and vinyl chlorine	No	Loss binder after 4k passes
Imation	More lubricant than Fuji	Urethane and vinyl chlorine	No	No significant wear after 4k passes
Maxell	Possible better binder material than Mp1	Urethane and vinyl chlorine	No	Very low wear
Mp3	Smaller magnetic particles, same binder material as Imation	Urethane and vinyl chlorine	No	Like Fuji tape

Table 3-27 Summary of LTO tape wear, all tapes are double layer MP tapes

Table 3-27 summarized major experimental results involved LTO tape system. There are more tape debris at higher temperature and higher water content conditions. The detail discussion of the wear of head and tape could be seen in Chapter 4.

4 Chapter 4 Discussion

Head wear; stain formation and PTR mechanisms are discussed in this Chapter. These mechanisms are dependent upon temperature and atmospheric water content, three-body particle generation mechanisms and contact pressure effects. Magnetic tape wear is also discussed in this chapter.

4.1 Problems in head tape systems

The experiments involved in this research project show Pole Tip Recession (PTR) occurred on all worn heads; stain is also a problem in some tape/head combinations. Maximum PTR reached 50-70nm in the Travan5 heads, and around 35-55nm in LTO heads. A huge amount of research data was obtained in this research work, including different tape effects, contact pressure effect, environmental atmosphere effects, PTR, stain formation and different material wear mechanisms during the wear procedure.

Physical spacing between head and tape remains the biggest factor in signal degradation and error growth and subsequently this effect limits attainable storage density. Thus, significant increase in densities can only be attained by minimising this physical spacing between media and sensors (pole tips). The major causes of spacing (and hence spacing losses) are Pole Tip Recession (PTR) and transferred materials from tapes to heads (stain). The recorded signal amplitude is only independent of the data being read if the spacing is zero. Thus, the level and more specifically the variation in head media spacing with device life must be a minimum to maximise signal output and minimised errors. It was the purpose of this programme to isolate and identify the mechanisms responsible for physical spacing between sensors and tape.

4.2 Contact Pressure Effect

For the thin film magnetic heads, the nominal contact pressure may be calculated from the relationship[72]:

$$P = \frac{T_{tape}}{R_{head} \cdot W_{tape}} \qquad \text{Equation-4-1}$$

Where P is the contact pressure, T_{tape} is the tape tension, R_{head} is the radius of the head and W_{tape} is the width of the tape. In this research work, the tape speed in LTO system was the same as Travan5 system (2.3m/s).

	Tape tension	Head radius	Tape width	Contact Pressure
LTO heads	0.8 N	6.55 mm	12.5 mm	9.8×10^3 N/M^2
Travan5 heads	0.6 N	2.28 mm	8.0 mm	3.4×10^4 N/M^2

Table 4-1 the contact pressure in the LTO and Travan5 heads

$$\frac{P_{Travan}}{P_{LTO}} = 3.5 \qquad \text{Equation 4-2}$$

Table 4-1 clearly shows that the contact pressure in the LTO system is less than one-third of the Travan5 system.

As is well known[20,46,47], the head wear is in proportion to the contact pressure and the sliding distance, head wear and tape wear are known to increase with increasing contact pressure. Thus, this difference in contact pressure has a large effect on wear, PTR and stain in the two recording systems used, as will be discussed in late sections.

4.3 Tape Wear

Tape wear was impossible to measure directly; the volumetric wear rate was far too small for measurement. Hence the only indication of wear and changes at the surface of the tape was to monitor the surface compositional changes with time of tape/head contact by mean of XPS. The removal of binder material was determined by measuring the change in composition of N and Cl that were both present in the co-polymer binder. Lubricant removal or surface removal was indicated by changes in the C-C/C-H component of C1S peak in the XPS spectra and changes in Al concentrate showed removal or exposure of Head Cleaning Agent (HCA) in the tape surface.

4.3.1 Travan5 Tape Wear

Synthesis of the Travan5 tape C1S peak (see section 3.1.4) revealed that five different chemical states contributed to the total carbon peak. This is similar to former work[11]. The major peak of C-C/C-H occurred at a binding energy of 284.6 eV and was used as a reference for the other peaks. C-C/C-H was a common bond in tapes and is also characteristic of the hydrocarbon contamination layer, the lubricant and the binder.

For the Travan5 tapes, the carboxyl (O=C-O) peak is characteristic of both the lubricant and binder material and as such is not a particularly useful indicator of the relative concentration of constituents in the near surface region of the tape. However, the C-N component provided a good indication of the relative changes in the concentration of binder material, since these peaks arise from bonds within the binder.

In all Travan5 experiments, XPS results (see section 3.1.4) show that the iron signal in worn Travan5 tape increases compared to virgin tape, while the nitrogen signal decreases compared to the virgin tape. Synthesis of the C 1s peak revealed that for every condition, lubricant was replenished at the surface during cycling (C-C/C-H increased, see section 3.1.4) and confirmed that binder (C-N) had decreased. The surface lubricant replenishment kept the total carbon composition constant. The lubricant replenishment process is the results of the lubricant migrating through the pores in magnetic layer. Lubricant will move to the surface of tape under the action of contact pressure. For the dual layer MP tapes, the non-magnetic layers beneath the magnetic layer not only provide a smooth layer for the magnetic layer to adhere, but also provide a lubricant reservoir which incorporate the lubricants and allow transfer the lubricants to the tape surface when the lubricants are needed.

The experiments show the iron composition in the central area of the tape increased more compared with the tape edge at the same experimental condition (see section 3.1.4). Binder (indicated by N) depletion occurred in the middle area of the tape more than the edge area of the tape. More tape wear occurred in the middle of the tape than at the edge of the tape due to the higher contact pressure in this area of the tape (see Figure 2-2, the polymer belt contacts the Travan5 tape only in the centre area of Travan5 tape) during the same experimental conditions.

Travan5 tape results showed that some surface degradation of the tape occurred at high temperature and high humidity (40°C, RH 80%). This was also confirmed by the rougher tape surface, the unused tape roughness (RMS) was about 15nm, and the worn tape roughness after 5k passes cycling reached 39nm at 40°C, RH 80%. This led to a different, thicker form of stain (mainly polymeric) being formed on the head surface under this condition. XPS results showed less change of N (binder) at 40°C, RH 80% for Travan5 tape, it is likely that the rate of removal was such that the surface layer remained similar to the unused tape surface with no time for transformation before removal. The long-term exposure of magnetic tapes to a hot and humid environment has been shown to result in tape degradation[20]. Tape become softer as the result of chain scission within the polymer due to water ingress aging probably due to decreased cross-linkage. The hot and wet environment increases the speed of aging of tape. Aged tape has a propensity for generating extensive debris. All these led to the Travan5 tape degradation at high temperature and high humidity (40°C, RH 80%).

4.3.2 LTO Tape Wear

Due to commercial confidentiality, the manufacturers would not provide the full details of specific component materials used in the different LTO tapes used during this investigation. Totally five different LTO tape types were used in this research project including Fuji tape, Maxell tape, Imation (production) tape, Imation Mp3 tape and Imation Mp1 tape. The Imation Mp1 tape was exactly similar in composition to Travan5 tape. Between the Fuji Tape, Imation (production) tape and Maxell tape, the lubricant level and composition varied. The Imation Mp3 tapes were quite similar to Imation (production) tape except that Fe metal particles inside Imation Mp3 tape are smaller than in Imation (production) tape.

Imation Mp1 tape XPS C1S peak synthesis revealed five different chemical components as did Travan5 tape. Synthesis of other LTO tapes (including Fuji, Maxell, Imation (production), Imation Mp3 tape) C1S peak revealed that six different chemical states contributing to the total carbon 1s peak. This can be seen in the different LTO tape wear results of Chapter three.

Analysis of the LTO tapes with the exception of the Imation production tape showed that, binder (N) depletion occurred and lubricant enhancement occurred with cycling for all environmental conditions. In these experimental results, the C-C/C-H component of the C1S peak signal increased with the tape cycling. It is possible chain scission was occurring in the tape binder resin resulting in phase segregation and low molecular weight short chain C-H polymers segregating to the surface of the tape, but the far more likely cause is due to the migration of the lubricant to the surface. Thus, two effects are evidence of removal of binder resin and lubricant replenishment on the surface of the tape.

The loss of binder was due to the removal of higher protruding tape asperities in the first stage of tape wear; high asperities on the tape were burnished during the first couple of hundred passes. The second stage of the wear of the tape was due to fatigue and results from continuous cyclic stressing of the media by contact with the heads. Sullivan[10, 27] stated that the tape asperities are alternately in compression and tension as a head asperity approaches and then moves away from the head. When two solid are in sliding contact, the maximum shear stress occurs not at the asperity junction, but below the surface[51]. The repeated contact between the tape and head makes the tape subsurface under cyclic stressing, the fatigue cracks beneath tape will eventually appear, this leads to the initiation of subsurface fatigue cracks which grow to the surface and produce delaminative removal of binder material and Fe particles.

For the Imation production tape (see section 3.5.6); examination of the C-C/C-H component indicated a lubricant loss. However, the initial lubricant concentration levels for Imation tape were significantly higher than for the other tapes, as was the final lubricant concentration.

Tape wear increased at higher contact pressure, higher temperature and water content conditions. During contact of a particulate tape with the head, tape debris consisting of binder and magnetic particles can be generated by adhesive, abrasive, and impact wear. Binder debris, loose magnetic particles, worn head material, or foreign contaminants are introduced between the sliding surfaces and results in three-body abrasion of the head and tape surface. The amount of debris generated as a result of tape wear depends on the

magnetic particles, binder, lubrication and cohesive and adhesive properties of the magnetic-coating formulation used to make the tape.

4.4 Head Stain

Stain formed on magnetic recording heads is defined as a transfer of material from tape to head. These deposits are not the readily removable tape debris. Stains are generally insoluble in most common solvents and require abrasive cleaning tapes for removal. In tribological terms, the formation of a transfer layer (stain) may be partially beneficial in reducing friction and wear; however, the layer may introduce unacceptable spacing losses between the tape and head that causes signal loss during the magnetic head reading and writing procedure and may under certain circumstances short out MR elements and shield pole[10].

The stains may contain organic or inorganic material. Organic stain is often called friction polymer[20]. Friction is essential for the formation of these materials; it is suggested that frictional heating allows the necessary chemical reaction to take place.

Conventional Fe stain is mainly inorganic stain. This Fe based stain is probably due to the adhesive force between the head and outer polymer layer of the tape being greater than the cohesive forces within the polymeric binder. This leads to dynamic formation of the transfer film (mainly the Fe particles) that attains and maintains constant critical thickness. The detail formation mechanism of Fe stain will be discussed later in this section.

4.4.1 Stain in Travan5 System

A Travan5 head has no components containing Fe; hence any traces of Fe detected on heads can only be due to a transfer magnetic material from tape to head. Thus the amount of Fe being deposited at each condition can be used as a reliable measure of the amount of stain formed.

Results (see section 3.1.1.11) show pole areas are the sites where stain forms preferentially. The pole and shared pole materials are metal thin films that are the most

active sites on the whole head. In this context an active site means that this part of the surfaces has a greater density of electrons in the conduction band, and promotes the formation of adhesive bonds between the tape materials and this part of head surface. Sullivan[10, 27, 77]suggested that the formation of conventional Fe based stain was dependent on an adhesive interaction between the outermost polymeric layer of the tape and the materials of the head. Sullivan has shown that Fe based stain formation is directly dependent on the electrical conductivity of the substrate, thus, the greater the density of electrons in the conduction band of the head components, the greater the probability of electron transfers and the more likely it is that these adhesive bonds will be formed. Stain easily formed on the materials with greater density of electrons in conduction band also was confirmed by Sourty and Sullivan' work[101, 103]. They found stain forms on the TiC phase of the ceramic in preference to the insulations Al_2O_3 phase; TiC has almost metallic electrical conductivity.

The bond energy between cross-linked polymers chains is of the order of the bond energy within the chain is about 10eV (via covalent bonding). The bond energy between the passivated magnetic particles and the polymer binder, via a good wetting agent, is almost certainly less than this[10, 27]. The weaker bonds in the tape magnetic layer are the binder-pigment bonds. This is the reason the separation tends to occur at the binder and magnetic particles interface. Fe and carbon bond energy is around 400kJ/mol (5eV/molecule), is less than the bond energy of the cross-linked polymers chains inside tape. With the tape under degradation or under constant fatigue wear, chains scission may occur, the magnetic particles possible were separated from tape binder, if the produced adhesive bond strength between the tape and head is greater than the internal cohesive bond strength between pigment particles and binder, materials transfer from tape to head may occur. Adhesive bond formation is a chemical process that is governed by temperature, thus the higher the contact temperature (high contact pressure) the higher the probability of adhesive bond formation and the greater the amount of transferred material (stain). Thus, an adhesive junction formed at the polymer/metal interfaces will be strong enough to produce shearing within the bulk of the magnetic layer. At the same time the recessed pole area will be less prone to removal of stain once formed.

By looking at the Fe:Co ratio (see section 3.1.2), where Co is the major constituent in the CoZrTa poles, it was possible to determine when a maximum occurred in the amount of Fe (hence Fe stain) present on the poles. It was shown that as the water content increased the Fe:Co ratio decreased indicating a decrease in coverage of the stain. It is proposed that Fe based stain was reduced at higher water content due to water saturation of active sites on the head preventing the formation of adhesive head/polymer bonds. But higher temperatures at the interface of tape and head assist the stain process by driving off water molecules. Thus the rate of a stain reaction increases exponentially with the absolute temperature following an Arrhenius type reaction. Sullivan[27] found that the mean contact temperatures for a similar linear tape system were over 130°C. Under higher ambient temperatures of tape-head interface, higher transient temperature occur between head and tape during tape cycling procedure. $T_{contact} = T_{ambient} + T_{flash}$, the higher interface temperature, the more stain formation.

Results confirmed that stain was concentrated on the poles and in all cases was of the order of around 30 nm thick (see section 3.1.3). This corresponded to a stain thickness approximately equivalent to the thickness of one magnetic particle. Fe particles from the tape normally consist of a pure Fe metal core with a Fe_2O_3 passivation layer. Thus a follow layer of stain can only be transferred to the Fe particles that already adhere to the poles. As mentioned early, the greater the density of electrons in the conduction band of the head components, the greater the probability of electron transfer and the more likely it is that these adhesive bonds will be formed. Because Fe_2O_3 is almost non-conductive material with few free electrons in its conductive band, the single layer of magnetic particles formed on the head surface will not bond strongly with the tape. It is probable that of bonds are formed, they are Van der Waals bond (with probably bond energy less than 0.5eV) or weak ionic bonds, thus a second layer of passivated Fe particles will not readily bond to the first adherent layer. The materials which do deposit will be easily removed by contact with the tape. At the same time, the Head Cleaning Agent (HCA) easily removes such weak bonded materials after it formed.

At the water content highest level (40°C, RH 80%), no conventional Fe stain was detected, but large amounts of loosely bound carbonaceous material transferred to the head, mainly of polymeric binder (see section 3.1.1.11). The material was also

significantly thicker than conventional Fe stain formed at the lower atmospheric water contents. At RH 80%, 40°C, the contact temperature and water content between the Travan5 head and tape were great enough to cause local surface binder softening and degradation[20] of the tape surface leading to the observed thick, polymeric stain.

4.4.2 Stain in LTO System

Fuji, Maxell, Imation (production) and Mp3 tapes showed very little staining of the head under any environmental condition (see Chapter three related sections). Only sparse Fe traces were detected on some ceramic regions.

LTO Mp1 tape had 2.5% HCA and produced Fe stain. The Fuji, Maxell, Imation (production) and Mp3 tapes have higher HCA content (5%) and these tapes did not produce stain. The reasons are possible as follows. The hard Al_2O_3 particles (so called head cleaning agents) provide bearing surfaces within the tape and increase its mechanical integrity. Thus the increased number of HCA particles produced more hard bearing surfaces at the tape contacts and additionally provide better hot-spot temperature distribution at the interface with consequently lower contact temperatures. The lower contact pressures in LTO system also ensured that the energy distribution at the real areas of contact is much lower. All these affects lead to a lower probability of material transfer, hence less stain.

Another postulated reason is due to the improved binder materials involved in these later generation Fuji, Maxell, Imation (production) and Mp3 tapes. Tape industry is continuing to develop binder materials that have high flexibility, elasticity, wear resistance and in the same time provide low coefficient of friction and low head wear. Meanwhile the binder still provides the cross linking necessary to hold all of the mix ingredients. Although details of the tapes was not revealed by industry, it is very likely the new LTO tapes involved here had better binder materials than LTO Mp1 tape (old Travan5 tape formation); this increases the cohesion force between the Fe particles and binder inside the tape, and makes the transfer materials more difficult than LTO Mp1 case. These low stain tapes had differences in lubricant levels (such as Imation production tape), slight differences in roughness, differences in magnetic particle size (such as Mp3 tape) and coercivity. However, none of these material variations affected

stain production (see Chapter three related different tape-stain sections). LTO stain results showed that stain is probably a function of tape formulation and structure; possible the dominant factor is the binder formulation and HCA inside tape.

With LTO Mp1 tape (see section 3.2.3), conventional Fe based head stain occurred under all conditions. Mp1 tape was specially made to exactly similar formulation as Travan5 tape. The extent and coverage of the stain on LTO heads, however, was much less than that of Travan5 system; this will be discussed in the section 4.4.3.

Water molecules' effect on the stain formation has been found. Figure 3-70 in section 3.2.3 represents the head stain at different water content but same temperature, this clearly indicated that water molecules occupation of active sites on the head reduces the stain formation at higher water content condition, but does not eliminate the formation of Fe stain. At high water content there are probably competing reactions between material transfer and water absorption on active sites on the head. Clearly the former is just dominant in this case.

Mp1 tape experiments (see section 3.2.3) at RH 15%, 15°C and RH 10%, 10°C results are quite similar, with less stain on the pole area indicating that low temperature and low water vapour content do not promote the dense stain under a low contact pressure system like LTO, the LTO contact pressure is around one third of Travan5 (see section 4.2). Extensive stain still formed on the poles in the condition of RH 40%, 22°C and RH 15%, 40°C. This is at total variance to previous results for Travan5 system where contact pressures are significantly higher.

Assuming that the chemical description of stain formation is valid, then it is likely that a certain threshold contact temperature (or perhaps energy dissipation) must be attained before substantive adhesive transfer of material from tape to the head will occur. In LTO the contact pressure between the head and tape is less than one-third of contact pressure in Travan5 system (see section 4.2), so the interface heating effect in LTO also was much lower due to low contact pressure, and it is therefore likely that this affects stain formation.

It must be assumed in the lower contact pressure LTO drives at ambient temperatures of 15°C or less the energy dissipated at the contacts was insufficient to increase the temperature to the threshold level necessary for significant adhesive transfer to occur, even though the water vapour conditions are such that stain might be favoured. An increase in ambient temperature above 22°C appears from the results to be just sufficient for the asperity contacts to exceed this threshold temperature and so stain form up to RH 40%, 22°C. Surprisingly, at much higher temperature and humidity, RH 80%, 40°C, conventional Fe based stain was also formed. This is again at variance with previous Travan5 results and clearly indicates a further contact pressure effect, but this time on the tape. Under these conditions, contact temperatures at the tape asperities are not sufficiently high to degrade the tape surface and thus to produce polymeric transfer films and high tape wear.

4.4.3 Contact pressure effect on the stain

Using an exactly similar formation tape (Travan5 and LTO Mp1) and same head materials within Travan5 head and LTO head, the contact pressure effect on the stain could be compared within Travan5 system and LTO system.

Four conditions which were carried out in both Travan5 and LTO Mp1 including RH 10%, 10°C; RH 40%, 22°C; RH 15%, 40°C and RH 80%, 40°C. There was more stain in the higher contact pressure case (Travan5) than that of LTO Mp1 in the same experimental condition (see section 3.1.2 and section 3.2.3). In all experimental conditions, except RH 80%, 40°C, Fe based stain completely covered the pole and insulator area so much that none of the original pole location could be identified by AES in Travan5 system. The LTO Mp1 experiments showed far less extensive stain cover on the surface of head, Fe stain mainly covered the pole area in LTO Mp1 system and no Fe stain covered insulator area.

It is well known that most forms of wear increase with contact pressure. As mentioned early, adhesive bond formation is a chemical process that is governed by temperature, thus the higher the contact pressure (higher interface temperature), the higher the probability of adhesive bond formation and the greater the amount of transferred

material (stain). This is possible reason for far more extensive stain formation in Travan5 under similar tape formulation.

In Travan5 system of 40°C, RH80% (see section 3.1.2), the stain consisted almost entirely of polymer material (AES results), this has been explained due to degradation of the surface of the tape under these hot wet conditions. At 40°C, RH 80%, the transfer of large amounts of polymeric material was not observed in the LTO system and in fact less Fe stain was observed (see section 3.2.3). The differences between LTO and Travan5 systems were due to differences in contact pressure. The lower contact pressure in LTO system reduced the tape degradation at the hot and wet condition (40°C, RH 80%).

4.4.4 Fe Stain Structure

Sullivan[10, 27] stated the Fe based stain mainly contains chemically un-changed MP particles from the tape and some binder and possible lubricant material that acts as an adhesive layer between MP particles and the materials of the head. Metal particles inside tape have pure metallic Fe core with a passivated Fe_2O_3 layer. XPS was used to study the structure of the Fe based stain in LTO Mp1 system, the Ar^+ etching was necessary useful to remove the passivation layer on the metal particles and reveal the iron cores. If the iron cores were seen in the head stain as well as in the etched tape, this would prove conclusively that the stain consisted of chemically un-changed metal particles and would validate our model that the Fe stains were formed from the same Fe metal particles and some binder, lubricant from the tape.

XPS results (see section 3.2.3) show the C, O, Fe and traces of N on the Fe stain. The only source of N from the head Fe stain surfaces was from the tape polymeric binder, indicating that some binder was also present in the Fe stain. XPS results (see section 3.2.3) show both head stain and tape sample had the Fe2p3/2 peaks of iron at a binding energy of 710.7eV. This value is characteristic of Fe_2O_3 2p3/2 line[153]. The low intensity (due to low concentration and very small area XPS analysis) of the Fe2p3/2 from the stain accounts for the peak broadening observed.

Stain and tape sample were etched and analysed (see section 3.2.3). The results showed that pure metallic Fe (binding energy 707.2eV) appeared in the surface of etched stain and on the etched tape sample as well. This is a very important result. The Fe 2p3 peak components from the etched tape MP pigment and from the etched Fe based stain have near identical binding energies, proving conclusively that the Fe stain mainly contain chemically un-changed MP particles from the tape and some binder and possible lubricant material. This result confirms Sullivan's Fe stain theory.

4.4.5 Summary of Stain Production Mechanism

In the case of thin film MR heads, stain formation was affected by interfacial contact temperature, tape formation and environmental operating conditions. In all the tapes used in this research project, only Travan5 tape and LTO Mp1 tape produced the traditional Fe stain. Other tapes produced very clean head surfaces, which occasionally had trace of polymer material transferred to the head surface.

Sullivan[77] indicated the stains formation was a dynamic process. Stain formation on the poles was influenced by whether the pole was energised or not and it was much greater on the energised pole, an obvious temperature effect. The thickness of the stain was constant, is related to the magnetic pigment size and corresponds to one particle thickness. In this research work, Fe stain was found to form a lumpy deposit in the initial stages and generally the areal coverage increased with number of passes.

Ceramics are brittle materials with low surface energy, high hardness, and low adhesion to contacting surfaces[175]. The ionic or covalent bonding in ceramic is directional; hence it is expected that tape asperity contacts have low adhesive strength. The pole and shared pole materials are thin film metal, which are the most active materials on the whole head. At the same time the pole area is the lowest recessed area in the head and possibly will have less contact with HCA (Head Cleaning Agent) after the stain formed. This means the stain formed at recessed pole area is difficult to be removed. All these make the pole area become the preferential area for the stain compared with other parts of the heads surface. This explains why stain preferentially deposits on the head pole area.

The experimental evidence suggests that the mechanism of stain production is as follows. Strong chemical bonding occurs between metals and polymers and preferentially at polymer/Metal contacts. This gives rise to strong adhesive junctions with bond strengths of about 10eV/atom (assuming covalent bond formation). This is probably greater than the cohesive forces between magnetic pigment and resin binder. Thus, an adhesive junction formed at the polymer/ceramic, polymer/metal interfaces will be strong enough to produce shearing within the bulk of the magnetic layer. This process inevitably results in the plucking out of a wear particle and transfer of material from media to head. With polymers such as those used in binder systems that are non-linear and of relatively low crystallinity, transfer occurs as a discontinuous lumpy film such as those observed in our experiments.

The presence of excessive water vapour at the interface saturates the surface bonds, reducing the adhesive junctions. Higher temperatures at the interface assist adhesion by driving off water molecules, hence increasing stain. The higher contact pressure in Travan5 increased stain formation due to the higher interface temperature produced. Conventional Fe stain was easily formed at the higher head-tape contact pressure condition like Travan5 system, the results suggest binder property and contact pressure play major role to decide the Fe stain.

It is postulated that in the case of the LTO tapes (except LTO Mp1) that did not produce Fe stain, each tape had improved binder materials that lead to greater bulk cohesive forces and at the same time, had higher HCA content (5%) to give greater bearing support by the hard particles. They were also subject to lower contact pressures in LTO system (less energy dissipated at the contact).

4.5 PTR of the head

4.5.1 Pole Wear and Pole Tip Recession

Pole tip recession, or PTR, is defined as the height difference between the air bearing surface, or ABS (ceramic substrate), and the pole tips. This height difference is a result of differential wear rates of the head materials. PTR is influenced not only by the pole

tip mechanical properties, but also by the mechanical properties of other materials in the head structure.

Sullivan[10, 27] stated two-body abrasion was not the important wear mechanism due to two criteria. One is the calculation of the plasticity index from the Greenwood and Williamson[57] relationship for the head-tape interface by insertion of roughness and elastic parameters for the materials, shows the contact between the head-tape to be almost entirely elastic. Another is considering the ultra-smooth surfaces and the consequently vanishing small asperity included angles calculated from Halliday[176] show that plastic deformation of the head components surface can not occur. On the basis of these two criteria two-body abrasion hardly occurs at the head-tape interface.

The head pole wears by three-body particles abrasive wear is the major reason for the pole tip recession. These three-body particles are produced from the surface of the head ceramic and also possible some three-body particles from the Head Cleaning Agent (HCA) in the tape. These abrasive wear particles produced during operation and trapped at the interface between the tape and head and cause growth in PTR by three-body abrasion.

If no Fe stain covered the pole and insulator, the pole and shared pole wear is thus a combination of adhesive removal of material, and three-body, abrasive wear. The poles are the softest component of the head surface (see Table 4-2) and therefore the three-body abrasion is more pronounced in these areas. The micro adhesive wear usually occurs in the initial stage of the wear, where the tape asperities are still in contact with the pole and insulator area. Later with the recessed area became deeper; the tape asperities can not reach the recessed pole areas, at this stage three-body particle wear became the major wear mode for the pole and shared pole and insulator area.

Materials	Insulator (Al_2O_3)	Amorphous CoZrTa	AlTiC	TiC	TiO_2
Knoop Microhardness (GPa)	7.0	4.9	21	27.5	7.0-10

Table 4-2 Hardness of materials

If Fe stain covered the pole and insulator, the covered stain could be a sacrificial protection layer to limit PTR if stain is extensive and heavy present on the surface of poles[10, 27]. The stains formation is a dynamic process, with removed of the stains causing the serious wear of pole area. The wear of the pole and insulator is a combination of adhesive removal of material and three-body abrasive wears.

4.5.2 Different Materials Wear Rates producing PTR

Absolute wear rates of heads are of obvious importance, particularly with thin film constructions. Far more important, however, is the different wear rate of different head component materials, for example the softer pole wear compared to the hard material of the head. The wear rate results of LTO heads cycling against Imation tapes could be seen in section 3.5.5.

The AlTiC ceramic wear rate was fairly constant with the cycling distance and the wear rate of the AlTiC ceramic was around 9nm every 5k passes (1000km) of tape cycling. The wear rate measurement shows that insulator and pole wear rate (~19nm) was higher at the first 5k passes cycling. The wear rate of insulator and pole occurred in the second 5k passes cycling distance is quite similar to AlTiC wear rate that is about 9nm/1000km.

The wear rates of AlTiC and Poles fit well with the PTR values obtained in the experiment (see section 3.5.4), PTR reached an equilibrium values after 5k passes of tape cycling and then kept constant[75]. This is because after a certain time of tape cycling, recession areas have become bigger enough that three-body particles no longer rub against both tape and recessed pole area, equilibrium values of PTR have been reached in this situation. However, with the further wear of AlTiC ceramic (tape bearing surface), the recessed pole areas become shallow again, then the three-body particles wear will start again and this cyclic behaviour will continue until both recessed pole and AlTiC (tape bearing surface) approach a new equilibrium situation.

Archard's law states[47]:

$$V = \frac{kWx}{H} \qquad \text{Equation 4-3}$$

Where V is the volume worn away, W is the normal load, x is the sliding distance, H is the hardness of the surface being worn away, and k is a non-dimensional wear coefficient dependent on the materials in contact and their exact degree of cleanliness. Then, since AlTiC is much harder than the pole and insulator (see Table 4-2), the wear rate of AlTiC is much smaller than that of CoZrTa (poles). Wear is very limited in the LTO system considering the dimension of the LTO heads. A commonly used equation[47] to compute the wear rate is $V_i = k_i F S$, where F is the normal load, S the sliding distance, V_i the wear volume and k_i the specific wear rate coefficient, the calculated wear rate for AlTiC was 7.2×10^{-21} $m^3m^{-1}N^{-1}$ (±30%). The wear rate of the AlTiC is lower than other application system[65]. In this work, the wear rate is only tested in two conditions, further work still requires in this field.

4.6 Three body Particles generation Mechanism

During all the experiments, ceramic pullout occurred in all head ceramic surfaces after cycling against tape. In these tape/head systems, three-body particles can be clearly seen in the pole region together with many scratches due to 3-body particle wear (for example, Figure 3-83). Auger analysis shows that Ti bearing particles appearing on the pole and insulator regions (see section 3.1.2 and section 3.3.2). Considering the head and tape materials, the only source of these particles is from delamination of the TiC grains. The particles are too small to unequivocally identify their chemical state by XPS. While AES does not give sufficient chemical information to make this possible.

Three-body particles wear and the presence of titanium on the thin film head region have been reported by the Aston Surface Science[77, 86, 101, 102]. The particles on the head thin film region were shown, by AES, to contain Ti. In order to identify the wear mechanism of formation of these particles, XPS was used to study the changes in the head ceramic surface before and after tapes cycling within the environmental conditions specified. The identification of the exact chemical composition of these three-body particles is one of the major findings of this work, since this allowed the author of this thesis to unequivocally identify the mechanism of generation of the Ti containing three-body abrasive particles responsible for PTR and wear.

Due to the similar head ceramics in Travan5 and LTO XPS experimental results were obtained from the different tape system. LTO heads that used the Maxell LTO tapes and LTO Imation production tapes were used as typical examples to discuss the AlTiC ceramic wear processes (see section 3.4.3 and section 3.5.3).

The result of AFM measurements on LTO heads in general showed little or no stain generation. Then the AlTiC ceramic wear could be studied in isolation from any complication transfer mechanism. AlTiC ceramic surface pullout depth from the TiC grains of the unused heads averaged 4nm. This increased to around 15-19 nm after 5k passes of tape sliding. Traces of titanium were detected (by AES) in the head thin film region.

In all cases including unused, worn and boiled heads, TiO_2 was found on the TiC grain surfaces (see section 3.4.3). It is clear from this and many previous studies that wear, differential wear and PTR are intimately connected to the fact that the TiC grains in the Al_2O_3-TiC ceramic matrix of the tape-bearing surface of heads delaminate and produces hard three-body abrasive particles. These particles, as has been reported[77, 86, 101, 102] are then carried across the head surface giving rise to three-body particles wear and surface distress.

XPS results show the variation of the TiO_2 : TiC atomic ratio increases with atmospheric water content after the wear test (see section 3.4.3). It also indicates that the oxidation rate was relatively insensitive to changes of ambient temperature in the range employed in these experiments. This latter result is not too surprising since the interface flash temperature between the head and tape may be very high[177, 178, 179]. Bhushan[177] speculated that if the exposed magnetic particles or alumina particles contact the slider surface, the transient temperature rise could be more than 1000°C in hard disk system; Sullivan[27] found that the mean contact temperatures for a similar linear tape system were over 130°C. Hence small increases in ambient temperature may be insignificant in the processes. The fact that after 1000 km of cycling against tape the TiO_2 increases with water content shows that TiO_2 formation is part of the wearing process. It also indicated that the presence of water vapour can have a significant effect on TiC oxidation. Zhang[108] found that significant static oxidation of TiC did not occur until

about 400°C, however, Sullivan [180] has shown that oxidation under tribological conditions can take place at much lower temperatures and at a rate several orders of magnitude greater than that occurring under static conditions at the same surface temperature due to increases of the entropy of the system and its consequent affect on the Arrhenius Constant.

As stated, PTR reaches an equilibrium value after several hundred kilometres tape cycling. The results (see section 3.5.3) strongly imply that the TiO_2 production rate was constant between the 5k and 10k tape cycling, thus the production of three-body particles was constant when the equilibrium PTR value was reached. Oxidation of TiC is a dynamic process and removal and production of TiO_2 were carried out in the same time, but the oxidation of TiC should gradually increase during initial tape cycling until TiO_2 composition on the AlTiC surface reach the saturated value under certain condition, at this stage, removed TiO_2 and produced TiO_2 from AlTiC surfaces maintain similar speed.

AFM line scan measurements indicated that the height of the eruptions on the surface of TiC grains was about 15 nm above the general ceramic surface for the unused AlTiC sample, and these eruptions on the TiC grains became about 80 nm for the boiled AlTiC sample (see section 3.4.3). Similar, but less pronounced results were found for the ceramic on real head subject to boiling. XPS results confirmed TiO_2 (TiC oxidation) covered the surface of TiC phase of AlTiC. No TiC was detected after boiling; XPS results showed no chemical change occurred for Al_2O_3 phase of AlTiC. This result confirmed TiO_2 could be thicker than 10nm after boiling, and at the same time, oxidation of TiC could occur at 100°C with water vapour present.

The density of TiC[53] is $4.9\times10^3 kg/m^3$ and the density of TiO_2[165] is $4.0\times10^3 kg/m^3$. For the same mass the volume of TiO_2 is greater than the TiC. This volumetric difference produces stress at the interface between oxide and carbide and makes the surface oxide layer unstable and prone to delamination when a critical thickness has been reached. This is typical of the oxidational wear process[180]. The Knoop hardness of TiO_2 is 7-10.0Gpa[165] which is harder than the pole amorphous CoZrTa and insulator material

amorphous Al_2O_3. Hence the delaminated TiO_2 particles will cause three-body abrasive wear at the pole and insulator surfaces, but preferentially at the poles. The hardness of amorphous CoZrTa thin film is 4.9Gpa[181]. Micro adhesive and abrasive wear occur in the initial stages of the wear, where the tape asperities were still in contact with the pole and insulator area. The more water was present, the greater was the rate of generation of these three-body particles. The oxidation of TiC and pullout of TiO_2 was dynamic process that played an important role in the headwear.

Particles released from the tape may possibly cause three-body abrasion, but our analysis has shown that the vast majority of this loose "tape debris" is polymeric in nature and therefore soft compared to the pole materials. In addition, tape XPS results showed the Al_2O_3 head cleaning agent (HCA) levels slightly increased with cycling as the particles become exposed, but no loss. Therefore, the effect of HCA, if it occurs, is small, The fact that we have shown the overwhelming presence of Ti in recessed pole regions leads us to the conclusion that it is laminar particles TiO_2 released from ceramic which are responsible for the PTR.

Aston group's former work[103] confirmed that there was no evidence of differential wear (pullout) occurred in dummy head single Al_2O_3 or TiO_2 single-phase surface. For the Al_2O_3 phase in the Al_2O_3/TiC, the wear was due to nano-scale adhesive interaction between the Al_2O_3 and tape during the tape cycling process. It is possible some abrasive wear occurred in the Al_2O_3 phase, but according the smoothness tape surface and hardness of the Al_2O_3 makes this process unlikely.

4.7 Contact pressure effect on Wear of the heads and PTR

As stated the contact pressure in Travan5 heads was about 3.5 times higher than the contact pressure in LTO system (see section 4.2); the mean contact temperatures in Travan5 are likely to be considerably higher than contact temperatures in LTO. Due to the similar tape materials using in LTO Mp1 tape and Travan5 tape, it was possible to compare directly the Travan5 and LTO head wear without regard to tape formation effects.

The depth of ceramic pullout in LTO is less than the depth of ceramic pullout in Travan5 (see section 3.1.1.11 and section 3.7.1). Section 4.6 has shown that chemical/oxidative wear occurs at the TiC grains and the pullout particles from the ceramic substrate are mainly the TiO_2 particles. It is possible that the lower contact pressure and subsequent reduction in interface temperature reduces the rate TiC oxidation in LTO. In addition to this, sub-surface stresses that give rise to the intra-granular delamination in the head ceramic are much closer to the surface in the case of LTO system. Sourty and Sullivan[182] explained this by calculation of the maximum shear stress depth close to the surface of thin film heads of similar design and having similar contact pressure. As a consequence of these effects the number and size of TiO_2 particles are less in the LTO system. The combination of the smaller less abundant three body wear particles and the lower contact pressure in the LTO system ensure that the three body abrasive wear is reduced in LTO, thus producing less depth of PTR.

Experimental results clearly show PTR in Travan5 was higher than that of LTO after the same conditions of cycling (see section 3.1.1.11and section 3.7.1). In Travan5 system, the pullouts from TiC ceramic (three-body particles) were thicker and more abundant than those of LTO due to higher contact pressure leads. Higher contact pressure leads to more damage for the pole during the three-body particles swiping the head thin film region.

The higher contact pressure in Travan5 system leads to more wear of all types compared with LTO system including PTR. From section 4.5.2 Archard' law, it is clearly shown that the wear of the system is proportional to the contact pressure, with increasing contact pressure, the wear becomes higher.

5 Chapter 5 Conclusions and Future Work

5.1 Tape Wear

Generally speaking the tape wear is very limited. Binder depletion occurred and lubricant "renewal" can be seen.

The relative humidity (as is used almost universally in this field) is not a suitable description for the environmental condition involved in the system. The absolute water content or the normalized water content will be a much better expression to demonstrate water effect.

The higher temperature and more water present at the head/tape interface, the more severe the wear of the tape. Increase the contact pressure; increased the wear of the tape. It was likely that tape binder material and HCA largely determines the materials transfer from the tape.

5.2 Head Stain

Stain formation was affected by tape formulation, interfacial contact temperature, contact pressure and environmental operating conditions.

For Travan5 tape and LTO Mp1 tape, the conventional Fe stain was produced on the surface of the heads. Other LTO Tapes such as Fuji, Maxell, Imation production, Imation Mp3 tapes did not produce conventional Fe stain.

The thickness of the Fe stain was around 25-30nm. Surface analysis has shown that stain consists of chemically un-changed passivated metal particles plus binder material and lubricant from the tape, thus confirming our earlier model of stain formation.

The stain formation mechanism has been identified from this work. Adhesive bond formation is a chemical process that is governed by temperature, thus the higher the contact pressure, the higher the contact temperature the higher the probability of adhesive bond formation and the greater the amount of transferred material (stain).

Water molecules at the interface saturate the surface bonds and makes adhesive junctions less likely. It is likely tape polymeric binder formulation and HCA have a significant role in stain formation, with the latest generation binders producing less transfer of material.

5.3 Contact Pressure Effects

The formation of three-body particles is directly related to contact pressure. Thus, the number of three-body wear particles produced was less and the particles were of smaller lateral size and thickness in the lower contact pressure (LTO) situation. The lower contact pressure LTO system, compared with higher contact pressure system (Travan5) ensures that fewer and smaller three-body abrasive particles were swept across the poles and insulator regions.

Lower contact pressure, as well as reducing tape wear, reduces head stain as described above. All other forms of wear were also reduced in the lower contact pressure case.

5.4 Three body particles and Head Wear

Micro adhesive wear, Micro-abrasion and three-body abrasion wear, tribo-chemical wear, fatigue wear were the major wear modes in the linear recording system.

PTR is the results of three-body abrasive wear. The three-body abrasive particles originated from tribo-oxidation of TiC grain surfaces within the AlTiC ceramic surface. Thin laminar sub-micron TiO_2 particles were removed from the ceramic by a delaminative wear process and were swept across the pole regions by the motion of the tape. There is possibility for some HCA particles as three body particles. For the Al_2O_3 phase of the head AlTiC ceramic, nano-abrasion and nano-adhesive wear occurred.

Higher water content and higher temperatures increase the TiC oxidation rate, leads to the higher wear of head and higher PTR value. The water content and interface flash temperature played critical role in the TiC oxidation.

Wear rate of the AlTiC ceramic in LTO system was around 9nm per 5k passes tape cycling, wear rate of AlTiC was 7.2×10^{-21} m^3/mN. The wear rates of pole and insulator were higher than the AlTiC wear rate during the first 5k passes of tape cycling, then later became similar wear rate. Wear rate of the Pole and ceramic material fitted the measurement of PTR value via tape cycling distance.

5.5 Pole Tip Recession

PTR is due to the different wear rate of the head materials during tape cycling. The three-body particles wear leads to wear of the poles. PTR reaches an equilibrium value after several hundred kilometres tape cycling.

Water content and temperature determine the extent of PTR in linear heads. Better design LTO heads can largely reduce the headwear. The final recommendation from this work is that Al_2O_3/TiC should not be used as a tape-bearing surface in linear data tape read/write heads.

5.6 Overall conclusion

The problem of stain in data tape recording heads appears to have been solved by a combination of low contact pressure, better head design and better tape formulation. The remaining problem and the one that severely limits tape performance and increased data density is PTR. It has been show in this thesis that the predominant mechanism for PTR is the generation of three-body wear particles by the oxidational wear of TiC phase in the two phase AlTiC ceramic tape bearing surface. Thus AlTiC should not be used for this application.

5.7 Future Work

In order to reduce the headwear, the research of the magnetic head generally carried out the incremental examination of the hardness of the head materials and an investigation of the protection layers. Meanwhile, the research of the magnetic tape takes certain measures to reduce the surface roughness and to reduce the friction coefficient through the optimisation of the lubricants, and reduces the tape tension.

Linear Tape Open (LTO) system is currently the best drive-tape system. In order to achieve the higher density of the recording, it still needs to improve the wear resistance of the system. Possible solutions for the reduction of the PTR and stains and increase the density of the recording system are as follows:

From the contact pressure point of view: Reducing the contact pressure will reduce the wear of the system. Continuing reducing the contact pressure but in the same time maintain the head-media space as low as possible will significantly reduce the wear of head and tape; maintain the head output and excellent tribology property. This is one of the major ways to reduce the wear of the tape head system.

From the head materials point of view: Better head materials properties will lead to less three-body particles production, this will lead to less wear (including pole materials and ceramic materials). The harder pole materials are needed to reduce the pole wear but in the same time still maintain the pole magnetic property. The small size of TiC grains will produce small and few TiO_2 particles, and then it is possible to reduce the wear of the heads. The possible solution for the three-body particles wear could be reduced by application of better ceramics as the tape-bearing surface, such as better designed single phase ceramic to be the tape bearing surface.

From the tape materials point of view: Better designed tapes formulation may reduce transfer of the materials and the wear rate of the heads; in this way better designed tapes will greatly reducing the space loss between the head and media, especially the binder materials and head-cleaning agent. The better lubricants materials inside the tape could reduce the wear of the tape head system. Efforts should be made to increase the

coercivity of MP and ME media, as this may be an important step in achieving the targeted linear recording density.

From the thin coating point of view: Coating is the efficient and highly supported way by the industry to reduce PTR and wear of head. The problems associated with spacing loss and stain could be solved by the application of a very thin coating (10nm) to the recording heads. Diamond like carbon (DLC) is one of the promising thin films. Some other thin film such as Cr_2O_3 is the possible coating as well. TiO_2 particles are pulled out at the Al_2O_3-TiC matrix surface and seem to initiate a chain of events that leads to the observed wear behaviour over time. When a thin coating like DLC is applied, obviously these TiO_2 particles are, at least in the first period of headwear, not generated anymore. Coating could protect the tape-bearing surface from HCA of the tape. Coating also protects the pole area during the tape cycling processing.

From the controlling environmental condition point of view: It is known that the higher temperature and higher water content increase the wear of the tape head system. Controlling the working condition of the drives would benefit the lifespan and performance of data storage system. Controlling the working environment could largely reduced the wear of the ceramic such as generation of three-body particles and stain formation on the head surface, reduction of the PTR become possible if the working environmental working conditions could be controlled under the suitable condition for the less wear and less stain condition.

Preliminary investigations show that there was a single-phase oxide tape-bearing surface like Al_2O_3 was used in tape heads, no three-body particles from the head ceramic would be produced and PTR would be reduced. Thin coatings like DLC can reduce the wear and PTR. The final recommendation from this research work is that Al_2O_3/TiC not an ideal material as a tape-bearing surface for the next generation linear data tape read/write heads.

[1] http:// www.seagate.com.

[2] Wood R, 2000, "Feasibility of magnetic recording at a terabit per square inch". IEEE Trans Magn, 36(1I): pp. 36-45.

[3] Robertson, J., 2003, "Rquirements of ultrathin carbon coatings for magnetic storage technology", Tribology International 36, pp. 405-415.

[4] Luitjens SB, Folkerts W, Van Kersteren HW, Ruigrok JJM, 1998, "Trends in digital magnetic recording; the application of thin film heads for tape recording". Philipp J Res; 51(1): pp. 5-19

[5] Robertson, J., 2002, "Diamond-like amorphous carbon", materials Science and Engineering, R 37, pp. 129-281.

[6] Wallace R.L, 1951, "The reproduction of Magnetically Recorded Signal", Bell system Technical Journal, 30, pp.1145-1173.

[7] Hempstock, M.S., Sullivan, J.L., 1996, "A study of the mechanical and magnetic performance of metal evaporated tape", Journal of Magnetism and Magnetic Materials, 155, pp.323-328.

[8] Bhushan, B., Theunissen, G.S.A.M., Li, X., 1997, "Tribologyical studies of chromium oxide films for magnetic recording applications", Thin Solid Films, 311, pp. 67-80.

[9] Patton, ST., Bhushan, B., 1996, "Micromechanical and tribological characterization of alternate pole tip materials for magnetic recording heads", Wear, 202, p. 99-109.

[10] Sullivan, J.L., 1998, "The tribology of flexible magnetic recording media-the influence of Wear on signal performance". Tribology International, 31(8), pp. 457-464.

[11] Hempstock, M.S., Mark, M.A., Sullivan, J.L., 1998, "A study of the durability of flexible magnetic media in a linear tape system". Tribology International, 31(8), pp. 435- 441.

[12] http://www.lto-technology.com.

[13] Mee, C.D. and Daniel, E.D., 1989, Magnetic recording handbook, technology and applications, McGraw-Hill Publishing Company.

[14] http://www.wtec.org/reports.htm

[15] Mallinson, J.C., 1987, "The foundations of magnetic recording", Academic Press, Inc. (London), pp. 1-30.

[16] Denis, C., Mee and Daniel, E., 1989, "Magnetic Recording Handbook", Printed and bound by R.R.Donnelley & Sons Company.

[17] United States Patent: 5,774,306.

[18] Nakagawa, S., Tanaka, S., Naoe, M., 1996, "Relationship between Ta content and soft magnetism of CoZrTa films for backlayers in perpendicular magnetic recording media", Journal of Magnetism and Magnetic Materials, 155, pp. 231-233.

[19] Bijker, M.D.,bastiaens, J.J.J., Draaisma, E.A., Jong, L.A.M.de., Sourty, E., Saied, S.O., Sullivan, J.L., 2003, "The development of a thin Cr2O3 wear protective coating for the advanced digital recording system". Tribology International 36, pp. 227-233.

[20] Bhushan, B., 1990, Tribology and mechanics of magnetic storage Devices, Spring-Verlag. New York InC.

[21] Fontana, R., 1990, "Magnetic thin film heads, A review on precessing issues", ECS Proc. Symp. Magn. Mater. Process Device 90-8, pp.205-219.

[22] Fontana, R., 1995, "Process complexity of magnetoresistive sensors: A Review", IEEE Trans. 31(6), pp. 2579-2584.

[23] Ichihara, T., Nakagawa, S., Naoe, M., 1998, "Analysis of stray magnetic field at the substrate and effect of applying external magnetic field field in facing targets sputtering", Vacuum, 51(4), pp. 715-718.

[24] Denis, C., Mee and Daniel, E., 1989, "Magnetic Recording Handbook", Printed and bound by R.R.Donnelley & Sons Company.

[25] Kaneo, M., Tsuyoshi, U., and Larissa V. Panina, 1997, "Recent advances of micro magnetic sensors and sensing application", Sensors and Actuators: Physical Volume 59, Issues 1-3, 1997, April, pp. 1-8.

[26] Yamamoto, H., Yamada, K., 1995, "The application of giant MR films to magnetic devices", Materials Science and Engineering, B31, pp. 207-211.

[27] Sullivan, J.L., 1996, "The tribology of flexible magnetic recording media", Journal of Magnetism and magnetic materials, 155, pp. 312-317.

[28] Chen, M., Nikles, D. E., 2001, "Surface Characterization of Iron particles Treated with a polyvinylchloride wetting binder", IEEE Transactions on magnetics, 137(4), pp. 1637-1639.

[29] Doshita, H., 1998, "Tribological characteristics of thin-layer magnetic particulate media", Tribology international, 31(9), pp. 541-545.

[30] Okamoto, K., Okazaki, Y., Nagai, N., Uedaira, S., 1996, "Advanced metal particles technologies for magnetic tapes", Journal of Magnetism and magnetic Materials, 155, pp. 60-66.

[31] Hisano, S., Saito, K., 1998, "Research and development of metal powder for magnetic recording", Journal of Magnetism and magnetic materials, 190, pp. 371-381.

[32] Sugita, N., Mackawa, M., Ohta, Y., Okinaka, K., Nagai, N., 1995, "Advances in fine magnetic particles for high density recording", IEEE Trans. Magn., 31, pp. 2854-2858.

[33] Hisano, S., Saito, K., 1998, "Research and development of metal powder for magnetic recording", J.Magn. Magn. Mater., 190, pp. 371-381.

[34] Li.XD., Bhushan,B., Inoue,M., 2001, "Time-dependent mechanical properties and tribological behavior of magnetic tapes", Wear 251, pp. 1150-1158.

[35] Doshita, H., 1999, "Tribological characteristics of thin-layer magnetic particulate media", Tribology International, 31(9), pp. 541-545.

[36] Weick, B L., Bhushan, B., 1995, "The tribological and dynamic behaviour of alternative magnetic tape substrates", Wear, 190, pp. 28-43.

[37] Weick, B.L., Bhushan, B., 1996, "Characterisation of Magnetic tapes and substrates", IEEE Transaction on Magnetics, 32, pp. 3319-3322.

[38] Mizoh, Y., 1996, "wear of tribo-elements of video tape recorders", Wear, 200, pp. 252-264.

[39] Xie, Y., Bhushan, B., 1996, "Fundamental wear studies with magnetic particles and head cleaning agents used in magnetic tapes", Wear, 202, pp. 3-16.

[40] Bhushan, B., Khatavkar, D., 1995, "Role of abrasivity on friction, Wear, staining and signal degradation in audio tapes", Wear, 190, pp. 16-27.

[41] Hirofumi, K., 1997, "Effect of double bonds on friction in the boundary lubrication of magnetic thin film media", Wear, 202, pp. 149-153.

[42] Osaki, H., Uchiyama, H., Honda, N., 1993, "Wear mechanisms of Co-Cr sputter deposited magnetic tapes in helical scan video tape recorders", IEEE Trans. Magnetics , 29, pp. 41-58.

[43] Patton, S.T. and Bhushan, B., 1997, "Environmental effects on the streaming mode performance of metal evaporated and metal particle tapes", IEEE Trans, Magnetics, 33, pp. 2513-2530.

[44] Bhushan, B. and Patton, S.T., 1998, "Tribology in ultra-high density tape drive systems: state of the art and future challenges". IEEE Trans. Magnetics , 34, pp. 1883-1888.

[45] Pattom, S.T., Bhushan, B., 1998, "Effect of diamond-like carbon coating and surface topography on the performance of metal evaporated magnetic tapes", IEEE Trans. Magn. 34, pp. 575-587.

[46] Wang, J., Mark, T., 1998, "Multi-channel, high speed, tape head contour", United States Patent: 5,774,306.

[47] Archard J.F., 1953, "Contact and rubbing of flat surfaces", Journal of Applied Physics, 24(8), pp. 981-988.

[48] Bhushan, B., 1996, Tribology and mechanics of magnetic storage devices, Spring Verlag, New York, 2nd,edn.

[49] Rabinowicz, E., 1965, Friction and wear of materials, Wiley, New York.

[50] Hertz, H., 1896, Hertz's Miscllaneous Papers; Chs.5 and 6. Macmilan, London, U.K.

[51] Hamilton, G.M., and Goodman, L.E, 1966, "The stress field created by a circular sliding contact", J.Appl.Mech., Trans. ASME 33, pp. 371-376.

[52] Suh, N.P., 1977, "An overview of the delamination theory of wear", Wear, 44, pp. 1-16.

[53] Bhushan, B., Gupta, B.K., 1991, Handbook of Tribology, Printed by R.R.Donnelley & Sons, Inc.

[54] Hand book of ThermoMicroscopes AFM, ThermoMicroscope, 2001.

[55] Topometrix Technical Brief-SPM overview, 1996, Topometrix Corporation, Santa Clara.

[56] Bhushan, B., 1984, " Analysis of the real area of contact between a polymeric magnetic medium and a rigid surface". J.Trib., Trans. ASME 106, pp. 26-34.

[57] Greenwood, JA., Williamson, JBP., 1966, Contact of normally flat surfaces. Proc Roy. Soc. Lond; A295: 300-319.

[58] Bhushan, B., 1985, "The real area of contact in polymeric magnetic media-II: Experimental data and analysis", ASLE Trans, 28, pp. 181-197.

[59] Bushan, B., Doverner, M.F.J., 1989, "Role of mechanical properties and surface texture in the real area of contact of magnetic rigd disks", T. Trib., Trans. ASME, 111, pp. 452-458.

[60] Hempstock, M.S., Sullivan, J.L., 1996, "A study of the mechanical and magnetic performance of metal evaporated tape", Journal of Magnetism and Magnetic materials , 155, pp. 323-328.

[61] Bhushan, B., 1985, "The real area of contact in polymeric magnetic media-II: Experimental data and analysis", ASLE Trans, 28, pp. 181-197.

[62] Bhushan, B., Doerner M.F., 1989, "The role of mechanical Properties and Surface Texture in the real Area of Contact of Magnetic Rigid Disks", J. Trib. Trans. ASME, 111, pp. 452-458.

[63] Tanaka, K., Miyazaki, O., 1981, "Wear of magnetic materials and audio heads sliding against magnetic tapes", Wear, 66, pp. 289-306.

[64] Bhushan, B., 1999, Principles and Applications of Tribology, Wiley, New York.

[65] Bhushan, B., Lowry, J.A., 1995, "Friction and wear studies of various head materials and magnetic tapes in a linear mode accelerated test using a new nano-scratch wear measurement technique". Wear, 190, pp. 1-15.

[66] Hahn, F.W., 1984, "Wear of recording heads by magnetic tape", Tribology and Mechanics of magnetic Storage System, 1, ASLE, Park Ridge, IL, pp. 41-48.

[67] Hahn J. F.W., 1975, "An Evaluation of a Wear Resistant Coating", IEEE Trans. Magn, 11, pp. 1242-1244.

[68] Bushan, B., Doverner, M.F.J., 1989, "Role of mechanical properties and surface texture in the real area of contact of magnetic rigd disks", T. Trib., Trans. ASME, 111, pp. 452-458.

[69] Bushan, B. and Majumdar.A, 1992, "Elastic-plastic contact model for bifractal surfaces", Wear, 153, pp. 53-64.

[70] Scott, W W. and Bhushan, B., 2000, "Loose debris and head-stain generation and pole-tip recession in modern tape drives: A critical review", J.Info. Storage Proc.Syst., 2. pp. 221-254.

[71] Sullivan, J.L. and Sharma.P.J, 1992, "Factors affecting the durability of repeatedly stressed flexible magnetic recording media", Journal of Physics D: Applied Physics, v 25, n 1A, Jan 14, 1992, p A321-A327.

[72] Scott, W. W., Bhushan, B.,2002, "Micro/nano-scale differential wear of multiphase materials: pole tip recession in magnetic-tape heads". Wear, 252, pp. 103-122.

[73] Bhushan, B., 1999, Principles and Applications of Tribology, Wiley, New York.

[74] Bhushan, B.,1992, Mechanics and reliability of flexible magnetic media, Spring Verlag, New York.

[75] Scott, WW. and Bhushan, B., "Pole tip recession in linear tape heads: measurement technique and influence of head materials, tape speed and tape tension". Proc Instn Mech Engrs, 213(J), pp. 139-150.

[76] Kulkarni, AV., Chilamakuri, SK., Gupta, B.K. and Menon, A., 2000, IEEE Transaction on magnetics, 36(5), pp. 2736-2738.

[77] Sullivan, J.L., Wild, M.A., Hempstock, M.S., 2003, "The tribology of linear tape/head interfaces and its impact on signal performance", Tribology International, 36, pp. 261-267.

[78] Bhushan, B., 1987, "Magnetic head-media interface temperature. Part 2 Application to magnetic tapes", ASME J. Tribol, 109, pp. 252-256.

[79] Lemke, J.U., 1972, Ferrite Transducers, in D.E. Speliotis and C.E.Johnson (eds.), Advances in Magnetic Recording, Ann, NY Acad.Sci.,189, pp. 171-190.

[80] Scott, W W. and Bhushan, B., 2000, "Loose debris and head-stain generation and pole-tip recession in modern tape drives: A critical review", J.Info. Storage Proc.Syst., 2. pp. 221-254.

[81] Sullivan, J.L. and Cardwell, M.J. "The tribology of flexible magnetic recording media in linear tape systems and its impact on signal performance", EPSRC Grant number GR/L18983. Private communication.

[82] Bhushan, B., Hahn, F., 1995, "Stains on magnetic tape heads", wear, 184, pp. 193-202.

[83] Kattner, M. and Nhushan, B., "Anylysis of stain formation and wear mechanism in a linear tape drive", Pro Instn Mech Engrs, 214(J), pp. 561-581.

[84] Prabhakaran, V., Kim, SK., Talke, FE., 1998, "Tribology of the helical scan head tape interface", Wear, 215, pp. 91-97.

[85] Ajayi, O.O., Ludema, K.C., 1990, "Mechanism of transfer film formation during repeat pass sliding of veramic materials", Wear, 140, pp. 191-206.

[86] Hempstock, M.S., Wild, M.A., Sullivan, J.L., 2000, "Interactions at the head-tape interface of a linear tape system", Tribology International, 33, pp. 391-399.

[87] Deryagin, B. and Abrikosova, I.I., 1956, J. Exp.Theor. phys., 3, 819.

[88] Israelachvili, J.N. and Tabor, D., 1972, Proc.R.Soc, A331, 19.

[89] Buckley, D.H and Brainard, W.A, 1974, Advances in Friction and wear of polymer, 5B, Plenum, New York, p 315.

[90] Bely, V.A., 1992, Friction and wear in polymer-based materials, Pergamon, Oxford.

[91] Stahle, C.M. and Lee, T.D., 1992,"Characterization of the deposits on helical scan heads", Adv, Inf. Storage Syst, 4, pp. 79-86.

[92] Buckley, D. and Miyashi, K., 1984, "Friction and wear of Ceramic", Wear,100, PP 333-353.

[93] Bhushan, B., 1993, "magnetic slider/rigid disk substrate materials and disk texturing techniques-status and future outlook", Adv.Info. Storage Syst, 5, pp. 175-209.

[94] Takahashi, K., Sawai, E., Yohda, H., Muraoka, S. and Ihara, K., 1979, "High frequency properties of CO-based alloy laminated film video head", Tech.Rep.IEICE, VR79-4, pp. 23-28.

[95] Evans, A.G., Marshall, D.B., 1981, Wear mechanisms in ceramics, in: D.A. Rigney (Ed.), Fundamentals of Friction and Wear of Materials, pp. 439-452.

[96] Hsu, S.M., Shen, M.C., 1996, "Ceramic wear maps". Wear, 200, pp. 154-175.

[97] Sasaki, S., 1989, "The effects of the surrounding atmosphere on the friction and wear of alumina, zirconia, silicon carbide, and silicon nitride", wear, 134, pp. 185-200.

[98] Fischer, T.E. and Tomizawa, H., 1985, "Interaction of tribochemistry and microfracture in the friction and wear of silicon nitride", wear, 105, pp. 29-45.

[99] Sasaki, S., 1990, "Adsorption activities and friction properties of sintered alumina, in Proc". Int. Conf. Nagoya, pp. 1431-1436.

[100] Xu, J., Kato, K., 1997, "The effect of water vapour on the agglomeration of wear particles of ceramics", Wear, 202, pp. 165-171.

[101] Sourty, E., Wild, M. and Sullivan, J. L. 2002, "Pole tip recession and staining at the head to tape interface of linear tape recording systems". Wear, 252 (3-4), pp. 276-299.

[102] Sourty, E., Sullivan, J.L., 2000, "The tribology of advanced digital recording (ADR) systems", Tribology International, 33, pp. 629-637.

[103] Sourty, E., Sullivan, J.L.and Jong, L.A.M.D., 2003, "Pole Tip recession in linear recording heads", IEEE Transaction on magnetics, 39(3), pp. 1859-1861.

[104] Harrison, M.J.K., Sullivan, J.L. and Theunissen, G.S.A.M. 1998, "Pole tip recession in sandwich heads incorporating a FeTaN soft magnetic track". Tribol. Int. 31, pp. 491-500.

[105] Xu, J. and Bhushan, B., 1998, "Pole tip recession studies of thin-film rigid disk head sliders. Part 1. Mechanisms of pole tip recession growth". Wear, 219, pp. 16-29.

[106] Tsuchiya, T. and Bhushan, B., 1995, "Metal core recession and head stain studies of MIG heads sliding against cobalt-doped gamma iron oxide and metal particle tapes". Tribol. Trans. 38, pp. 941-949.

[107] Zhang, L., 2001, "Tribo-chemical Wear of Amprphous carbon overcoats and TiC in Al2O3-TiC sliders", Journal of Tribology, Transactions of ASME, 123, pp. 324-329.

[108] Zhang, L., kova, R. V., 1998, "A study on the oxidation and carbon diffusion of TiC in alumina-titanium carbide ceramic using XPS and Raman spectroscopy", Materials Chemistry and physics, 57, pp. 23-32.

[109] Patton, S T., Bhushan, B., 1996, "Micro-mechanical and tribological characterization of alternate pole tip materials for magnetic recording heads", Wear, 202, pp. 99-109.

[110] Halliday, JS., 1955, "Surface examination by reflection electron microscopy". Proc Inst Mech Eng; 169:777-81.

[111] Bhushan, B., Khatavkar, D V., 1996, "Role of water vapour on the wear of Mn-Zn ferrite heads sliding against magnetic tapes", Wear, 202, pp. 30-34.

[112] Bhushan, B., 1992, "Magnetic head-media interface temperature-part 3:application to rigid disks", ASME Journal of Tribology, 114, pp. 420-430.

[113] Bair, S., Green, I. and Bhushan, B., 1991, "Measurements of Asperity temperatures of a read/write head slider bearing in hard magnetic recording disks", ASME Journal of Tribology, 113, pp. 547-554.

[114] Kim, J H. and Shin, KH., 2000, "A numerical model Incorporating friction induced temperatures for contact recording applications", IEEE Transactions on Magnetics, 36, pp. 2692-2695.

[115] Carroll, J.F. and Gotham, R.C., 1966, "The measurement of abrasiveness of magnetic tape". IEEE Trans. Magn., MAG-2, pp. 6-13.

[116] Bhushan, B., 1999, Principles and Applications of tribology, Printed by Wiley, New York.

[117] Bhushan, B., 1999, "Chemical, mechanical and tribology characterization of ultra-thin and hard amorphous carbon coating as thin as 3.5nm:recent developments", Diamond and relatived Materials, 8, pp. 1985-2015.

[118] Huu, T.L., Zaidi, H., Paulmier, D., 1995, "lubricating properties of diamond–like coating", Wear, 181-183, pp. 766-770.

[119] Robertson, J., 2002, "Diamond-like amorphous carbon", Materials Science and Engineering R, 37, pp. 129-281.

[120] Robertson, J., 1986, "AMORPHOUS CARBON", Advances in Physics, v 35, n 4, Jul-Aug, 1986, p 317-374.

[121] Gupta, B.K., Nhushan, B., 1995, "Mechanical and tribological properties of hard carbon coating for magnetic recording heads", Wear, 190, pp. 110-122.

[122] Bull, S.J., 1995, "Tribology of carbon coating: DLC, diamond and beyond", Diamond and related materials, 4, pp. 827-836.

[123] Lee, J-W; Kim, S.H., Park, Y.S.; Shinn, M.N, 1997, "Retardation of the onset time for signal dropout arising from wear debris using diamond-like carbon overcoats on the VCR head", IEEE Tractions on Magnetics, 33, pp. 828-835.

[124] Xu, J., Bhushan, B., 1998, "Pole tip recession studies of thin film rigid disk head sliders II Effects of air bearing surface and pole tip region designs and carbon coating". Weaar 219, pp. 30-41.

[125] Bijker, M.D., Draaisma, E.A., Eisenberg, M., Jansen, J., Persat, N., Sourty, E., 2000, "Future directions in advanced digital recording technology", Tribology international, 33, pp. 383-390.

[126] Sourty, E., Sullivan, J.L., Bijker, M.D., 2003, "Chromium oxide coatings applied to magnetic tape heads for improved wear resistance, Tribology International, 36, pp. 389-396.

[127] Bushan, B., 1991, Tribilogy and machanics of magnetic storage device, Springer-Verlag, p 625.

[128] Nishida, Y., Nishida, Y., Kikkawa, M. and Kondo, H. 1999, "Behavior of lubricant migration in particulate magnetic recording media", IEEE Transaction on magnetics, 35(5), pp. 2451-2453.

[129] Zhao, X. and Bhushan, B., "Studies on degradation mechanisms of lubricants for magnetic thin-film rigid disks", Proc Instn Mech Engrs, 215(J), pp. 173-180.

[130] Zhao, X., Bhushan, B.and Kajdas, C., "lubrication studies of head-disk interfaces in a contralled environment Part 2: degradation mechanisms of perfluoropolyether lubricants", Proc Instn Mech Engrs, 214(J), pp. 547-559.

[131] Li, Y. and Bhushan, B., "Degradation of perfluoropolyether lubricants on magnetic recording disks during sliding", Proc Instn Mech Engrs, 211(J), pp. 279-288.

[132] Zhao, Z. and Bhushan, B, 1999, "Tribological performance of PFPE and X-1P lubricants at head-disk interface,part I:experimental results". Tribology lett., 6, pp. 129-139.

[133] Wagner, C.D., Riggs, W.M., Davis, L.E., Moulder, J.F. and Muilenberg, G.E., Handbook of X-ray photoelectron spectroscopy, published by perkin-Elmer Corporation.

[134] Beanson, G., and Briggs, D., 1992, High Resolution XPS of Organic polymers. New York:John Wiley& Sons.

[135] Kuroe, A., Uenaka, H., Hirokoh, M. and Itoh, N., 1990, "A short-time measuring method of head wear in VCR", Trans.Inst.Electron. Inf.Commun. Engr, J73-C-II, pp. 803-812.

[136] Bhushan, B., Khatavkar, D.V., 1995, "Role of tape abrasivity on friction, Wear, staining and signal degradation in audio tape", Wear, 190, pp. 16-27.

[137] Sharma, P.J., 1989, "Factors affecting the durability of floppy diskette media and mechanisms of wear". Aston University, Birmingham.

[138] Bhushan, B. and Patton, S. T., 1998, "Tribology in ultra-high density tape drive systems: state of art and future challenges", IEEE Trans. Magnetics, 34, pp. 1883-1888.

[139] Topoleski, J J. and Bhushan, B., 2001, "Magnetic and tribological evaluation of metal particle and metal-evaporated tapes in a linear tape drive", Pro Instn Mech Engrs, 215(J), pp. 157-170.

[140] Patton, S.T., Bhushan, B., 1998, "Effect of diamond-like carbon coating and surface topography on the performance of metal evaporated magnetic tapes", IEEE Trans.Magn. 34, pp. 575-587.

[141] Gupta, B.K., Bhushan, B., Zhou, Y., Winograd, N. and Krishnan,K., 1995, "Chemical analysis of stains formed on Co-Nb-Zr metal in gap heads sliding against oxide and metal particle magnetic tapes". J.Mater.Res., 10, pp. 1795-1810.

[142] Scott, WW. and Bhushan, B.,1999, "Generation of magnetic tape debris and head stain in a linear tape drive", Proc Instn Mech Engrs, 213(J), pp. 127-138.

[143] Kelly, J. 1982, Tape and head wear. In "Magnetic tape recording for the Eighties", pp. 7-22. NASA Reference Publication 1075, Washington, D.C.

[144] Smith, D., 1998, "Tribology of the belt driven data cartridge". Tribology International, **31**, pp. 465–477.

[145] Smith, DP., 1998, "Tribology of the belt-driven data tape cartridge", Tribology International, 31 (8), pp. 465-477.

[146] http://www.usatoday.com/weather/

[147] Briggs, D. and Seah, M.P., 1990, Practical Surface Analysis, Printed in Great Britain by Biddles Ltd, Guildford, Surrey.

[148] Watts J F, 1994, X-ray photoelectron spectroscopy, Vaccu, 45, pp.653-671.

[149] Siegbahn, K. et al., 1969, ESCA Applied to free molecules, North Holland, Amsterdam.

[150] YU, W., 1995, Ion bombardment induced compositional changes in compound semiconductor surfaces studied by XPS combined with LEISS, PhD thesis, Aston University in Birmingham.

[151] Shirley, D.A., 1972, "High resolution X-ray photoemission spectrum of valence band of gold", Phys Rev, B5, pp. 4709-4714.

[152] Bishop, H. E., 1981, "PRACTICAL PEAK AREA MEASUREMENTS IN X-RAY PHOTOELECTRON SPECTROSCOPY", Surface and Interface Analysis, v 3, n 6, Dec, 1981, p 272-274.

[153] http://srdata.nist.gov/xps/

[154] Wagner, C.D., Riggs, W.M., davis, L.E., Moulder, J.F., 1979, Handbook of X-Ray photoelectron spectroscopy, Perkin-Elmer Corporation, Physical Electronic Division. Printed in USA.

[155] Beanson, G.and Briggs, D., 1992, High resolution XPS of Organic Polymers. New York: John Wiley & Sons, p 240.

[156] Chastain, J. and King, R.C., 1995, Handbook of X-Ray Photoelectron Spectroscopy, MN: Physical electronic, Inc.

[157] McIntyre, N.S. and Zetaruk, D.G., 1975, "X-ray photoelectron spectroscopic studies of iron oxides," Environ. Sci. Technol., 9, p 336.

[158] Binnig, G., Quate. C.F. and Gerber, Ch., 1986, "Atomic force microscopy". Phys. Rev. Lett. **56**, pp. 930–933.

[159] Binnig, G., Gerber, Ch., Stoll, E., Albrecht, T.R. and Quate, C.F. 1987, "Atomic resolution with atomic force microscope". Europhys. Lett. **3**, pp. 1281–1286.

[160] Thermo Microscopes handbook, copyright 1992-2000 by ThermoMicroscopes, delivered with machines.

[161] Bhushan, B., 1999, "Nanoscale tribophysics and tribomechanics", Wear, 225-229, pp. 465-492.

[162] Bhushan, B., Gupta, B.K., 1991, Handbook of Tribology, Printed by R.R.Donnelly & Sons, Inc.

[163] Harrison, M.J.K., Sullivan, J.L. and Theunissen, G S A M., "Wear mechanisms of sandwich-type video heads", Proc Instn Mech Engrs, 211(J), pp. 263-277.

[164] Wahi, R.P., Iischner, B., 1980, "Fracture behaviour of composites based on Al_2O_3-TiC", J.Mater.Sci, 15, pp. 875-885.

[165] http://www.matweb.com/

[166] Doshita, H., 1999, "Tribological characteristics of thin-layer magnetic particulate media", Tribology International, 31(9), pp. 541-545.

[167] Private communication with Imation Company.

[168] Private communication with Hewlett-Packard.

[169] Scott,WW., Bhushan,B., 2000, "Corrosion and wear studies of uncoated and ultra-thin DLC coated magnetic tape-write heads and magnetic tapes", Wear, 243, pp. 31-42.

[170] http://www.lto-technology.com

[171] http://www.ultrium.com/

[172] Hempstock, M.S. and Sullivan, J.L., 1998, "Characterization of surface changes to metal evaporated and metal particle media following durability tests in helical scan Hi-8 recorders at ambient and high humidity condition", Tribology International, 31(8), pp. 419-424.

[173] Choudhury, T., Saied, S.O., Sullivan J.L.and Abbot, A.M., 1989, "Reduction of oxides of Iron, cobalt, titanium and niobium by low-energy ion bombardment", J.Phys. D: Appl. Phys, 22, pp. 1185-1195.

[174] Bhushan, B., 1990, "Tribology and Mechanics of Magnetic Storage Device", Springer-Verlag, pp. 471-474.

[175] Chandrasekar, S., Bhushan, B., 1990, "Friction and wear of ceramic for magnetic recording spplicstions-Psrt I A Review", Journal of Tribology, Transaction of ASME, 112, pp. 1-16.

[176] Halliday, JS. 1955, "Surface examination by reflection electron microscopy". Proc Inst Mech Eng, 169:777-81.

[177] Bhushan, B., 1992, "Magnetic head-media interface temperature-part 3:application to rigid disks", ASME Journal of Tribology, 114, pp. 420-430.

[178] Bair, S., Green, I. and Bhushan, B., 1991, "Measurements of Asperity temperatures of a read/write head slider bearing in hard magnetic recording disks", ASME Journal of Tribology, 113, pp. 547-554.

[179] Kim, JH. and Shin, KH., 2000, "A numerical model Incorporating friction induced temperatures for contact recording applications", IEEE Transactions on Magnetics, 36(5), pp. 2692-2695.

[180] Sullivan, J.L. 1987,"The role of oxides in the protection of tribological surfaces - Part 1 and II", Proc.I.Mech.E, Special Issue on 50 Years of Tribology, 1, 283-292 and 293-301.

[181] Unpublished results in our group.

[182] Sourty, E., Sullivan, J.L., Bijker, M.D., 2002, "Numerical modeling of sub-surface stress in magnetic data tape heads due to the dynamic contact with a tape", Tribology International, 35, pp. 171-184.

ELSEVIER

Tribology International 36 (2003) 335–341

TRIBOLOGY INTERNATIONAL

www.elsevier.com/locate/triboint

A study of tribology of Travan heads in linear tape recording

M.A. Wild *, Baogui Shi, J.L. Sullivan, S.O. Saied

Surface Science Research Group, School of Engineering and Applied Science, Aston University, Birmingham, B4 7ET, UK

Study of Generation Mechanism of Three-Body Particles in Linear Tape Recording

Baogui Shi
e-mail:shib@aston.ac.uk
Fax: +44 (0)121-359-0156

J. L. Sullivan

M. A. Wild

S. O. Saied

Surface Science Research Group
School of Engineering and Applied Science
Aston University
Birmingham, B4 7ET, United Kingdom

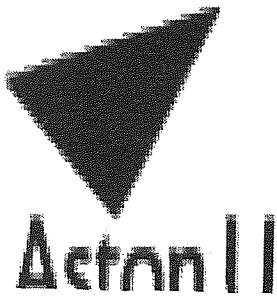

ELSEVIER

Tribology International 38 (2005) 699–708

TRIBOLOGY INTERNATIONAL

www.elsevier.com/locate/triboint

Contact pressure effects on pole tip recession and head stain in linear digital tape systems

Baogui Shi*, M.A. Wild, J.L. Sullivan, S.O. Saied

Surface Science Research Group, School of Engineering and Applied Science, Aston University, Birmingham B4 7ET, UK

Available online 2 March 2005

ELSEVIER

Tribology International 38 (2005) 709–716

TRIBOLOGY INTERNATIONAL

www.elsevier.com/locate/triboint

A study on the formation and structure of LTO head stains

Baogui Shi*, J.L. Sullivan, S.O. Saied, M.A. Wild

Surface Science Research Group, School of Engineering and Applied Science, Aston University, Birmingham B4 7ET, UK

Available online 2 March 2005

ELSEVIER

Tribology International 38 (2005) 633–640

TRIBOLOGY INTERNATIONAL

www.elsevier.com/locate/triboint

A study of three-body particle generation and subsequent pole tip recession in linear tape recording heads

Baogui Shi*, J.L. Sullivan, M.A. Wild, S.O. Saied

Surface Science Research Group, School of Engineering and Applied Science, Aston University, Birmingham B4 7ET, UK

Available online 25 February 2005

ELSEVIER

Tribology International xx (2005) 1–8

TRIBOLOGY INTERNATIONAL

www.elsevier.com/locate/triboint

Microtribological studies of two-phase Al_2O_3–TiC ceramic at low contact pressure

J.L. Sullivan*, Baogui Shi, S.O. Saied

Surface Science Group, School of Engineering and Applied Science, Aston University, Birmingham B4 7ET, UK